

Measurement of Liquid Film Thickness during Upward Annular Air-Water Flow in Vertical Pipe
Using Planar Laser-Induced Fluorescence (PLIF) Technique

by

Doszhan Mamedulanov

A thesis submitted in partial fulfillment of the requirements for the degree of

Master of Science

in

Petroleum Engineering

Department of Civil and Environmental Engineering
University of Alberta

© Doszhan Mamedulanov, 2016

Abstract

Experimental investigation of vertical annular two phase flow is the main scope of this thesis. Flow parameters such as pressure drop, temperature and film thickness were recorded and analyzed at low liquid and moderate gas flow rates. Film thickness measurement was done using Planar Laser Induced Fluorescence (PLIF) technique.

Liquid film thickness in annular gas-liquid flow is of significant importance for mechanistic modeling of this flow regime. It is required for calculation of gas core diameter, distribution of dynamic interfacial roughness which affects interfacial shear and the pressure drop in annular two-phase flow. The current experimental study examined the variation of film thickness in annular air-water flow in one-inch vertical clear acrylic tube. Planar laser-induced fluorescence (PLIF) technique combined with high magnification imaging was used for visualisation of the liquid film. Average film thickness distribution was found to increase with increase of liquid flow rate and decrease with increase of gas flow rate.

Visualization of liquid film was performed in two steps. First, recording of flowing film was done with laser aligned with the center of the pipe at low liquid flow rates of 20, 25, 30 liters per hour. Second, laser position was moved away from pipe center closer to camera in order to reduce obstruction of imaging path by air bubbles at liquid flow rates from 20 to 60 liters per hour. The film thickness was obtained from digital images by converting them into binary images using threshold level. Correction number was acquired by comparing images from two setups at low liquid flow rates of 20, 25, 30 liters per hour.

Further calculations of liquid film thickness at higher liquid flow rates gave inconsistent results due to increasing concentration of air bubbles in liquid phase that made it challenging to distinguish liquid film edge.

Results were compared against mechanistic models of Hughmark (1973), Henstock and Hanratty (1976) and Ansari (1994) and experiments with similar geometry and conditions.

Acknowledgments

I would like to thank my supervisor, Dr. Ergun Kuru for his patience, support and guidance that he gave me throughout this research.

I would like to thank my co-supervisor Dr. Sina Ghaemi for his assistance and technical knowledge and support that he provided me during this study.

Special thanks to my colleagues Majid Bizhani, John Nichol and Todd Kinnee for their help with technical aspects of research.

I would like to thank my parents Sarkyt and Gulzhan for their unconditional love and support.

Special thanks to many of my friends, Aigerim Raimbay, Amin Jorati, Kais Ben Abdallah, Yevgenyi Zagaevskiy, Joshua Black and others.

No table of figures entries found.

Table of contents

ABSTRACT	
ACKNOWLEDGMENTS	
TABLE OF CONTENTS	
LIST OF TABLES	
LIST OF FIGURES	
NOMENCLATURE	
1.1 OVERVIEW	2
1.2 STATEMENT OF THE PROBLEM	2
1.3 OBJECTIVES AND TASKS.....	4
1.4 METHODOLOGY	4
1.5 CONTRIBUTIONS OF RESEARCH	5
1.6 STRUCTURE OF THE THESIS	6
2.1 MULTIPHASE FLOW IN TUBING OR PIPES.....	9
2.2 ANNULAR TWO-PHASE GAS-LIQUID FLOW	10
2.3 OVERVIEW OF MECHANISTIC MODELS	24
3.1 VERTICAL FLOW LOOP.....	32
3.2 MEASUREMENT TOOLS AND TECHNIQUES	34
3.2.1 LIQUID FLOW METER	34
3.2.2 MASS FLOW CONTROLLER FOR AIR	35
3.2.3 DIFFERENTIAL PRESSURE TRANSDUCER.....	36
3.2.4 ABSOLUTE PRESSURE TRANSDUCER.....	37
3.2.5 PURGING ABSOLUTE AND DIFFERENTIAL PRESSURE LINES	39
3.2.6 CALIBRATION OF DIFFERENTIAL PRESSURE AND ABSOLUTE PRESSURE TRANSDUCERS	39
3.3 PLANAR LASER INDUCED FLUORESCENCE (PLIF) COMPONENTS	41
3.3.1 TEST SECTION FOR PLIF SETUP	42
3.3.2 CAMERA	43
3.3.3 FILTER.....	47
3.3.4 LASER.....	47
3.3.5 SOFTWARE.....	48
3.3.6 FLUORESCENT DYE (RHODAMINE B).....	49

3.4 EXPERIMENTAL RUN	49
3.4.1 CALIBRATION	49
3.4.2 CALIBRATION PROCEDURE	52
3.4.3 CALIBRATION PROCEDURE IN DAVIS	53
3.4.4 EXPERIMENTAL PROCEDURE.....	56
3.5 FILM THICKNESS CALCULATION.....	57
4.1 PRESSURE DROP, ABSOLUTE PRESSURE AND TEMPERATURE.....	60
4.2 VISUAL OBSERVATION (ENTRAINMENT)	63
4.3 CORRECTION NUMBER.....	72
4.4 COMPARISON WITH THEORETICAL MODELS.....	80
4.5 COMPARISON WITH EXPERIMENTAL DATA FROM LITERATURE	85
4.6 SENSITIVITY ANALYSIS	94
5. CONCLUSION.....	98
5.1 RECOMMENDATIONS FOR FUTURE WORK	98
6. REFERENCES	99

List of tables

TABLE 3- 1: MAIN DESCRIPTION OF WATER ROTAMETER	35
TABLE 3- 2: DATA POINTS WITH PRESSURE VALUES FOR CALIBRATION OF TRANSDUCERS	40
TABLE 3-3: PRESSURE POINTS WITH CORRESPONDING VALUES IN SIGNAL EXPRESS	41
TABLE 3-4: TECHNICAL CHARACTERISTICS OF IMAGER INTENSE CAMERA	43
TABLE 3-5: GENERAL SYSTEM SPECIFICATIONS OF CAMERA	44
TABLE 3-6: CCD SENSOR.....	45
TABLE 3-7: CCD CONTROL AND A/D- CONVERTER	45
TABLE 3- 8: TECHNICAL SPECIFICATIONS OF LENS	46
TABLE 3-9: TECHNICAL SPECIFICATIONS OF LASER.....	48
TABLE 3- 10: SPECIFICATIONS OF CALIBRATION TARGET	50
TABLE 4-1: PRESSURE GRADIENT, ABSOLUTE PRESSURE AND TEMPERATURE VALUES FROM EXPERIMENT	61
TABLE 4-2: FILM THICKNESS VALUES OBTAINED WHEN LASER WAS IN THE CENTER OF TUBE	72
TABLE 4-3: FILM THICKNESS VALUES OBTAINED WHEN WITH LASER OFFSET	73
TABLE 4-4: CORRECTION NUMBERS	74
TABLE 4- 5: FILM THICKNESS VALUES OBTAINED AFTER CALCULATION WITH CORRECTION	77
TABLE 4-6: FILM THICKNESS VALUES (NOT CORRECTED) TO TEST REPEATABILITY OF EXPERIMENT (40 LPH OF LIQUID RATE).....	78

List of figures

FIGURE 1-1 GAS LIQUID FLOW REGIME MAP WITH REGION OF INVESTIGATED FLOW RATES.....	6
FIGURE 2-1 TWO PHASE FLOW REGIMES IN VERTICAL TUBING (A, B, C, D, E).....	10
FIGURE 2-2 SAMPLING PROBE DEVICE FROM ANDERSON AND MANTZOURANIS EXPERIMENT	12
FIGURE 2-3 TWO PHASE FLOW MAP WITH IMAGES OF FLOW REGIMES	13
FIGURE 2-4 IMAGES TAKEN WITH X-RAY (LEFT) AND FLASH PHOTOGRAPHY (RIGHT) FROM EXPERIMENT OF BENNET (1960).....	17
FIGURE 2-5 AXIAL VIEW OF ANNULAR TWO PHASE FLOW (HEWITT, 1969).....	18
FIGURE 2- 6 LFD METHOD FROM HAZUKU ET AL. (2005)	22
FIGURE 2-7 PROCESSED IMAGES FOR LIQUID FILM THICKNESS CALCULATION, ASHWOOD (2010)..	23
FIGURE 2-8 BASE FILM AND INTERFACIAL WAVES, RODRIGUEZ (2004)	23
FIGURE 3-1 SIMPLIFIED SCHEMATIC OF VERTICAL FLOW LOOP.....	33
FIGURE 3-2 WATER ROTAMETERS WITH DIFFERENT RANGES	34
FIGURE 3-3 AIR FLOW CONTROLLER	36
FIGURE 3-4 OMEGA PX2300-1DI DIFFERENTIAL PRESSURE TRANSDUCER.....	36
FIGURE 3-5 SCHEMATIC OF DIFFERENTIAL PRESSURE TRANSDUCER.....	37
FIGURE 3-6 PX419-2.5GI ABSOLUTE PRESSURE TRANSDUCER.....	37
FIGURE 3-7 NATIONAL INSTRUMENTS SIGNAL PROCESSING BOX.....	38
FIGURE 3-8 CALIBRATION GRAPH FOR SIGNAL EXPRESS	40
FIGURE 3-9 PLIF TEST SECTION.....	42
FIGURE 3-10 IMAGER INTENSE CAMERA	43
FIGURE 3-11 NIKON AF MICRO-NIKKOR 60 MM F/2.8D LENS	46
FIGURE 3-12 CAMERA AND LASER SETUP DURING CALIBRATION	47
FIGURE 3-13 RHODAMINE B	49
FIGURE 3-14 CALIBRATION TARGET	50
FIGURE 3-15 DIMENSIONS OF BASE OF CALIBRATION TARGET	51
FIGURE 3-16 CALIBRATION TARGET BASE WITH CALIBRATION GRID ATTACHED TO IT	52

FIGURE 3-17 TAKING IMAGE BEFORE RUNNING CALIBRATION IN DAVIS	52
FIGURE 3-18 UNMARKED IMAGE OF CALIBRATION GRID	53
FIGURE 3-19 COMPLETED CALIBRATION	54
FIGURE 3-20 CALIBRATION GRID AFTER CORRECTION (WORLD TO RAW)	55
FIGURE 3-21 RAW IMAGE (LEFT) AND IMAGE AFTER CONVERSION (RIGHT) GREYSCALE THRESHOLD VALUE (60)	58
FIGURE 4-1 RECORDED DIFFERENTIAL PRESSURE COMPARED AGAINST MODELS (20 LPH OF LIQUID RATE).....	62
FIGURE 4-2 RECORDED DIFFERENTIAL PRESSURE COMPARED AGAINST MODELS (40 LPH OF LIQUID RATE).....	62
FIGURE 4-3 500 AND 600 SLPM OF GAS RATE AT 20 LPH OF WATER RATE	63
FIGURE 4-4 900 AND 1200 SLPM OF GAS RATE AT 20 LPH OF LIQUID RATE	64
FIGURE 4-5 600 AND 900 SLPM OF GAS RATE AT 30 LPH OF LIQUID RATE	64
FIGURE 4-6 AT 1200 SLPM OF GAS RATE FROM LEFT TO RIGHT: 20, 30, 40, 50, AND 60 LPH OF WATER RATE	65
FIGURE 4-7 20 LPH OF LIQUID FLOW RATE AT AND 700, 1100 AND 1500 SLPM OF GAS FLOW RATES	65
FIGURE 4-8 IMAGES TAKEN WITH LASER OFFSET AT 20 LPH OF LIQUID FLOW RATE AND AT 700, 1100 AND 1500 SLPM OF GAS FLOW RATES	66
FIGURE 4-9 IMAGES TAKEN WITH HIGH SPEED CAMERA AT 30 LPH OF LIQUID FLOW RATE AND AT 700, 1100 AND 1500 SLPM OF GAS FLOW RATES	67
FIGURE 4-10 IMAGES TAKEN WITH HIGH SPEED CAMERA AT 40 LPH OF LIQUID FLOW RATE AND AT 900, 1100 AND 1300 SLPM OF GAS FLOW RATES	67
FIGURE 4-11 IMAGES TAKEN WITH LASER OFFSET AT 40 LPH OF LIQUID FLOW RATE AND AT 600, 900 AND 1200 SLPM OF GAS FLOW RATES	68
FIGURE 4-12 IMAGES TAKEN WITH HIGH SPEED CAMERA AT 60 LPH OF LIQUID FLOW RATE AND AT 800, 900 AND 1100 SLPM OF GAS FLOW RATES	69
FIGURE 4-13 IMAGES TAKEN WITH LASER OFFSET AT 60 LPH OF LIQUID FLOW RATE AND AT 600, 900 AND 1200 SLPM OF GAS FLOW RATES	69
FIGURE 4-14 FILM THICKNESS VARIATION DURING RECORDING.....	70

FIGURE 4-15 FILM THICKNESS VARIATION DURING RECORDING.....	71
FIGURE 4-16 CORRECTION NUMBER VALUES WITH FIT EQUATION.....	75
FIGURE 4-17 FILM THICKNESS VARIATION WITH NUMBER IMAGES AT 600 SLPM OF GAS RATE AND DIFFERENT LIQUID FLOW RATES	75
FIGURE 4-18 FILM THICKNESS VARIATION WITH NUMBER IMAGES AT 1200 SLPM OF GAS RATE AND DIFFERENT LIQUID FLOW RATES	76
FIGURE 4-19 FILM THICKNESS VALUES OBTAINED FROM EXPERIMENT.....	78
FIGURE 4-20 DATA OBTAINED FROM 3 DIFFERENT EXPERIMENTAL RUNS AT 40 LPH OF WATER RATE	79
FIGURE 4-21 COMPARISON OF EXPERIMENTAL RESULTS AT 20 LPH OF LIQUID RATE WITH THREE MODELS	80
FIGURE 4-22 COMPARISON OF EXPERIMENTAL RESULTS AT 25 LPH OF LIQUID RATE WITH THREE MODELS	80
FIGURE 4-23 COMPARISON OF EXPERIMENTAL RESULTS AT 30 LPH OF LIQUID RATE WITH THREE MODELS	81
FIGURE 4-24 COMPARISON OF EXPERIMENTAL RESULTS AT 35 LPH OF LIQUID RATE WITH THREE MODELS	81
FIGURE 4-25 COMPARISON OF EXPERIMENTAL RESULTS AT 40 LPH OF LIQUID RATE WITH THREE MODELS	82
FIGURE 4-26 COMPARISON OF EXPERIMENTAL RESULTS AT 45 LPH OF LIQUID RATE WITH THREE MODELS	82
FIGURE 4-27 COMPARISON OF EXPERIMENTAL RESULTS AT 50 LPH OF LIQUID RATE WITH THREE MODELS.....	83
FIGURE 4-28 COMPARISON OF EXPERIMENTAL RESULTS AT 55 LPH OF LIQUID RATE WITH THREE MODELS	83
FIGURE 4-29 COMPARISON OF EXPERIMENTAL RESULTS AT 60 LPH OF LIQUID RATE WITH THREE MODELS	84
FIGURE 4-30 COMPARISON OF CALCULATED FILM THICKNESS VALUES WITH EXPERIMENTAL DATA FROM LITERATURE, SCHUBRING (2009), TUBE ID=22.4 MM	85
FIGURE 4-31 COMPARISON OF CALCULATED FILM THICKNESS VALUES WITH EXPERIMENTAL DATA FROM LITERATURE, FUKANO, TUBE ID=26 MM.....	86

FIGURE 4-32 COMPARISON OF CALCULATED FILM THICKNESS VALUES WITH EXPERIMENTAL DATA FROM LITERATURE, WONGWISES (2001), TUBE ID=29 MM	87
FIGURE 4-33 COMPARISON OF CALCULATED FILM THICKNESS VALUES WITH EXPERIMENTAL DATA FROM LITERATURE, WOLF TUBE ID=31.8 MM.....	87
FIGURE 4-34 COMPARISON OF CALCULATED FILM THICKNESS VALUES WITH EXPERIMENTAL DATA FROM LITERATURE, WOLF TUBE ID=31.8 MM.....	88
FIGURE 4-35 COMPARISON OF CALCULATED FILM THICKNESS VALUES WITH EXPERIMENTAL DATA FROM LITERATURE, WOLF TUBE ID=31.8 MM.....	88
FIGURE 4-36 COMPARISON OF CALCULATED FILM THICKNESS VALUES WITH EXPERIMENTAL DATA FROM LITERATURE GILL, (1963), ID =31.75 MM	89
FIGURE 4-37 COMPARISON OF CALCULATED FILM THICKNESS VALUES WITH EXPERIMENTAL DATA FROM LITERATURE GILL, (1963), ID =31.75 MM	90
FIGURE 4-38 COMPARISON OF CALCULATED FILM THICKNESS VALUES WITH EXPERIMENTAL DATA FROM LITERATURE BELT, (2010), ID =50 MM.....	91
FIGURE 4-39 COMPARISON OF CALCULATED FILM THICKNESS VALUES WITH EXPERIMENTAL DATA FROM LITERATURE BELT, (2010), ID =50 MM.....	92
FIGURE 4-40 COMPARISON OF CALCULATED FILM THICKNESS VALUES WITH EXPERIMENTAL DATA FROM LITERATURE BELT, (2010), ID =50 MM.....	93
FIGURE 4-41 FILM THICKNESS VARIATION WITH PRESSURE DROP	94
FIGURE 4-42 PRESSURE VS FILM THICKNESS	94
FIGURE 4-43 FILM THICKNESS SENSITIVITY TO LIQUID REYNOLDS NUMBER	95
FIGURE 4-44 FILM THICKNESS VARIATION WITH GAS FLOW RATE	96

Nomenclature

A : cross-sectional area of the pipe m^2

A_c : cross-sectional area of the pipe m^2

τ_w : wall shear stress,

τ_i : interfacial shear stress

P : pressure Pa

L : length of test section m

g : acceleration due to gravity m/s^2

ρ_L : liquid density kg/m^3

ρ_G : gas density kg/m^3

R : pipe Radius m

D : pipe diameter m

D_c : core diameter m

U_G : gas velocity in core m/s

f : friction factor

δ : film thickness m

Re_L : liquid Reynolds number

U_{SL} : superficial liquid velocity m/s

U_{SG} : superficial gas velocity m/s

μ_L : dynamic liquid viscosity Pa*s

$y_L^+ = yu_i^*/\nu_L$

u_i^* : shear velocity $[(\tau_w + \tau_i)/2 \rho_L]^{1/2}$

ν_L : kinematic viscosity of liquid

$\alpha = W_E \rho_G / W_G \rho_L$: quantity of entrainment based on volumetric flow ratio

$$y_G^+ = y u_G^* / \nu_G$$

u_G^* : shear velocity $[(\tau_w + \tau_i)/2 \rho_G]^{1/2}$, where τ_i , τ_w interfacial and wall shear respectively

ν_G : kinematic viscosity of gas

ϕ : empirical parameter related to film thickness

$$F = \frac{\gamma (Re_{LF}) \nu_L}{Re_G^{0.9} \nu_G} \sqrt{\frac{\rho_L}{\rho_G}}: \text{dimensionless group containing flow rates and fluid properties}$$

X, X_{vt}, X_{tt} : Martinelli flow parameter

A_F : cross sectional area of the film

σ : interfacial tension between air and water dyne/cm

π_2 : Paleev and Fillipovich empirical parameter for estimation of entrainment

E : entrained fraction

S_W : wall perimeter m

S_i : interfacial perimeter m

A_F : cross sectional area of film m^2

α_C : void fraction of the core

f_i : interfacial friction factor

Re_c : core Reynolds number

U_c : core velocity

ρ_C :core density kg/m³

μ_c :core viscosity Pa*s

μ_G : gas viscosity Pa*s

Chapter 1

Introduction

Overview of the current state in research of annular gas-liquid flow is given in this section of the thesis. Statement of the problem, objectives and methodology of research are presented. The contributions of this experimental study and outline of thesis are given at the end.

1.1 Overview

Annular gas-liquid flow is one of the widely studied multiphase flow regimes. It is encountered in the oil and gas industry, in gas and gas condensate wells, and in many industrial heat transfer applications. Understanding the nature of pressure drop, affecting flow parameters are of significant importance for mechanistic modeling of this flow regime. Pressure gradient variations are often linked to changes in dynamic roughness of liquid film, interfacial features of the liquid film like ripple and disturbance waves and their frequency, entrainment rate of liquid droplets to the core, and the rate of mass transfer between core and film. Properties of phases such as density and viscosity also have considerable influence on pressure drop.

Comparing to other flow patterns annular flow regime is the least understood one. The importance is quite significant as almost all gas and gas condensate wells operate in annular flow regime. The main scope of numerous experiments was on investigating liquid film and entrained phase parameters and their effect on pressure drop.

Interfacial roughness is dynamic due to variation in liquid film thickness, film flow rate and frequency of different types of waves. Interfacial friction factor are often connected with film thickness when applied to predict pressure drop

1.2 Statement of the Problem

Annular two phase flow is one of the least understood flow patterns in the industry. Over the years there have been numerous studies of this flow regime with proposed models based on experiments. Annular two phase flow is the most common flow regime that is encountered in production of hydrocarbons in gas and gas-condensate wells. Annular two-phase flow is characterized by the presence of thin liquid film and gas core. Also, sometimes depending on the gas and liquid flow rates the liquid phase can be entrained in the gas core in forms of droplets.

Entrainment is caused by disturbance waves that cause inception of droplets to the gas core. When the critical flow rate of upward flowing gas is not able to lift the entrained droplets it causes the flow regime change and liquid starts accumulating in bottomhole, liquid starts to drain down and liquid loading occurs. It is commonly assumed that dispersed phase causes loading, when the minimum gas velocity is not sufficient to keep the largest droplet present in the gas core. It causes liquid loading and becomes an obstacle in production of gas.

Due to its complex nature annular two-phase flow is challenging for investigation. Understanding mechanisms that affect pressure drop, mass and heat transfer in this flow regime is crucial. Over the years a large number of experiments were performed on various factors as liquid film and entrained phase parameters in order to build proper pressure drop models. However, each technique has its limitations and models not always follow their pattern when compared to the obtained experimental data. Improvement in accuracy of techniques, changing operational conditions aim to create better annular flow maps and models

Over the years there have been many studies to measure parameters such as liquid film flow rate, liquid film thickness, entrained droplet size, disturbance wave frequency, and pressure drop and to develop proper models and predict those parameters. Entrained phase parameters were tested mainly with extraction of liquid film. Liquid film thickness is one of the parameters that were studied many times. The main technique that was used in these experimental investigations was conductance probe. Wire or flush mounted probe, calibrated to certain conductivity based on liquid film thickness, was installed in test sections of setups. Image based measurements techniques using high speed cameras and lasers were also used. Using this approach gives an opportunity to directly measure the film thickness and visualize liquid film thickness and observed the disturbance waves.

There is lack of high accuracy data in terms of investigating vertical annular two-phase flow. The main goal of current project is to determine liquid film thickness in fully developed annular flow in 1 inch tube by using PLIF technique.

The PLIF technique has numerous advantages over intrusive method like conductance probe when it comes to measuring liquid film thickness.

It is a non-intrusive method that allows direct visualization of the film with all its features such as ripple, disturbance waves and entrained air bubbles. The average liquid film thickness that is in most liquid and gas flow rates does not exceed 1 mm and most of the time in order of only several hundred microns presents a challenge for accurate measurement by methods such as conductance probe. Entrained air bubbles can create great difficulty in terms of receiving right conductance signal, hence providing good measurement accuracy. It does not allow to directly visualize the film.

1.3 Objectives and tasks

Ultimate goal is focused on investigation of annular flow particularly measuring pressure drop and film thickness. Overall experimental study of liquid film thickness and its behavior and variation with changing liquid and gas flow rates.

The thesis project consists of three parts:

- Experimental investigation of pressure drop variation within annular flow and comparing it with the existing pressure drop models and mapping region of interest onto annular flow map.
- Experimental investigation of film thickness and its behavior with implementation of modified PLIF technique and extensive study of film characteristics are main goals of this research
- Performing extensive analysis of film thickness values and comparing them with existing models and experimental results from literature.

1.4 Methodology

Methodology is based on using modified PLIF technique to visualize and record liquid film. It is carried out by.

- Measuring film thickness with the laser sheet passing through the center of the tube.
- Measuring film thickness with a laser offset and adjusting obtained values with correction factor.

1.5 Contributions of research

Current study of annular gas-liquid flow is focused on investigating liquid film thickness and its sensitivity to gas, liquid flow rates and pressure drop. Visual description and interpretation of images is also in the scope of this research. Particularly determining at which gas and liquid flow rates there is an entrainment of liquid droplets into core and entrainment of air bubbles into liquid film. New approach was used in order to calculate liquid film thickness. PLIF technique was used to record images of liquid film. Two different setup configurations were used for recording. First images were obtained with laser sheet in the center of the pipe and second, laser sheet was moved away from center closer to the camera in order to avoid obstruction caused by rough surface of the film and increasing air bubble concentration in the film. Research is motivated by lack of data being collected using direct film visualization technique such as PLIF at low liquid flow rates. Collected data compared to existing pressure drop models that incorporate film thickness as of its crucial parameters. Obtained images and results are useful for further study of this flow regime, specifically potential study of entrained droplet size and bubble concentration.

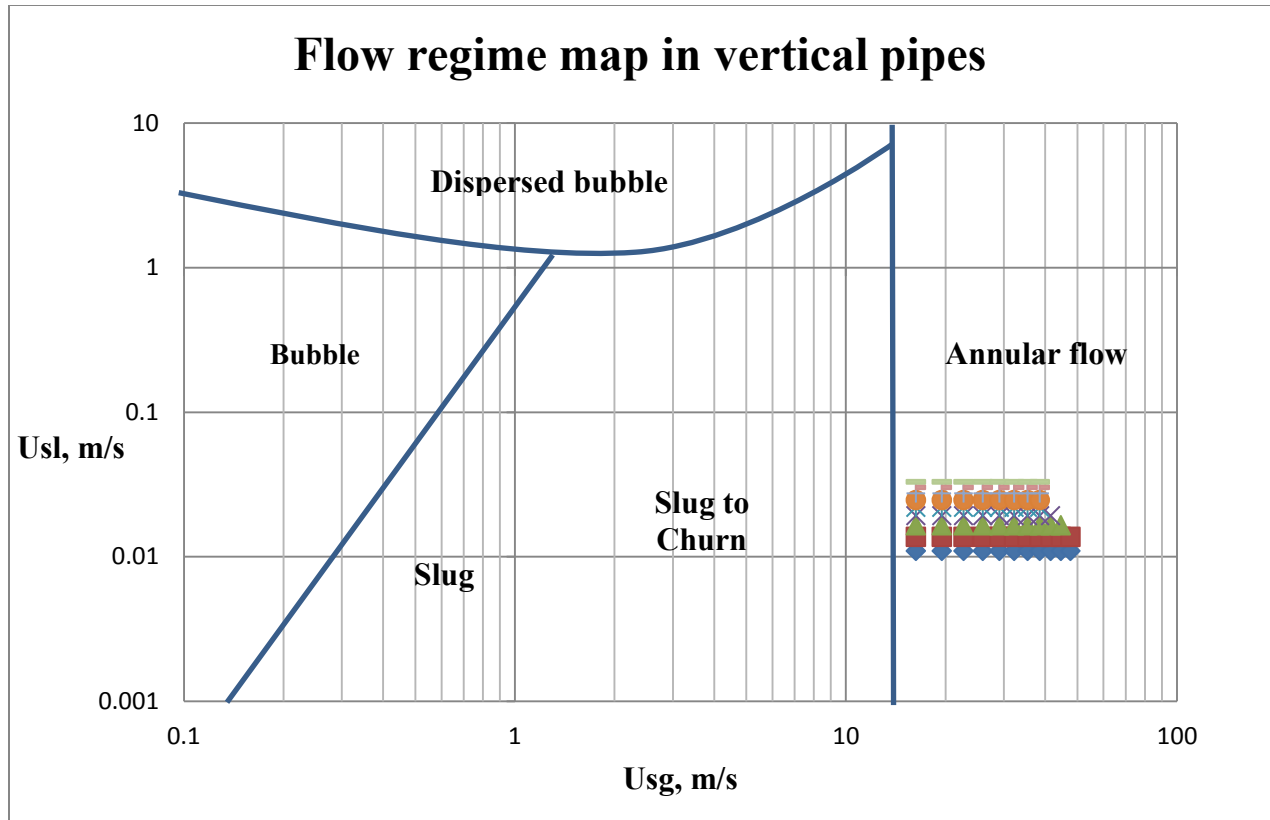


Figure 1-1 Gas liquid flow regime map with region of investigated flow rates

1.6 Structure of the Thesis

This Thesis is focused on investigating annular two-phase gas liquid flow by measurement of characteristics such as pressure gradient and film thickness.

Literature review of the background information is presented in the second chapter. It covers experimental and theoretical investigations of vertical annular gas-liquid flow. Multiphase flow is shortly covered in this section with following material dedicated to annular two phase flows studies. Towards the end of the chapter information on recent visual investigation methods is mentioned.

Chapter 3 covers experimental setup and procedure. It includes technical specifications of all instruments and calibration procedure.

Chapter 4 includes information on PLIF and its components. Calibration process prior recording and user inputs and settings in Davis software are explained in this part of the Thesis. This chapter also covers image acquisition procedure, image processing, and estimation of film thickness in Matlab.

Chapter 5 discusses results of PLIF experimental investigations. Results compared against several available empirical and semi-mechanistic models and experiments with similar conditions and geometry. Explanation of each mechanistic model is included. Sensitivity and error analysis are also given.

Chapter 6 includes conclusive information on the importance of the current experimental data and recommendations for further study of annular gas-liquid flow.

Chapter 2:
Literature Review and
Background

2.1 Multiphase flow in tubing or pipes

Multiphase flow is concurrent flow of materials at different phases or states. One of the most common multiphase flows is flow of gas with liquid. It is present in industrial heat exchangers, gas and gas condensate wells, chemical reactors, transport and pumping systems. Gas and liquid flow in tubing and flow lines is categorized based on liquid and gas rates. Whalley [1] studied and described flow patterns in vertical two-phase flow. The following flow regimes are present in tubing or pipes depending on feed rate of gas and liquid:

Bubbly flow or dispersed bubbly flow (Figure 2-1a):

This flow regime is described by presence of separate distorted gas spherical bubbles that flow in the liquid.

Slug or plug flow (Figure 2-1b):

This flow pattern is characterized by bullet shaped gas flowing upwards and thin liquid film flowing downwards. It is caused by coalescence of gas bubbles. Upward flowing gas creates bullet shaped gas pockets divided by bubbly flow liquid regions. These bullet shaped upward flowing gas are known as Taylor bubbles.

Churn flow (Figure 2-1c):

It is unstable gas-liquid flow regime where increased gas rate causes the liquid to oscillate but does not lift it completely in upward direction. Although it is similar to slug flow, churn flow being unstable have characteristic liquid motion. The regions of liquid between Taylor bubbles become narrower and get constantly broke down by increasing concentration of gas.

Annular flow (Figure 2-1d):

Annular flow is flow regime where gas flows in the core of the pipe or tube whereas liquid flows alongside as the thin film on the walls. Depending on gas and liquid flow rates the entrainment of liquid is present.

Annular flow regime itself can be divided into sub-regimes defined by gas and liquid flow rates that affect film thickness and its behavior, mass and heat exchange between gas and liquid phases. It will be discussed further in this work.

Wispy annular flow (Figure 2-1e):

In this flow regime increasing gas rate increases entrainment rate which causes the entrained liquid droplets to coalesce and form wisp like liquid streaks or lumps.

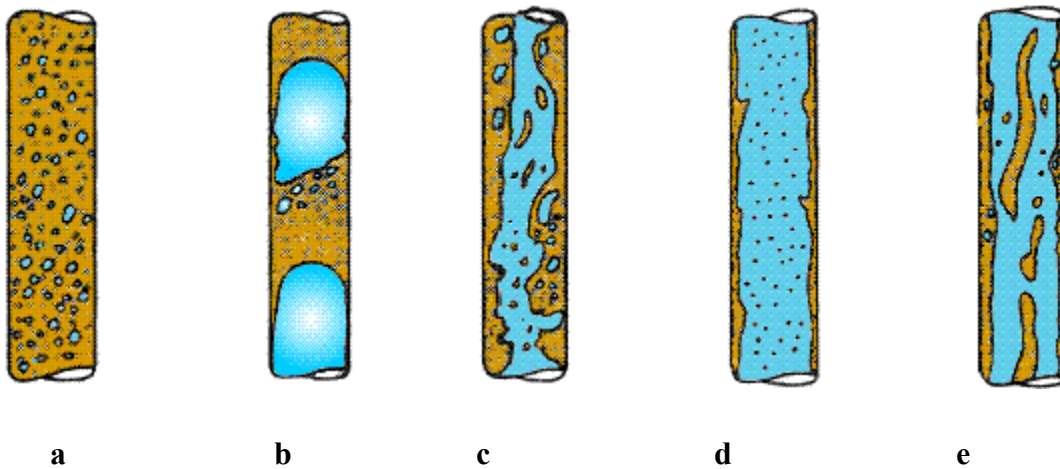


Figure 2-1 Two phase flow regimes in vertical tubing (a, b, c, d, e)

Retrieved from <http://thermopedia.com/content/2/>

2.2 Annular two-phase gas-liquid flow

One of the most important aspects of two-phase flow regime is pressure gradient. It is important to understand and predict its pressure drop in two-phase flow. Pressure gradient is affected by various factors such as pipe diameter, roughness of the tubing material, density and viscosity of liquid and gas phases, surface tension etc. Over the years there were numerous studies of annular two-phase flow regimes using various techniques which evolved with improvement of

technologies. Many researchers and their collaborators studied and experimentally investigated different factors that cause pressure drop or transition from one flow regime to another.

In horizontal and vertical annular two phase flow the following characteristics were studied.

Liquid film:

Film thickness, film flow rate, film velocity, film roughness, frequency of disturbance and ripple waves were studied and integrated into pressure drop models.

Entrainment:

Also many experiments were performed in order to investigate entrainment phenomena. Entrainment and deposition rate, size of entrained liquid droplets were examined and used to build proper mechanistic models for describing annular flow regime.

In addition, the effect diverse parameters (tubing size, length of development) and physical properties of phases (density, viscosity) were studied.

Chronological literature review of annular two-phase flow regime is presented. Many characteristics of this flow regime were experimentally investigated over the years and there were numerous proposed mechanistic models as attempts to describe transition and pressure drop using different variables as a function of proposed equations. Since in most of experiments several measurable parameters (pressure drop, film thickness, film flow rate, characteristics of liquid interfacial features, entrainment) were recorded, literature review is given in chronological order. The review shows the improvements and development in measuring techniques and progression in study of annular flow.

Anderson and Mantzouranis [2] studied annular two-phase flow in 0.5 inch glass tube and attempted to develop theory for pressure drop prediction. The experiment was performed using liquid and vapor and liquid hold-up and pressure drop were measured. In addition based on these experimental results and studying data from literature of the time the film thickness prediction was attempted and claimed to be in the margin of $\pm 15\%$. Also, proposed model allowed predicting the transition between slug and annular flow.

Based on the obtained data and proposed theory was found to be successful over the wide range of conditions within annular flow. Authors stated that presence of ripple waves in the film did not have significant effect on average film thickness. However, due to frictional pressure drop being linked to dynamic film roughness it was recommended that film thickness and effective roughness characteristics of film like ripple and disturbance waves needed to be thoroughly experimentally studied.

As the explanation for deviation of predicted values of film thickness the liquid entrainment phenomena was studied by Anderson and Mantzouranis [3]. Using the brass sampling probe (Figure) placed inside of the pipe where annular flow was simulated the samples of entrained droplets were collected and measured. In addition to that impact pressure of core mixture of gas and entrained liquid was recorded. Experiment showed 20 % reproducibility accuracy when it was repeated. It was found that proportion of entrained liquid in the gas core at high gas rates can be 40 % and higher. After introducing liquid entrainment correction factor the dimensionless film thickness results from previous study did not deviated substantially compared to initial results. No correlation model was build based on experimental data on entrainment.

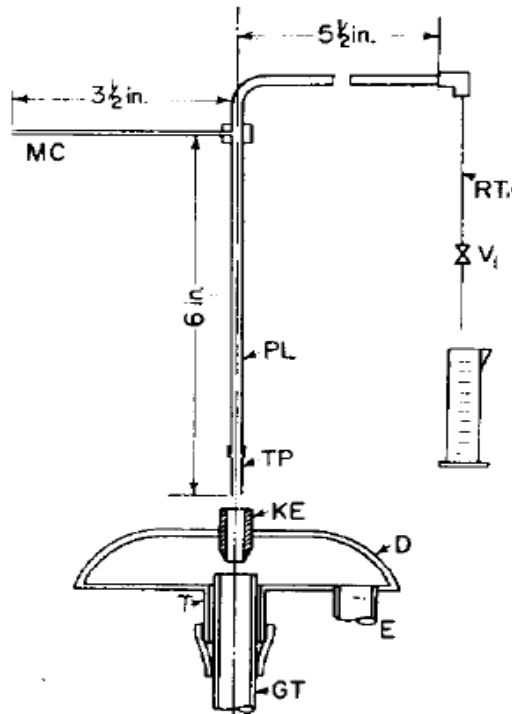


Figure 2-2 Sampling probe device from Anderson and Mantzouranis experiment [3]

The series of experimental studies were done by Govier and his collaborators. These investigations were aimed to study effect of various variables on pressure drop, hold-up and flow pattern. The effect of liquid and gas rates were studied by Govier, Radford and Dunn 4]. The experimental investigation was performed in 1.025 inch ID bore tube and regimes leading to annular film flow were identified. Regime III and IV precede annular film flow. Regime III described as froth flow. It is characterized with minimum motion between gas and liquid phases. With increasing gas flow rate it transitions to ripple wave regime. Ripple wave regime is short lived and described more as transitional state to annular film flow (Regime IV)

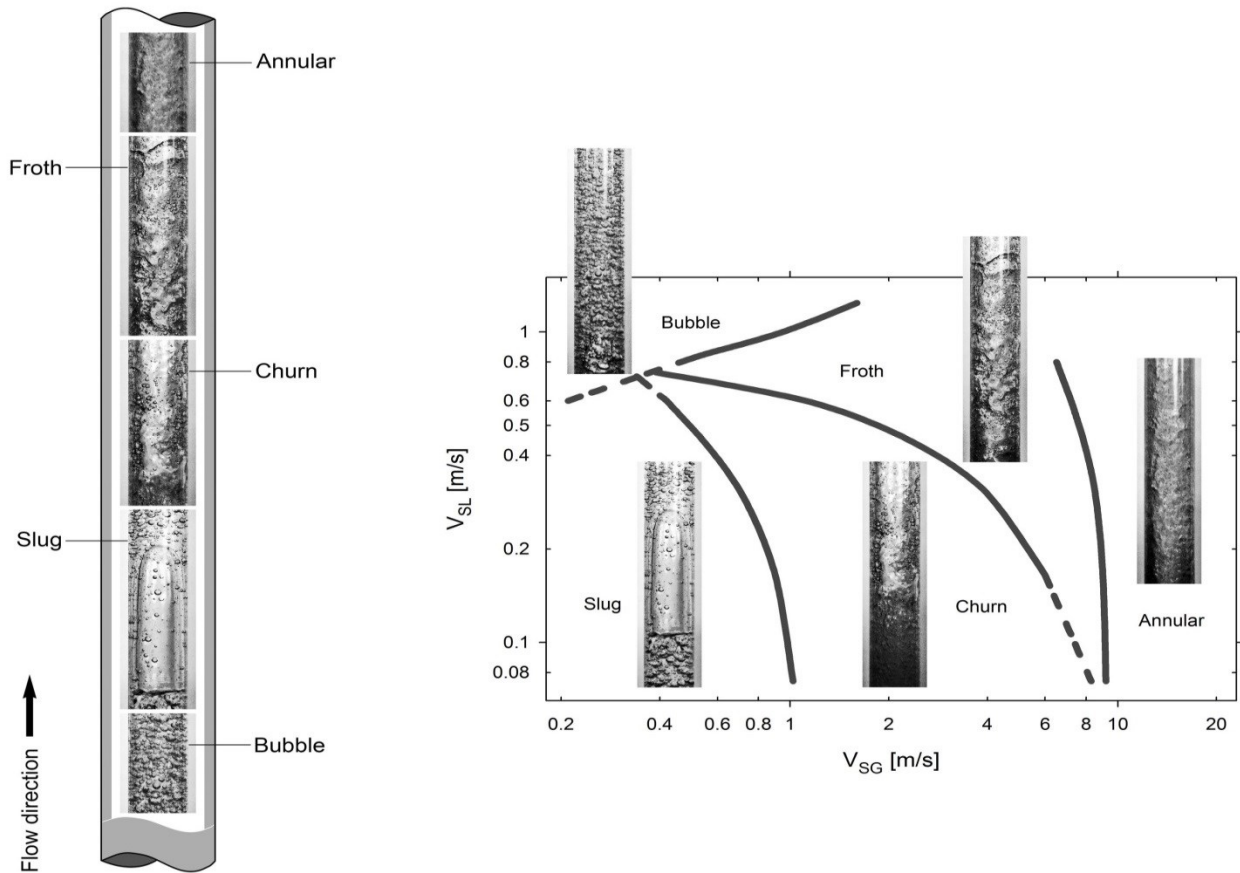


Figure 2-3 Two phase flow map with images of flow regimes

Retrieved from <http://hmf.enseeiht.fr/travaux/bei/beiep/book/export/html/1771>

Effect of tubing diameter was inspected by Govier and Leigh Short 5]. The diameter of used tubes ranged from 0.630 inch to 2.5 inch. It was found that tubing diameter has considerable

influence on boundary regions between slug to froth and froth to ripple, annular film flow regimes.

Brown, Sullivan and Govier [6] studied the effect of gas phase density on flow pattern, liquid hold up and pressure drop in vertical air-water flow. The experiment was done in 1.5 inch ID copper tube. The average air density was varied from 0.0015 gm/cc to 0.0088 gm/cc whereas superficial water velocities were between 0.02 m/s to 2.24 m/s.

Significant portion of studies on two-phase flow were done from 1960 to 1970. Authors like Hall Taylor, Dukler, Hewitt, Govier and Wallis did extensive studies of annular two-phase flow in both vertical and horizontal tubing. Numerous mechanistic pressure drop models were introduced that integrated different variables that were more extensively studied during this period. Numerous experiments with extensive research of film characteristics and entrainment were performed. One of them being study of Brown and Govier [7] where authors carried out experimental investigation of two-phase flow using high-speed photography in University of Alberta. The main focus of study was analysis of motion, shape and velocity of bubbles in bubbly and slug flow. Possibility of studying ripple, disturbance wave velocities and amplitude and periodic appearance of waves were discussed.

In work of Carter and Huntington [8] air-water flow was studied also by using high-speed camera alongside with measurements of pressure drop and in-place ratio of gas to liquid. This study was carried out in 2.125 inch ID and 20 feet long open vertical Tenite tube as well as in annulus of 0.9375 X 2.125 inches. The purpose was to compare the difference of pressure drop, in-place ration and motion of gas-liquid flow between annular and annuli flow.

Bennet and Thornton [9] performed experimental investigation of annular and dispersed flow in similar conditions to current study in 1.25 inch Perspex tube. Liquid rate was varied from 4.5 liters to 45 liters per hour and gas rate was varied from 580 LPM to 3500 LPM. Later Collier and Hewitt [10] did film thickness and entrainment analysis in same apparatus with extended liquid flow rate of up to 680 LPH. Film thickness measurements were obtained between 4.5 and 45 LPH due to technical limitations of conductance probe that was not able to get consistent results of film thickness larger than 250 microns. Establishment of relationship between parameters like

film thickness, film liquid flow rate and frictional pressure drop was attempted. Entrainment data was used for calculation of gas phase density and film flow rate.

Hall Taylor, Hewitt and Lacey [11] examined the function of disturbance wave in air-water annular two-phase flow. Disturbance wave appearing conditions were closely studied with measurements of wave velocity, distance between waves and their frequency. The role of disturbance wave as transporter of liquid was determined as the result of observation of increasing wave frequency with increasing water rate. The apparatus of experiment was similar to previous study of Bennet and Thornton (1961) and Collier and Hewitt (1961). From the experiment, annular flow was classified under for four sub regimes:

- Non-wetting region, when water does not wet the whole internal surface of the tube. This regime was observed at very low flow rates of water of less than 16 LPH in current experiment.
- Region of ripple waves only, when only ripple waves appear in the film.
- The disturbance wave region. These waves are superimposed in the film and appear in complete developed form in fully developed flow section and become stable.
- Also intermediate region between ripple and disturbance wave region was observed where waves are not of constant frequency but appear in pulses. It might have been related to oscillation in the system or type of air injection system.

In this study alongside with conductance probe method cine film visual method was used. This was done in order to record and observe the position of large waves and see their separation. Numerous separation patterns were observed and classified.

Later similar experiment with different apparatus and wider range of variables was carried out by Nedderman and Shearer [12]. The frequency of waves was found to be dependent on length of development section. However, wave velocities were found to be similar to the values in the work of Hall Taylor indicating that they don't depend on geometry of apparatus. Occurrence of disturbance waves indicates transition of single phase flow from laminar to turbulent.

It is important to note the experimental work of Gill et al. [13]. It is traversing probe studies of annular two-phase flow in 1.25 inch ID and 20 feet long bore acrylic tube focused on examining the effect of length on phase and velocity distribution. Using 0.062 inch ID pitot-type traversing

probe the impact pressure of gas core and entrained liquid phase was measured at 175000 LPH of air rate and 453 LPH of water rate at different locations along the tube. Along the tube number of flush mount resistance probes was installed in order to measure film thickness at different locations from inlet. Small amount of sodium chloride was mixed with water for film thickness measuring purposes. The results of experimental work indicated that velocity profile of gas phase changes from flat topped form to sharp peaked from which indicated that dynamic roughness of liquid reduces velocity of gas core. The film thickness data varied from 500 microns at short distance from inlet to around 320 microns at 20 feet distance from inlet where fully developed annular flow was achieved. Usage of longer tube was suggested in order to study effect of length on various parameters.

Later on the same apparatus the effects of phase flow rates on phase and velocity distribution was investigated by Gill [14]. As in previous study film thickness and pressure drop data was obtained where range of air rate was varied from 35 m³/h to 245 m³/h and water flow rate from 14 LPH to 570 LPH. Film thickness varied from 75 microns to around 760 microns at lowest gas rate and highest liquid rate. Based on the results of work it was concluded that liquid mass velocity cannot be assumed to be constant across the tube at given liquid and gas rates.

New approaches of flow visualization were used by Bennett [15]. Previous known technique of high-speed cine photography alongside with x-ray was applied to investigate and examine steam-water flow patterns in 0.497 inch ID Pyrex tube at absolute pressures of 3500 and 6900 kPa with wide range of mass velocities. X-ray was used to investigate the flow regimes in in test section made from titanium and allowed to detect new flow regime previously described as “wispy annular flow” that was detected at high mass velocities. One of the advantages of x-ray method is that it allows visualizing two-phase flow in non-transparent materials like metals. In addition to that using x-ray allowed visualizing agglomerated entrainments in wispy annular flow regime comparing to flash photography.

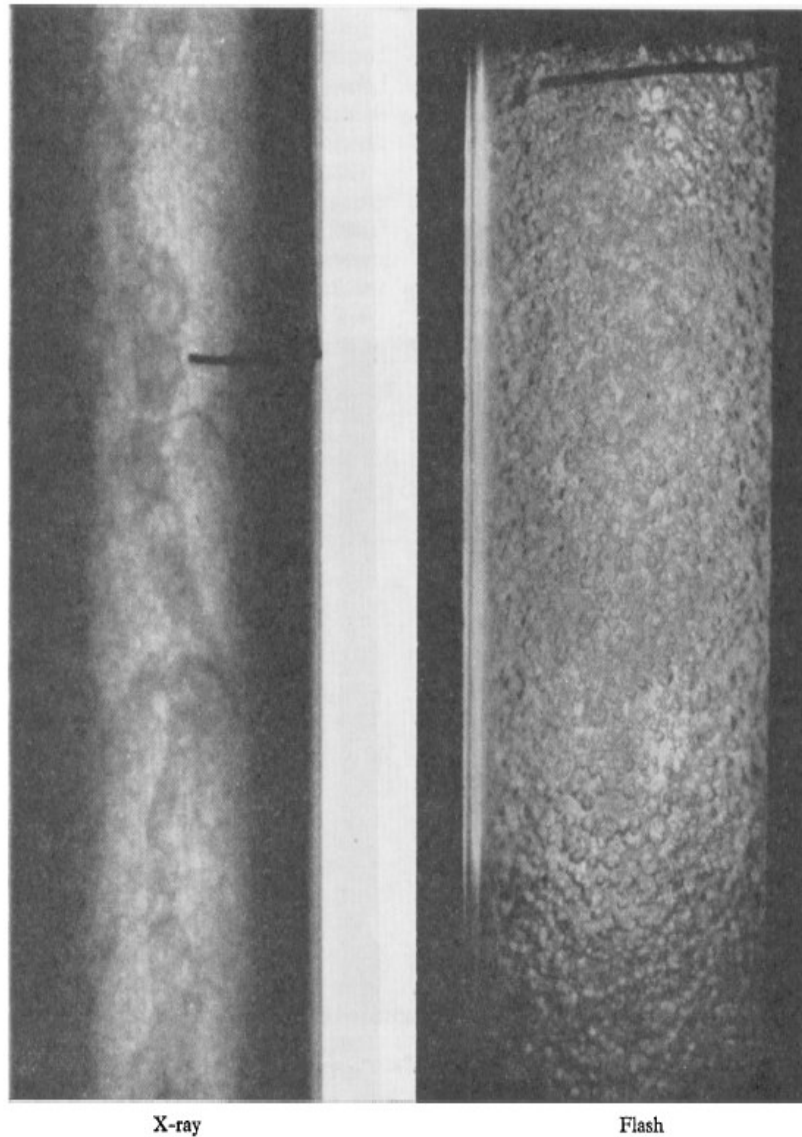


Figure 2-4 Images taken with X-ray (left) and Flash Photography (right) from experiment of Bennet [15]

Also, Chien [16] performed visual studies of falling film and film in vertical downward annular flow using high speed photography.

The subject matter of experimental work of Hall Taylor and Nedderman [17] was examination of coalescence disturbance waves in annular two-phase flow in 1 inch glass tube. The frequency and velocity of disturbance waves was measured using conductance probe at the close distance to inlet and cine film technique was used for flow visualization at fully developed regions. By studying behavior of disturbance waves and measuring mentioned above parameters it was

concluded that film can be divided into three regions. Wave formation region, where waves are formed typically close to injector. It is followed by wave coalescence region and quasi-steady state region where there is minimum coalescence of wave as they are sufficiently distanced from each other.

In the later work of Hewitt [18] liquid film was investigated by new methods such as fluorescent technique for thickness measurements and film velocity measurements using optical-mechanical stroboscopic device. Using the fluorescent technique allowed measuring true local wave amplitude in the film that was previously averaged out over the distance of approximately 0.5 inches. In addition, axial flow visualization was done by installing flat viewing window on the top of the tube. Experimental data showed that wave frequency and velocity was independent of travelled distance and it gave reason to assume that there is equilibrium between entrainment and deposition of droplet rate.

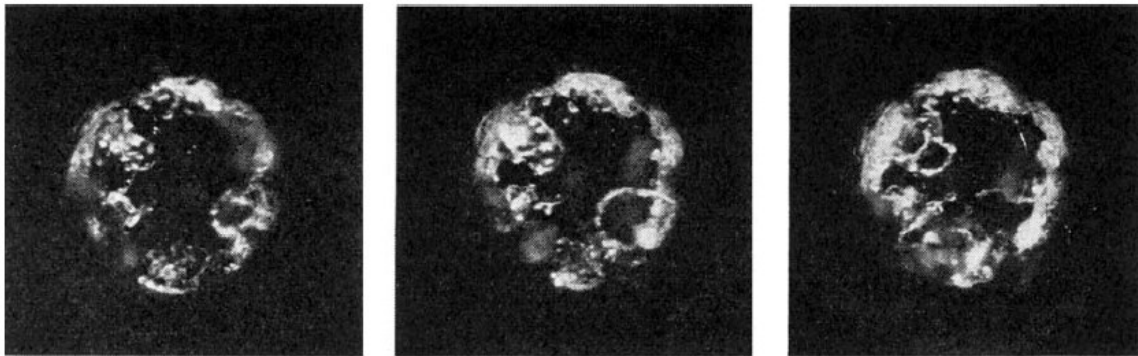


Figure 2-5 Axial view of annular two phase flow (Hewitt [18])

Investigation of annular two phase gas-liquid flow was carried out in 1 inch I.D. acrylic tube in series of experiments performed by Jagota and his collaborators. Interchange and entrainment was studied using tracer measurement technique [19]. Steady injection of tracer (5 % sodium chloride solution) allowed obtaining satisfactory values of these two parameters. Results obtained from this experiment showed that when boundary conditions of model are met interchange and entrainment can be modeled by assuming two homogeneous flows of liquid.

Same approach was used for measuring film and droplet velocities in annular flow [20]. Film thickness was also measured. One of the main difficulties of using conductance probe in measuring film thickness was the size of probe that should be smaller than measured thickness.

As the result of that conductance probe measurement was restricted by certain range of liquid flow rates. Stainless steel sleeve with the probe was used to measure the amount of tracer in the core. Steady constant injection of tracer was necessary as sudden pulses did not give reasonable results.

Lopes and Duckler [21] investigated entrainment phenomena in vertical annular flow and its effects on momentum transfer. Work was motivated for developing better correlation that accounted pressure drop not only for rough surface of the flowing film but for transfer rates of liquid between film and gas core. Experiment was carried out in 50.74 mm Plexiglas tube using air and water. Three quartz rods were installed at different radial positions in order to measure the droplet size. Axial and radial velocities of droplets were also measured.

In the work of Hewitt [22], the influence of liquid injector type on annular two-phase flow was studied. Porous and central jet injector effects were tested in 31.75 mm ID acrylic resin pipe. Parameters such pressure gradient, liquid mass flux, impact pressure and velocity alongside with film thickness were measured at different distances from injector. Jet injection gave much higher entrainment values hence lower liquid film thickness whereas porous injector caused higher liquid film thickness hence higher pressure drop values.

In the research of Jepson [23] examination of effect of gas phase properties on droplets was carried out in 10.26 mm ID stainless steel vertical tube. Helium and air were two gas phases used for comparison. Laser diffraction technique was used for droplet size measurements. Each one of the 30 photosensitive detector elements was related to certain droplet size range. By detecting angular distribution of scattered light (caused by Fraunhofer diffraction of parallel beam of monochromatic light) from droplets the size of them were determined. Detailed description of apparatus can be found in the source. Film flow rate and deposition of droplets were determined by extracting liquid through porous section of the wall. Porous wall of the tube was used for measuring the rate of liquid withdrawal for finding film flow rate. Remaining deposition of liquid flow was measured in upper section of the tube to find deposition rate. As the results of experiments indicated droplet size decreased with increasing gas phase superficial velocity. It was visually confirmed by current experiment in vertical flow loop. Gas with lower density causes less entrainment which can be explained by lower shear stress. Observations of Azzopardi et al, (1983) regarding the relating droplet size to entrainment mechanism was discussed in this

work. Two liquid breakup types of causes different size distribution of droplets. Bag break up at low liquid flow rates produces larger droplets whereas ligament break up at higher liquid flow rates causes entrainment of smaller droplets. Both breakup mechanisms assumed to be present in the flow. As the droplet concentration increases smaller droplets coalesce which causes an increase in the size of droplets.

In the work of Wolf, Jayanati and Hewitt [24], the nature of ephemeral waves were studied in annular flow regime. Alongside with flow visualization, film thickness measurements were carried out in 31.8 ID tube. Section made from fluorinated ethylene propylene was used for flow visualization. Images were obtained using high frame rate video camera and stroboscopic light. Based on results of visualization it was determined that ephemeral waves are present before occurrence of disturbance waves which is below liquid Reynolds number of 500. They are similar to disturbance waves but move much more slowly and with increasing liquid flow rate they are overtaken by disturbance waves.

One of the important works to be noted in this field is studying flow development in vertical annular flow by Wolf [25]. Values of pressure gradient, film thickness, wall shear stress disturbance wave velocity and frequency were obtained at different axial distances from inlet. Experiments were carried out in 31.8 mm ID and 10.8 m long copper pipe. Based on the experiments it was concluded that most of flowing interfacial features of flowing film and its parameters such as wave spectrum, disturbance wave velocity and its frequency did not vary much at distances from the inlet in order of 100-300 diameters. However, pressure gradient, film thickness and film flow rate varied considerably from at different distances from inlet depending on water and gas flow rate. At lower gas flow rates variation in film flow rate and film thickness persisted from 100 to 300 diameter distances from inlet. At highest gas flow rates their value stabilized. Although parameters such as pressure gradient, shear stress, film flow rate and film thickness showed variation at different distances, order of 100 and more diameters is considered enough as they respond slowly to the distance from inlet.

Liquid viscosity affects shear stress and pressure drop. This parameter was tested with different liquids by Fukano [26]. Different concentrations of water and glycerol were used to test variation in average liquid film thickness, wave height and interfacial stress between gas and liquid in 26

mm ID acrylic resin tube. Four solutions with different viscosities were tested and these conclusions were reported:

Liquid viscosity has significant influence on interfacial structure of the film. Liquid film thickness increased with increased viscosity whereas interfacial friction factor decreased. Pressure drop decreased with increased viscosity.

In the article by Nakazatomi [27] experiment on entrainment were done at range of pressures between 0.3 MPa to 20 MPa. While most of the models that were used were able to predict with considerable accuracy the low pressure results, at higher pressure greater than 7 Mpa they were not able to provide reasonably accurate results.

The influence of film structure, specifically wave height on interfacial friction was studied in the work of Wang [28] at normal and microgravity conditions. Dynamic interaction between two phases is vital and directly affects pressure drop. Investigation was carried out in order to observe the effect of gravity on interfacial structures during interaction of gas and liquid phases and its effect on pressure drop in 9.525 mm ID tube. Interfacial roughness decreased with increasing gas flow rate and at microgravity condition roughness was less than half of normal gravity values. Interfacial friction factor increased with increasing interfacial roughness and decreased with increasing gas Reynolds number. Interfacial shear stress in microgravity was close and in some cases larger than in normal gravity. It was linked to main causes which are slightly higher friction factor in microgravity and higher gas velocity in microgravity.

With wide range of experiments being done using conductance probes to measure liquid film interfacial structures and film thickness researchers started using more advanced visual measurement techniques to characterize liquid film. For instance Laser focus displacement meter (LFD) method was used to measure interfacial wave structures in vertical annular two phase flow and test these structures at different axial locations from inlet to see the development of liquid film in 11 mm ID and 3 m long acrylic pipe [29]. LFD method was capable of accurately recording momentary changes in liquid film structure. As the results of experiment indicated, the frequency of disturbance waves and film thickness decreased with axial development of the flow and remained in this pattern until exit given an implication that flow might never reach fully developed stable state.

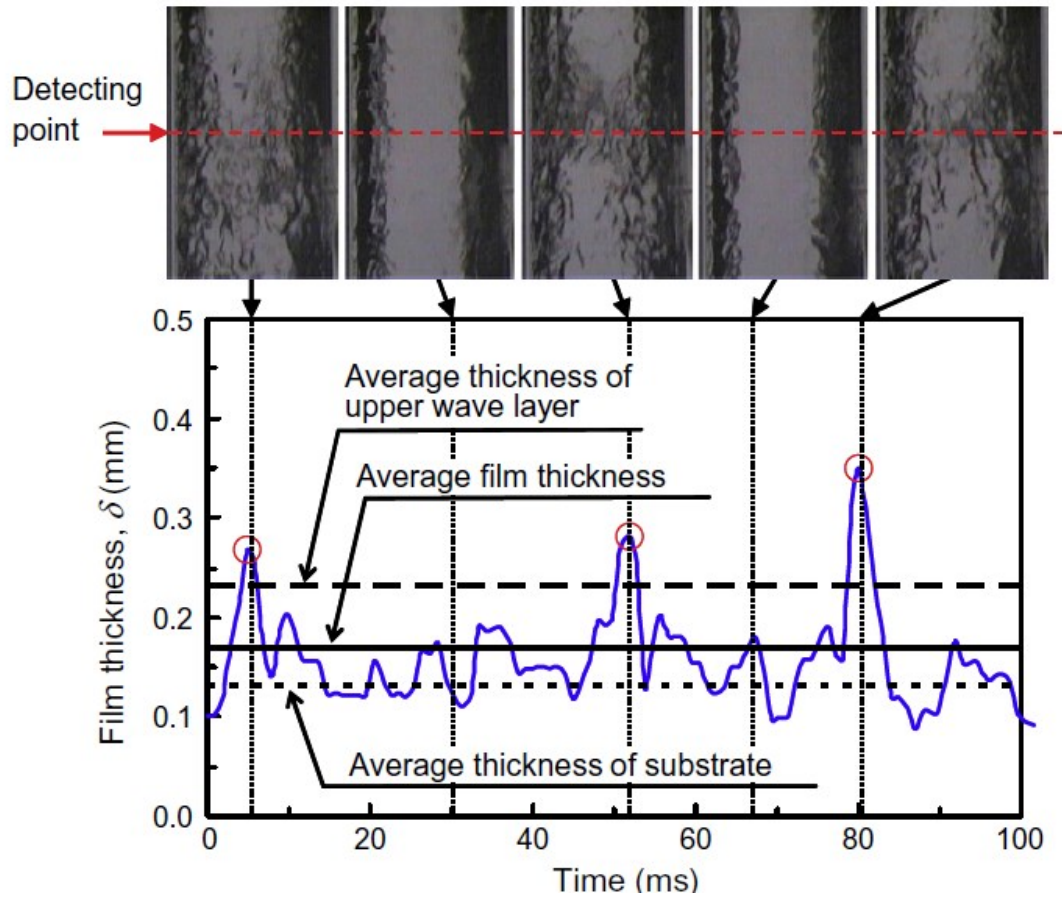


Figure 2-6 LFD method from Hazuku [29]

Total internal reflection technique developed by Shedd and Newell (1998) used for film thickness measurements (base film) was used by Ashwood [30] for liquid film roughness measurements. Planar laser induced fluorescence was also applied to measure film roughness in 22.4 mm ID FEP test section. These two optical approaches gave reasonably accurate in terms of measuring base film thickness and film roughness. Roughness distribution was well represented by standard deviation of the film thickness meaning that smooth film will be like smaller diameter pipe.

Similar approach (PLIF) was used by Shedd and Rodriguez [31] for investigation of annular flow in horizontal pipe. Cross sectional imaging was performed in 15.1 mm ID FEP tube. Technique allowed visualizing liquid film with as close as 10 microns from the tube wall. Based on

experiment it was concluded that size and shape of waves are dependent on gas flow rate, whereas an increase in frequency of waves is linked to increasing liquid flow rate.

Using flush mount conductance probes are one of the non-intrusive methods for measuring film thickness and interfacial structures. This particular approach was applied by Belt [32]. 32 probes with 6 mm spacing between each other around circumference of the 50 mm ID pipe were installed at 10 different axial locations. Although technique does not capture film features smaller than 6 mm in length, it allows measuring and characterizing large structures like disturbance waves and inconsistent height fluctuations. It was found that length of disturbance waves approximately equal to pipe diameter.

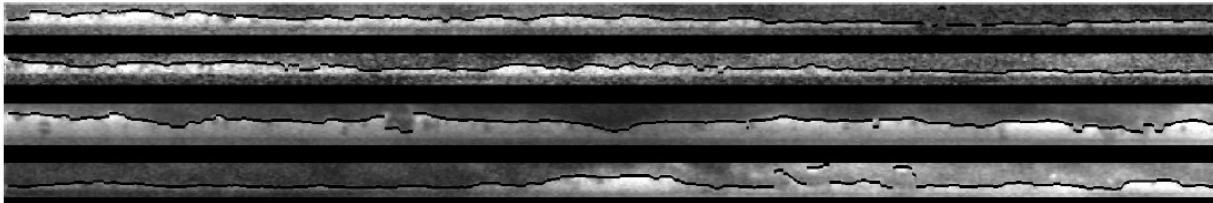


Figure 2-7 Processed images for liquid film thickness calculation, Ashwood [30]

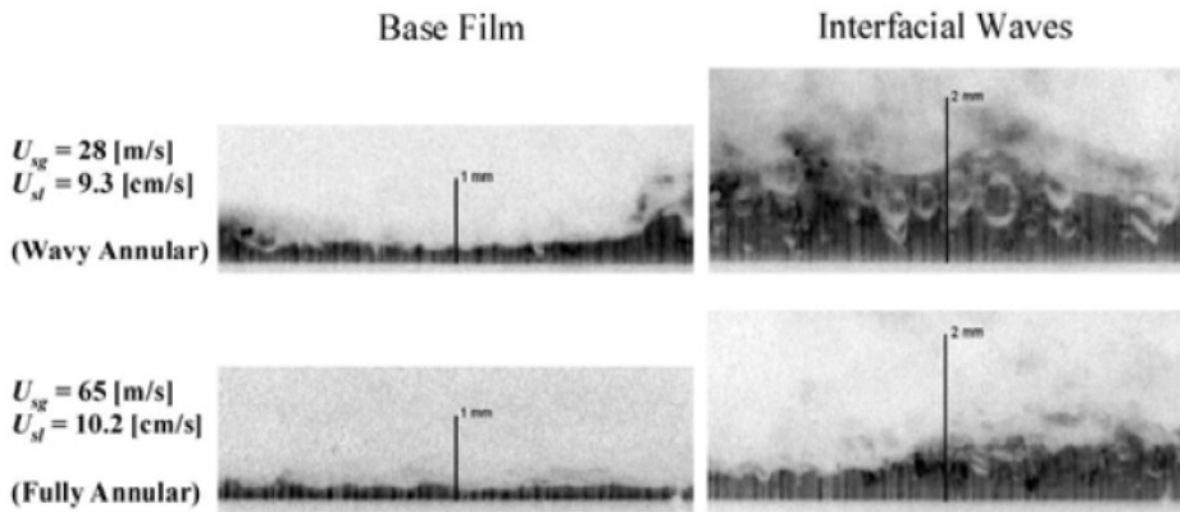


Figure 2-8 Base film and interfacial waves, Rodriguez [31]

2.3 Overview of mechanistic models

There various models of predicting pressure drop and film thickness. One of them is Hughmark [33] model for predicting pressure drop, film thickness and entrainment. Given inputs are water flow rate and gas flow rate. With measuring instruments differential pressure, absolute pressure and temperature were recorded. Volumetric gas flow rate is recorded in unites of SLPM and it needs to be converted to LPM. Standard conditions were set at 14.696 psi and 288.15 K. In order to convert it next formula is used:

The wall and interfacial shear stresses are represented by:

$$\tau_w = \left[\left(-\frac{dP}{dL} \right) - g\rho_L \left(1 - \frac{a^2}{R^2} \right) - g\rho_G \frac{a^2}{R^2} \right] \frac{R}{2} \quad (1)$$

$$\tau_i = \left[\left(-\frac{dP}{dL} \right) - g\rho_G \right] \frac{a}{2} \quad (2)$$

Relationship between friction factor and pressure gradient is described by:

$$f = \frac{dP/dL D_c}{2U_G^2 \rho_G} \quad (3)$$

L - length of the test section where pressure drop is recorded,

D_c – core diameter

U_G - gas velocity in core

Friction factor is given by:

$$f = 0.005 \left(1 + 149 \frac{\delta}{R} \right) \quad (4)$$

δ – film thickness,

R – radius of the pipe,

Based on various experimental data of previous works Hughmark developed empirical fit correlation:

With given inputs liquid film Reynolds needs to be known:

$$Re_L = \frac{\rho_L v_L D_H}{\mu_L} \quad (5)$$

Where ρ_L is density of water assumed to be constant $\rho_L=1000 \text{ kg/m}^3$,

v_L - mean liquid velocity in m/s equal to superficial liquid velocity:

$$U_{SL} = \frac{Q_L}{A} \quad (6)$$

Q_L is volumetric flow rate of liquid and A is cross sectional area of the pipe:

$$A = \pi \left(\frac{D_P}{2}\right)^2 \quad (7)$$

D_P -pipe diameter equal to hydraulic diameter D_H

In order to find dynamic viscosity of water μ_L inputs of temperature are needed. Recorded temperature needs to be converted from Celsius to Fahrenheit as it is used for calculation of liquid dynamic viscosity:

$$^{\circ}F < \frac{9}{5}T(^{\circ}C) + 32 \quad (8)$$

Dynamic viscosity of liquid phase in cp is given by:

$$\mu_L = e^{[1.003-0.01479T(degF)+0.00001982T(degF)^2]} \quad (9)$$

Based on calculated Re_L one of three correlations for y_L^+ is selected:

$$2 < Re_L < 100, \quad y_L^+ = 0.66 (Re_L)^{0.53}$$

$$100 < Re_L < 1000, \quad y_L^+ = 0.347 (Re_L)^{2/3} \quad (10)$$

$$1000 < Re_L, \quad y_L^+ = 0.13 (Re_L)^{0.81}$$

Where y_L^+ is described as:

$$y_L^+ = y u_i^* / \nu_L$$

u_i^* - shear velocity $[(\tau_w + \tau_i) / 2 \rho_L]^{1/2}$, where τ_i , τ_w interfacial and wall shear respectively

ν_L - kinematic viscosity of liquid

Furthermore model provides quantity of entrainment α given by volumetric flow ratio:

$$\alpha = W_E \rho_G / W_G \rho_L \quad (11)$$

Where, W_E , W_G are mass flow rate of entrainment and gas

Air density ρ_G depends on absolute pressure and temperature in the core

$$\rho_G = \frac{P_{abs}}{R_{air} T} \quad (12)$$

Where, absolute pressure is calculated by:

$$P_{abs} = P_a + P_{measured} \quad (13)$$

P_a and $P_{measured}$ are atmospheric pressure and pressure measured in test section respectively,

$R_{air} = 287.058 \text{ J/kgK}$ specific gas constant for dry air

Empirical correlations for α are:

$$y_G^+ < 36, \quad \alpha = 0$$

$$36 < y_G^+ < 42, \quad \alpha = -0.000442 + 0.000013 y_G^+$$

$$42 < y_G^+ < 60, \quad \alpha = -0.000625 + 0.0000172 y_G^+ \quad (14)$$

$$60 < y_G^+, \quad \alpha = 5 * 10^{-8} (y_G^+)^{2.2}$$

Where,

$$y_G^+ = y u_G^* / \nu_G$$

u_G^* - shear velocity $[(\tau_w + \tau_i) / 2 \rho_G]^{1/2}$, where τ_i , τ_w interfacial and wall shear respectively

ν_G - kinematic viscosity of gas

Relationship between y_G^+ and y_L^+ is given by:

$$y_G^+ = (\rho_G/\rho_L)^{1/2}(\mu_L/\mu_G) y_L^+ \quad (15)$$

$$\frac{y}{R} \frac{(f/R)^{1/2}}{(1-2y/R)(1-y/R)^{1/2}} = \frac{y_L^+ \mu_L}{RU_{SG}(\rho_G \rho_L)^{1/2}} = \phi \quad (16)$$

$$\phi < 0.00069, \quad \frac{y}{R} = 3.85 \phi^{0.815}$$

$$0.00069 < \phi < 0.0057, \quad \frac{y}{R} = 1.18 \phi^{0.655} \quad (17)$$

$$0.0057 < \phi, \quad \frac{y}{R} = 0.78 \phi^{0.577}$$

$$y = \phi R$$

In mechanistic model of Henstock and Hanratty [34], film thickness over tube diameter related to dimensionless group F ,

$$\frac{m}{d_t} = \frac{6.59F}{(1+1400F)^{1/2}} \quad (18)$$

Where F is

$$F = \frac{\gamma(Re_{LF})}{Re_G^{0.9}} \frac{\nu_L}{\nu_G} \sqrt{\frac{\rho_L}{\rho_G}} \quad (19)$$

To find F , Martinelli flow parameter needs to be known,

For $Re_L < 1000$ $Re_G > 1000$

$$X = X_{vt} = 16.9 \left(\frac{\mu_L}{\mu_G}\right)^{0.5} \left(\frac{\rho_G}{\rho_L}\right)^{0.5} \left(\frac{W_L}{W_G}\right)^{0.5} Re_G^{-0.4} \quad (20)$$

For $Re_L > 1000$ $Re_G > 1000$

$$X = X_{tt} = \left(\frac{\mu_L}{\mu_G}\right)^{0.1} \left(\frac{\rho_G}{\rho_L}\right)^{0.5} \left(\frac{W_L}{W_G}\right)^{0.9} \quad (21)$$

Then relations below are obtained

For $Re_L < 1000$ $Re_G > 1000$

$$F = 0.0379X_{vt} \quad (22)$$

For $Re_L > 1000$ $Re_G > 1000$

$$F = 0.0379X_{tt} \quad (23)$$

Ansari's [35] mechanistic model is based on that pressure gradient for core and liquid film is same.

$$\left(\frac{dP}{dL}\right)_F = \tau_W \frac{S_W}{A_F} - \tau_i \frac{S_i}{A_F} + \rho_L g \sin\beta \quad (24)$$

$$\left(\frac{dP}{dL}\right)_C = \tau_i \frac{S_i}{A_c} + \rho_c g \sin\beta \quad (25)$$

$$\left(\frac{dP}{dL}\right)_C = \left(\frac{dP}{dL}\right)_F \quad (26)$$

All the parameters that are necessary for calculation of pressure drop are dependent on film thickness. By adjusting film thickness two pressure drop are equalized and pressure drop for given liquid and gas flow rate is calculated.

First interfacial tension between air and water is calculated from:

$$\sigma = \frac{(52.5 - 0.006P(\text{psi})) + (280 - T(^{\circ}F))}{206(76 \exp(-0.00025P(\text{psi})) - 52.5 - 0.006P(\text{psi}))} \quad (27)$$

Entrainment is calculated from Paleev and Fillipovich empirical correlation that gives a fraction of entrained liquid:

$$\pi_2 = U_{SG} \frac{\mu_G}{\sigma} \left(\frac{\rho_G}{\rho_L} \right)^{0.5} \quad (28)$$

$$E = \frac{100 - 121e^{-1229\pi_2}}{100} \quad (29)$$

Wall perimeter and interfacial (where film assumed as circle inside of the tube) perimeters are given by:

$$S_W = \pi D \quad (7)$$

$$S_i = \pi(D - 2\delta) \quad (8)$$

Cross sectional area of liquid film A_F and core A_C given by:

$$A_F = \pi D \delta - \pi \delta^2 \quad (30)$$

$$A_C = \frac{\pi(D-2\delta)^2}{4} \quad (31)$$

Void fraction of the core is given by:

$$\alpha_C = \frac{U_{SG}}{U_{SG} + U_{SLE}} \quad (32)$$

Shear stress that acts against the wall is given by:

$$\tau_W = f_m \frac{\rho_L U_F^2}{8} \quad (33)$$

$$U_f = U_{SL} \frac{(1-E)D^2}{4\delta(D-\delta)} \quad (34)$$

Friction factor f_m is calculated from Blasius correlation:

When $Re < 2300$,

$$f_m = \frac{Re}{64} \quad (35)$$

When $Re > 2300$,

$$f_m = \frac{0.18}{Re^{0.2}} \quad (36)$$

Interfacial shear stress is given by,

$$\tau_i = f_i \frac{\rho_c (U_c - U_c)^2}{8} \quad (37)$$

Core velocity, is given by

$$U_c = \frac{(U_{SG} + U_{SLE})D^2}{(D - 2\delta)^2} \quad (38)$$

Core density,

$$\rho_c = \rho_G \alpha_c + \rho_L (1 - \alpha_c) \quad (39)$$

Interfacial friction factor is calculated from Wallis correlation

$$f_i = f_c \left(1 + 300 \frac{\delta}{D}\right) \quad (40)$$

Core Reynolds number is defined by,

$$Re = \frac{\rho_c U_c (D - 2\delta)}{\mu_c} \quad (41)$$

Core viscosity is given by,

$$\mu_c = \mu_G \alpha_c + \mu_L (1 - \alpha_c) \quad (42)$$

Chapter 3:

Experimental setup and instrumentation

3.1 Vertical flow loop

Vertical flow loop was specially designed for investigation of different two-phase flow regimes. The figure 1 in the next page shows the simplified schematic of flow loop. On the left side of schematic diagram water reservoir (1) is shown. It provides water feeding to the system. This reservoir is a 6 inches (OD) x 0.25 inch (thickness) x 10ft long PVC pipe. Desired water flow rate is achieved by setting water head at certain level. There is no pump in the system for controlling water rate. The liquid flow rate is controlled by water head, water flow meter (2) valves, throttling valve (3) and air flow rate. There are three water rotameters (2) installed right after water reservoir on PVC pipe which is 2 inches in diameter. Depending on desired liquid mass flow rate range one of them is opened. The throttling valve was installed to control the oscillation in the system that was caused by back pressure from point where air and water mixed. Mixing chamber (4) is a 2 inch PVC pipe where the air is introduced and mixed with the liquid and lifts the liquid to the top. Air is injected through the nozzle capped with porous material. Air feeding is provided from University compressor and controlled by gas flow controller (5). The main pipe is a 1.0 inch (25.4mm) ID transparent acrylic pipe which consists of the development section and the test section. The test section (6), which is 0.76m in length, is used for observation and PLIF measurements. Absolute pressure transmitter, differential pressure transducer and thermocouple are installed alongside the test section. They are connected to PC (7) through National Instruments I/O connecting block for data acquisition. Camera and laser (8) are placed perpendicular to each other and connected to PC (9) from Lavisision for data acquisition. Laser has separate power supply and water cooling system. At the top of flow loop 2 inch ID PVC pipe with filter (10) is installed for discharging the air while liquid returns to the water reservoir. The access to the test section is provided by 2 levels scaffolding which is not illustrated in this figure.

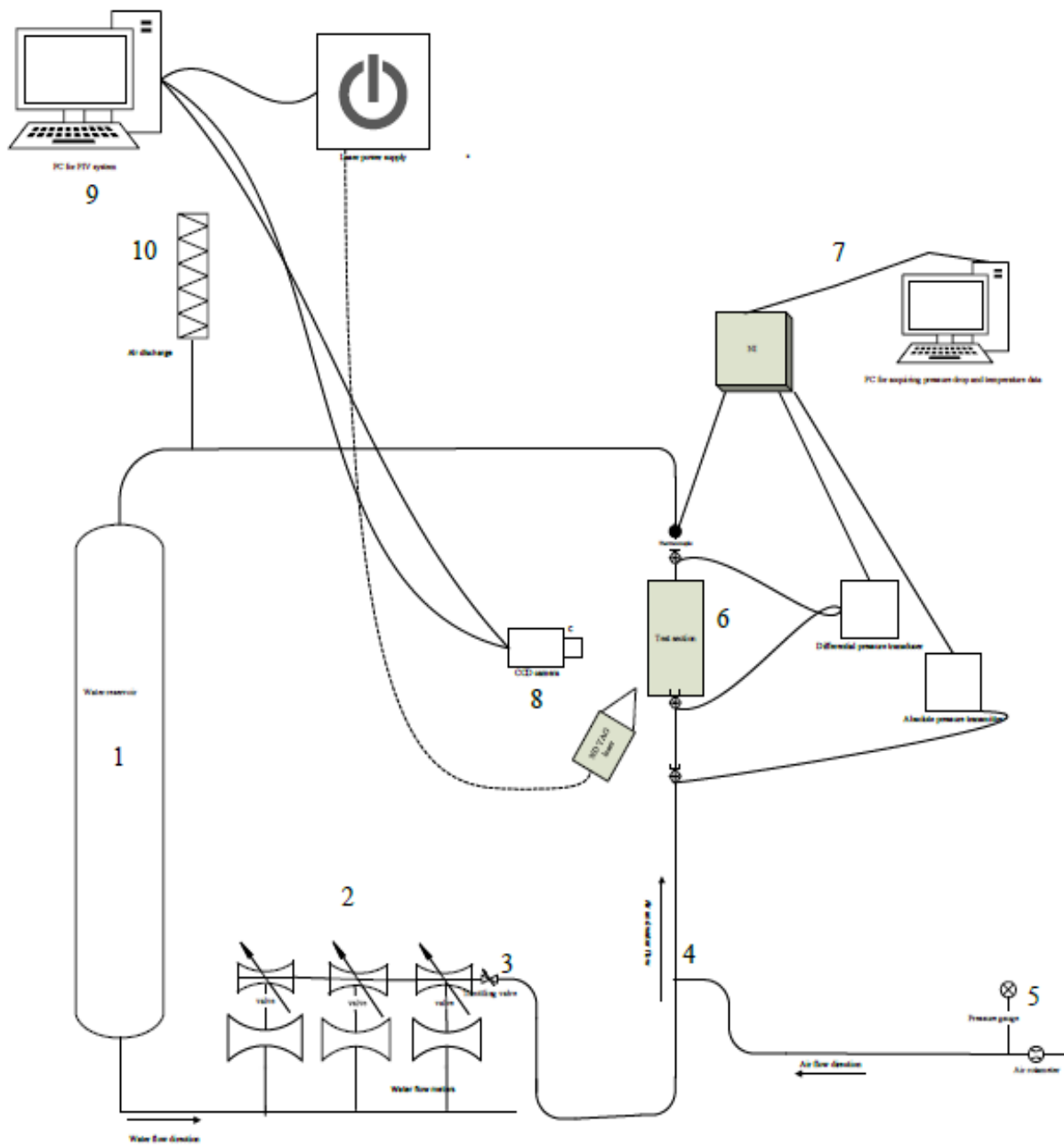


Figure 3-1 Simplified schematic of vertical flow loop

3.2 Measurement tools and techniques

Characteristic values of flow regime such as pressure drop, absolute pressure and temperature needed to be recorded in test section. Alongside with that essential input values of the experiment were recorded using water rotameter and gas flow controller. In the next several pages selected measurement tools are discussed.

3.2.1 Liquid flow meter

As it was mentioned earlier water flow rate was dictated by air flow rate, hydrostatic head in reservoir and by adjusting throttling valve and valve of rotameter.

Three rotameters (Fig. 2) were installed to the pipe connected to water reservoir. Each one has certain range of flow rates (from left to right: 100-1000 LPH, 16-160 LPH and 2-20 LPH). Investigated water flow rate region was between 20 LPH and 100 LPH. For that reason only one flow meter out of three was used with measuring range of 16-160 LPH. It is Kobold (V31-60301S-01-CW2-F-F-A-1-0-2-0-2-00000-K) variable area flowmeter with shatter proof protection and with an accuracy of $\pm 1.6\%$ at full scale.



Figure 3-2 Water rotameters with different ranges

Table 3- 1: Main description of water rotameter

Fitting	1/2" NPT F SS
Range of measurement	16-160 lph or 4.2-42 GPH water
Type of float	Stainless steel float not guided
Accuracy	1.6% full scale
Length	375 mm
O-ring	Viton o-ring
Type of float stop	PVDF float stops

3.2.2 Mass flow controller for air

Omega FM-2621A (Figure 3) gas flow controller was selected as the instrument for controlling and measuring the volumetric flow rate of gas phase. Flow controller works based on the principle of differential pressure within laminar flow. Measuring differential pressure within flow controller and viscosity of given gas is used to accurately determine volumetric flow rate of the gas. The detailed description of work principle of flow meters of FMA-2600 series can be found in website of omega flow meters. The unit of measurement of air flow rate was set as SLPM (standard liters per minute) at standard condition of 15C and 101.325 kPa. The general characteristics of flow meter are given below.

- 20+ Gas Calibrations, Including: He, O₂, Neon, N₂O, N₂, Air, Argon, CO, CO₂, Methane, Ethane, Propane, Butane, Acetylene, Ethylene, H₂
- Pressure, Temperature, Volumetric & Mass Flow Simultaneously Displayed
- Easy Operator Push Button Interface
- NIST Traceability Standard
- Full Scale Ranges from 0.5 SCCM to 3000 LPM
- Response Time of 100 milliseconds Typical
- Turndown Ratio of 100:1 Typical
- Position Insensitive
- Accuracy of ±1% Full Scale
- No Warm Up Time

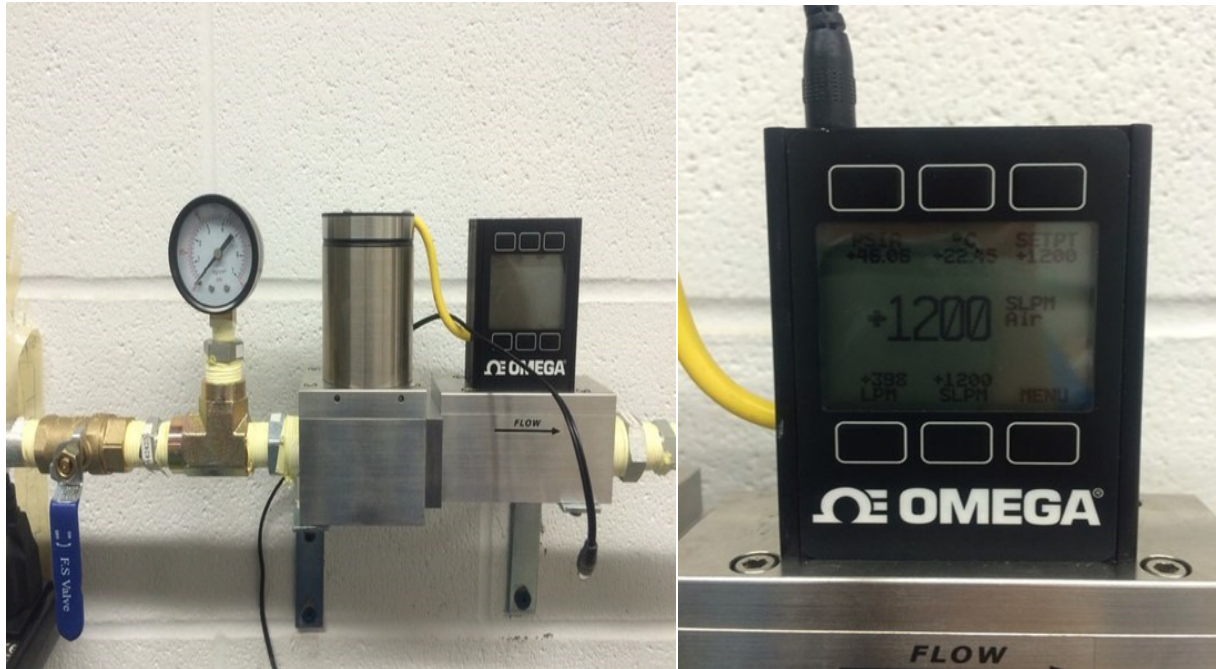


Figure 3-3 Air flow controller

3.2.3 Differential pressure transducer

Omega PX2300-1DI unidirectional wet/wet differential pressure transducer was used for measuring pressure drop in test section. The measuring range of transducer is from 0 to 1 psi with an accuracy of $\pm 0.25\%$ at constant temperature and response time to pressure change is 50 ms. Operating temperature falls between -18°C and 80°C .



Figure 3-4 Omega PX2300-1DI differential pressure transducer

Retrieved from <http://www.tuner.tw/OMEGA%20CD/Pressure/pdf/PX2300.pdf>

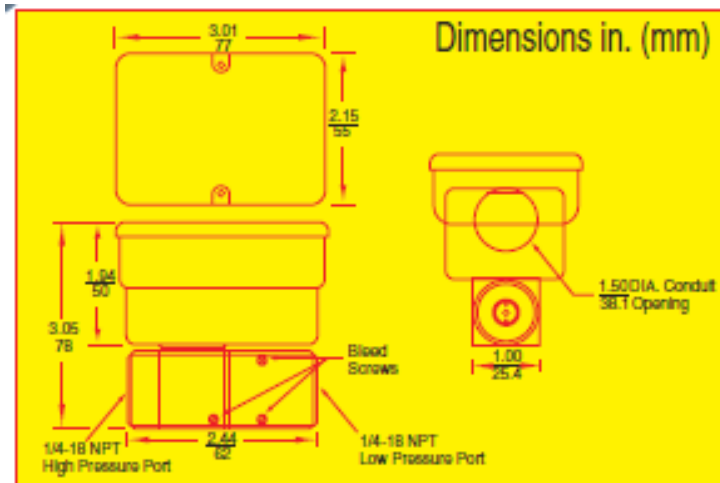


Figure 3-5 Schematic of differential pressure transducer

Retrieved from <http://www.tuner.tw/OMEGA%20CD/Pressure/pdf/PX2300.pdf>

3.2.4 Absolute pressure transducer

Absolute pressure transducer PX419-2.5GI with high accuracy of $\pm 0.08\%$ and range of 0-2.5 psi was selected for measuring absolute pressure in the test section. Transducer has stainless steel case with 316 stainless steel wetted parts and operates between -29°C and 85°C .



Figure 3-6 PX419-2.5GI Absolute pressure transducer

Retrieved from http://dtpvietnam.com.vn/assets/shops/2016_02/px419.1.jpg

Both transducers connected to Omega U24Y175 regulated power supply which is connected to National Instruments data acquisition box.



Figure 3-7 National instruments signal processing box

Temperature is measured by thermocouple which is connected to NI signal processing box.

3.2.5 Purging absolute and differential pressure lines

Before each experiment absolute and differential pressure transducer lines need to be purged in order to remove trapped air bubbles from tubes. The procedure is performed in several steps:

1. Throttling valve is completely closed in order to fill the 1 inch tube with distilled water
2. The cap on the side of 1 inch tube is opened and tube is filled with distilled water so it passes thermocouple
3. First top line of pressure transducer is disconnected from the tube in order to remove all the air bubbles from the line and fill it with fresh distilled water and then it is reconnected.
4. Same procedure is repeated for bottom pressure line of differential pressure transducer and absolute pressure tap
5. Pins on transducer box is loosened (1-1.5 turn maximum) in order to drain the water with possible trapped air from the box. Draining 3-4 droplets is enough.
6. Throttling valve is opened in order for level hydrostatic head on both sides of flow loop

3.2.6 Calibration of differential pressure and absolute pressure transducers

It is important to calibrate the pressure transducers properly as values of obtained pressure are small and it requires high accuracy measurement with minimum error. Calibration is performed in several steps

Calibration of absolute and differential pressure transducers

1. Completely closing the throttling valve.
2. Filling the 1 inch tube with water above the thermocouple
3. Draining the water through the transducer lines to make sure that there is no any air
4. Loosening the pins to drain the water through transducer box
5. Connecting the calibrator to the transducer line

6. Finding the current for every pressure step (for example 0, 0.2, 0.41 psi)

Table 3- 2: Data points with pressure values for calibration of transducers

Calibrator input, psi	First pressure reading in voltage, volt	Second pressure reading in voltage, volt	Average, volt
0	0.01846	0.01837	0.018415
0.2	0.01522	0.01522	0.01522
0.25	0.01457	0.01461	0.01459
0.4	0.01199	0.01214	0.012065
0.6	0.00895	0.00899	0.00897
0.8	0.00571	0.00579	0.00575
1	0.00295	0.00295	0.00295

7. Building the current vs pressure graph in excel and defining fit formula for that graph

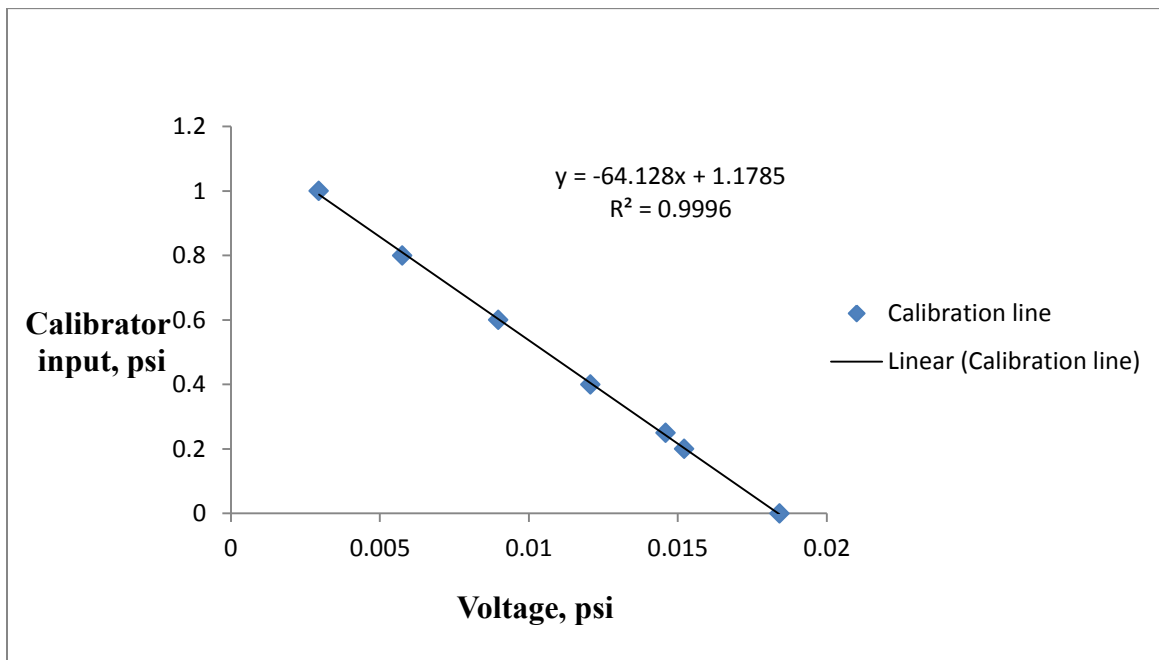


Figure 3-8 Calibration graph for Signal Express

Insert this formula ($y = -64.128x + 1.1785$) into calibration graph in Signal Express for correction

8. Then calibrator is connected to transducer tubes again in order to check the accuracy of calibration

Table 3-3: Pressure points with corresponding values in Signal Express

Calibrator input, psi	Measured value in Signal Express, psi
1	0.988
0.8	0.816
0.6	0.607
0.4	0.407
0.25	0.246
0.2	0.199
0	-0.007

Data acquisition on Signal Express (temperature, differential and absolute pressure)

Data was acquired simultaneously with recording images. Data was recorded and exported to Excel sheet for every set of liquid and gas flow rates. User can define frequency of recording in the software.

3.3 Planar laser induced fluorescence (PLIF) components

Planar laser induced fluorescence is widely used technique for flow visualization. It is mainly used for concentration, velocity, temperature and pressure measurements. In case of this experiment it is used for visualizing flowing film. PLIF system consists of light source which is usually laser, fluorescent medium (mix of distilled water and Rhodamine B) and collection optics with detector (high speed CCD camera from Lavision).

3.3.1 Test section for PLIF setup

The test section (figure) for PLIF measurements is 1ft in length. The CCD (1) camera and laser (2) are placed by 90° from each other. The box (3) is filled with glycerol (4) that possess similar refraction index to acrylic glass (5). The aluminium frame (not shown in the picture) is used to fix the laser and camera and can be changed based on desired location for other potential measurements.

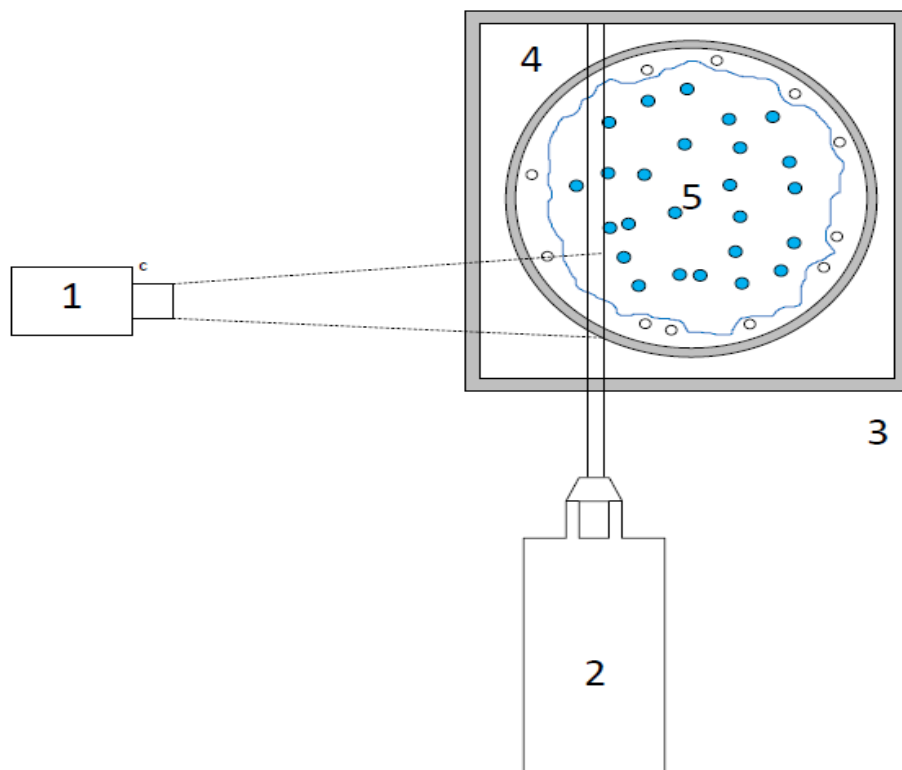


Figure 3-9 PLIF test section

Figure above illustrates setup with laser offset. Laser moved closer to the camera in order to reduce obstruction of liquid film image by rough surface of the film and increasing air bubble concentration in the film with increasing liquid and gas flow rates.

3.3.2 Camera

Imager intense (figure 9) the camera used in the LaVisionFlowMaster PIV system was selected for this particular experiment. It is sensitive camera with low readout noise. The camera delivers 12 bit digital images and it features a built in electronic shutter with exposure times as short as 500ns. In the table below it is compared to other cameras of Lavisision. It represents the overview of CCD cameras from Lavisision. Imager Intense and Imager QE cameras have lower readout noise comparing to other cameras from the list. Imager intense is equipped with 2/3” and 1376x1040 pixel CCD. Operating temperature of CCD is -12°C which is the reason for low readout noise.



Figure 3-10 Imager Intense camera

Retrieved from http://www.lavisision.de/en/products/cameras/piv_cameras.php

Table 3-4: Technical characteristics of Imager Intense Camera

Imaging parameters	Spectral response	Sensitivity	Image rate	Spatial resolution		Time resol-n.	Intensity resolution	
				CCD Chip Size	CCD Pixel Size		Full Well (e-pixel)	Digitization
Camera ¹	Spectral Range	Read-Out Noise	Frames/s ² (Pixel Rate)	CCD Chip Size	CCD Pixel Size	Exposure	Full Well (e-pixel)	Digitization
Imager QE Imager intense	290-1100nm	<5 e-	10 (12.5MHz)	1376 x104 0	6.45μm	100ns - 1000s	18 k	12bit

¹ pro X models have built-in memory (512 MB - 4 GB available)

²can be increased by image reduction (binning, windowing)

General specifications of the camera are listed in table below.

Table 3-5: General system specifications of camera

Double Shutter	Two images with 500ns interframing time
Exposure time	500 ns ... 1 ms or 1ms...1000s (software selectable)
Digital output	12 bit @ 16 MHz
Serial link	coaxial (≤ 10 m) or fiber optic (≤ 300 m)

Table 3-6: CCD sensor

Number of pixels	1376 x 1040 pixels
Pixel size	6.45 μm x 6.45
Sensor format	2/3"
Full-well capacity	18.000 electrons
Spectral range	290 – 1100 nm
Max. QE	65 % @ 500 nm
Cooling type	2-stage Peltier, forced air (optional liquid)
CCD temperature	-12°C

Table 3-7: CCD Control and A/D- Converter

Dynamic range	12 bit
A/D conversion factor	2 e ⁻ /count (high gain), 4 e ⁻ /count (low gain)
Readout (scan) rate	16 MHz
Readout noise	4-5 e ⁻ @ 16 MHz (high gain), 5-6 e ⁻ @ 16 MHz (low gain)
Frame rate	10 frames/s
Dark current	< 0.1 e ⁻ /pixel/s
Electronic shutter	down to 500 ns
Binning	1-8 (h) 1-32 (v)

3.3.3 Lens

Nikon AF Micro-Nikkor 60 mm f/2.8D lens was used. Two extension rings were added to the lens before mounting it to the camera. It is standard macro lens with manual aperture control with minimum aperture of F32 and maximum aperture of F2.8. Main technical specifications of lens are given in the table below.



Figure 3-11 Nikon AF Micro-Nikkor 60 mm f/2.8D lens

Retrieved from <http://www.photozone.de/Reviews/219-micro-nikkor-af-60mm-f28-d-review--test-report>

Table 3- 8: Technical specifications of lens

Equiv. focal length	60 mm (full format equivalent)
Equiv. aperture	f/2.8 (full format equivalent, in terms of depth-of-field)
Optical construction	12 elements in 9 groups
Number of aperture blades	9
min. focus distance	0.185 m (max. magnification ratio 1:1)
Dimensions	70 x 60 mm
Weight	428 g
Filter size	62 mm (non-rotating)



Figure 3-12 Camera and laser setup during calibration

3.3.3 Filter

Image filter with wave lengths cut-off threshold of 540nm was selected. When illuminated with green laser light Rhodamine and distilled water mix illuminates light up to 565 nm and filter cuts off everything below 540 nm. It is also prevents CCD chip from oversaturation hence burning out.

3.3.4 Laser

Selected laser ND YAG SOLO III-15. This laser from New Wave Research Inc. The laser is optimal configurations for this experiment. It has 50mJ power for green laser, good beam divergence and beam pointing, and beam diameter can be adjusted between 0.5 mm and 3.5 mm

Table below shows the specifications of laser.

Table 3-9: Technical specifications of laser

	Solo III-15
Energy ¹	
532nm	50mJ
266 nm	
Stability ² 532 nm	± 4 %
Stability 266 nm	
Pulse width ³	3-5ns
Beam divergence ⁴	< 4mrad
Beam pointing ⁵	< 100μrad
Jitter	± 0.5ns
Beam Diameter	3.5mm

1. Optical losses due to optional attenuator will reduce maximum energy by 10%
2. Pulse-to-pulse for 98% of shots after 30 minute warm up
3. Full width half maximum
4. Full angle for 86% of the energy, 1/e² point
5. Full angle for 86% of the energy, 1/e² point

3.3.5 Software

Processing of data and is done on DaVis 7.2 software.

3.3.6 Fluorescent dye (Rhodamine B)

Rhodamine B was selected as tracer dye. Rhodamine B was mixed with distilled water in the amount of 150 mg to liter of distilled water. It should be mixed with distilled water as it chlorinated tap water decomposes Rhodamine B. Rhodamine B and distilled water mixture absorbs light up to 545 nm and emits at maximum 565nm.



Figure 3-13 Rhodamine B

3.4 Experimental run

Calibration is done prior to the run of flow loop and camera position and laser is not being changed during the run while images are taken.

3.4.1 Calibration

Due to the image distortions caused by curvature of the tube, the field of view needs to be calibrated from physical to pixel space. For this particular experiment, custom made distortion target with 25 x 25 mm dimension, 0.5 mm spacing and with dot diameter of 0.25 mm was chosen (figure 12). Target was made from paper and was laminated in order to prevent the paper from getting wet. Grid pattern was printed using 2400*2400 dpi high resolution printer.

Table below outlines main specifications of this target:

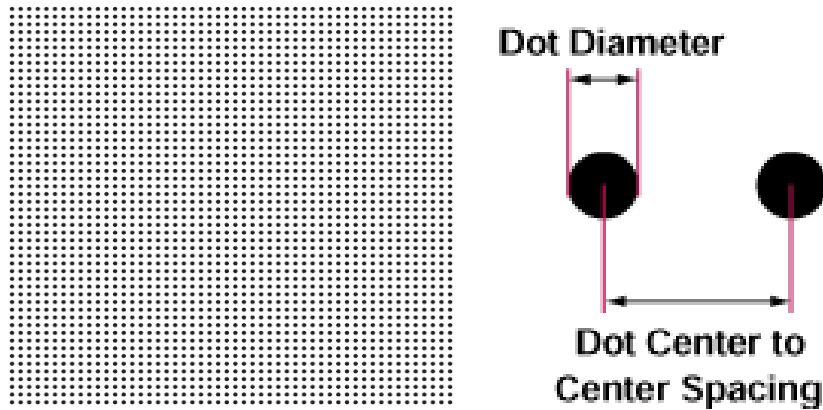


Figure 3-14 Calibration target

Retrieved from <http://www.edmundoptics.com/test-targets/distortion-test-targets/fixed-frequency-grid-distortion-targets/58509/>

Table 3- 10: Specifications of calibration target

Type	Chrome on Glass
Dimensions (inches)	2 x 2
Pattern Size (mm)	25 x 25
Dot Diameter (mm)	0.25
Dot Spacing (mm)	0.5

As experiment is performed in 1 inch tube it is necessary to have a mount for holding calibration target. The half-cylinder base was made from nylon with three magnets inserted in it for adjusting the position of target. Calibration target was cut to fit the tube. Target was attached to the surface of the base by double-sided tape. Figure 13 represents the dimensions of the base in mm.

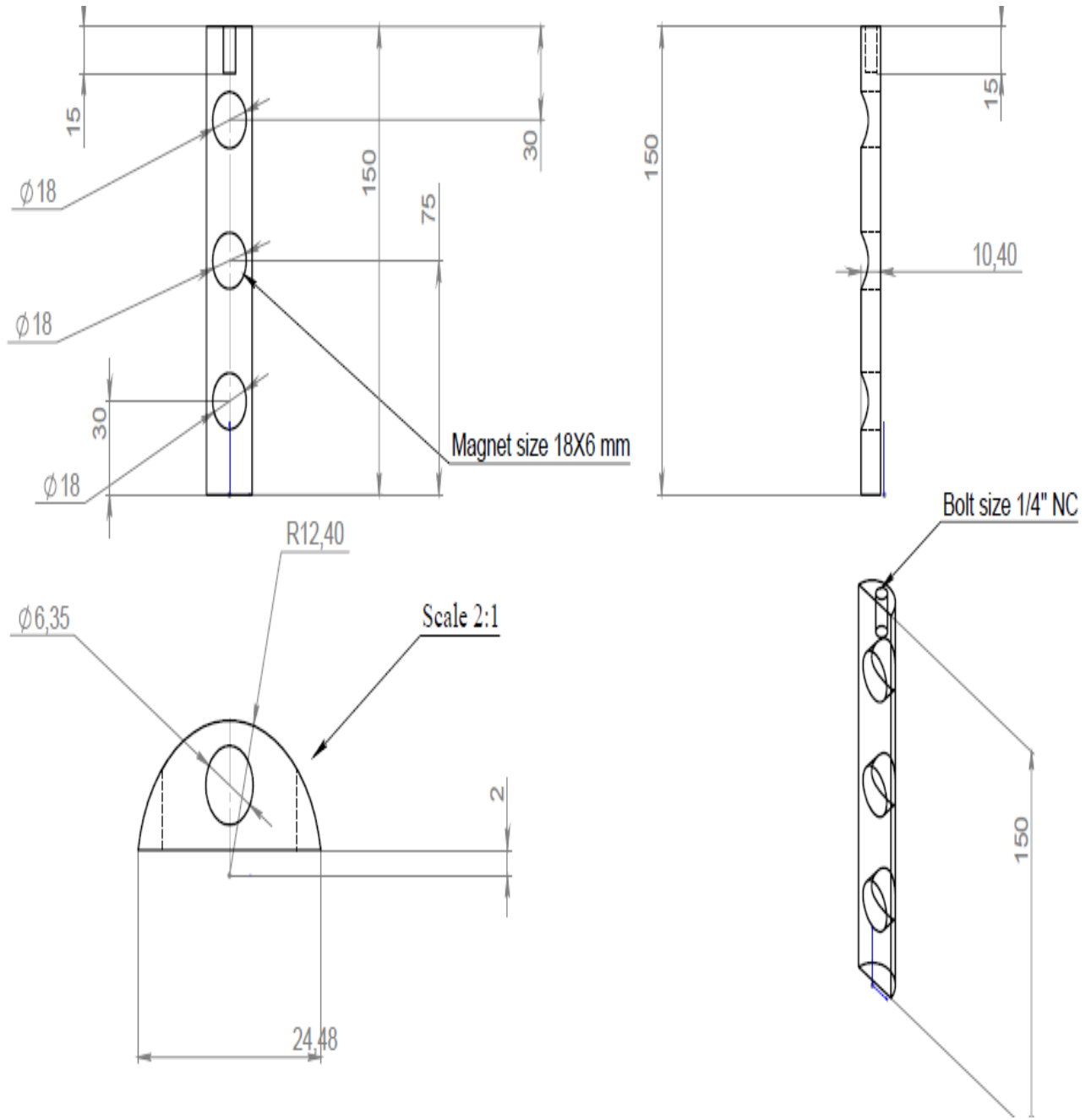


Figure 3-15 Dimensions of base of calibration target

Calibration was done in water as it gave more accurate position of the wall comparing to calibration in air.



Figure 3-16 Calibration target base with calibration grid attached to it

3.4.2 Calibration procedure

1. Putting the calibration target inside of the tube and fixing it with help of magnets at desired spot where experimental data will be collected.

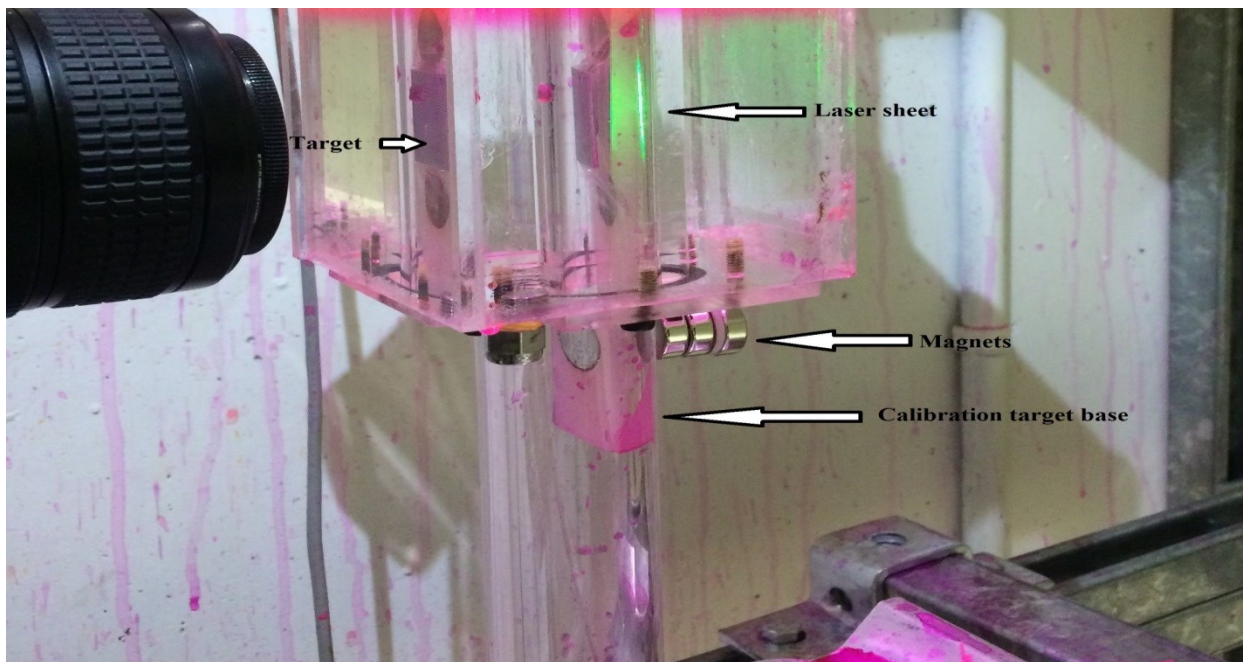


Figure 3-17 Taking image before running calibration in Davis

2. Adjusting the camera position and optics to make sure that clear image of grid from region of interest is taken.

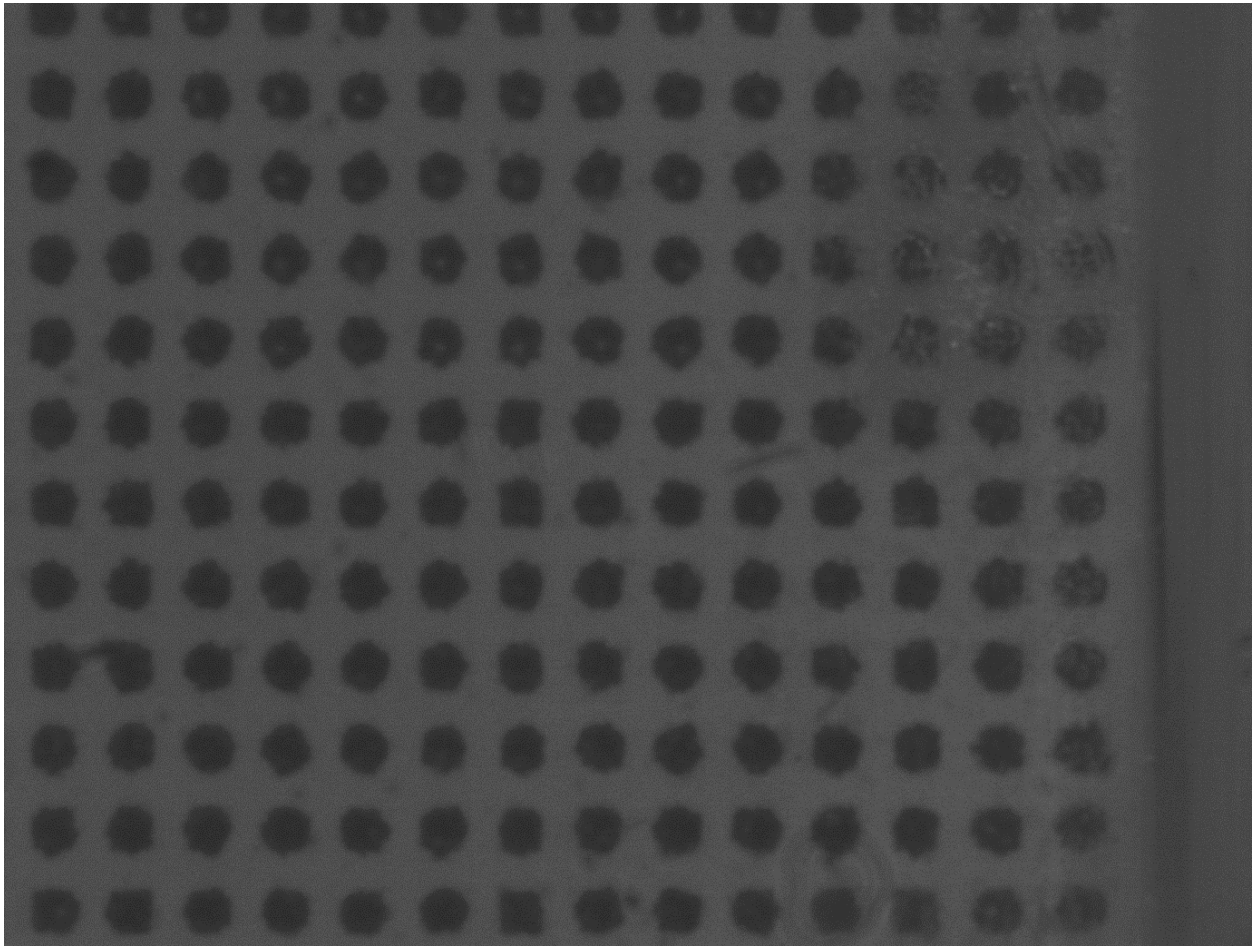


Figure 3-18 Unmarked image of calibration grid

Next calibration steps were done using DaVis 7.2 software.

3.4.3 Calibration procedure in Davis

1. Defining the experimental setup type. For this project it is one camera and 2D.
2. Defining coordinate system
3. Defining the calibration target type
4. Image of calibration target is taken
5. Defining exposure time
6. Taking the image

7. Marking the reference mark, defining the neighbour mark by clicking one on the right and one on the top

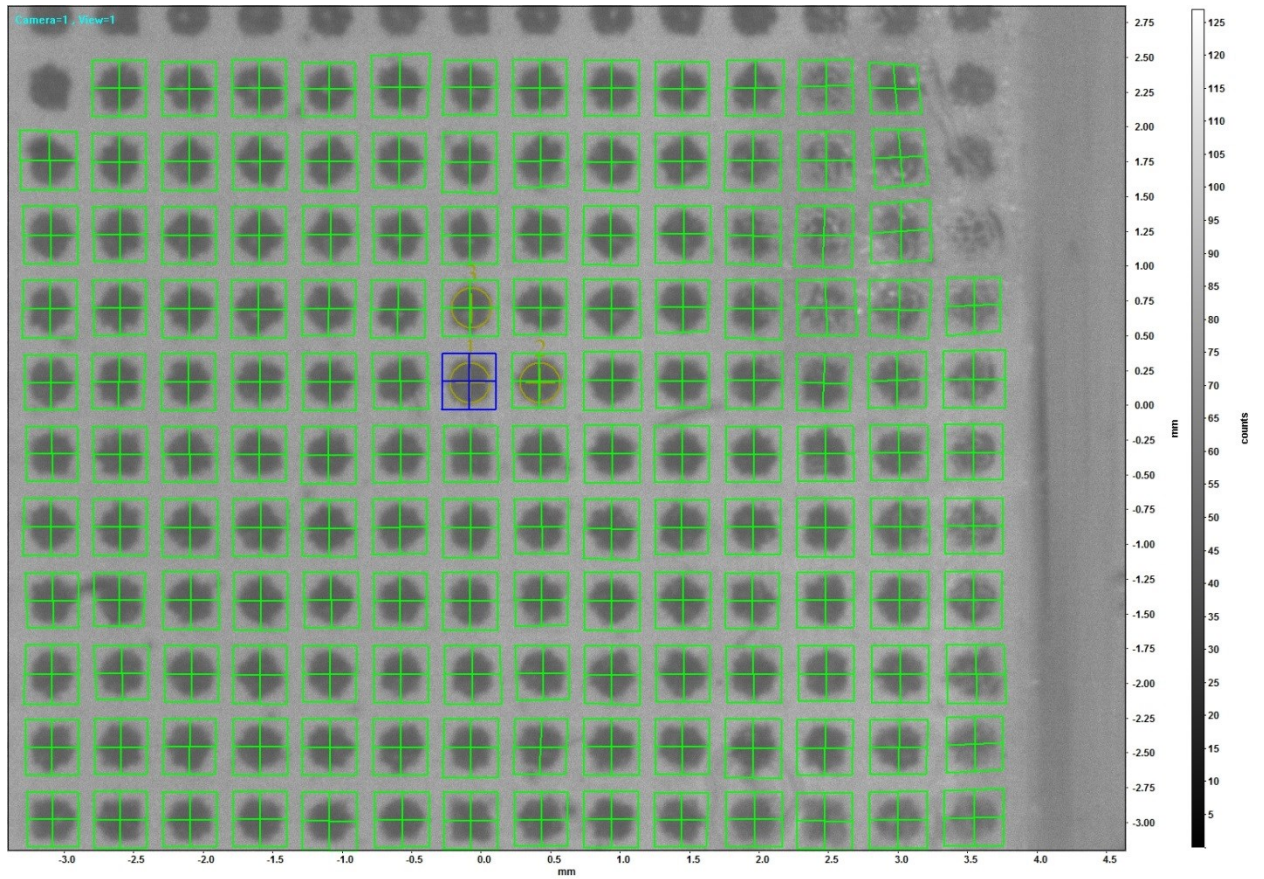


Figure 3-19 Completed calibration

8. Run the calibration
9. Fitting the mapping function

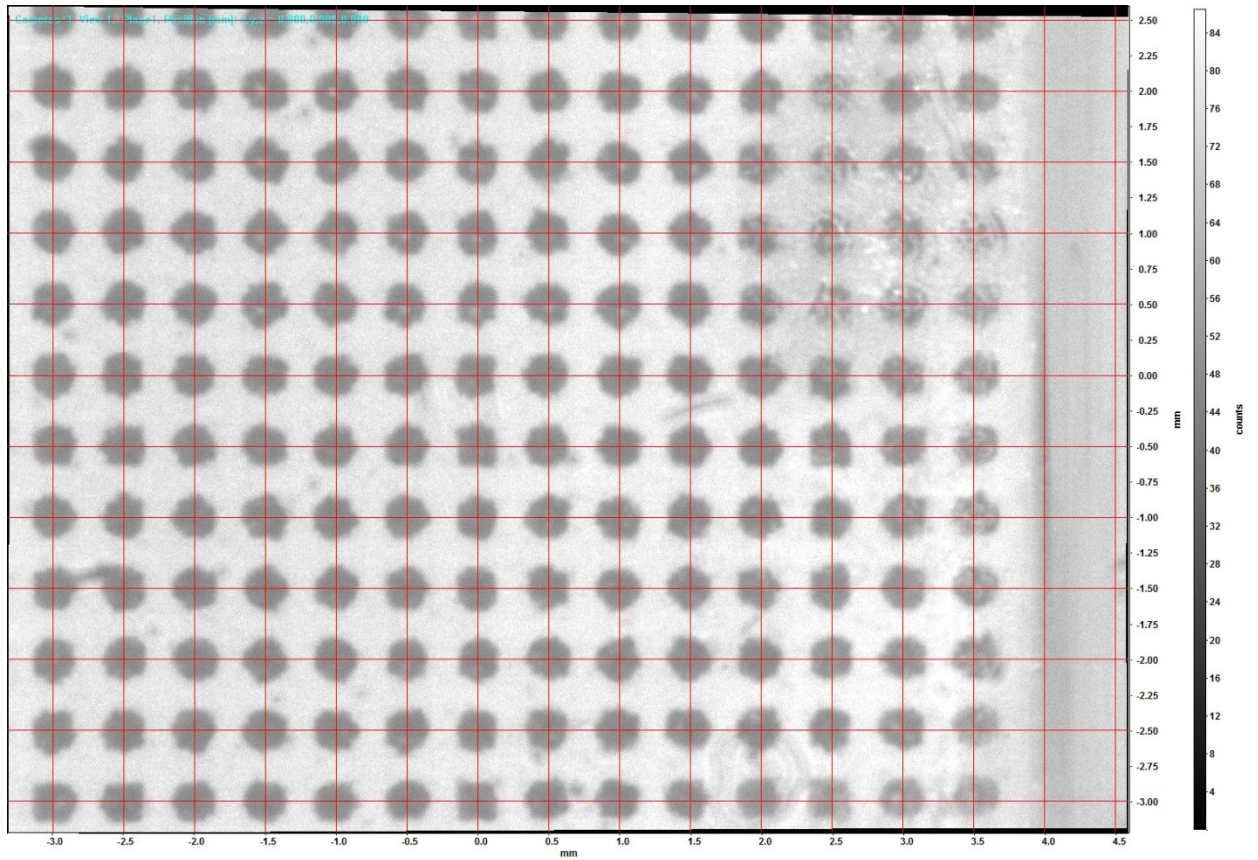


Figure 3-20 Calibration grid after correction (world to raw)

In this experiment the most accurate calibration was achieved with RMS pixel fit of 1.31 for offset setup and 5.75 for setup when laser was in the center and further attempts to reduce the value were not satisfactory. Scaling factor for offset setup is 200 pixels per mm whereas for setup when laser was in the center 323.89 pixels per mm.

3.4.4 Experimental procedure

1. The water reservoir needs to be filled to desired level
2. The valve from university air compressor is opened to provide air feeding
3. With help of gas flow controller the air flow rate is set at desired value
4. One of three liquid flow meters is selected depending on investigated liquid flow rate (other two needs to be kept closed)
5. Water flow rate is adjusted and stabilized by adjusting throttling valve and liquid flow meter valve
6. It is necessary for flow regime to stabilize. For that reason duration of 5 minutes is selected.
7. The Davis software is started and project selected
8. The Signal Express software is started
9. The recording of 1500 images on Davis and recording of absolute pressure, differential pressure and temperature on Signal Express is initiated at the same time by pressing record button on both software interfaces
10. As the recording on Davis is 5 frames per second it takes approximately 5 minutes to gather one set of data at one water and gas flow rates
11. The recording on Signal Express is stopped at the same time when recording on Davis stops automatically
12. The next air flow rate is selected and steps 2-11 are repeated

Settings before recording images

Number of images: 1500

Power of laser pulse: 50%. In this experiment only one pulse is chosen.

3.5 Film thickness calculation

Calculation of film thickness was done in two steps:

The film thickness was obtained from original set up when laser sheet was aligned with center of the tube to prevent any sort of refraction. However, due to difference in refractive index of acrylic glass and water with increasing water flow rate the images got distorted due to that difference. Also, concentration of air bubbles in the film increased with increasing water flow rate which was an obstacle for obtaining clear unclouded images of the film. As the result, only three liquid flow rates of 20, 25, 30 LPH were used for calculation of correction coefficients set of gas flow rates from 500 SLPM to 1400 SLPM.

Calculation explained

- Images are loaded from given directory (folder from external hard drive or internal hard drive of PC)
- Each separate image is cropped in region of interest defined by user.
- Then images are converted from greyscale to binary image. Threshold is defined by user depending on minimum greyscale index value in liquid film region.
 - ✓ For the setup with laser aligned with center of the pipe threshold value is 60
 - ✓ For the setup with laser offset threshold value is 50
- Once image is converted liquid appears white while rest of the picture is black
- Program calculates total number of white pixels and divides it by scaling factor (323.89 pixels/mm for setup with laser aligned with center of the pipe and 200 pixels/mm with an offset) and height
- Each liquid film thickness is calculated this way and value stored in 1*1500 arrays
- At the end mean function calculates average of 1500 images

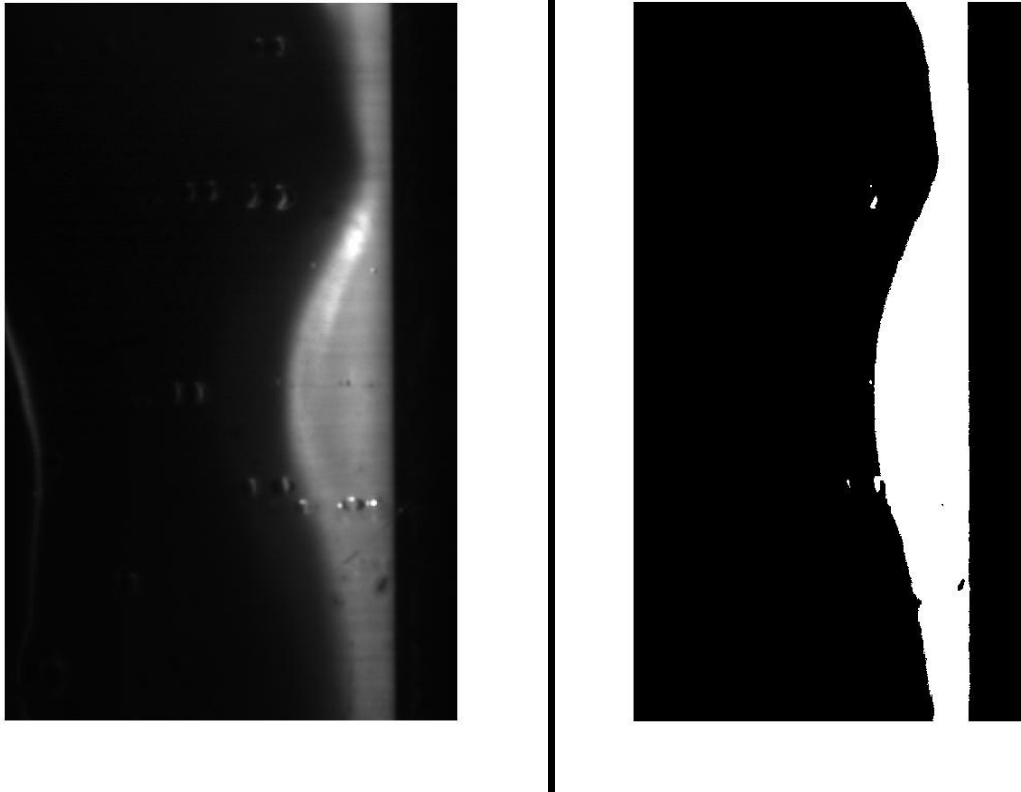


Figure 3-21 Raw image (left) and Image after conversion (right) Greyscale Threshold Value (60)

Chapter 4:

Results and discussion

In this chapter, the measured film thickness values along with pressure drop, absolute pressure and temperature are presented. Also values of film thickness from two different measurements in the literature are presented and correction number calculation is explained. Results are compared against existing theoretical models and experimental data from literature.

4.1 Pressure drop, absolute pressure and temperature

Pressure drop, absolute pressure and temperature were recorded simultaneously with recording liquid film. Table below presents values of these measurable parameters from 20 to 60 LPH of liquid flow rate and from 500 to 1200 SLPM of gas flow rate. Values of these parameters are necessary for calculation of film thickness in models. Absolute pressure and temperature are needed in order to determine dynamic viscosity and density of liquid phase and core.

Table 4-1: Pressure gradient, absolute pressure and temperature values from experiment

Liquid flow rate, LPH	20	30	40	50	60	Gas flow rate, SLPM
Pressure drop, Pa	409.85	452.78	530.98	561.81	624.52	500
Absolute pressure, Pa	10244	102752	102930	103109	103258	
Temperature, C	15.36	19.2	17.49	16.69	16.91	
Pressure drop, Pa	438.56	495.01	576.29	643.77	712.96	600
Absolute pressure, Pa	102448	102745	102926	103125	103296	
Temperature, C	14.59	18.69	17.14	15.76	16.07	
Pressure drop, Pa	504.29	575.48	667.7	745.28	841.6	700
Absolute pressure, Pa	102473	102802	102997	103223	103425	
Temperature, C	14.27	18.55	16.89	14.72	14.95	
Pressure drop, Pa	621.4	626.81	785.97	874.33	987.79	800
Absolute pressure, Pa	102610	102911	103121	103385	103523	
Temperature, C	14.17	16.71	16.72	14.8	17.05	
Pressure drop, Pa	729.86	748.28	918.19	983.21	1141.5	900
Absolute pressure, Pa	102713	103041	103264	103538	103711	
Temperature, C	13.98	16.47	16.51	15.04	16.57	
Pressure drop, Pa	843.88	842.14	1079.3	1253.4	1318.2	1000
Absolute pressure, Pa	102833	103108	103455	103750	103911	
Temperature, C	13.71	16.21	16.33	16.81	16.19	
Pressure drop, Pa	958.37	1003.5	1239.4	1413.2	1512.4	1100
Absolute pressure, Pa	102983	103284	103637	104001	104235	
Temperature, C	13.35	16.16	16.25	15.11	16.07	
Pressure drop, Pa	1123.6	1195.4	1444.7	1609.5	1718	1200
Absolute pressure, Pa	103209	103508	103894	104205	104416	
Temperature, C	13.06	15.89	16.14	15.35	15.49	

Data was compared to Hughmark's (1973) and Ansari's(1994) models. Recorded values are on average 25-30 % lower from models.

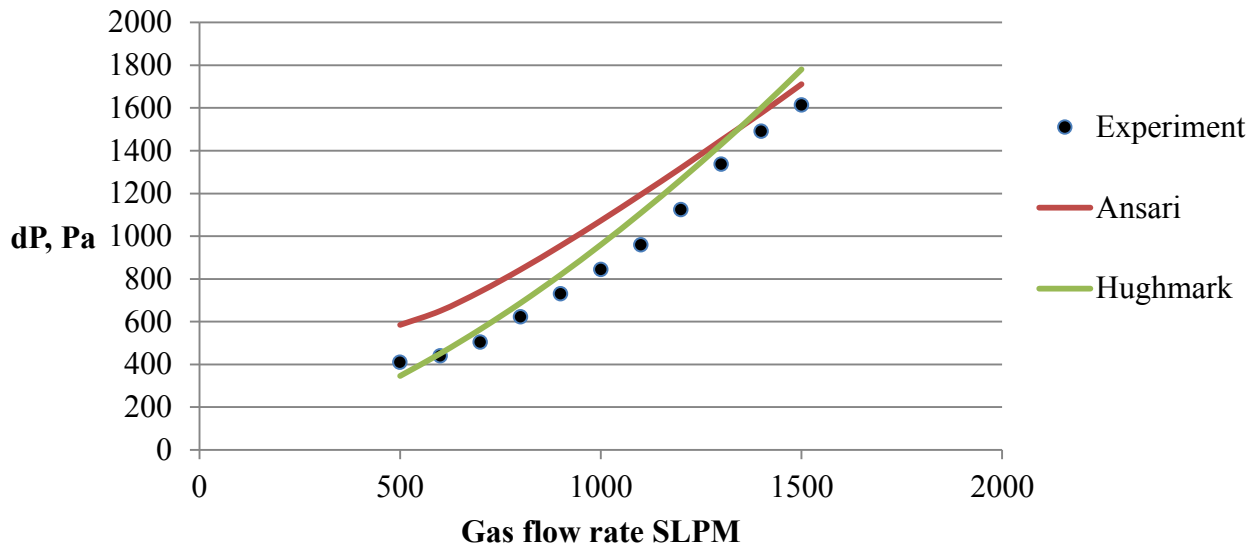


Figure 4-1 Recorded differential pressure compared against models (20 LPH of liquid rate)

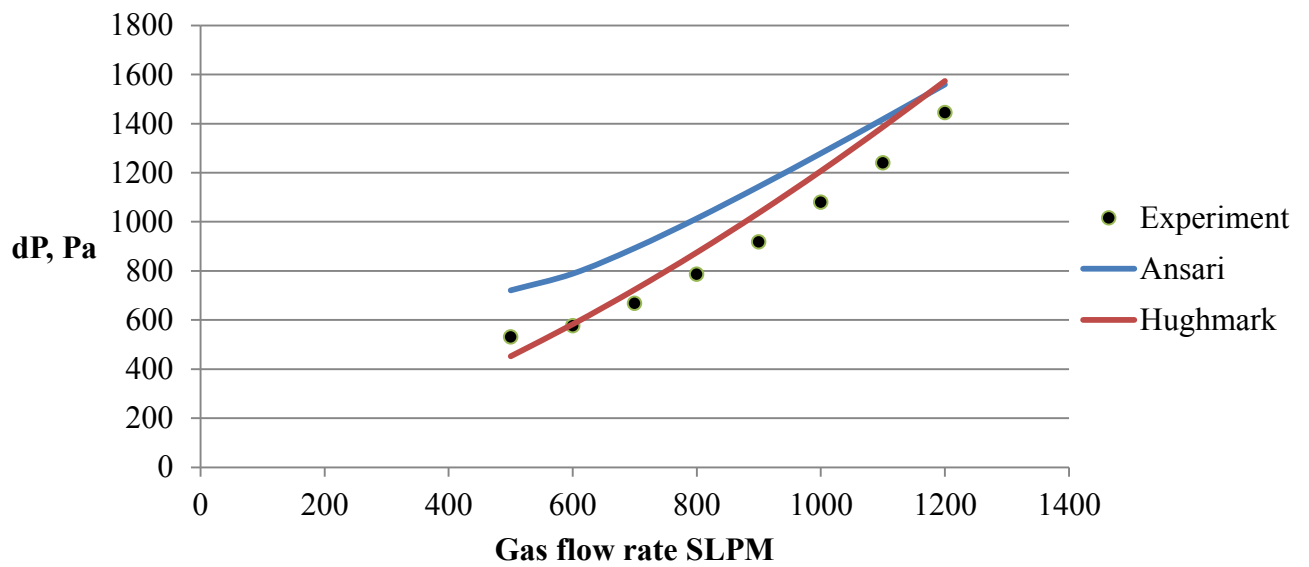


Figure 4-2 Recorded differential pressure compared against models (40 LPH of liquid rate)

4.2 Visual observation (entrainment)

According to Ansari's (1994) model entrainment took place at all superficial liquid velocities (0.011m/s to 0.033 m/s hour) starting from superficial gas velocity of 19 m/s (approximately 600 SLPM). However, images obtained at 20 and 30 liters per hour of liquid flow rate show that there is an entrainment at U_{sg} of 16.25-16.3 m/s which is 500 SLPM. Images were obtained low magnification. Below some images from 20 and 30 liters per hour of liquid rates are presented.

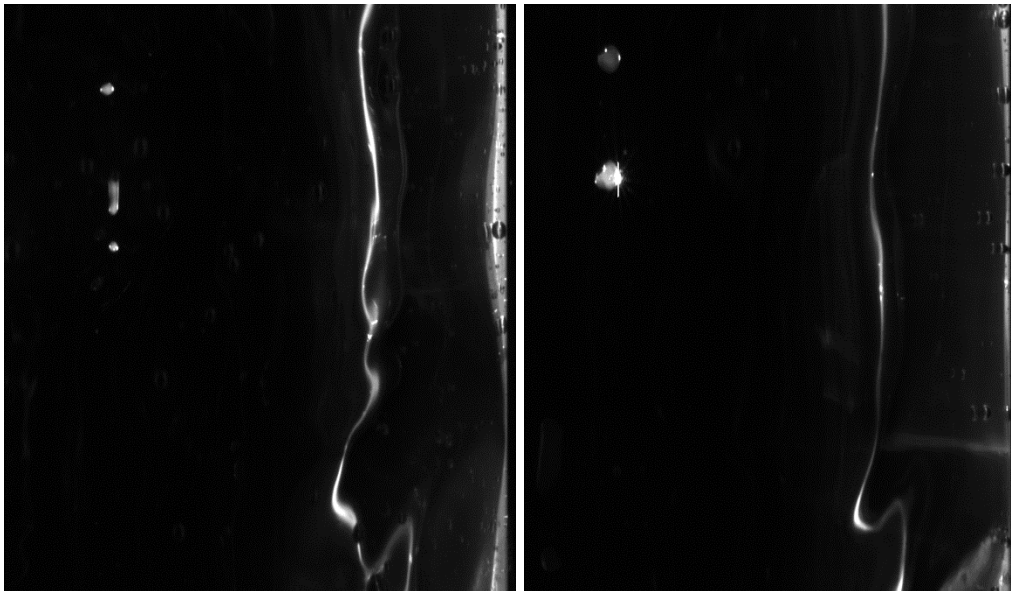


Figure 4-3 500 and 600 SLPM of gas rate at 20 LPH of water rate

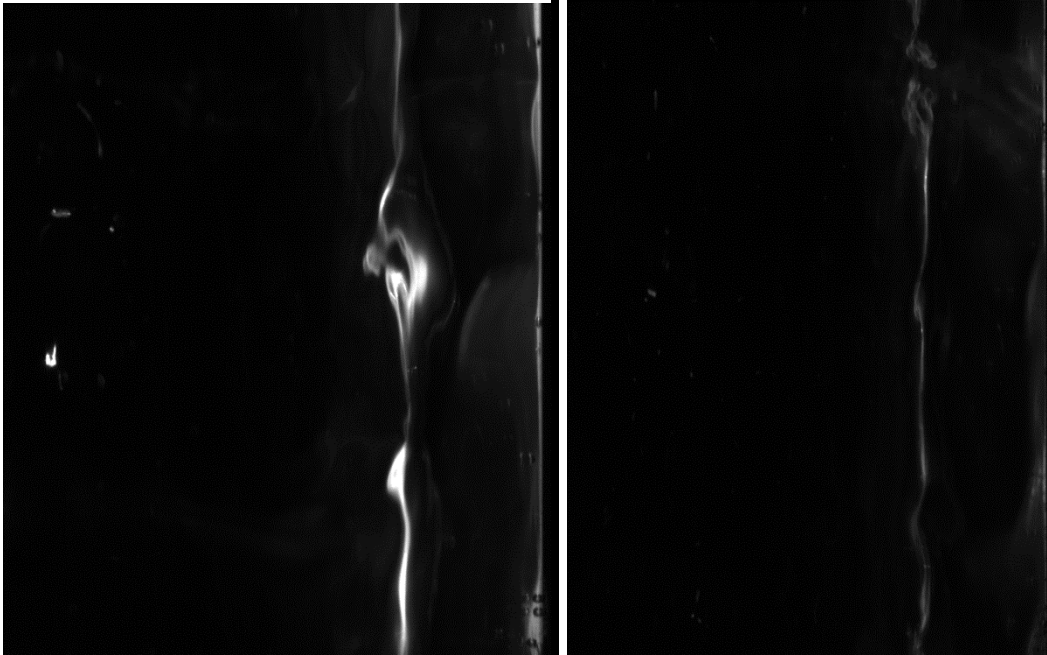


Figure 4-4 900 and 1200 SLPM of gas rate at 20 LPH of liquid rate

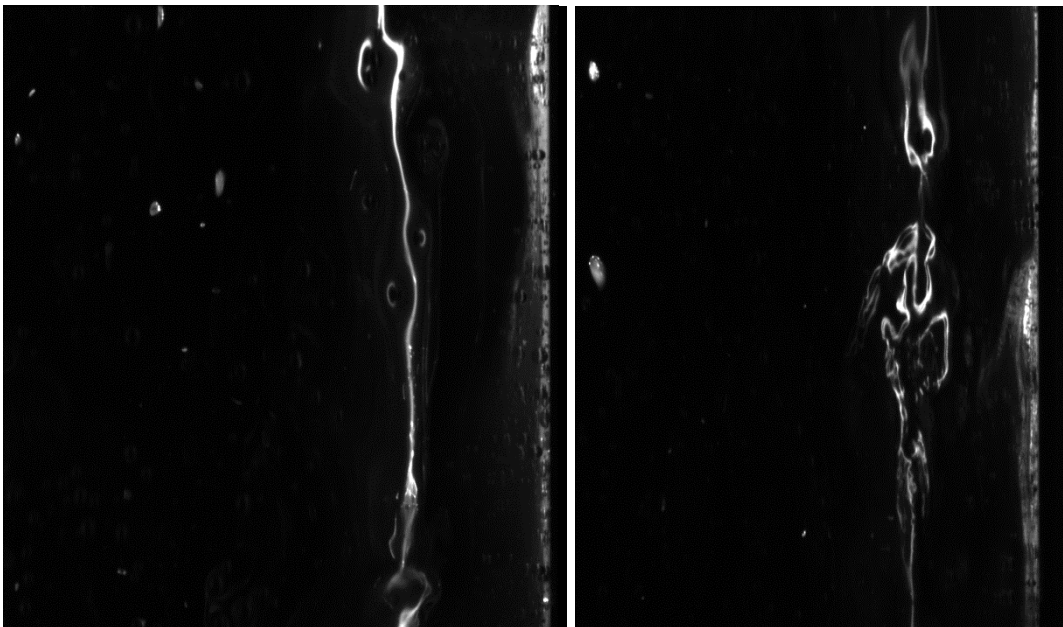


Figure 4-5 600 and 900 SLPM of gas rate at 30 LPH of liquid rate

As it can be observed droplet size decreases with increasing gas flow rate. It can be explained by gas drag force that breaks down droplets into smaller droplets. Droplet concentration increases with increasing liquid flow rate.

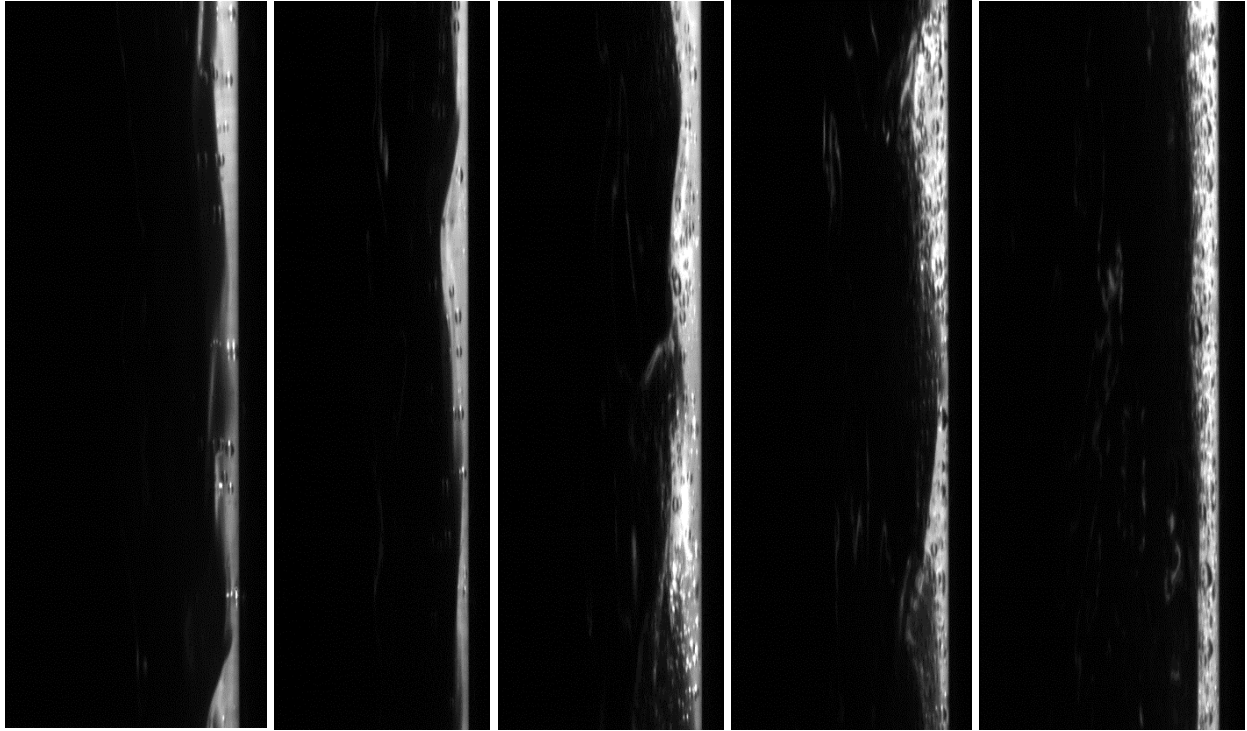


Figure 4-6 At 1200 SLPM of gas rate from left to right: 20, 30, 40, 50, and 60 LPH of water rate

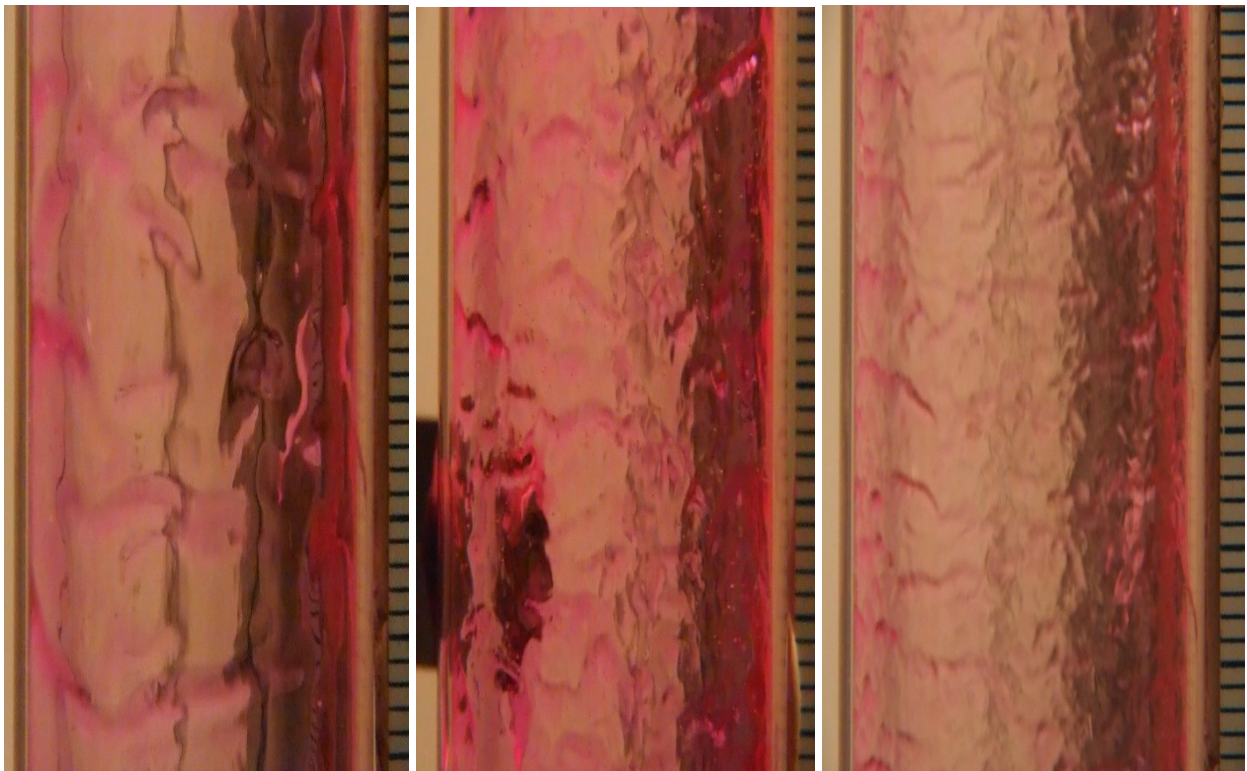


Figure 4-7 20 LPH of liquid flow rate at and 700, 1100 and 1500 SLPM of gas flow rates

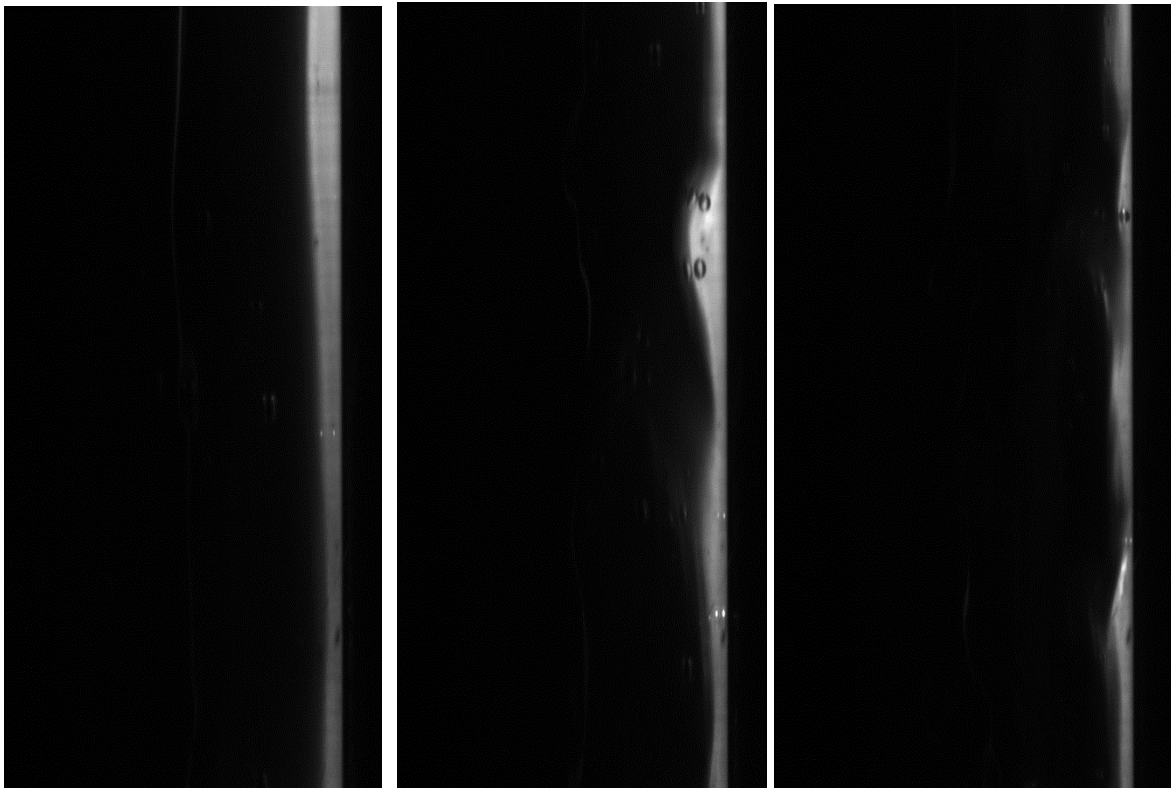


Figure 4-8 Images taken with laser offset at 20 LPH of liquid flow rate and at 700, 1100 and 1500 SLPM of gas flow rates

At low liquid flow rates liquid film appears smooth at low gas rates. There is very low concentration of air bubbles in the film. With increasing gas flow rate film roughness increases which causes increase in pressure drop.

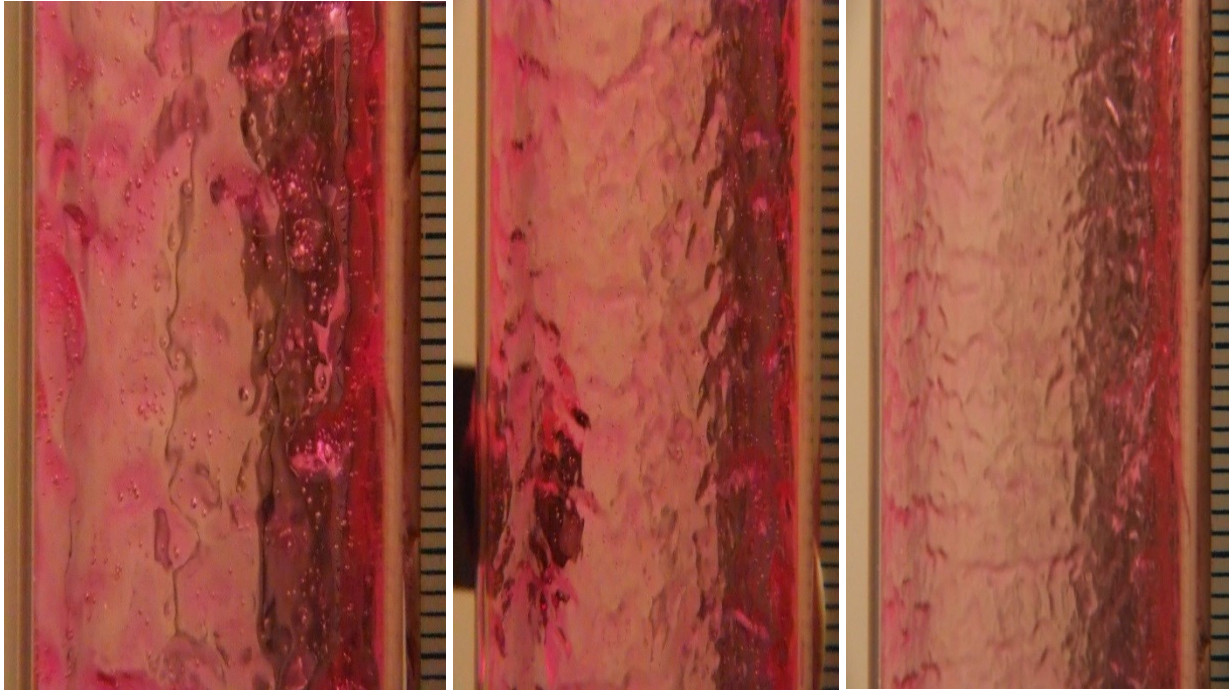


Figure 4-9 Images taken with high speed camera at 30 LPH of liquid flow rate and at 700, 1100 and 1500 SLPM of gas flow rates

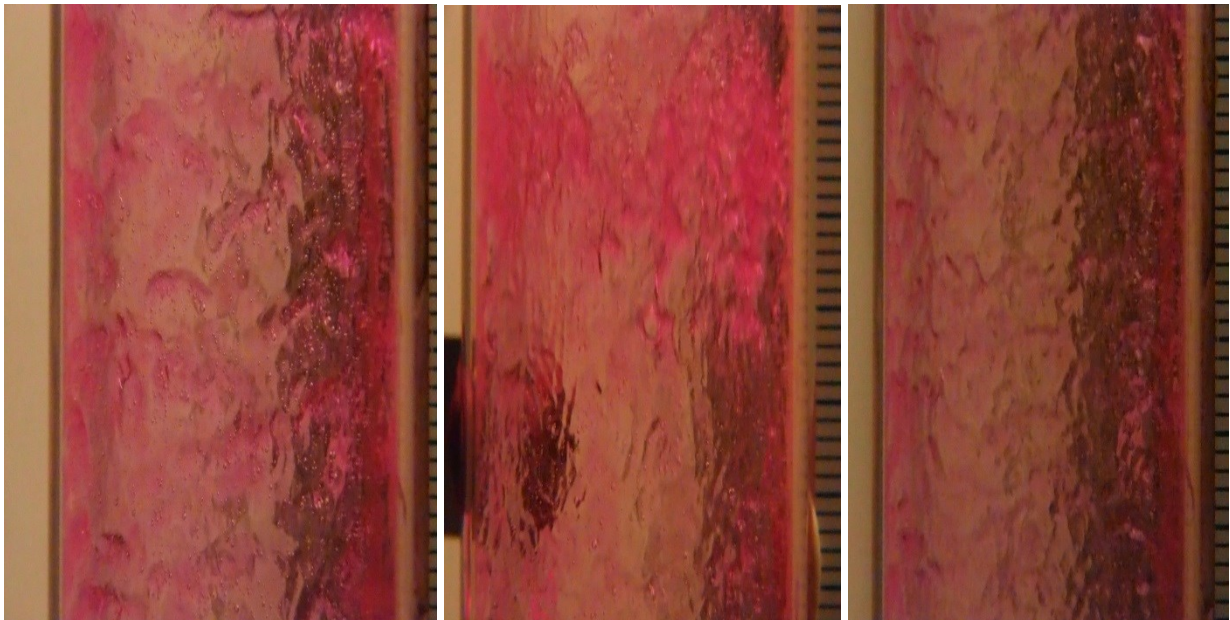


Figure 4-10 Images taken with high speed camera at 40 LPH of liquid flow rate and at 900, 1100 and 1300 SLPM of gas flow rates

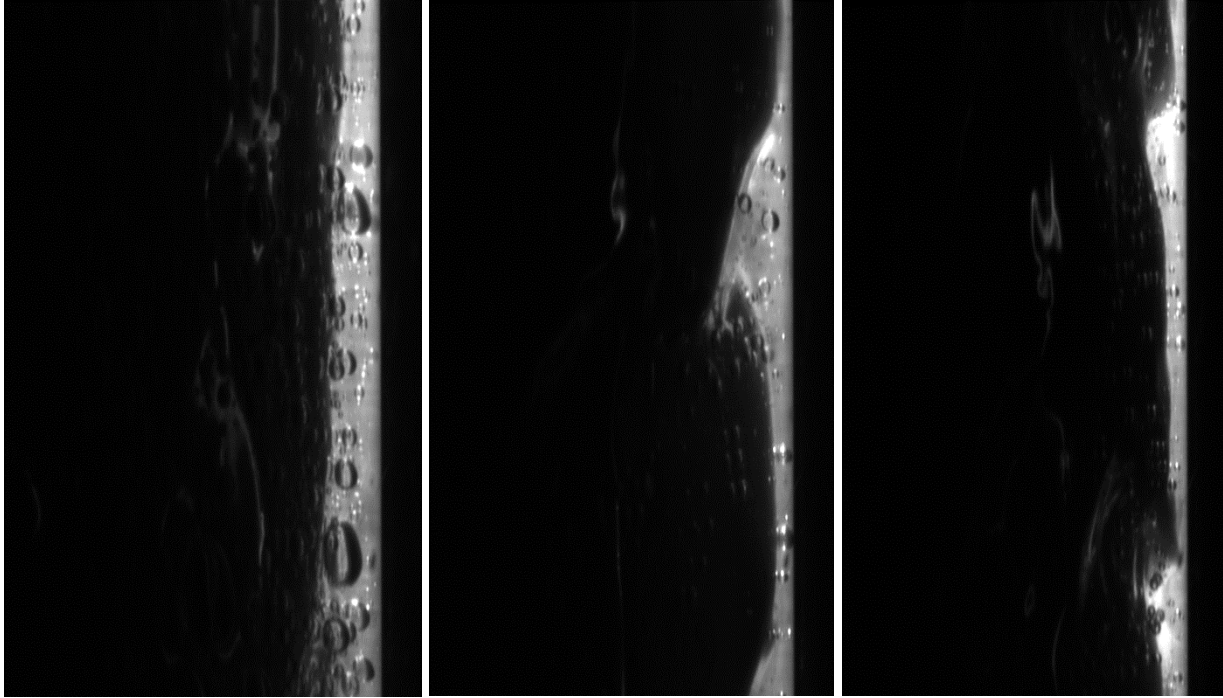


Figure 4-11 Images taken with laser offset at 40 LPH of liquid flow rate and at 600, 900 and 1200 SLPM of gas flow rates

With increasing liquid flow rate film gets thicker and entrainment volume is higher. Disturbance waves can be observed. Air bubble concentration increases. Similar to entrained droplet size, size of bubbles decreases with increasing gas rate.



Figure 4-12 Images taken with high speed camera at 60 LPH of liquid flow rate and at 800, 900 and 1100 SLPM of gas flow rates

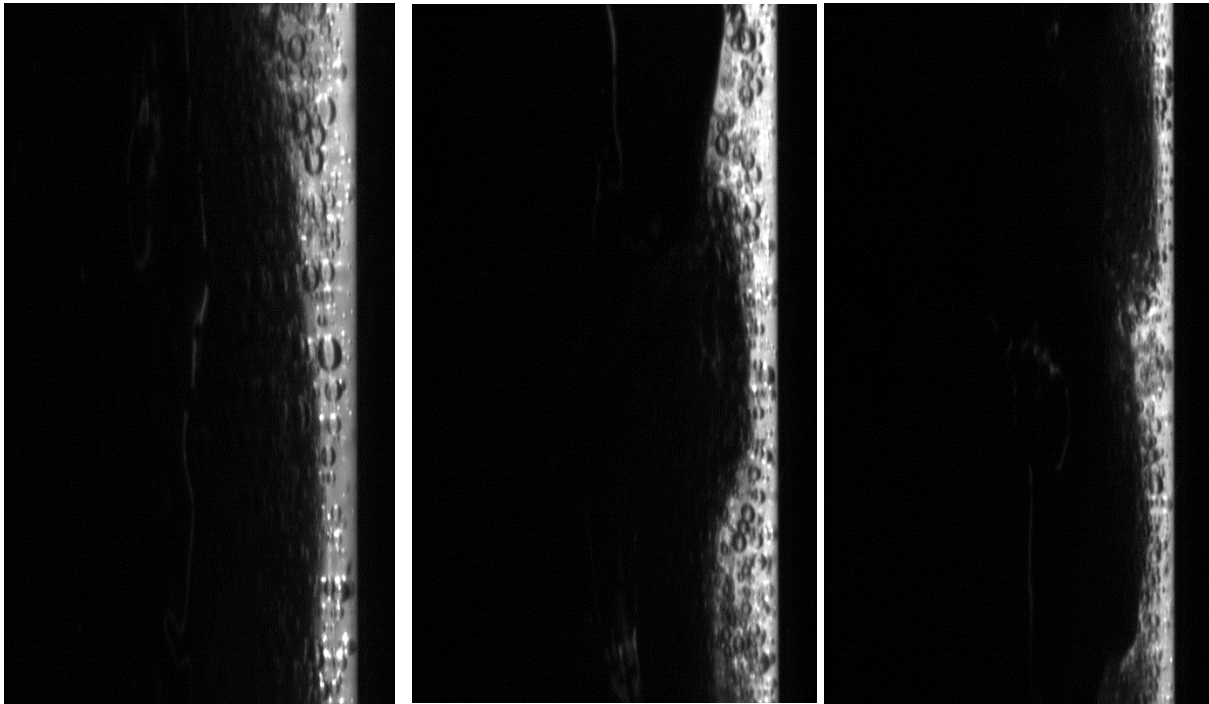


Figure 4-13 Images taken with laser offset at 60 LPH of liquid flow rate and at 600, 900 and 1200 SLPM of gas flow rates

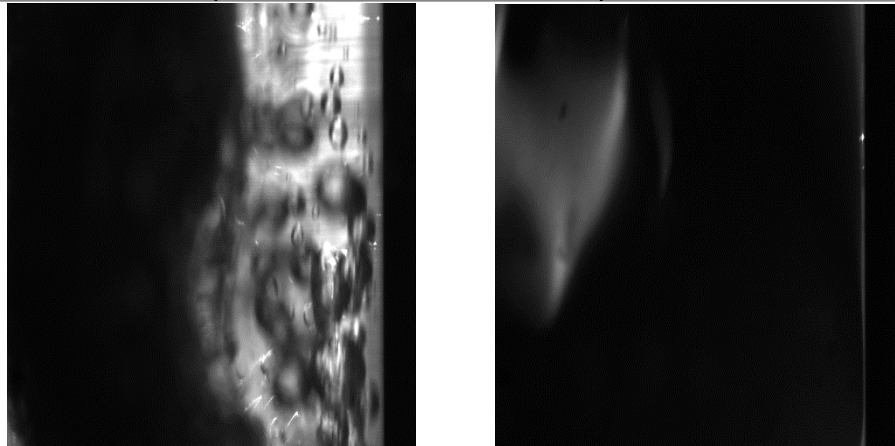
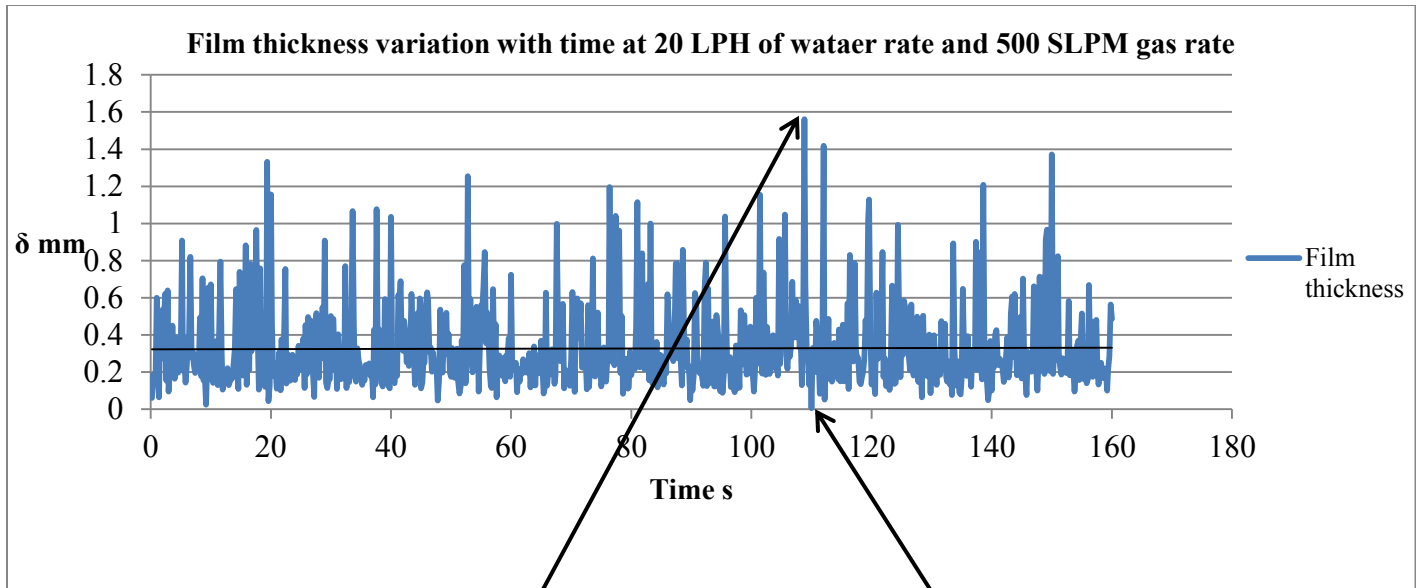


Figure 4-14 Film thickness variation during recording

Film thcikness varies significantly during annular flow. At low gas rates the ratio between maximim and minimum film thickness is significant at can be as high as 500 times.

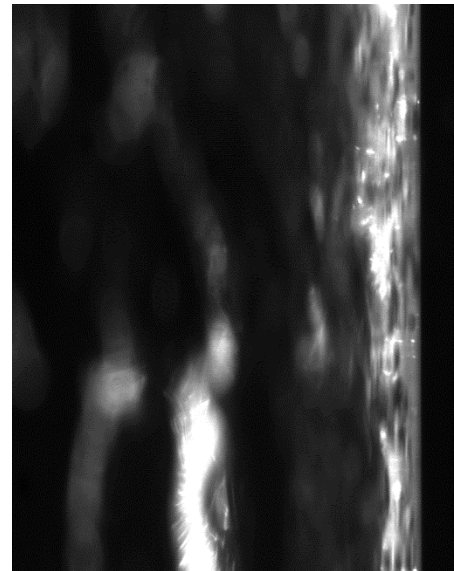
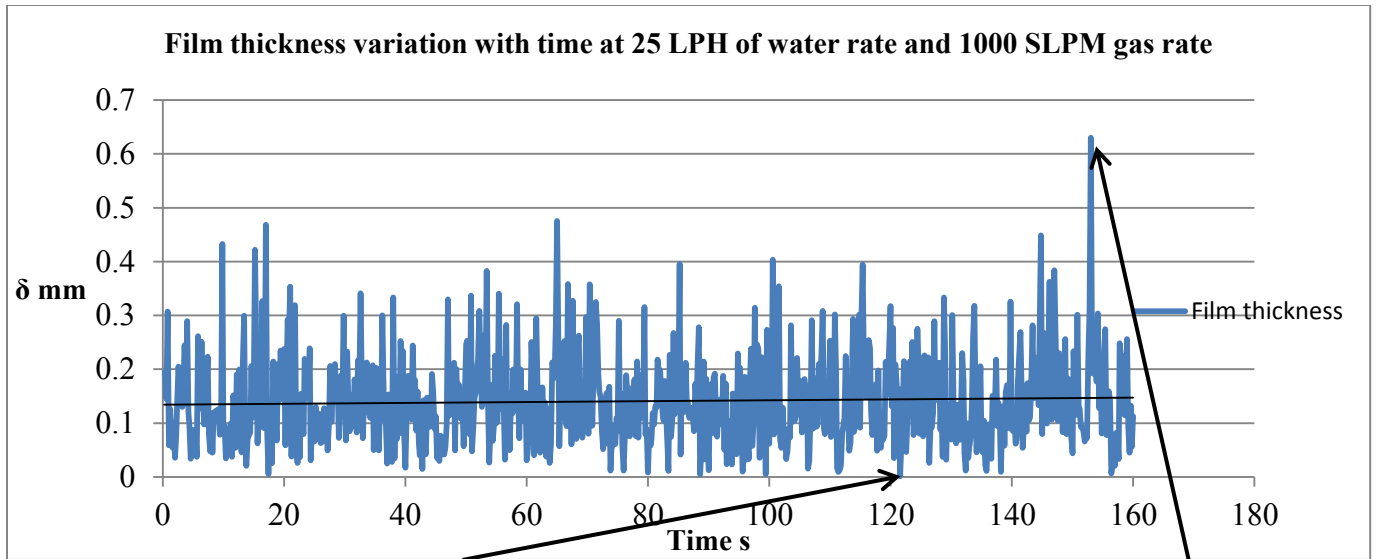


Figure 4-15 Film thickness variation during recording

4.3 Correction number

Correction number is number obtained from dividing film thickness values from two different PLIF setups. Film thickness values obtained with laser aligned with center of the pipe are assumed to be correct. Film thickness values that were obtained at 20, 25, 30 LPH of water rate are compared against images at same flow rates when laser was moved away from the center closer to the camera.

Table 4-2: Film thickness values obtained when laser was in the center of tube

Liquid flow rate LPH	20	25	30
Gas flow rate SLPM	Film thickness mm		
500	0.335	0.349	0.365
600	0.258	0.273	0.286
700	0.212	0.231	0.244
800	0.171	0.188	0.213
900	0.156	0.168	0.188
1000	0.134	0.144	0.156
1100	0.110	0.124	0.132
1200	0.088	0.103	0.111
1300	0.072		
1400	0.064		

Table 4-3: Film thickness values obtained when with laser offset

Liquid flow rate LPH	20	25	30
Gas flow rate SLPM	Film thickness mm		
500	0.790	0.850	0.867
600	0.707	0.744	0.799
700	0.628	0.710	0.707
800	0.598	0.629	0.657
900	0.545	0.589	0.640
1000	0.499	0.527	0.567
1100	0.468	0.514	0.562
1200	0.438	0.486	0.530
1300	0.419		
1400	0.405		

Each film thickness value is divided by corresponding film thickness value (laser in the center) in order to obtain ratio of difference between two setups at given liquid and gas flow rate.

Table 4-4: Correction numbers

Liquid flow rate LPH	20	25	30
Gas flow rate SLPM	Correction numbers		
500	2.361	2.433	2.375
600	2.738	2.728	2.790
700	2.959	3.079	2.899
800	3.496	3.352	3.079
900	3.507	3.501	3.407
1000	3.721	3.645	3.628
1100	4.257	4.136	4.252
1200	5.002	4.731	4.756
1300	5.834		
1400	6.364		

Correction numbers were calculated by dividing two set of values of film thickness from two different setups. Calculated ratio values are reasonably close and give a reason to obtain fit equation.

Fit equation ($y = 2E-06x^2 - 0.0005x + 2.2206$, y-correction number and x-gas flow rate) was obtained in Excel. Gas flow rate of 1500 SLPM was not recorded when laser was aligned with center of the tube. Correction number for it was interpolated using fit equation.

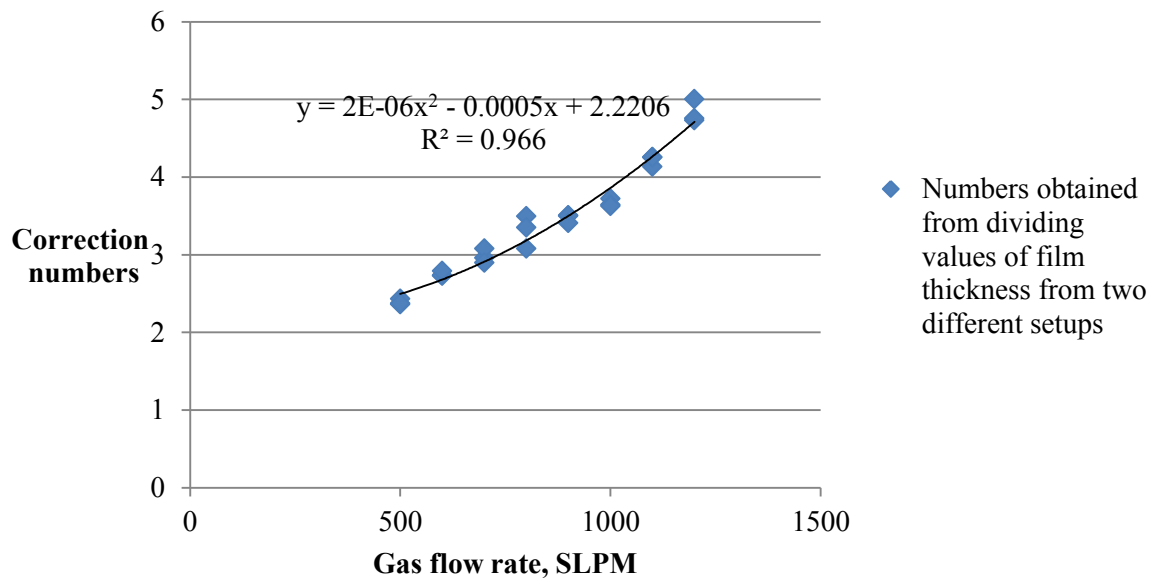


Figure 4-16 Correction number values with fit equation

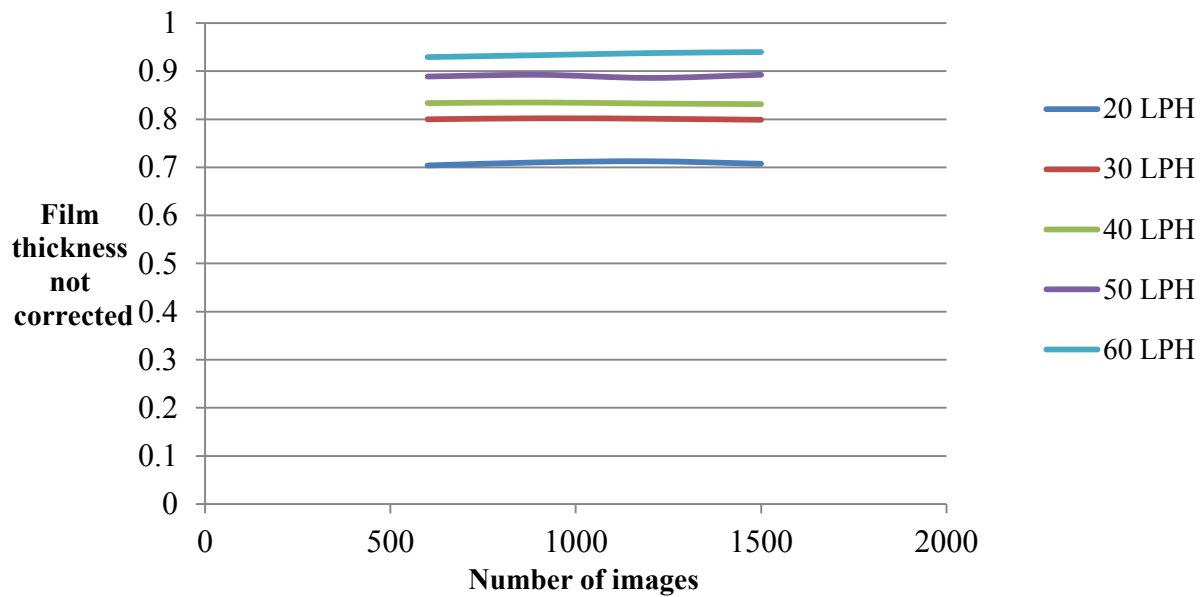


Figure 4-17 Film thickness variation with number images at 600 SLPM of gas rate and different liquid flow rates

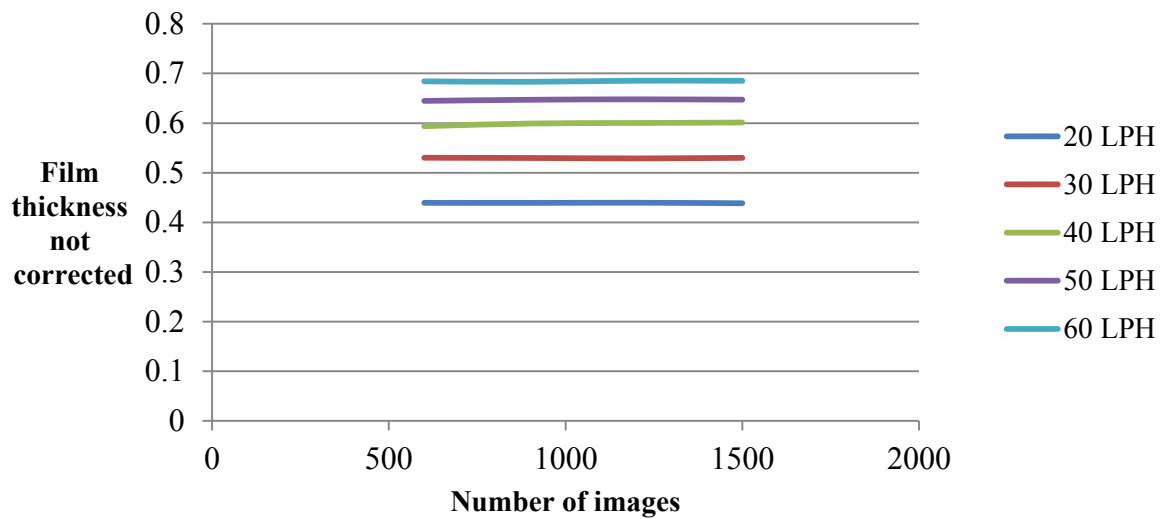


Figure 4-18 Film thickness variation with number images at 1200 SLPM of gas rate and different liquid flow rates

Film thickness dependence on number of images recorded was tested. Numbers were obtained at 600, 900, 1200 and 1500 images. As results show the variance between values is less than 1% which indicates that number of images does not affect film thickness values.

Table 4- 5: Film thickness values obtained after calculation with correction

U_{sg} m/s	16.24	19.43	22.55	25.94	29.08	32.21	35.30	38.37	41.52	44.61	47.69
U_{sl} m/s	Film thickness in mm										
0.011	0.334	0.258	0.212	0.171	0.156	0.134	0.110	0.088	0.072	0.063	0.063
0.014	0.349	0.273	0.231	0.187	0.168	0.144	0.124	0.103	0.093	0.081	0.070
0.016	0.365	0.286	0.244	0.213	0.188	0.156	0.132	0.111	0.104	0.089	
0.019	0.361	0.310	0.260	0.218	0.195	0.156	0.144	0.127	0.111		
0.022	0.369	0.315	0.266	0.227	0.210	0.167	0.154	0.133			
0.025	0.383	0.328	0.274	0.236	0.218	0.172	0.161	0.139			
0.028	0.393	0.338	0.289	0.243	0.225	0.182	0.168	0.144			
0.03	0.401	0.351	0.299	0.248	0.233	0.201	0.178	0.151			
0.033	0.410	0.356	0.312	0.266	0.238	0.206	0.179	0.152			

Table above presents final film thickness values after calculation with correction.

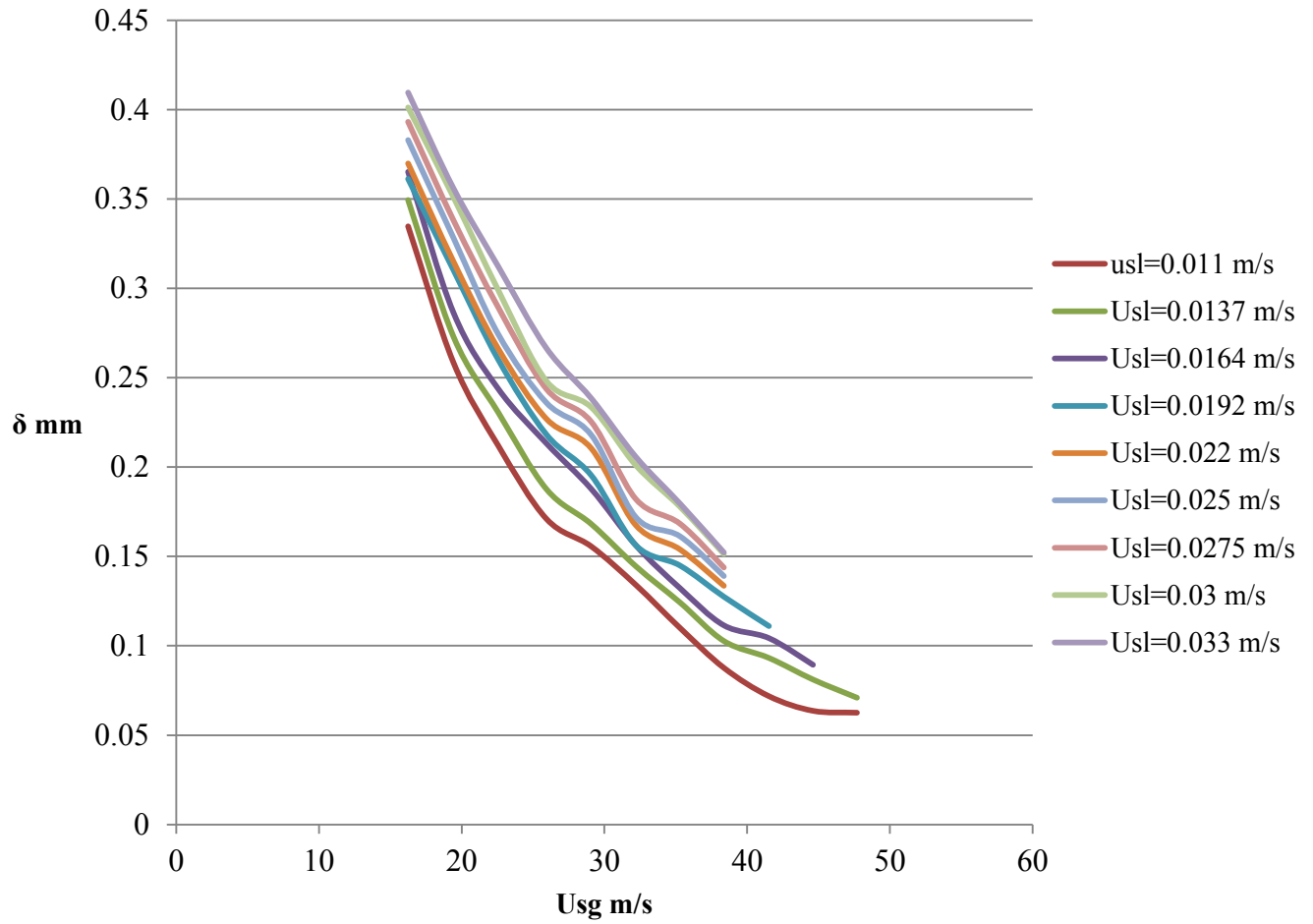


Figure 4-19 Film thickness values obtained from experiment

Table 4-6: Film thickness values (not corrected) to test repeatability of experiment (40 LPH of liquid rate)

Gas rate flow rate SLPM	500	600	800	1100
1	0.91393	0.83148	0.73177	0.62949
2	0.89441	0.82044	0.71453	0.66192
3	0.90835	0.82799	0.71639	0.63915

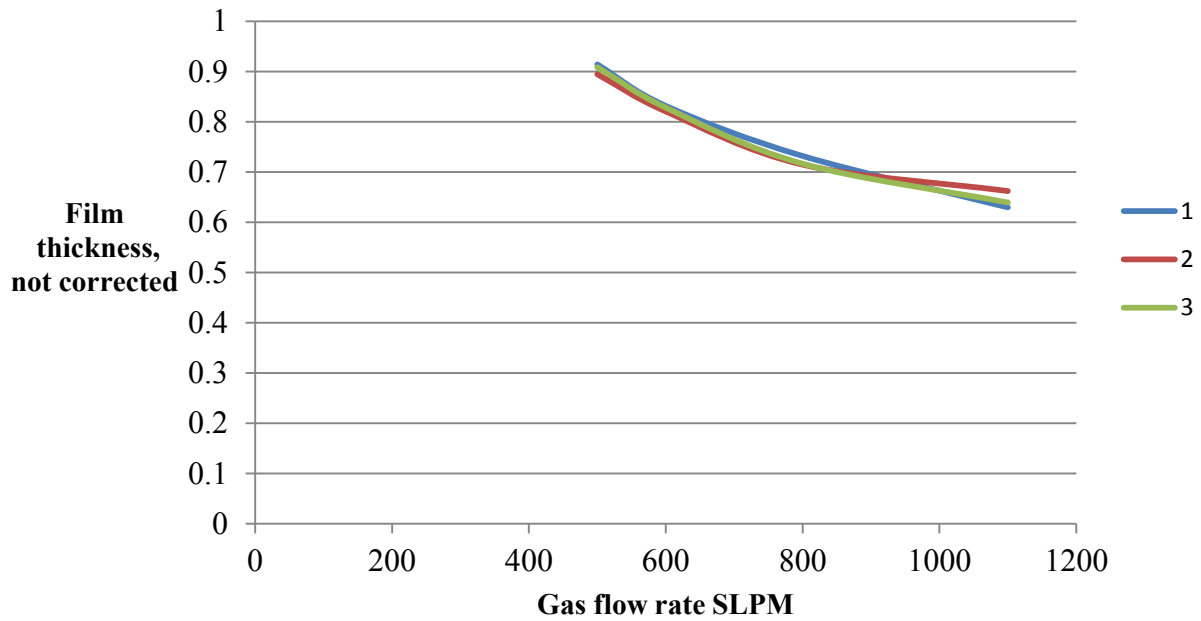


Figure 4-20 Data obtained from 3 different experimental runs at 40 LPH of water rate

Experiment repeatability was tested at 40 LPH and 500 to 1200 SLPM gas rates. The difference between three experiments was maximum 2-5 % at highest gas flow rates.

4.4 Comparison with theoretical models

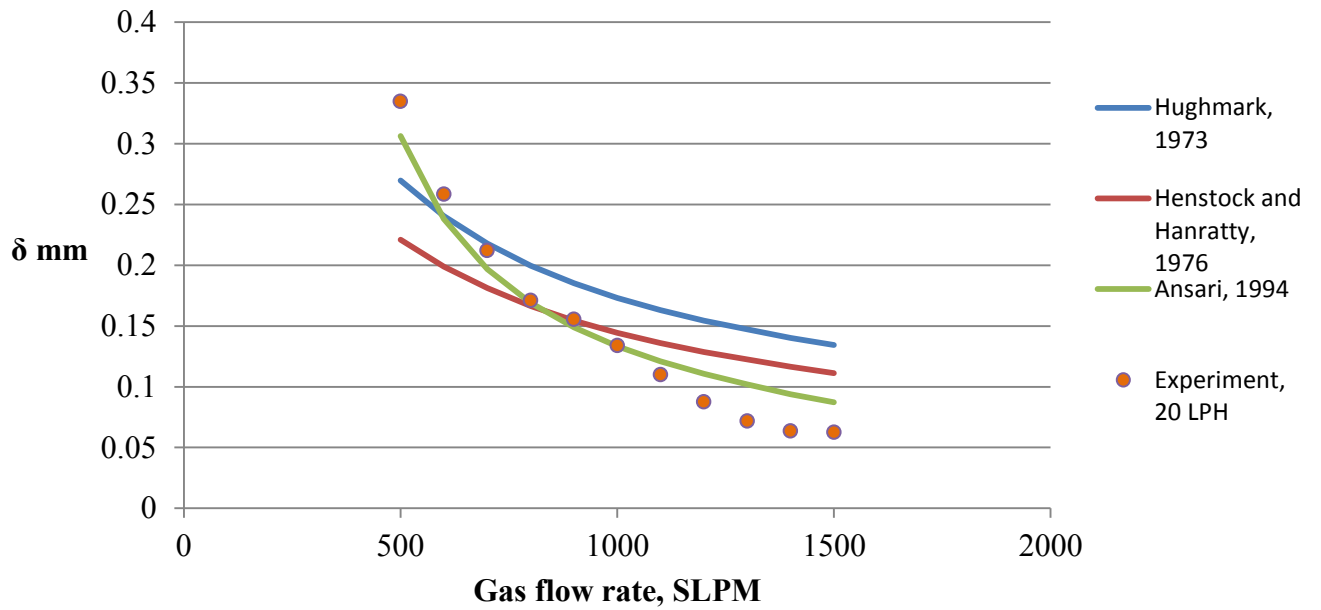


Figure 4-21 Comparison of experimental results at 20 LPH of liquid rate with three models

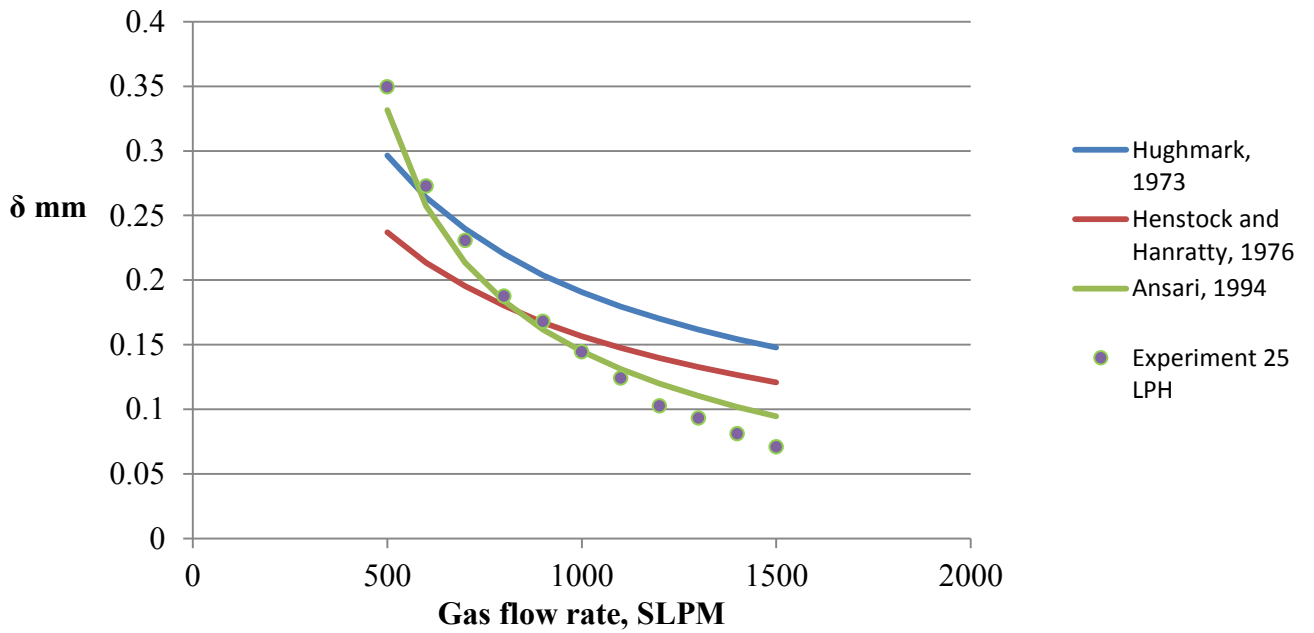


Figure 4-22 Comparison of experimental results at 25 LPH of liquid rate with three models

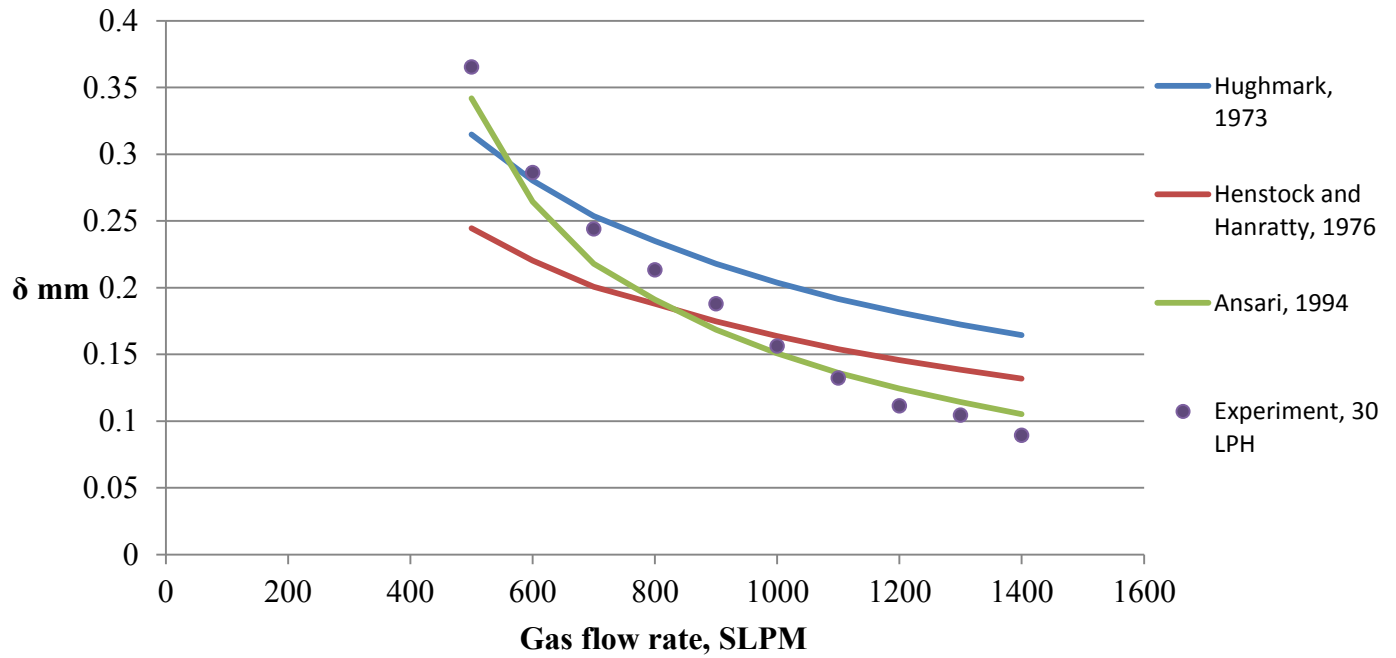


Figure 4-23 Comparison of experimental results at 30 LPH of liquid rate with three models

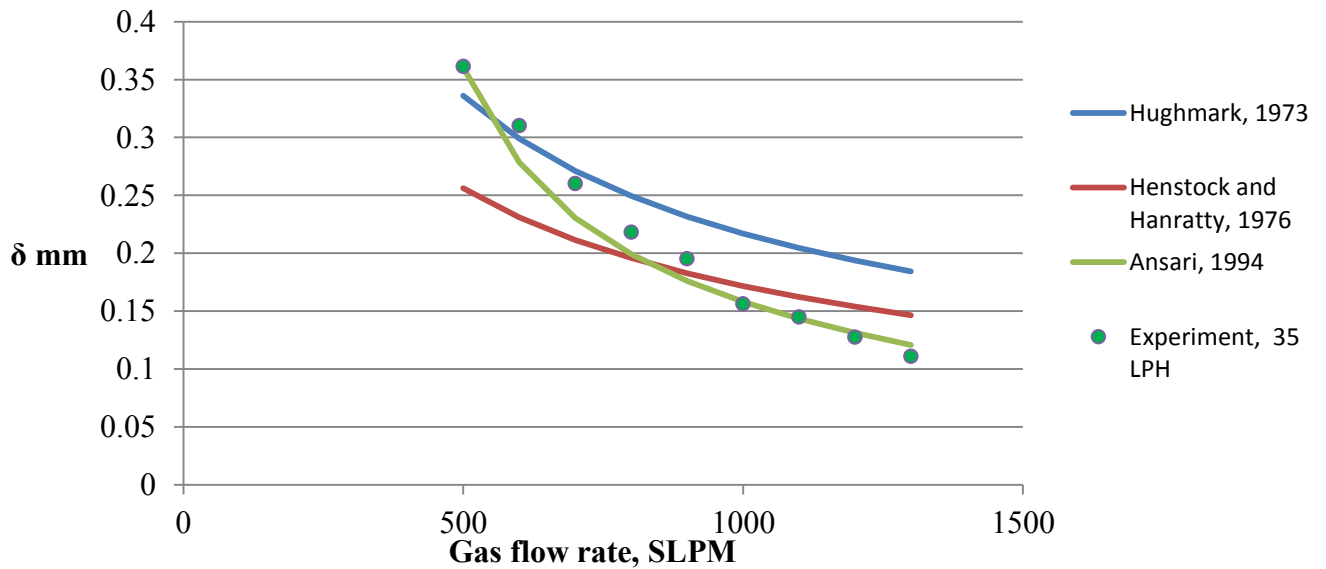


Figure 4-24 Comparison of experimental results at 35 LPH of liquid rate with three models

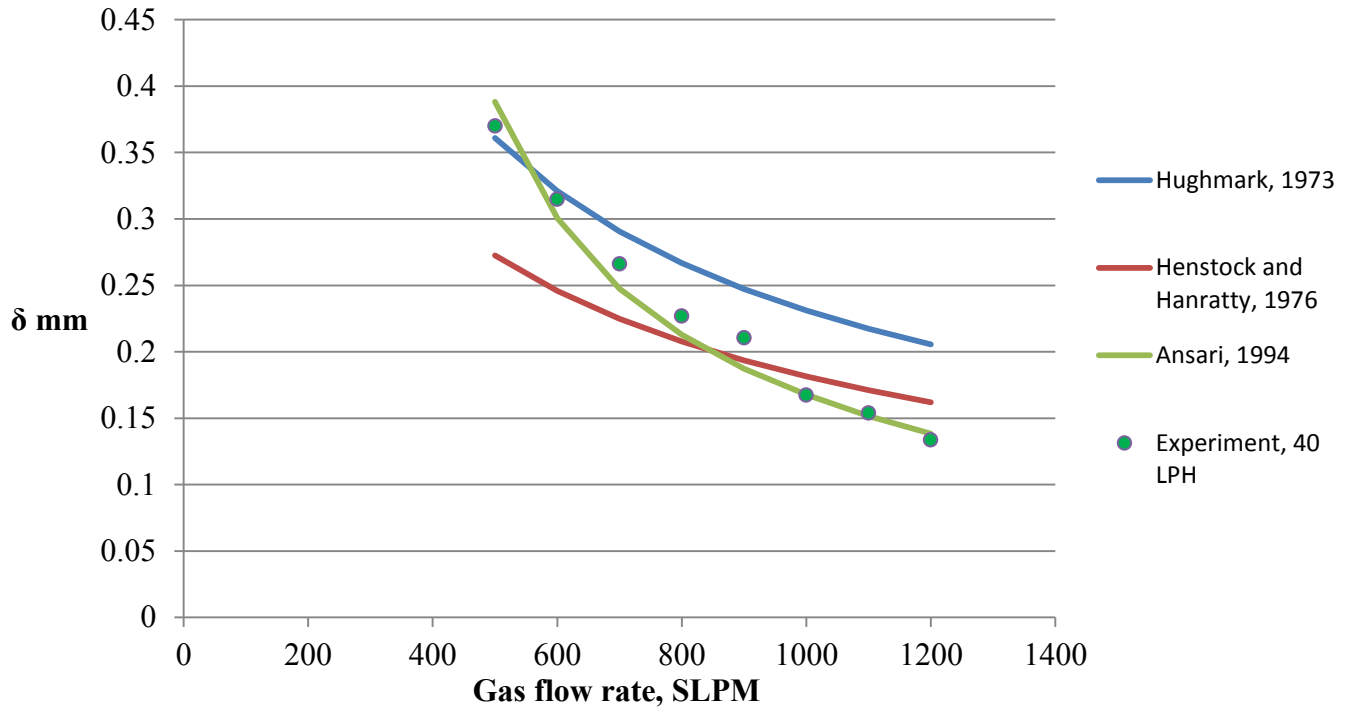


Figure 4-25 Comparison of experimental results at 40 LPH of liquid rate with three models

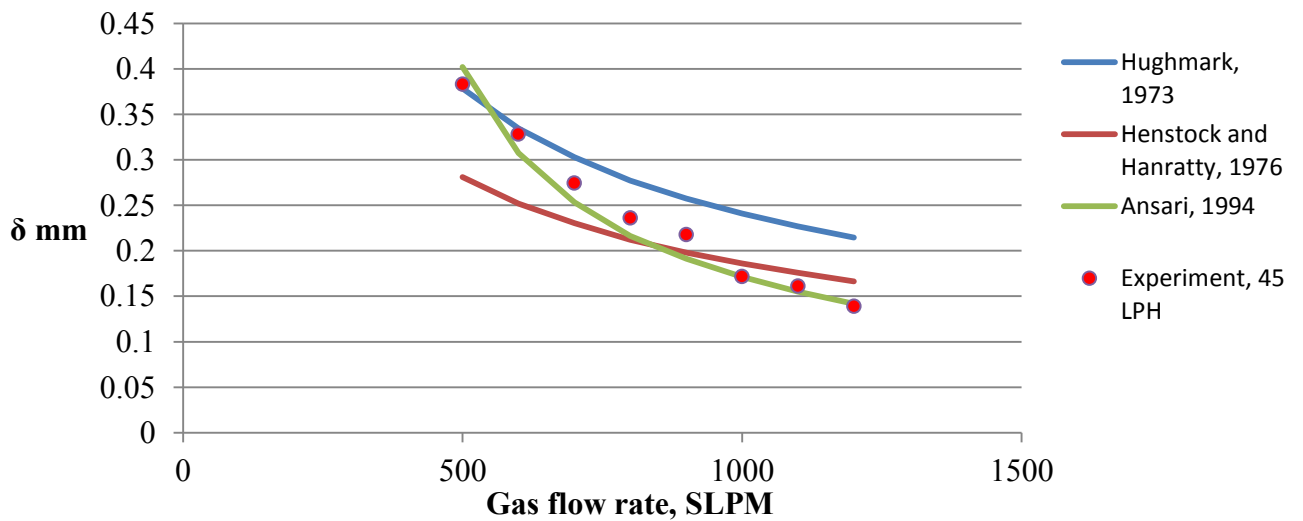


Figure 4-26 Comparison of experimental results at 45 LPH of liquid rate with three models

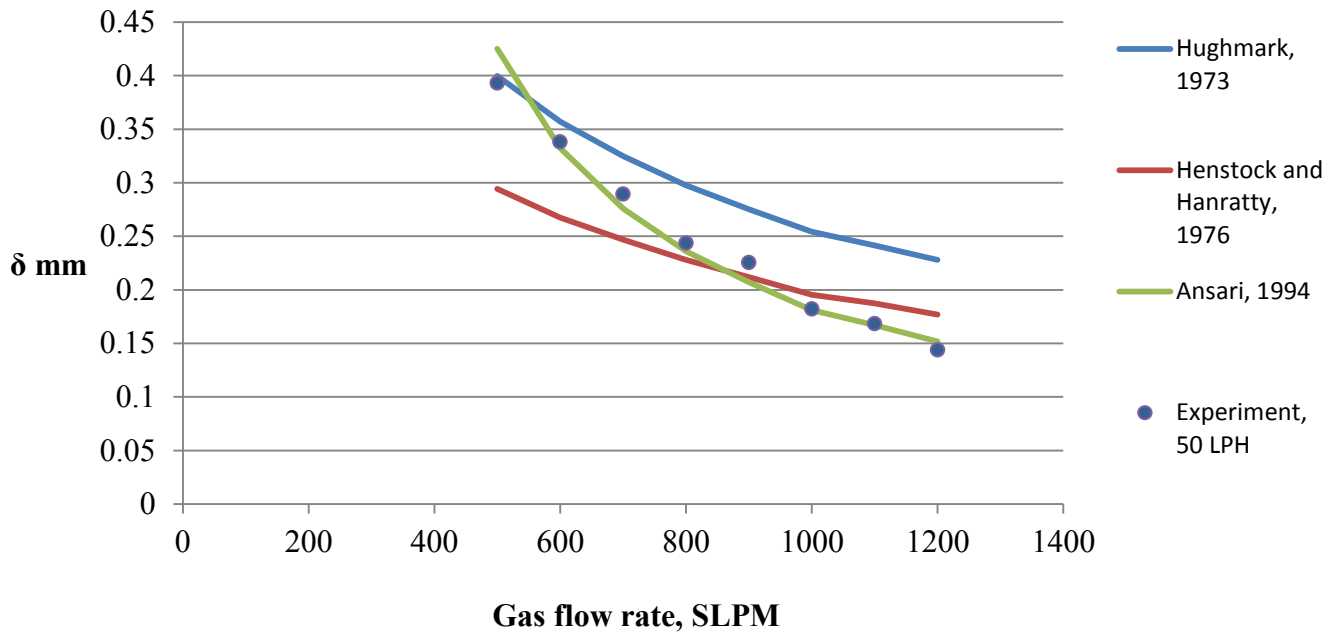


Figure 4-27 Comparison of experimental results at 50 LPH of liquid rate with three models

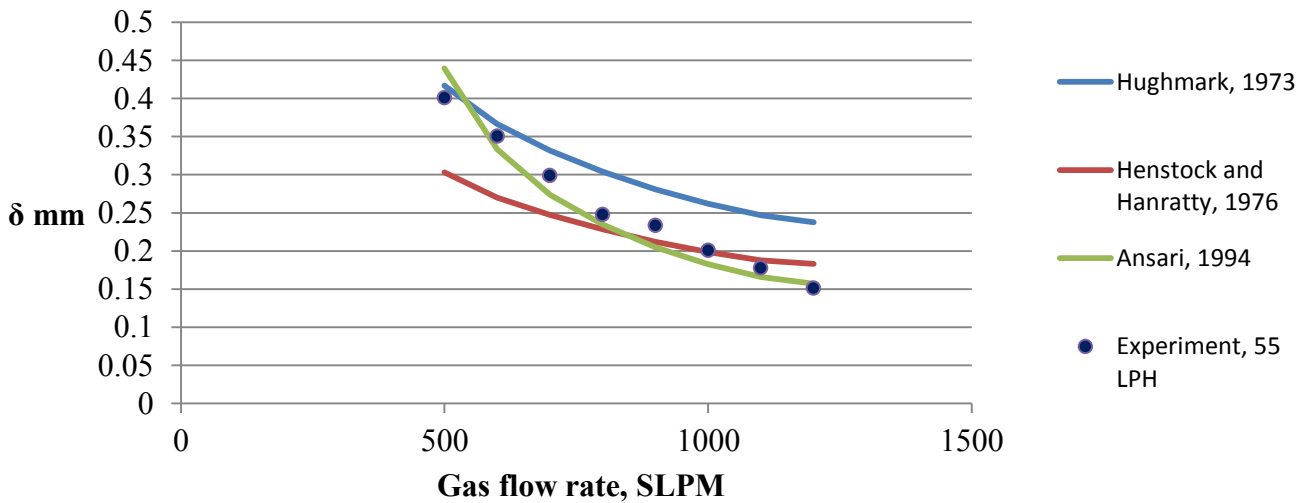


Figure 4-28 Comparison of experimental results at 55 LPH of liquid rate with three models

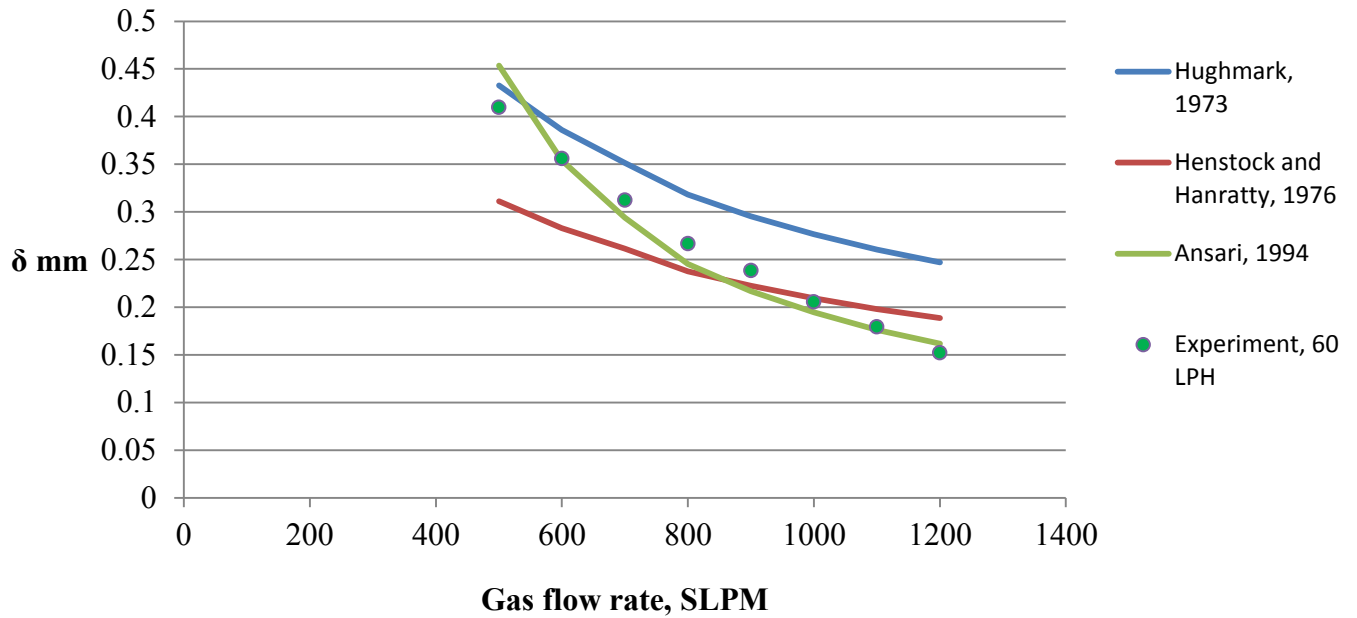


Figure 4-29 Comparison of experimental results at 60 LPH of liquid rate with three models

When compared to models that predict film thickness and pressure drop most accurate one was the Ansari model. As it was visually confirmed it predicted closely entrainment comparing to other two. Recorded film thickness values were maximum 10 % off from the model. Whereas Hughmark model give satisfactory prediction at low liquid flow rates but with increasing liquid rate results considerably diverged. Henstock and Hanratty model gave lower liquid film thickness at low liquid flow rates and higher liquid film thickness at high liquid flow rates when compared to experimental data.

4.5 Comparison with experimental data from literature

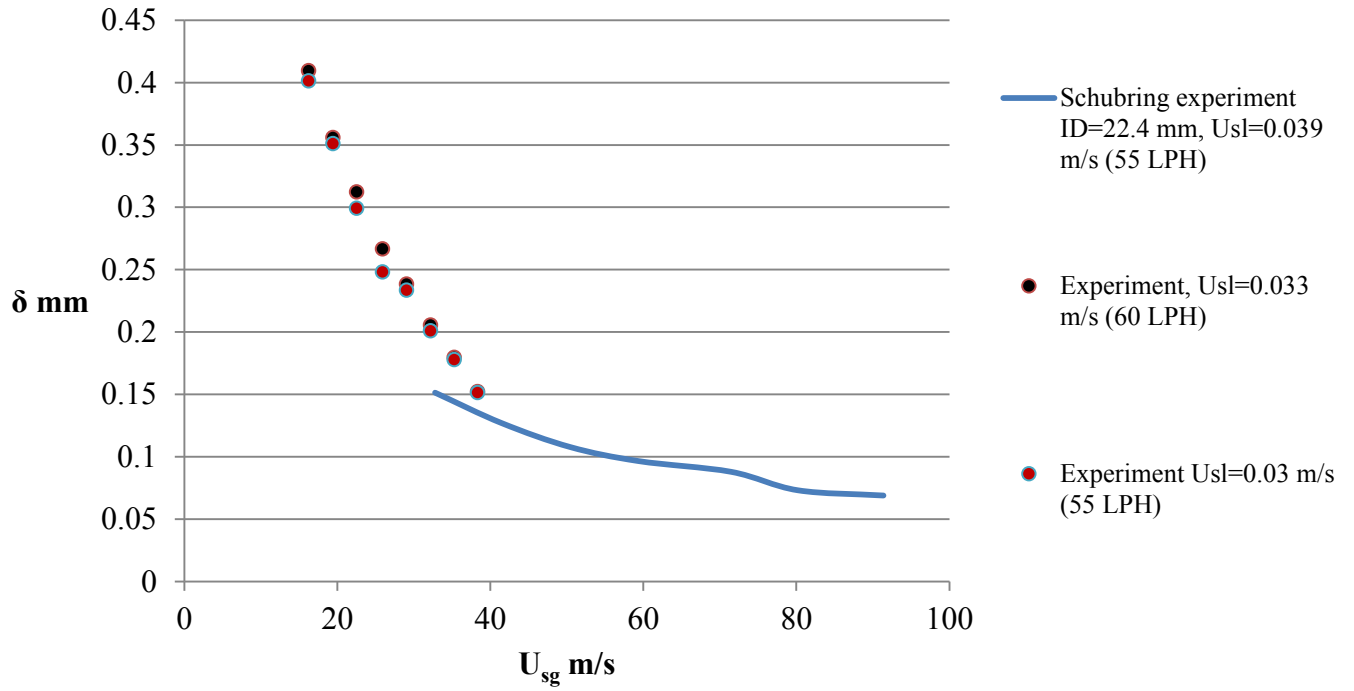


Figure 4-30 Comparison of calculated film thickness values with experimental data from literature, Schubring [35], tube ID=22.4 mm

Film thickness values follow similar trend when compared to data from Schubring [35]. The test section in their experiment was made from 22.4 ID FEP tube.

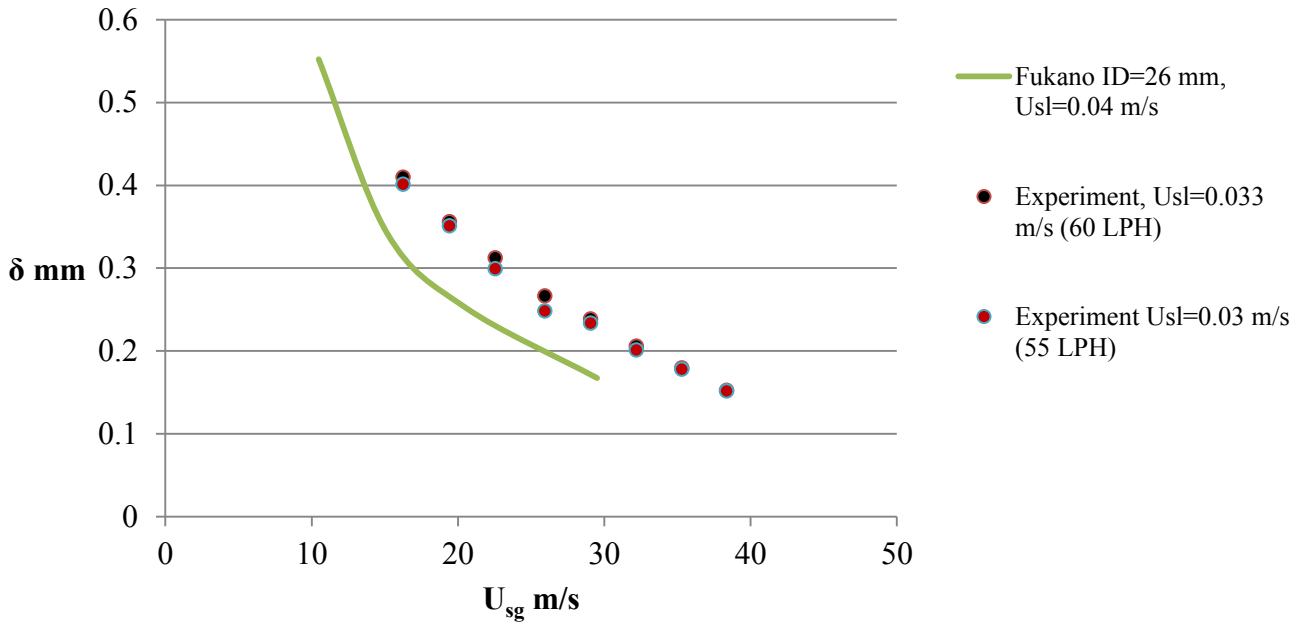


Figure 4-31 Comparison of calculated film thickness values with experimental data from literature, Fukano [26], tube ID=26 mm

Lowest superficial velocity in experiment of Fukano [26] is 0.04 m/s which is close to 80 LPH of water rate. Results obtained from current experiment are on average 25 % higher than Fukano experimental results. It might be explained by few reasons. Development section in current experiment is 108 L/D where in Fukano's experiment 133. Air injector type also might have affected film thickness as in current experiment the holes were drilled on the side of injector whereas in Fukano's experiment is it vertical holes.

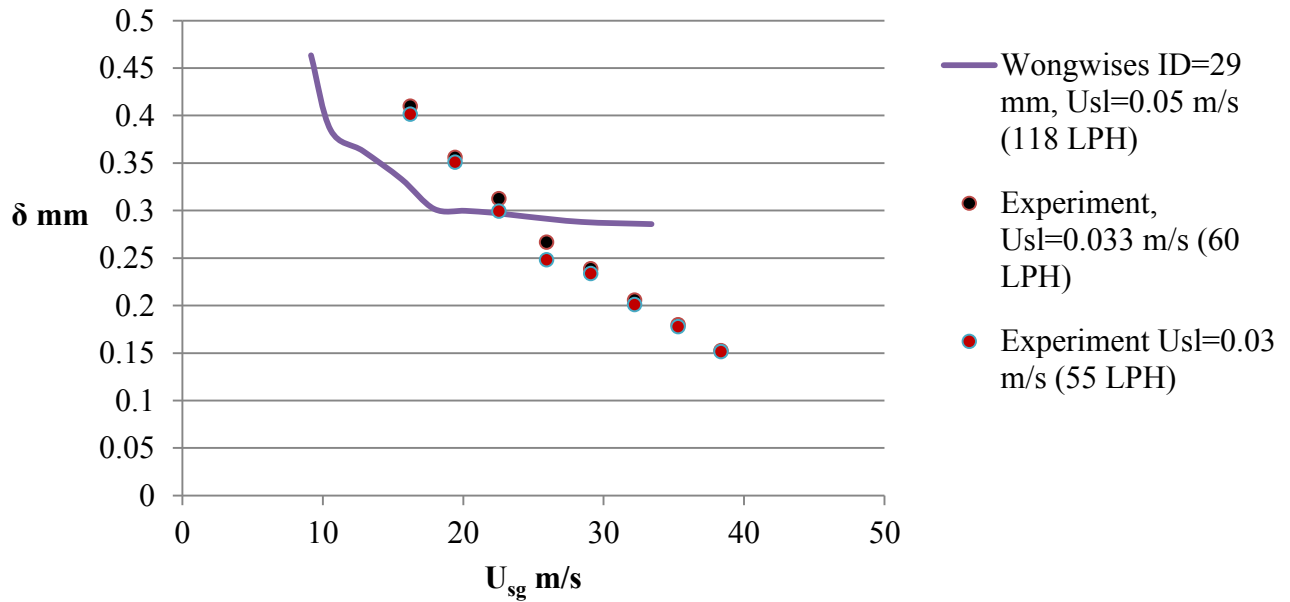


Figure 4-32 Comparison of calculated film thickness values with experimental data from literature, Wongwises [36], tube ID=29 mm

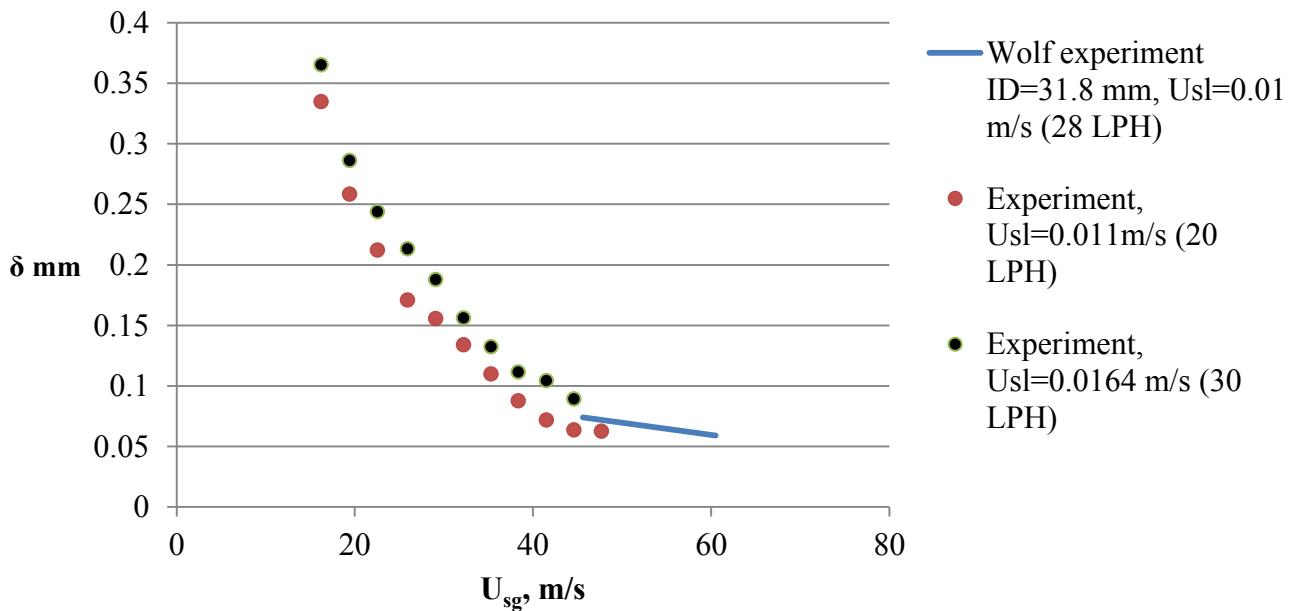


Figure 4-33 Comparison of calculated film thickness values with experimental data from literature, Wolf [24] tube ID=31.8 mm

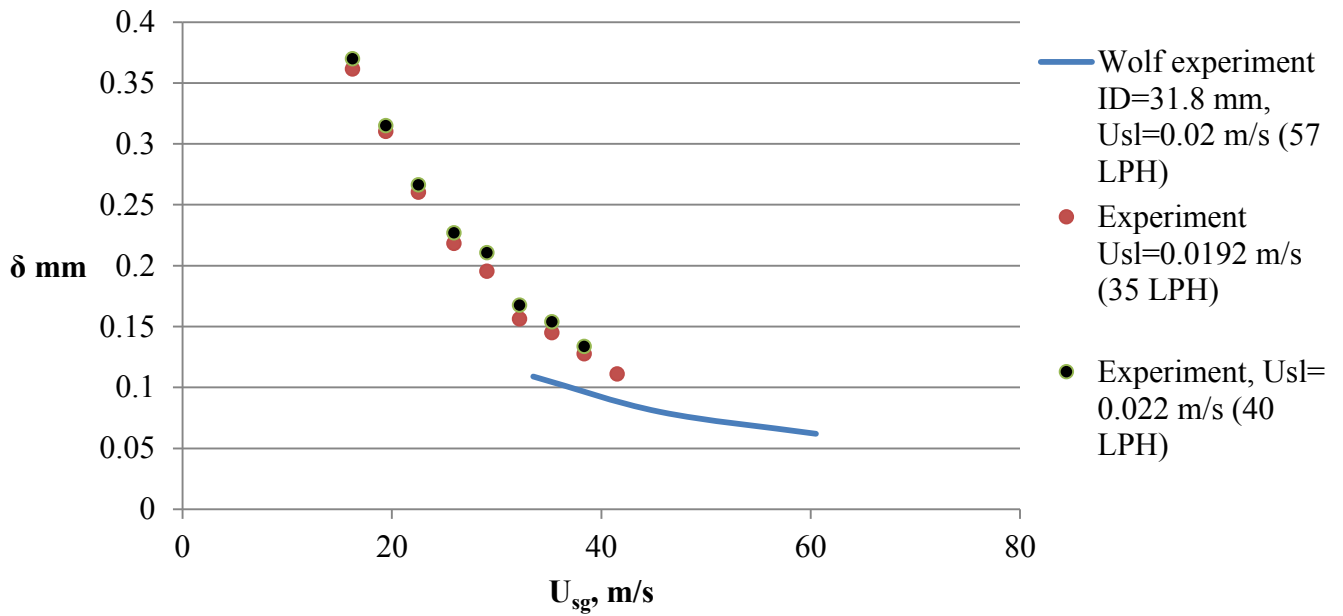


Figure 4-34 Comparison of calculated film thickness values with experimental data from literature, Wolf [24] tube ID=31.8 mm

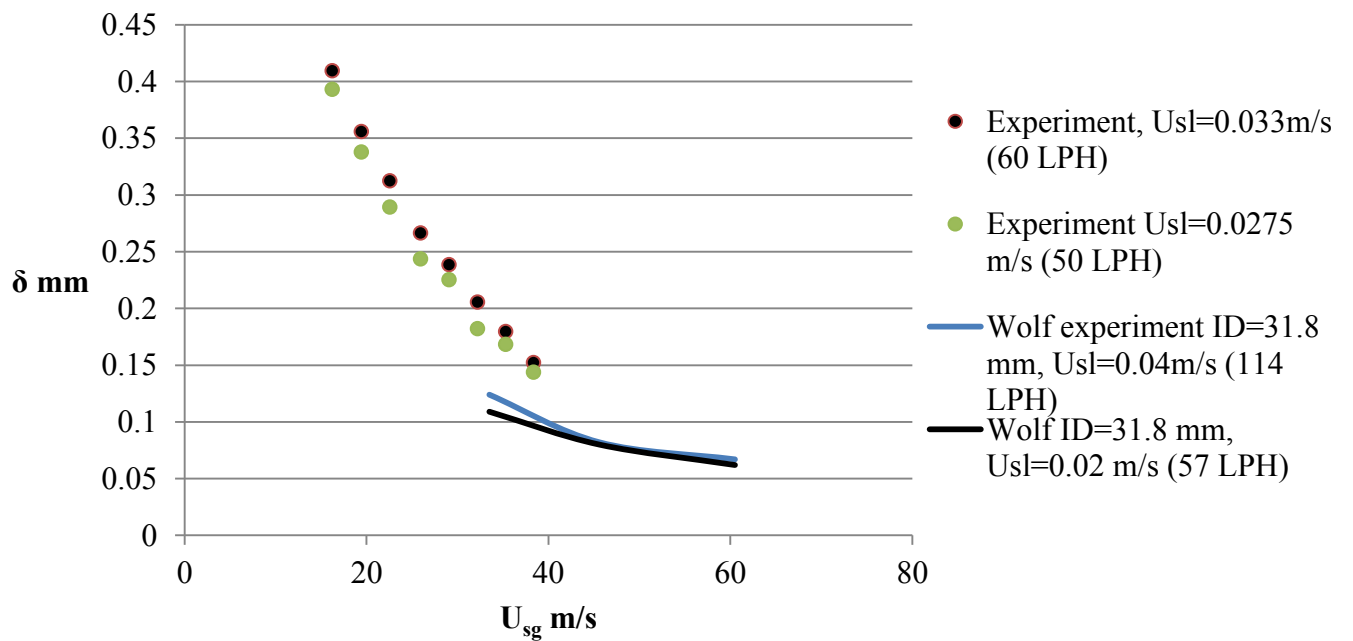


Figure 4-35 Comparison of calculated film thickness values with experimental data from literature, Wolf [38] tube ID=31.8 mm

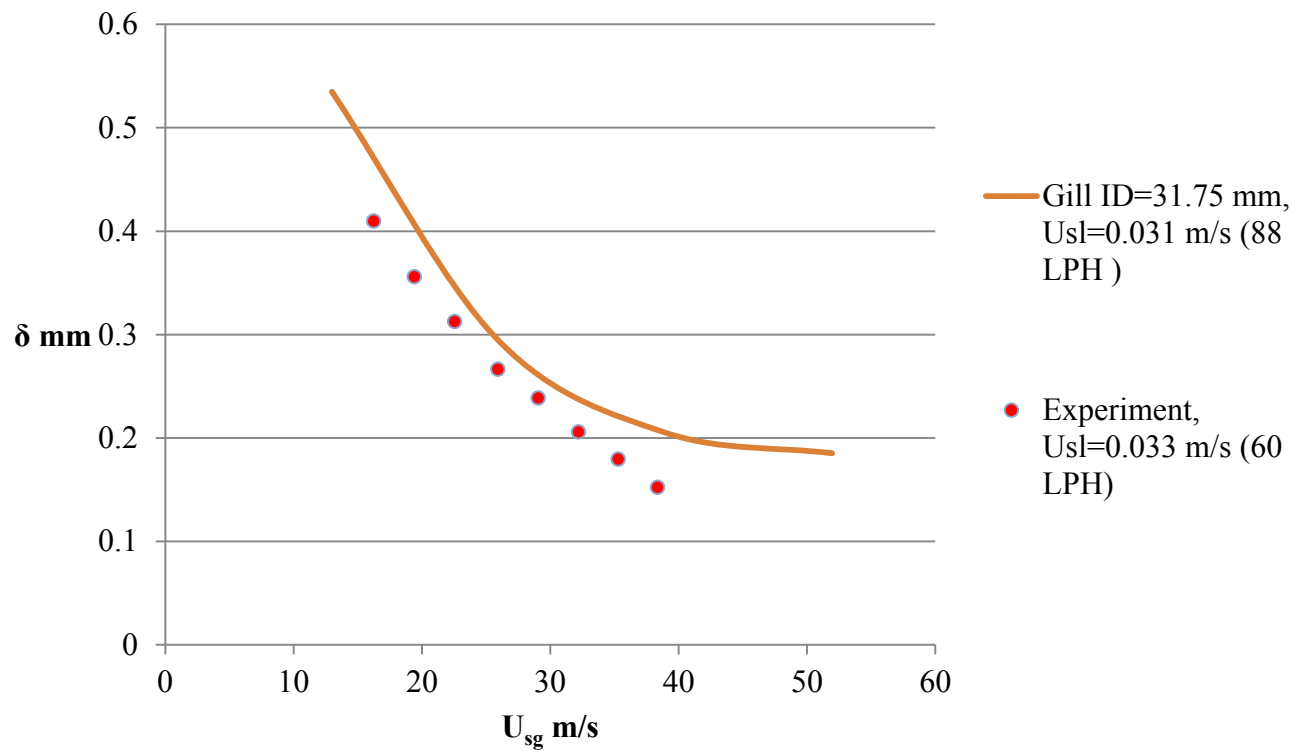


Figure 4-36 Comparison of calculated film thickness values with experimental data from literature Gill [14] tube ID =31.75 mm

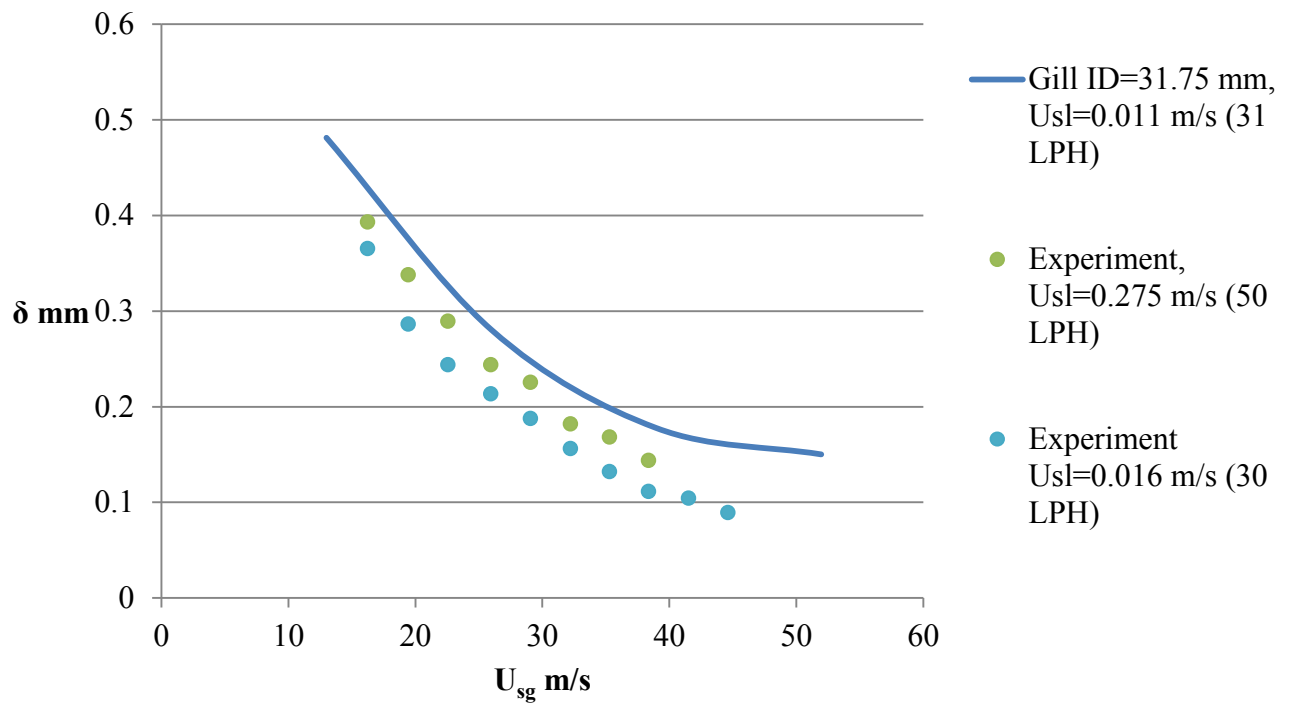


Figure 4-37 Comparison of calculated film thickness values with experimental data from literature Gill, (1963) [14], ID =31.75 mm

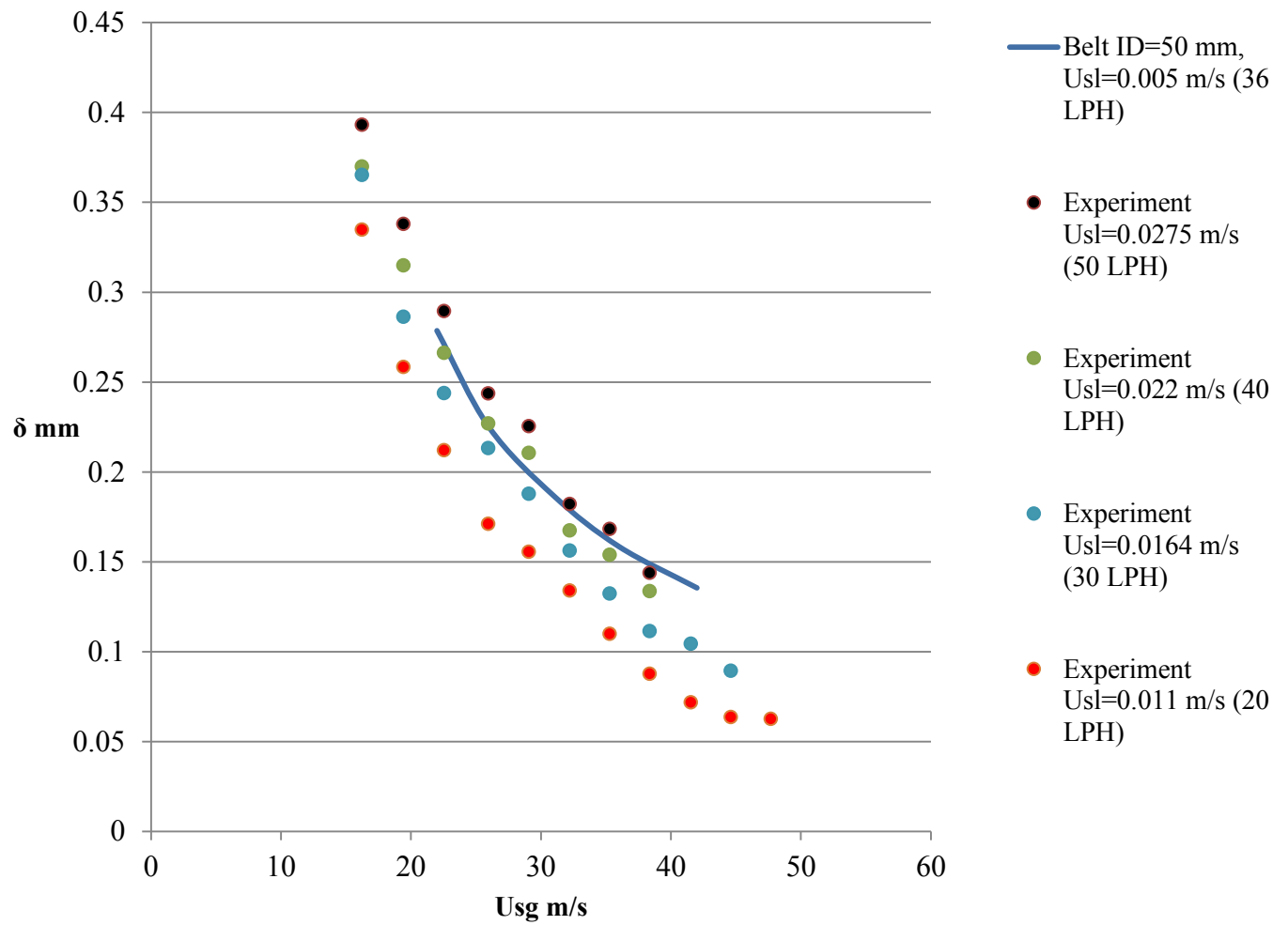


Figure 4-38 Comparison of calculated film thickness values with experimental data from literature Belt [37] tube ID =50 mm

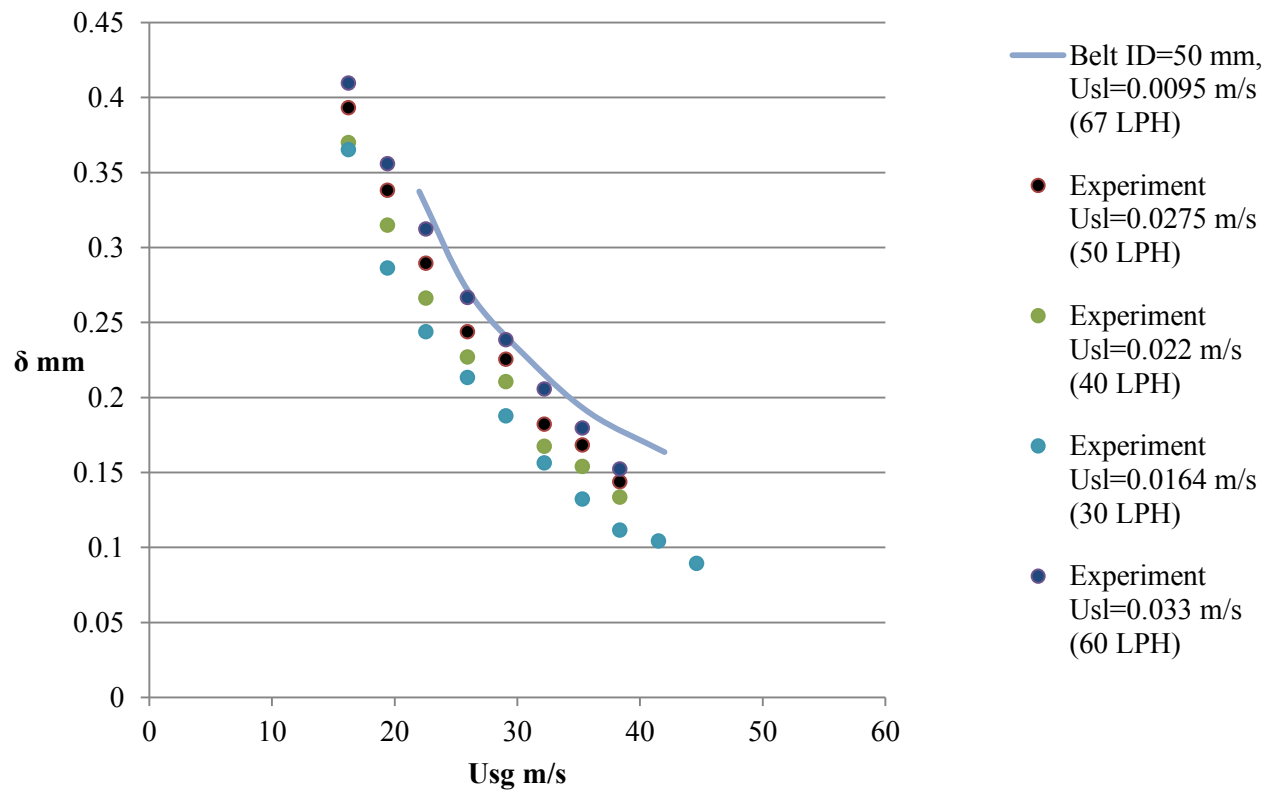


Figure 4-39 Comparison of calculated film thickness values with experimental data from literature Belt [37] tube ID =50 mm

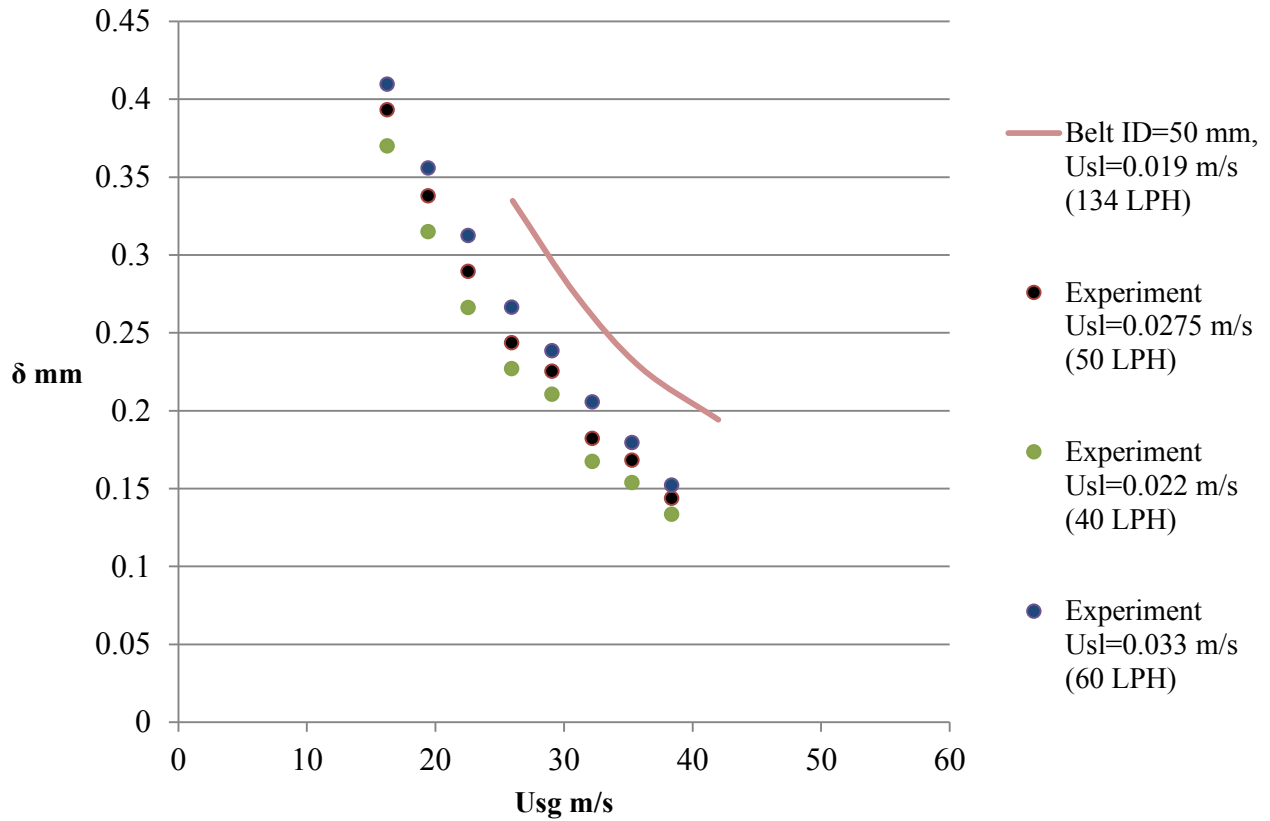


Figure 4-40 Comparison of calculated film thickness values with experimental data from literature Belt [37] tube ID =50 mm

Overall when compared to experimental data from literature current datum is reasonably close in values. Divergence in results might be explained by several factors as air and water injection type, pressure inside of the tube, development length of experimental setup and accuracy of used instrument.

4.6 Sensitivity analysis

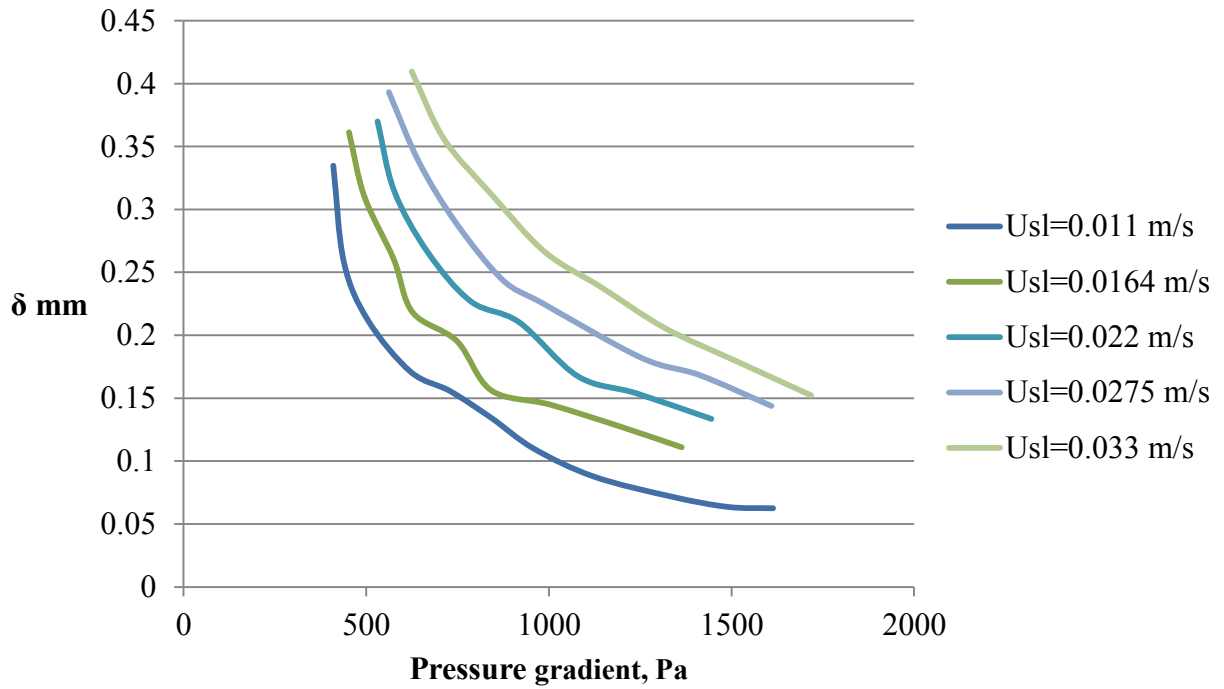


Figure 4-41 Film thickness variation with pressure drop

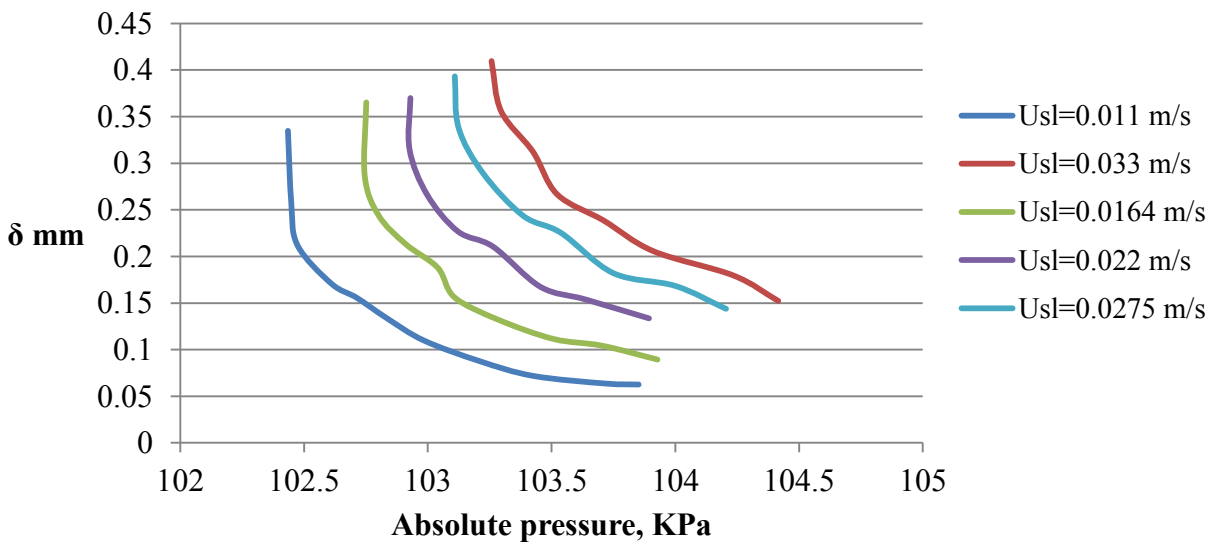


Figure 4-42 Pressure vs film thickness

Film thickness decreases with increasing pressure drop.

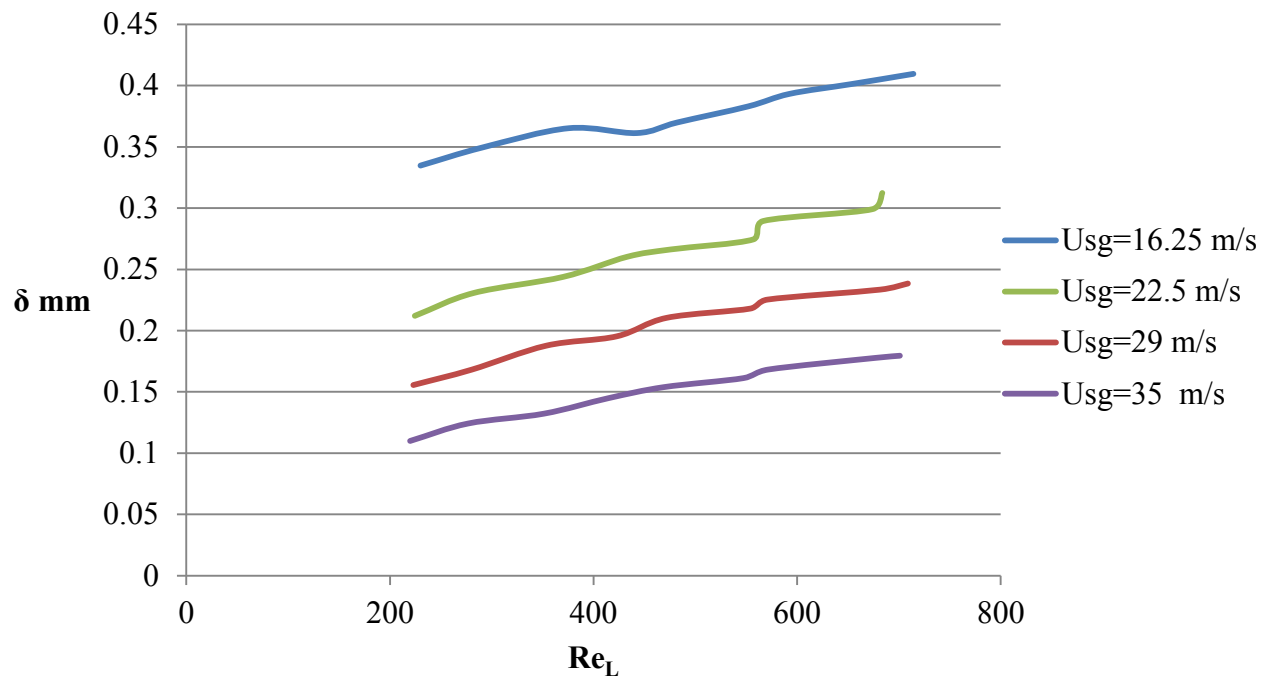


Figure 4-43 Film thickness sensitivity to liquid Reynolds number

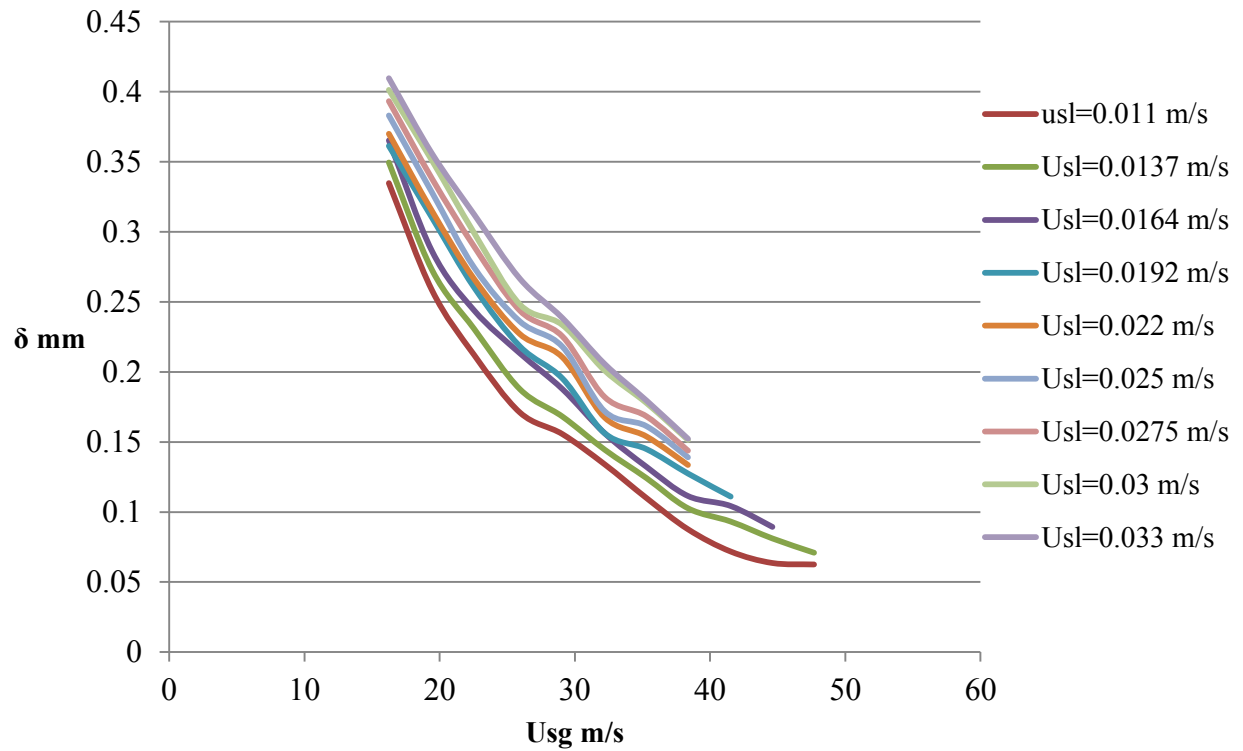


Figure 4-44 Film thickness variation with gas flow rate

Film thickness variation is strongly dependant on gas flow rate. The decrease is sharp when superficial gas velocity goes from 16 m/s to 19 m/s and then steady gradual decline with increasing gas flow rate and magnitude of variation decreases with increasing gas flow rate.

Chapter 5:

Conclusions and

Recommendations for Future

Works

5. Conclusion

- Film thickness increased with increasing liquid flow rate and decreased with increasing gas flow rate. The size of droplet entrained in the core flow decreased and droplet number density increased decreased with increasing gas flow rate.
- Obtained film thickness values were compared with experimental results from literature and was found to be reasonably close in values when compared to similar liquid and gas flow rates.
- Obtained experimental data was compared with three models. Ansari (1994) model was able to predict film thickness with 10 % uncertainty. It also accurately predicted the liquid and gas flow rates where entrainment occurs.
- Pressure drop values were compared to models. Divergence from models was on average around 25 %.

5.1 Recommendations for future work

- Liquid and air injection types needs to be tested in order to see the difference and their effect on measurable parameters like liquid film thickness, pressure drop and liquid film interfacial features.
- Entrained air bubble size can be investigated using PLIF.
- Investigation of entrained droplet size needs to be carried out.

6. References

- [1]. K.W. McQuilann and P.B. Whalley, 1985, "Flow patterns in vertical two phase flow" , International Journal Multiphase Flow Vol. 11, No 2, pp 161-175.
- [2]. G. H. Anderson and B. G. Mantzouranis, 1960, "Two-phase (gas-liquid) flow phenomena-I Pressure drop and hold-up for two-phase flow in vertical tubes", Chemical Engineering Science Vol.12, pp.109 to 126.
- [3]. G. H. Anderson and B. G. Mantzouranis, 1960, "Two-phase (gas-liquid) flow phenomena-II Liquid entrainment", Chemical Engineering Science Vol.12.
- [4]. G.W.Govier, B.A. Radford and J.S.C Dunn, 1957, "The Upward Vertical Flow of Air-Water Mictures I. Effect of Air and Water Rates on Flow Pattern, Holdup and Pressure drop", Canadian Journal of Chemical Engineering, August.
- [5]. G.W. Govier and W. Leigh Short ,1958, "The Upward Vertical Flow of Air-Water Mictures II. Effect of Tubing Diameter on Flow Pattern, Holdup and Pressure drop", Canadian Journal of Chemical Engineering, October.
- [6]. R. A. S. Brown, G. A. Suallivan and G. W. Govier, 1960, "The Upward Vertical Flow of Air-Water Mictures II. Effect of Gas Phase Density on Flow Pattern, Holdup and Pressure drop", Canadian Journal of Chemical Engineering, April.
- [7]. R. A. S. Brown, and G. W. Govier, 1961, "High-Speed Photography in the Study of Two-Phase Flow", Canadian Journal of Chemical Engineering, August.
- [8]. Cecil O. Carter and R.L. Huntington, 1961, "Concurrent Two-Phase Upward Flow of Air and Water Through an Open Vertical Tube and Through Annulus", Canadian Journal of Chemical Engineering, December.
- [9]. J.A.R. Bennet and J.D.Thornton, 1961, "Data on the vertical flow of air-water mixtures in the annular and dispersed flow regions. Part I: Preliminary study", TRANS. INSTN. Chem. ENGRS, Vol. 39.
- [10].J.G Collier and G.F.Hewitt , 1961, Data on the vertical flow of air-water mixtures in the annular and dispersed flow regions. Part II: Film thickness and entrainment data and analysis of pressure drop measurments", TRANS. INSTN. Chem. ENGRS, Vol. 39.

- [11]. N. Hall Taylor, G. F. Hewitt and P. M. C. Lacey, 1963, "The motion and frequency of large disturbance waves in annular two-phase flow of air-water mixtures", *Chemical Engineering Science*, Vol. 18.
- [12]. R. M. Nedderman and C. J. Shearer, 1963, "The motion and frequency of large disturbance waves in annular two-phase flow of air-water mixtures", *Chemical Engineering Science*, Vol. 18, pp. 661-670.
- [13]. L. E. Gill, G. F. Hewitt, J. W. Hitchon and P. M. C. Lacey, 1963, "Sampling probe studies of the gas core in annular two-phase flow-1 .The effect of length on phase and velocity distribution" *Chemical Engineering Science*, Vol. 18, pp.525-535.
- [14]. L. E. Gill, G. F. Hewitt, and P. M. C. Lacey, 1964, "Sampling probe studies of the gas core in annular two-phase flow-1 .Studies of the effect of phase flow rates on phase and velocity distribution" *Chemical Engineering Science*, Vol. 19, pp.665-682.
- [15]. W. Bennett, G. F. Hewitt, H. A. Kearsy, R. K. F. Keeys, and P. M. C. Lacey, 1965, "Flow Visualization studies of boiling at high pressure", *Proc Instn Mech Engrs* 1965-66, Vol. 180.
- [16]. Sze-Foo Chien and W. E. Trele, 1966, "Photographic study of the interfacial disturbances of liquid films in falling film flow and in vertical, downward annular two-phase flow", 1966, *Int. J. Heat Mass Transfer*. Vol 10. pp1016-1018.
- [17]. N. S. Hall Taylor and R. M. Nedderman, 1968, "The coalescence of disturbance waves in annular two phase flow", *Chemical Engineering Science*. Vol. 23, pp. 551-564.
- [18]. G. F. Hewitt, 1969 "Disturbance waves in annular two-phase flow", *Proc Instn Mech Engrs* 1969-70, Vol. 184.
- [19]. A. K. Jagota, E. Rhodes, and D. S. Scott, 1973 "Tracer Measurements in Two Phase Annular Flow to Obtain Interchange and Entrainment" ,*The Canadian Journal of Chemical Engineering*, Vol. 51.
- [20]. A. K. Jagota, E. Rhodes, and D. S. Scott, 1973 "Measurement of Residence Times, and Film and Drop Velocities in Two Phase Annular Flow" ,*The Canadian Journal of Chemical Engineering*, Vol. 51.
- [21]. J. C. B. Lopes, A. E. Dukler, 1986, "Droplet Entrainment in Vertical Annular Flow and Its Contribution to Momentum Transfer", *AIChE Journal*, Vol. 32, No. 9.
- [22]. G.F. Hewitt, 1987, "Experimental data set No.3: Developing annular flow", *Multiphase Science and Technology*, Vol. 3, pp 163-183.

- [23]. D. M. Jepson, B. J. Azzopardi and P. B. Whalley, 1988, “The effect of gas properties on drops in annular flow”, *Int. J. Multiphase Flow*, Vol. 15, No. 3, pp. 327-339.
- [24]. A. Wolf, S. Jayanti and G. F. Hewitt, 1996, “On the nature of ephemeral waves in vertical annular flow”, *Int. J. Multiphase Flow* Vol. 22, No. 2, pp. 325-333.
- [25]. A. Wolf, S. Jayanti, G. F. Hewitt, 2001, “Flow development in vertical annular flow”, *Chemical Engineering Science* 56 (2001) 3221-3235.
- [26]. T. Fukano and T. Furukawa, 1997, “Prediction of liquid viscosity on interfacial shear stress and frictional pressure drop in vertical upward gas-liquid annular flow”, *Int. J. Multiphase Flow* Vol. 24, No. 4, pp. 587-603.
- [27]. Masao Nakazatomi, 1996, “Effect of Pressure on Entrainment Flow Rate in Vertical Upward Gas-Liquid Annular Flow. Part II: An assessment of Published Correlations of Entrainment Flow Rate through High-Pressure Data and Proposal of New Correlations”, *Heat Transfer – Japanese Research* 25(5).
- [28]. Zhaolin Wang, Kamiel S. Gabriel, Devon L. Manz, 2004, “The influences of wave height on the interfacial friction in annular gas-liquid flow under normal and microgravity conditions”, *International Journal of Multiphase Flow* 30 (2004) 1193–1211.
- [29]. Tatsuya Hazuku, Tomoji Takamas, Yoichiro Matsumoto, 2008, “Experimental study on axial development of liquid film in vertical upward annular two-phase flow”, *International Journal of Multiphase Flow* 34 (2008) 111–127.
- [30]. Andrea C. Ashwood, DuWayne Schubring, Timothy A. Shedd, 2009, “Direct measurement of liquid film roughness for the prediction of annular flow pressure drop”, *ECI International Conference on Boiling Heat Transfer Florianopolis-SC-Brazil*, 3-7.
- [31]. Daniel J. Rodriguez, Timothy A. Shedd, 2004, “Entrainment of gas in the liquid film of horizontal, annular, two-phase flow”, *International Journal of Multiphase Flow* 30 (2004) 565–583
- [32]. G. A. Hughmark, 1973, “Film Thickness, Entrainment, and Pressure Drop in Upward Annular and Dispersed Flow”, *AIChE Journal* (Vol. 19, No. 5).

- [33]. W. H. Hentsch and T. J. Hanratty, 1976, “The Interfacial Drag and the Height of the Wall Layer in Annular Flows”, *AIChE Journal* (Vol. 22, No. 6).
- [34]. A.M. Ansari, N.D.Sylvester, C.Sarica, O. Shoham and J.P.Brill, 1994, “A Comprehensive Mechanistic Model for Upward Two-Phase flow in Wellbores”, *SPE Production and Facilities*, May.
- [35]. D. Schubring, A.C. Ashwood, T.A. Shedd and E.T. Hurlburt, 2010, “Planar laser-induced fluorescence (PLIF) measurements of liquid film thickness in annular flow. Part I: Methods and data”, *International Journal of Multiphase Flow* 36 (2010) 815–824.
- [36]. Somchai Wongwises and Wittaya Kongkiatwanitch, 2001, “Interfacial friction factor in vertical upward gas-liquid annular two-phase flow”, *Int. Comm. Heat Mass Transfer*: Vol. 28, No. 3, pp. 323-336.
- [37] R.J. Belt, J.M.C. Van't Westende, L.M. Portela, 2009, “Prediction of the interfacial shear-stress in vertical annular flow”, *International Journal of Multiphase Flow* 35 (2009) 689–697.

APPENDIX A

Matlab script for calculation of film thickness

```
clear all
close all
clc

scale=200; %% pix/mm scaling factor
pathdata = 'H:\tiff\40-500-50p-2\'; % file location
rootdata = 'B0' ; % root name of image
firstseq = 1 ; % first image
lastseq = 1500; % last image

for i=firstseq:lastseq

% load the X, Y, and Z grids from the first file
filename = [pathdata rootdata makestr(i) '.tif'] ;
%filename = [pathdata rootdata, num2str(i),'.tif'] ;
data(:,:,i) = imread(filename);
disp(['reading ' pathdata filename]);
end

close all
for i=1:1500
%figure; imshow(data(:,:,i));
%set(gca,'clim',[0 100])

[datab(:,:,i) position]=imcrop(data(:,:,i),[671.5 21.5 650 1007]); % cropping the image
%BW = edge(datab(:,:,i));
%figure, imshow(datab(:,:,i));
%mask = false(rows, columns);
databw(:,:,i)=im2bw(datab(:,:,i), 0.2); % converting image into binary image
%figure; imshow(databw(:,:,i));
%colormap('gray');
databwh(:,:,i)= imfill(databw(:,:,i),'holes'); % filling holes from air bubbles
databwf(:,:,i) = bwareaopen(databw(:,:,i),0); % removes white pixels that are not in the film
%figure; imshow(databwf(:,:,i));
%colormap('gray');
thickness(i)=sum(sum(databwf(:,:,i)))/size(databw(:,:,i),1)/scale; % calculated film thickness

end

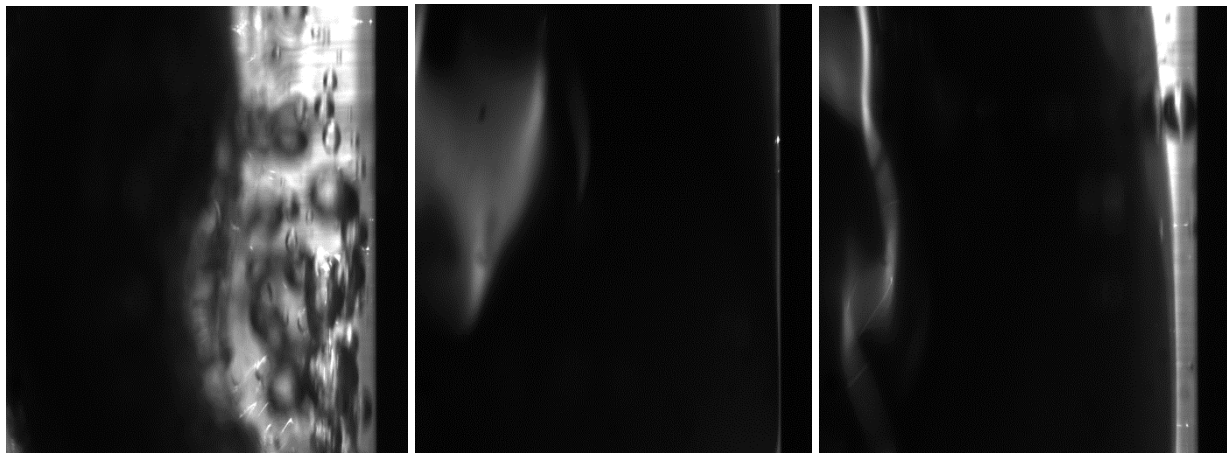
m=mean(thickness) % finds average value of film thickness
```

APPENDIX B

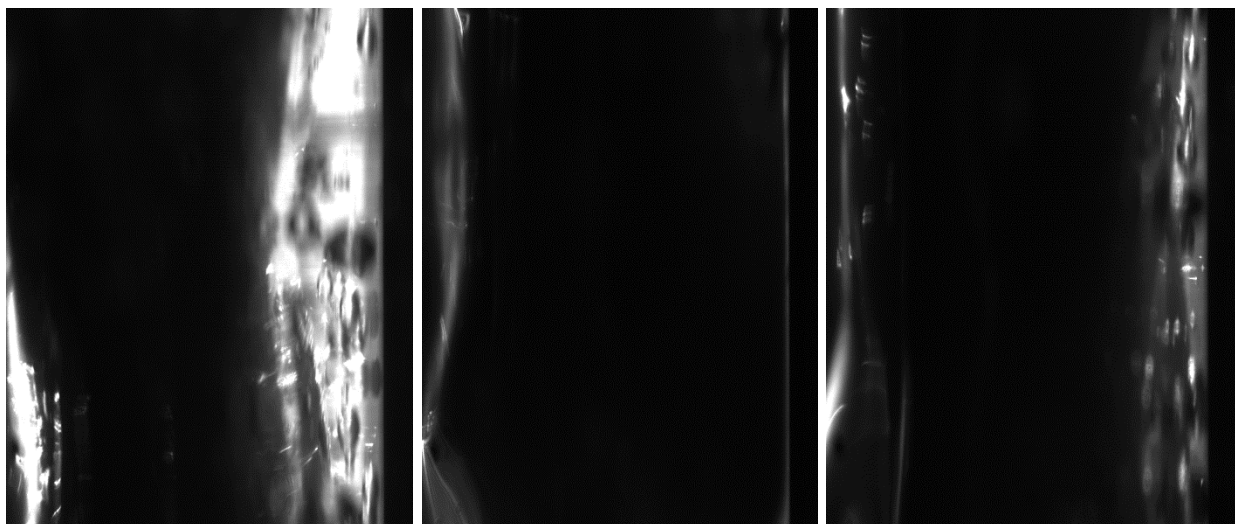
Corresponding images for maximum, minimum and average value of film thickness for every gas and liquid flow rate

First setup (laser sheet aligned with center of the pipe):

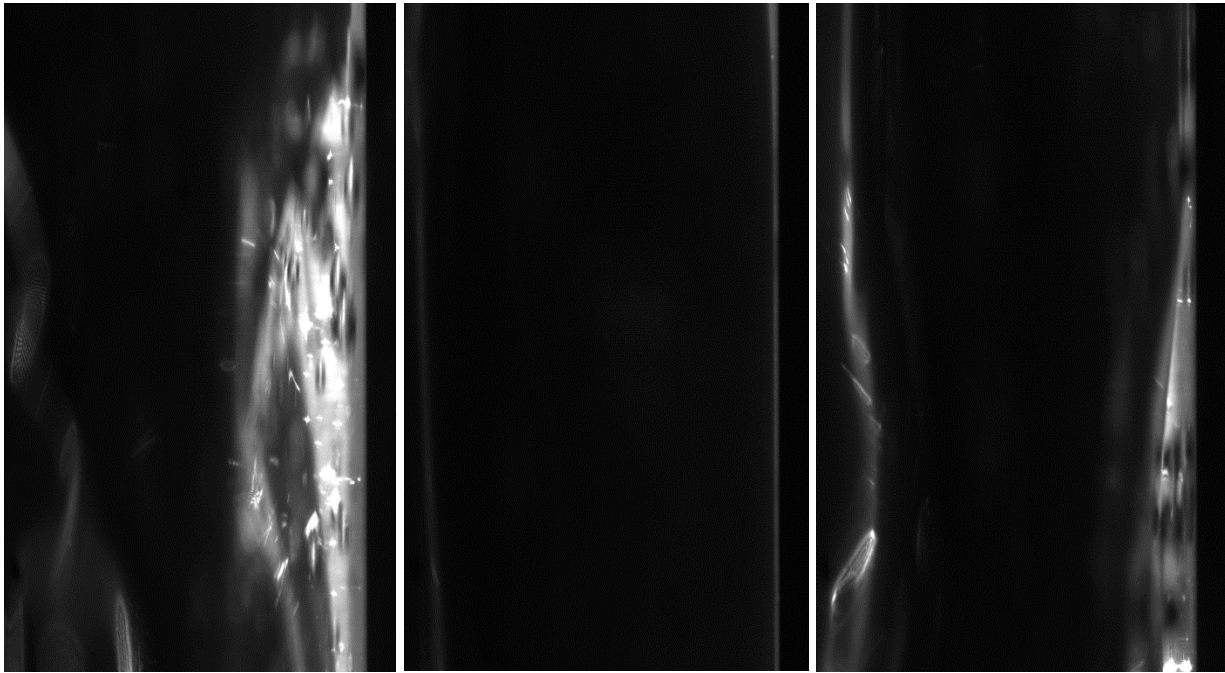
20 LPH (liquid rate) and 500 SLPM (gas rate) (left to right: maximum, minimum, and average)



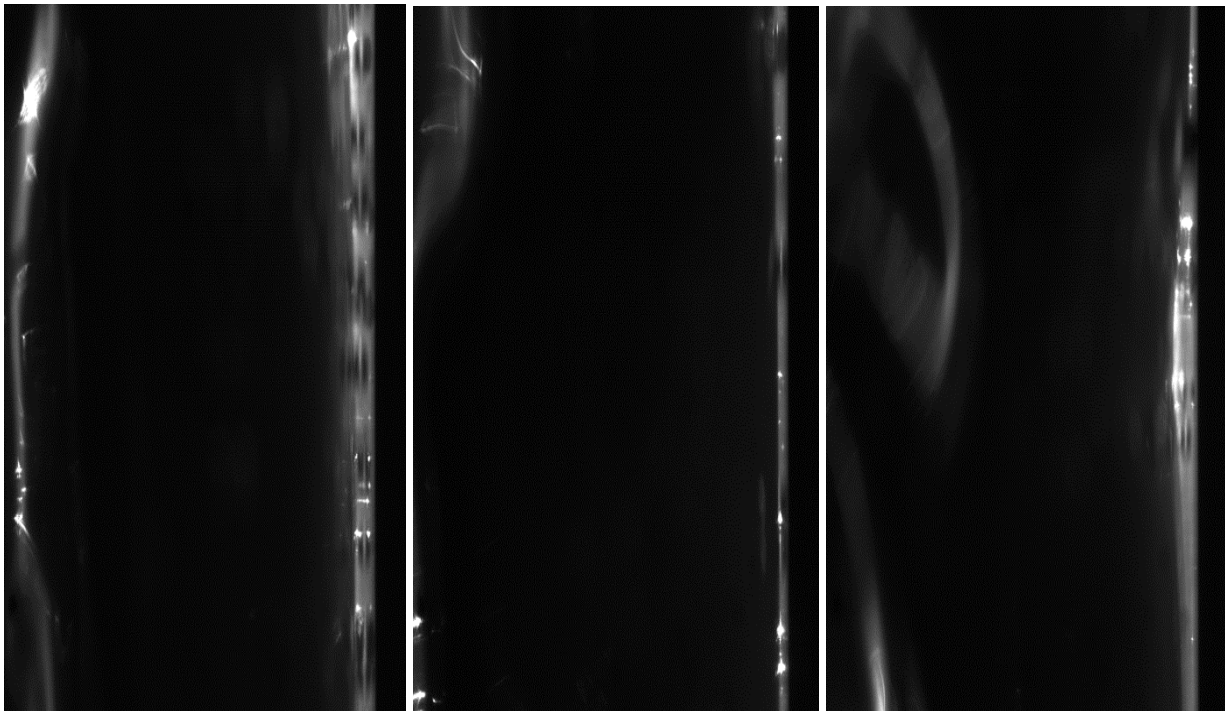
20 LPH (liquid rate) and 600 SLPM (gas rate) (left to right: maximum, minimum, and average)



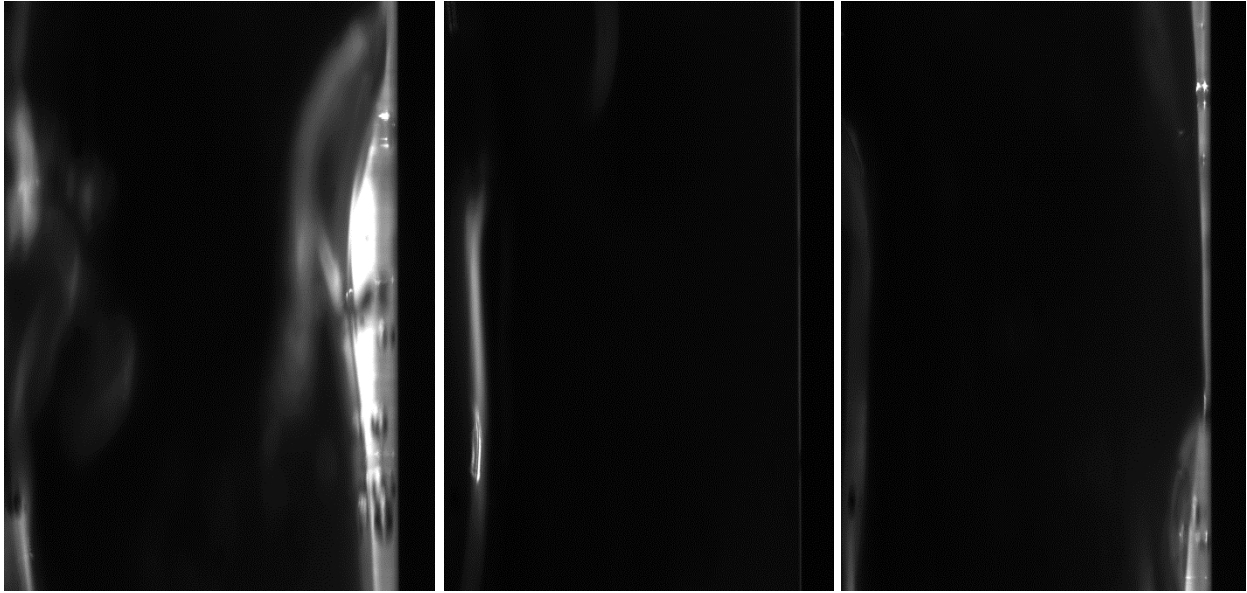
20 LPH (liquid rate) and 700 SLPM (gas rate) (left to right: maximum, minimum, and average)



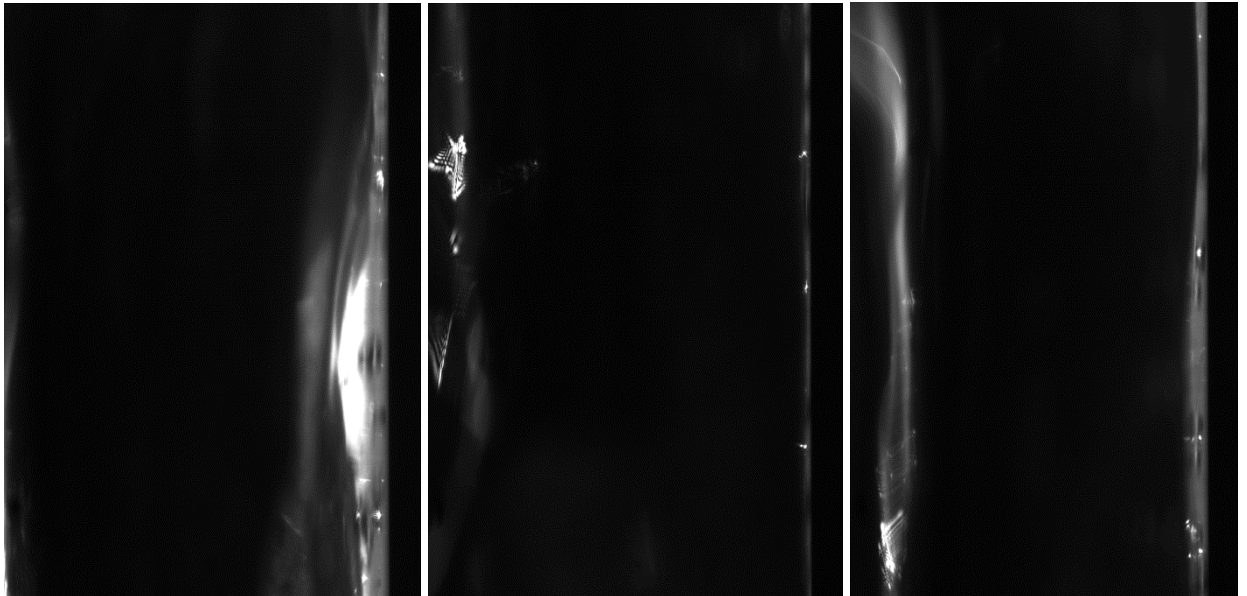
20 LPH (liquid rate) and 800 SLPM (gas rate) (left to right: maximum, minimum, and average)



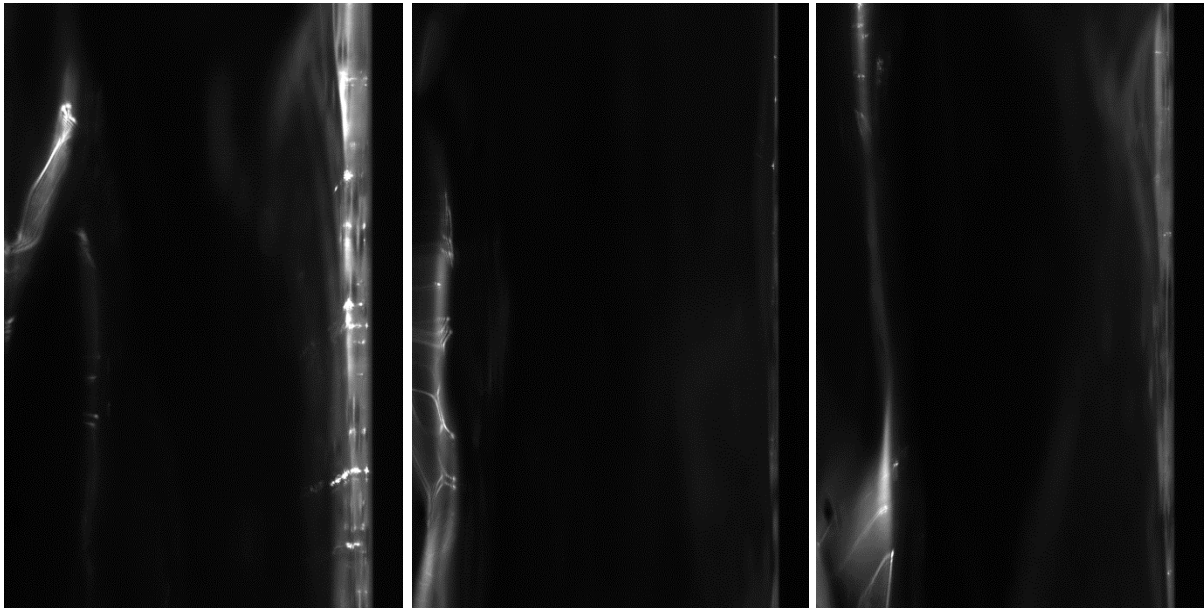
20 LPH (liquid rate) and 900 SLPM (gas rate) (left to right: maximum, minimum, and average)



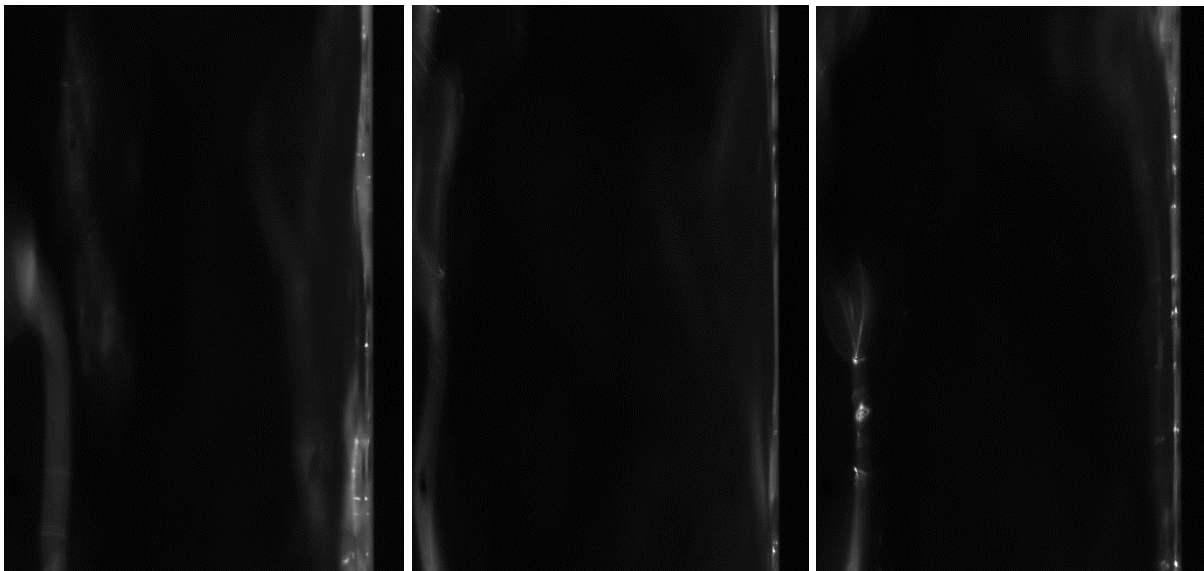
20 LPH (liquid rate) and 1000 SLPM (gas rate) (left to right: maximum, minimum, and average)



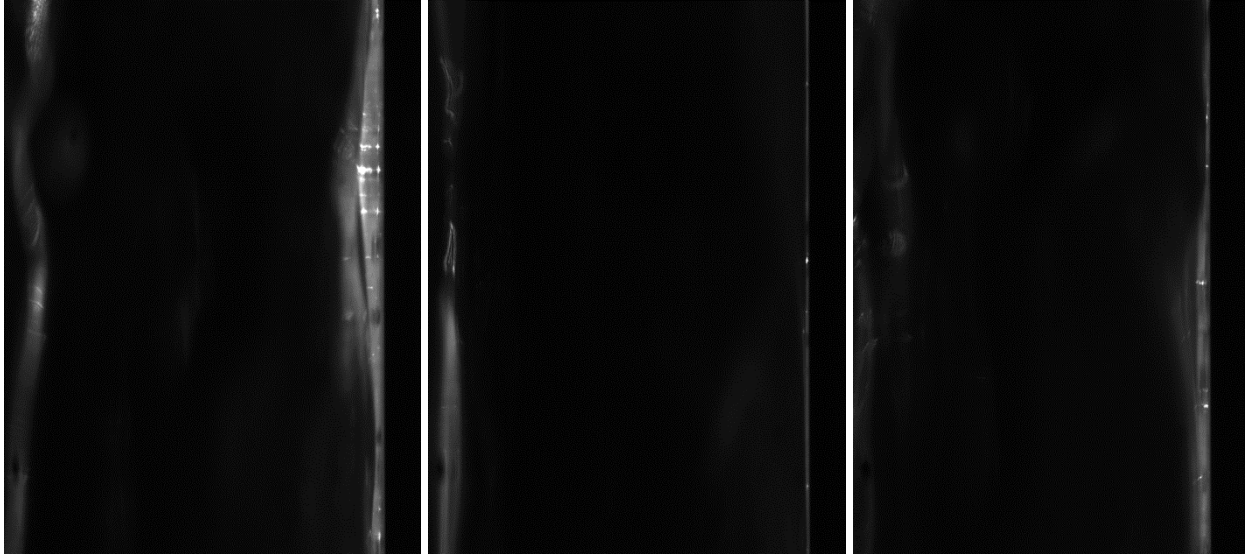
20 LPH (liquid rate) and 1100 SLPM (gas rate) (left to right: maximum, minimum, and average)



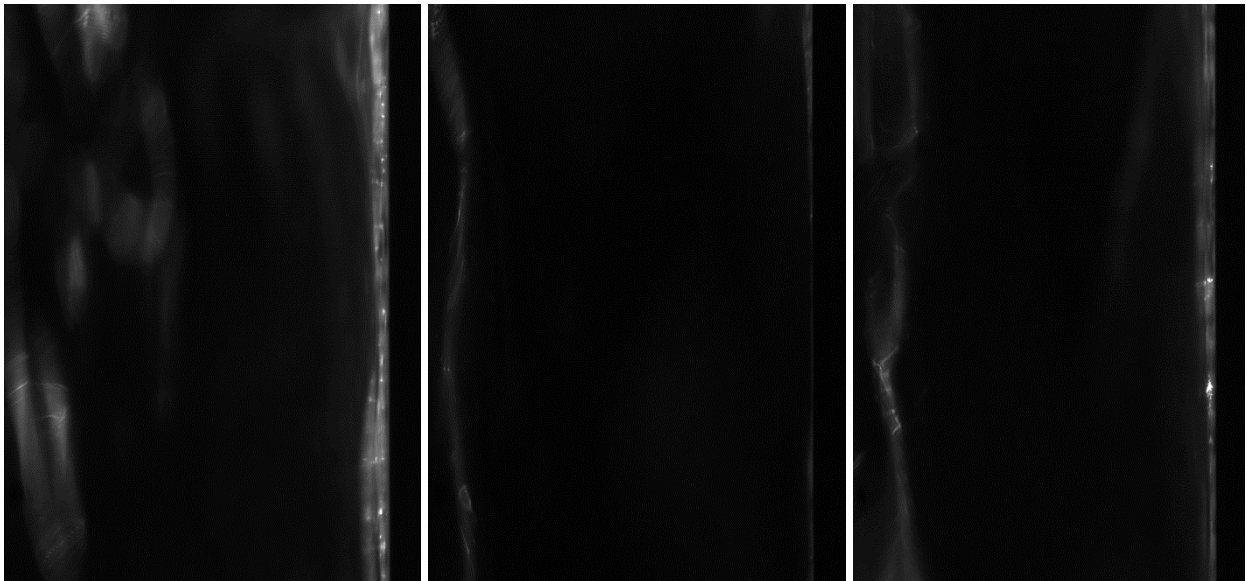
20 LPH (liquid rate) and 1200 SLPM (gas rate) (left to right: maximum, minimum, and average)



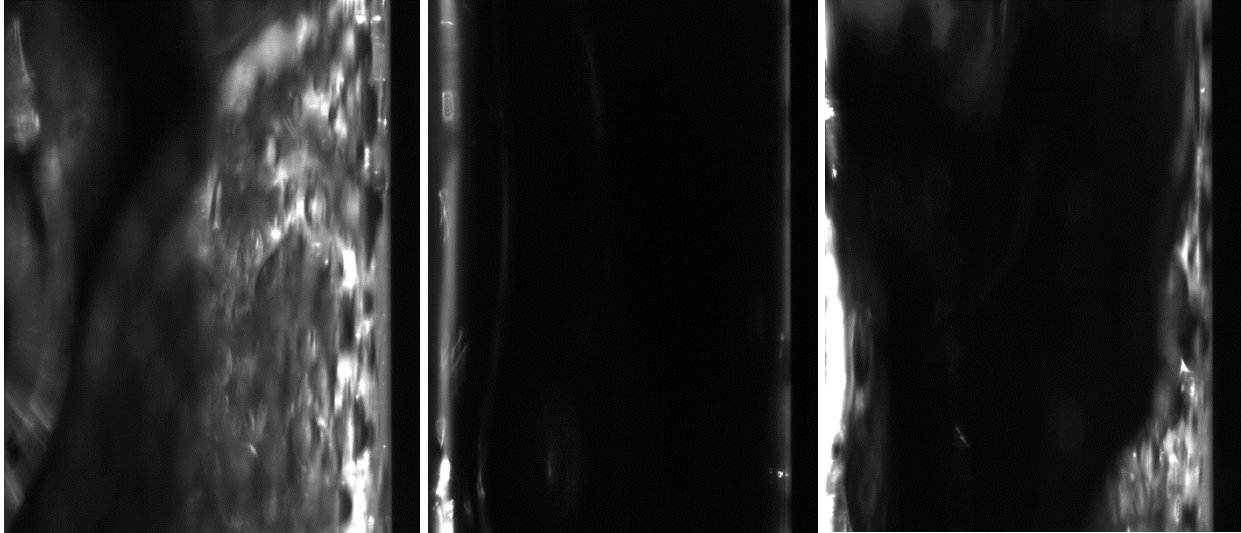
20 LPH (liquid rate) and 1300 SLPM (gas rate) (left to right: maximum, minimum, and average)



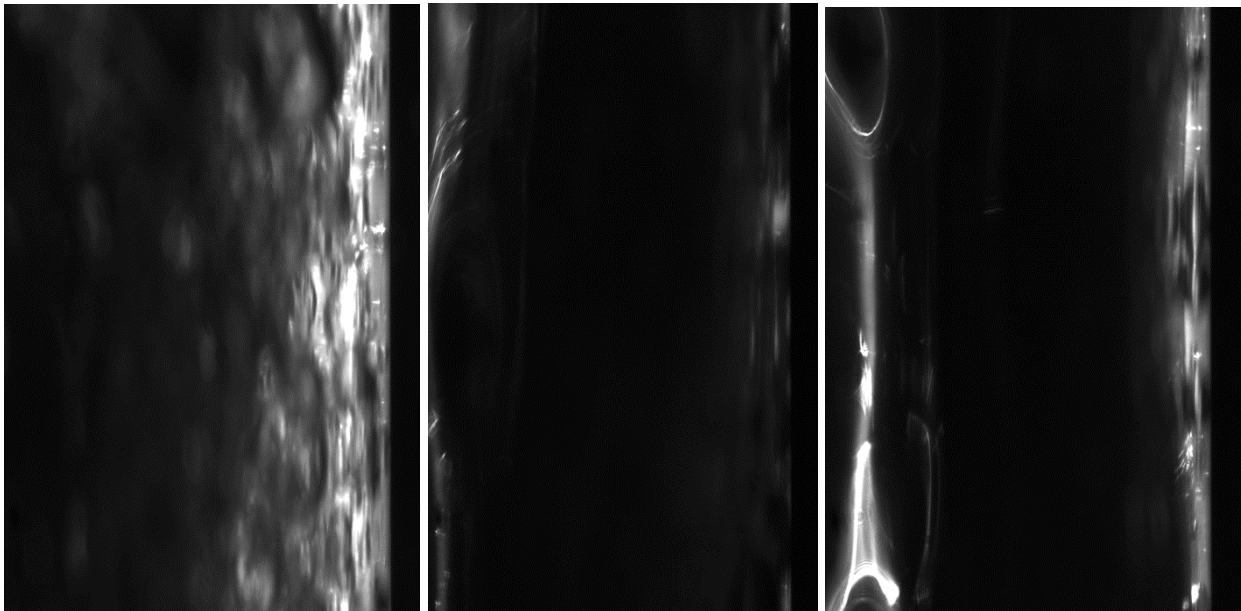
20 LPH (liquid rate) and 1400 SLPM (gas rate) (left to right: maximum, minimum, and average)



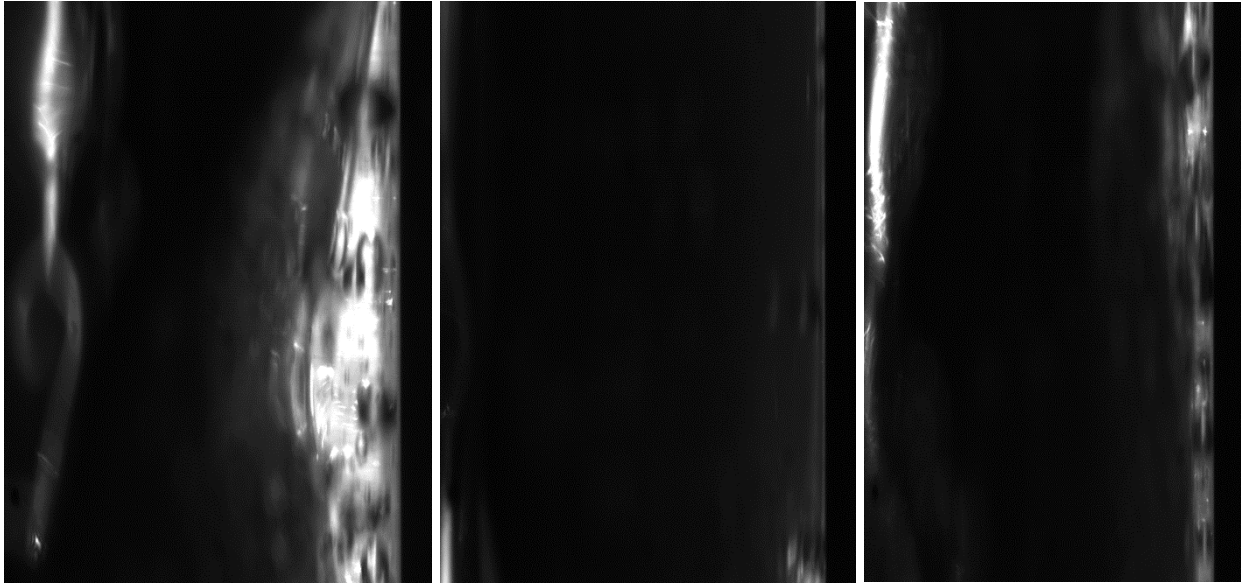
25 LPH (liquid rate) and 500 SLPM (gas rate) (left to right: maximum, minimum, and average)



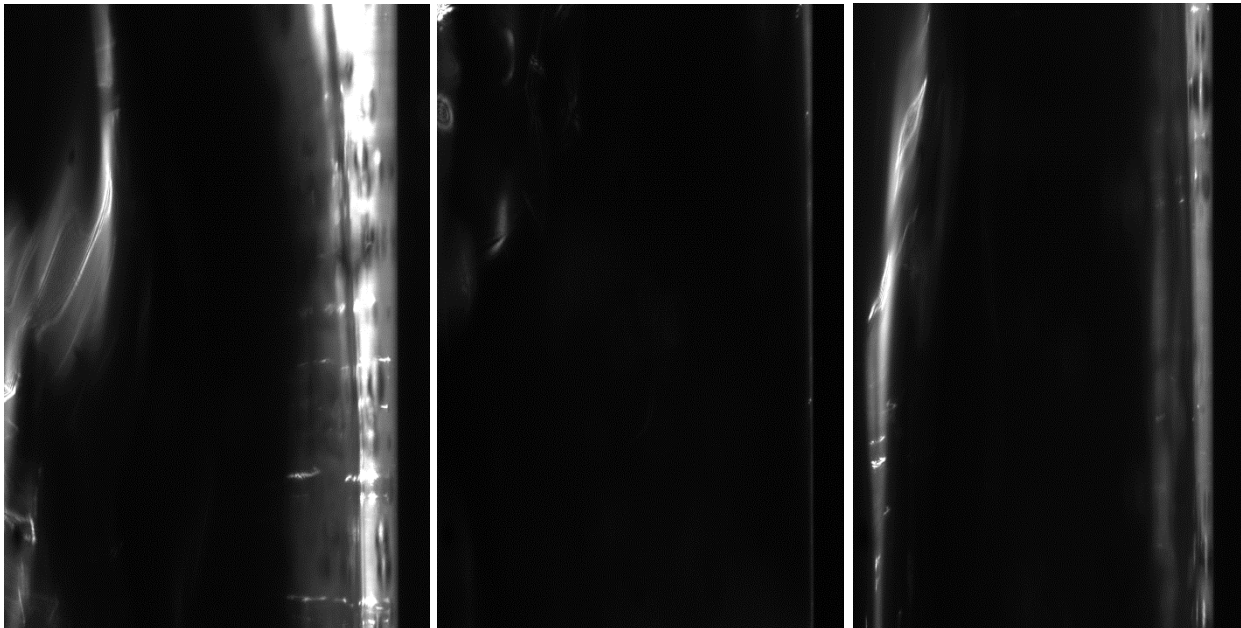
25 LPH (liquid rate) and 600 SLPM (gas rate) (left to right: maximum, minimum, and average)



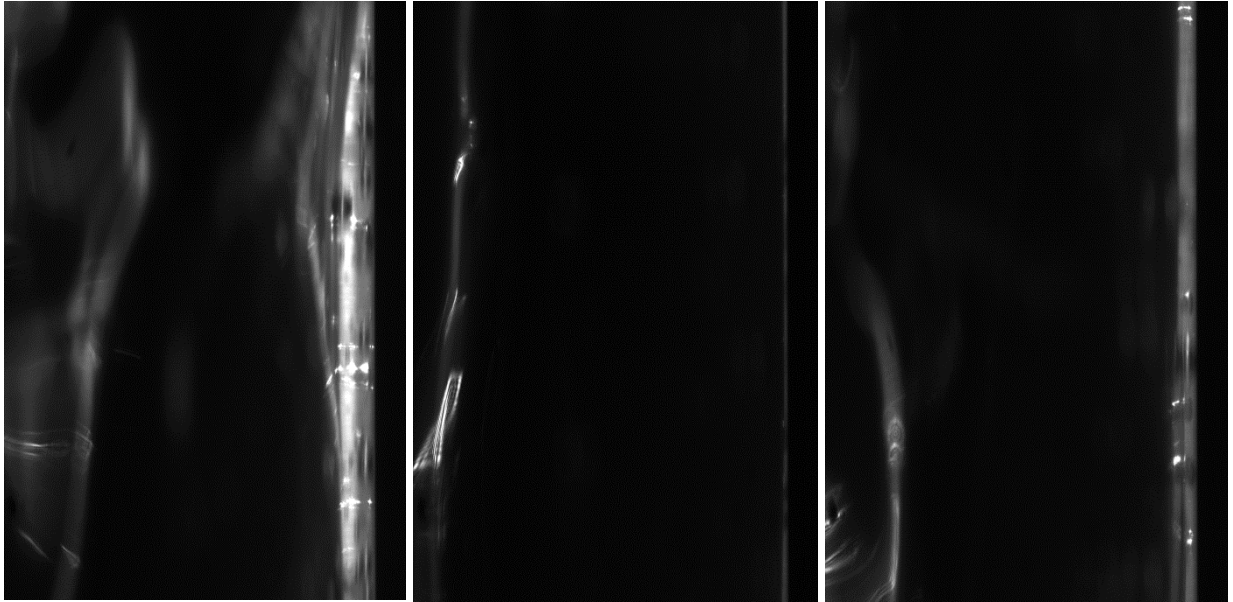
25 LPH (liquid rate) and 700 SLPM (gas rate) (left to right: maximum, minimum, and average)



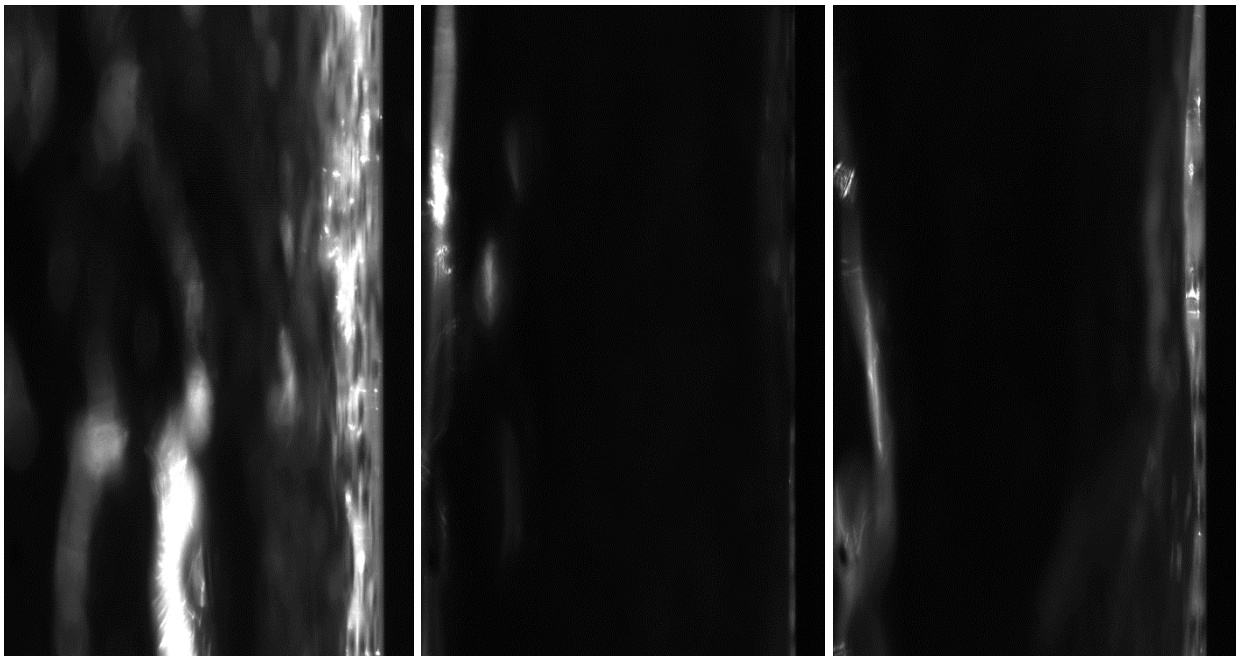
25 LPH (liquid rate) and 800 SLPM (gas rate) (left to right: maximum, minimum, and average)



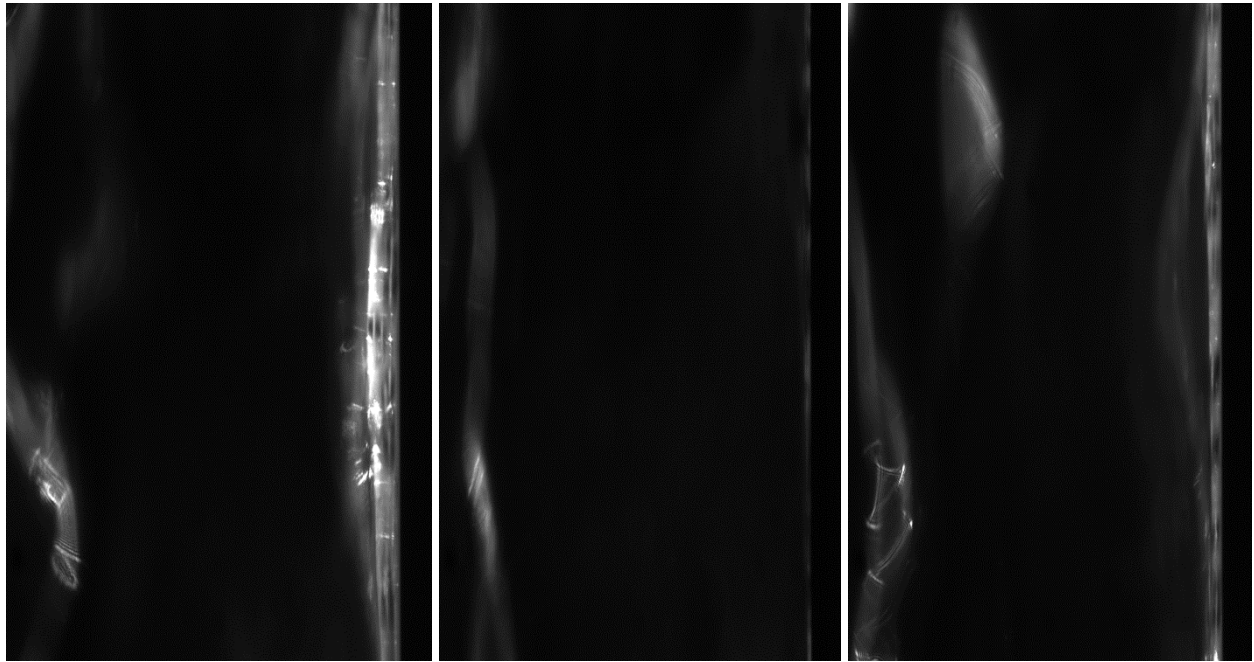
25 LPH (liquid rate) and 900 SLPM (gas rate) (left to right: maximum, minimum, and average)



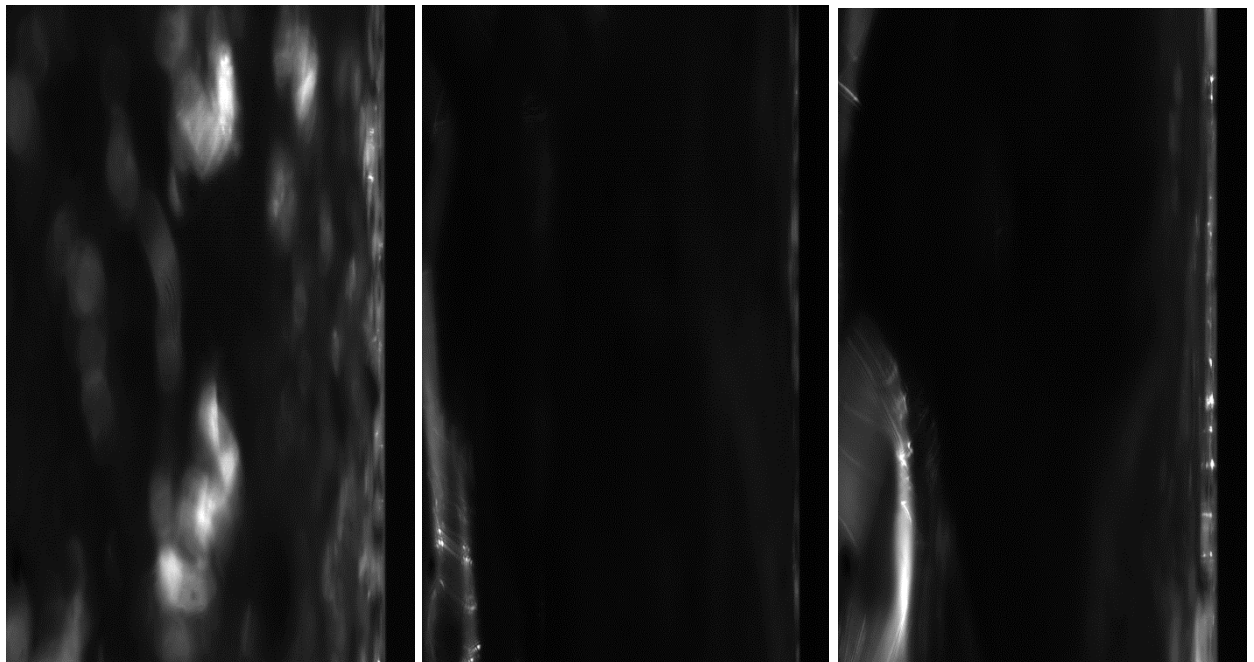
25 LPH (liquid rate) and 1000 SLPM (gas rate) (left to right: maximum, minimum, and average)



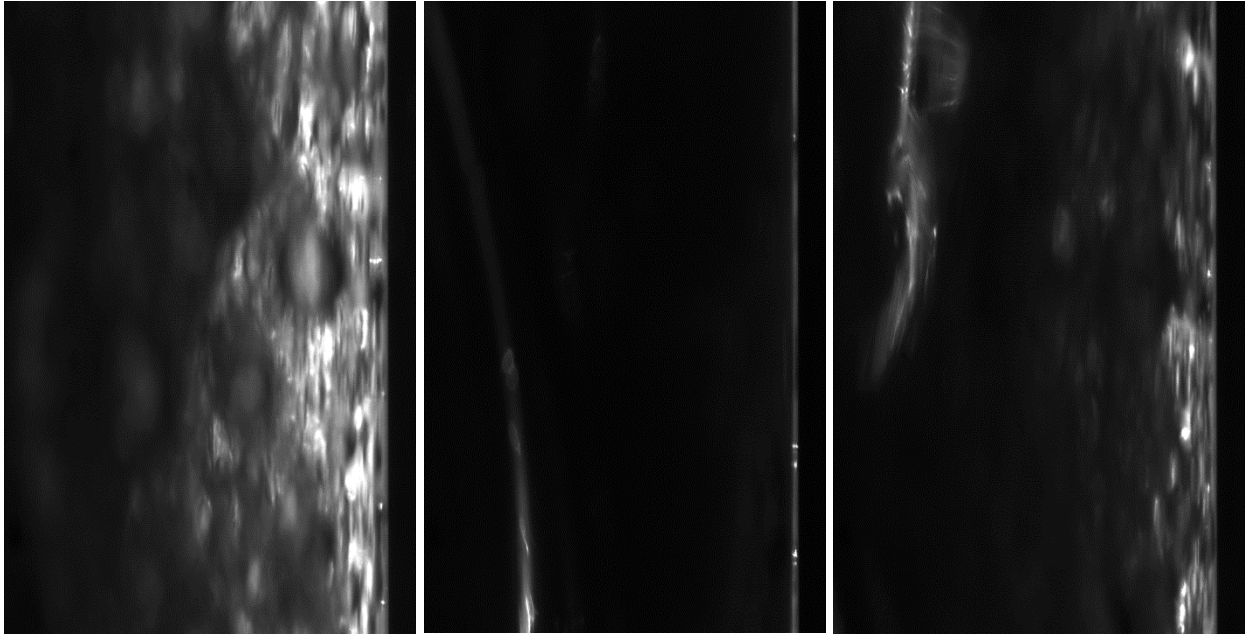
25 LPH (liquid rate) and 1100 SLPM (gas rate) (left to right: maximum, minimum, and average)



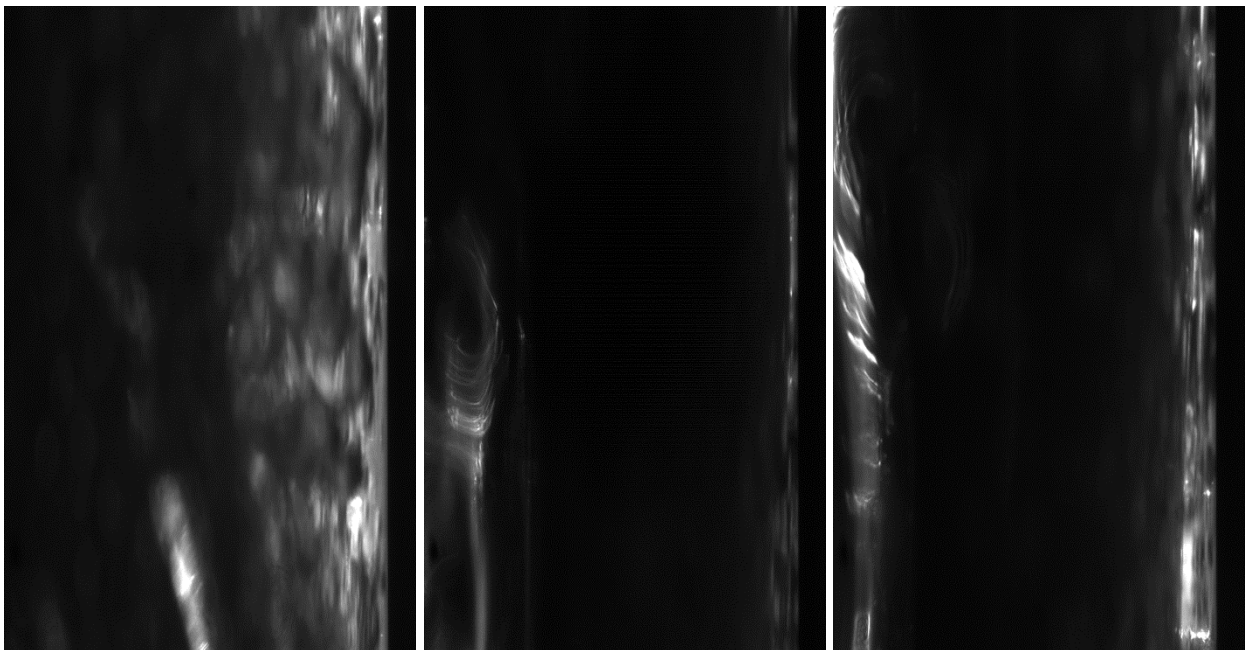
25 LPH (liquid rate) and 1200 SLPM (gas rate) (left to right: maximum, minimum, and average)



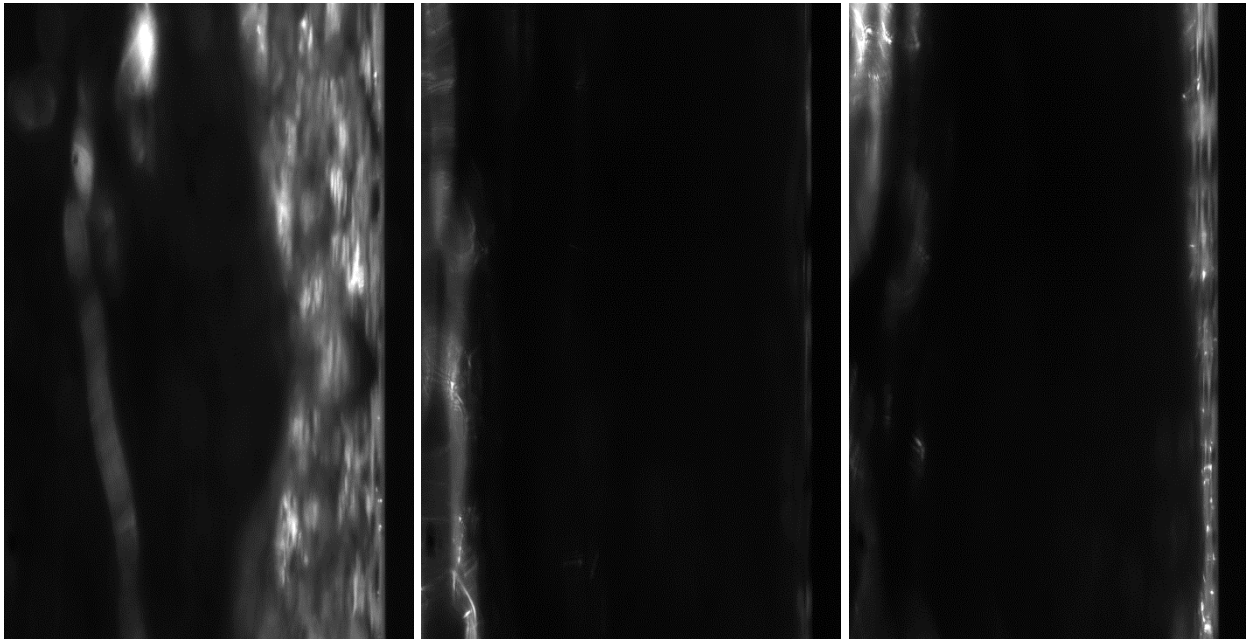
30 LPH (liquid rate) and 500 SLPM (gas rate) (left to right: maximum, minimum, and average)



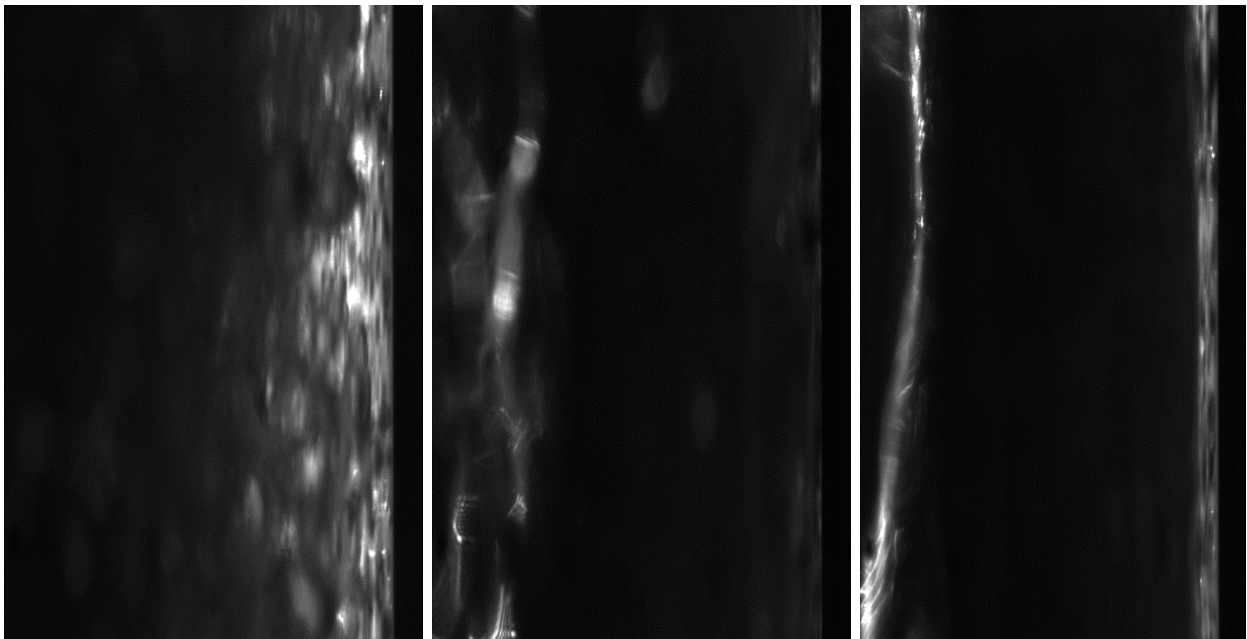
30 LPH (liquid rate) and 600 SLPM (gas rate) (left to right: maximum, minimum, and average)



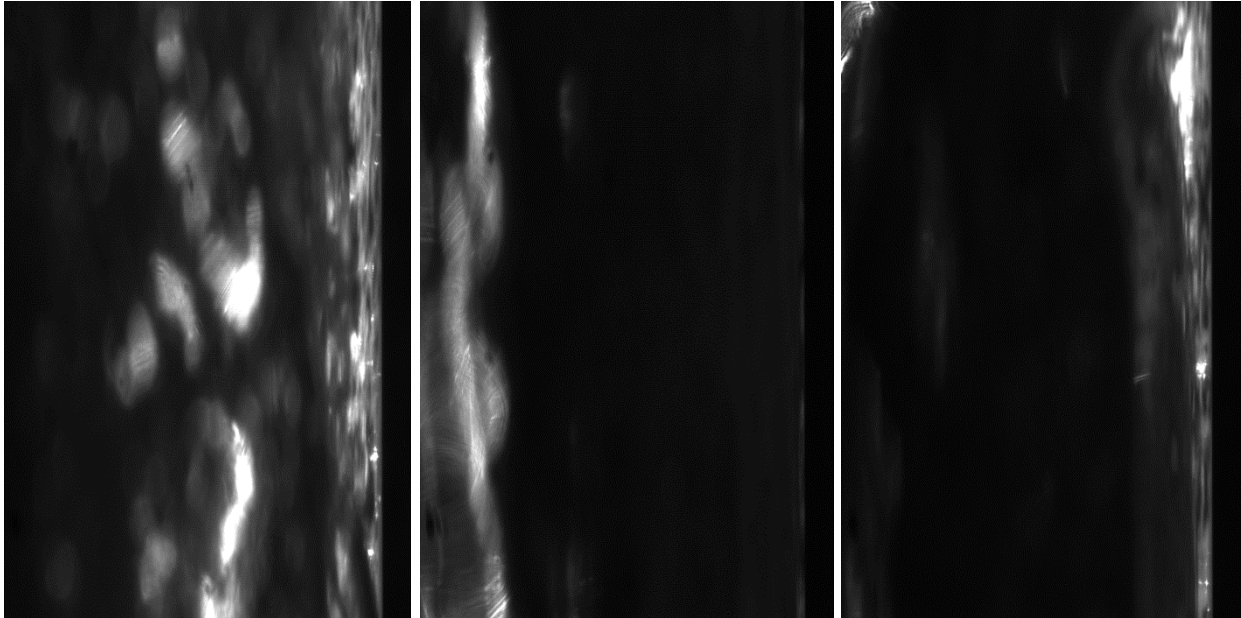
30 LPH (liquid rate) and 700 SLPM (gas rate) (left to right: maximum, minimum, and average)



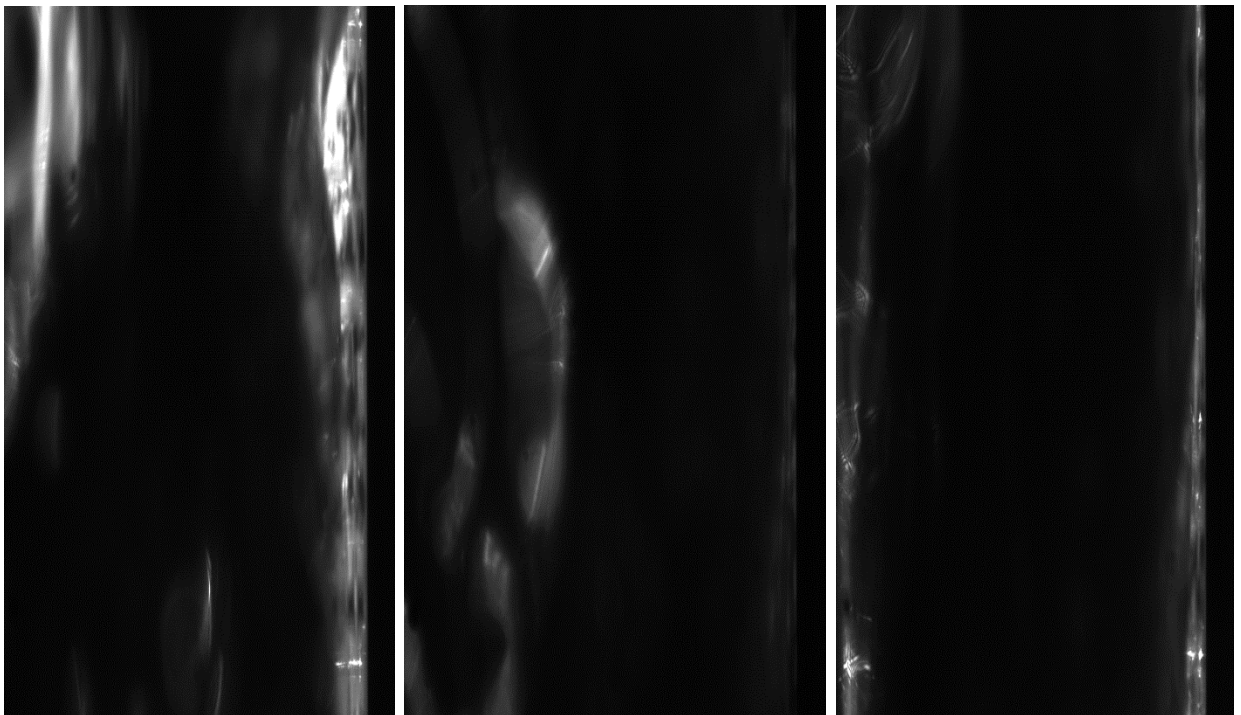
30 LPH (liquid rate) and 800 SLPM (gas rate) (left to right: maximum, minimum, and average)



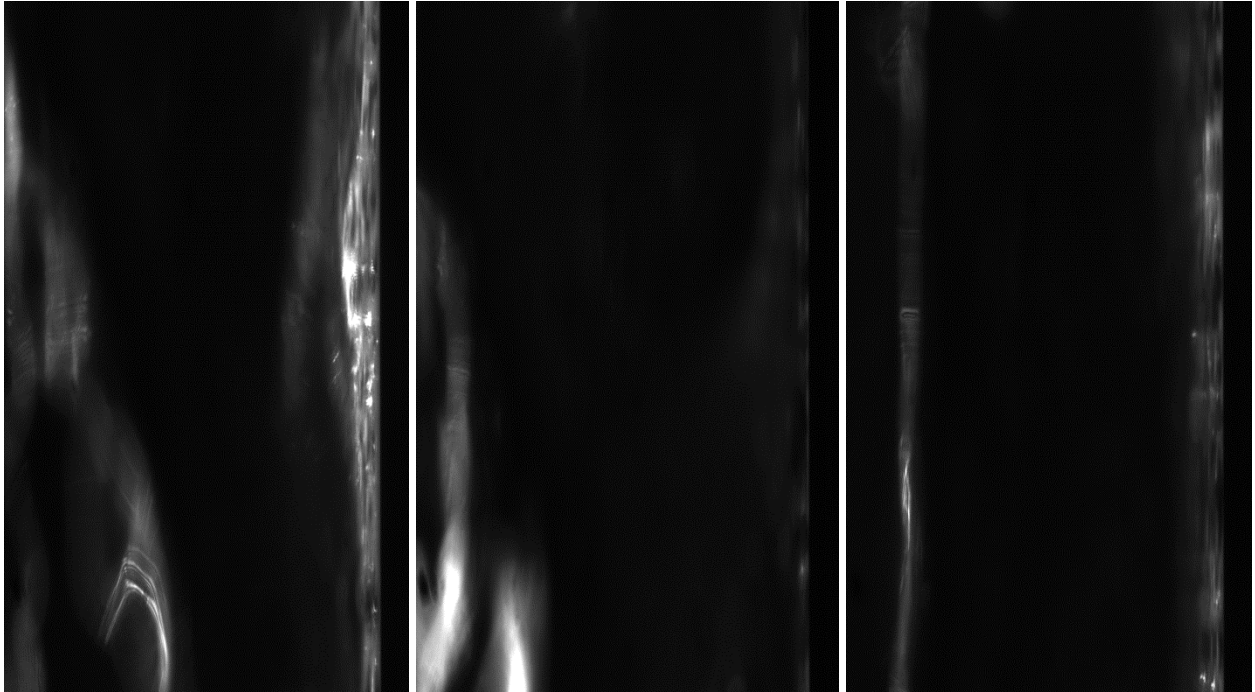
30 LPH (liquid rate) and 900 SLPM (gas rate) (left to right: maximum, minimum, and average)



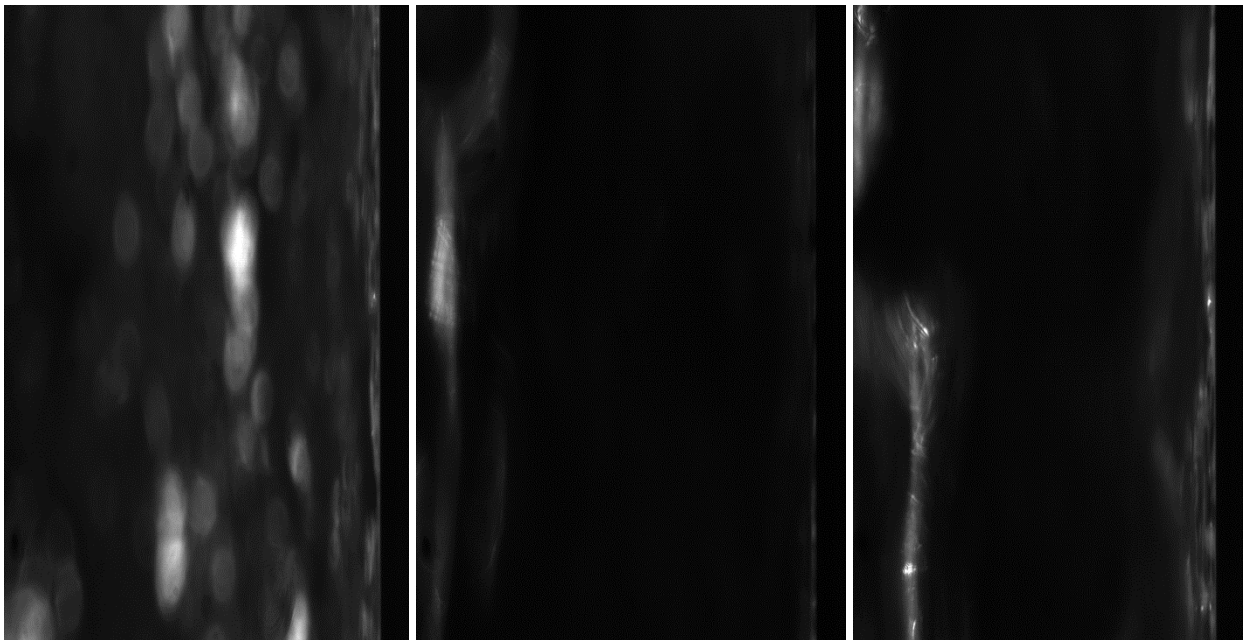
30 LPH (liquid rate) and 1000 SLPM (gas rate) (left to right: maximum, minimum, and average)



30 LPH (liquid rate) and 1100 SLPM (gas rate) (left to right: maximum, minimum, and average)

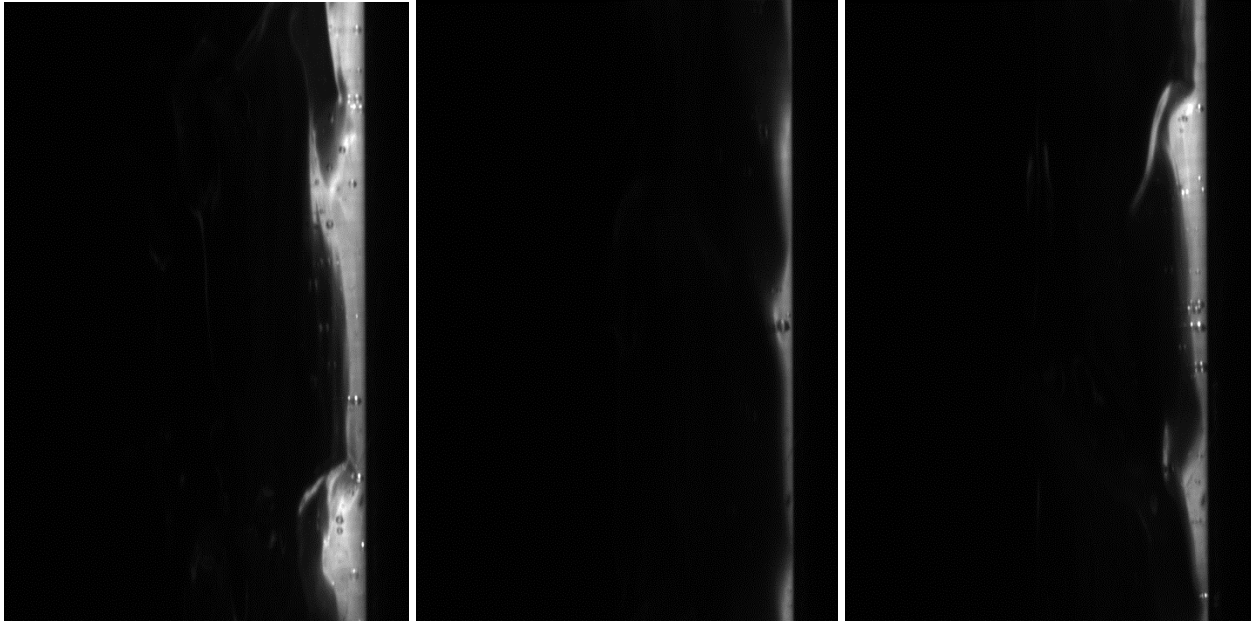


30 LPH (liquid rate) and 1200 SLPM (gas rate) (left to right: maximum, minimum, and average)

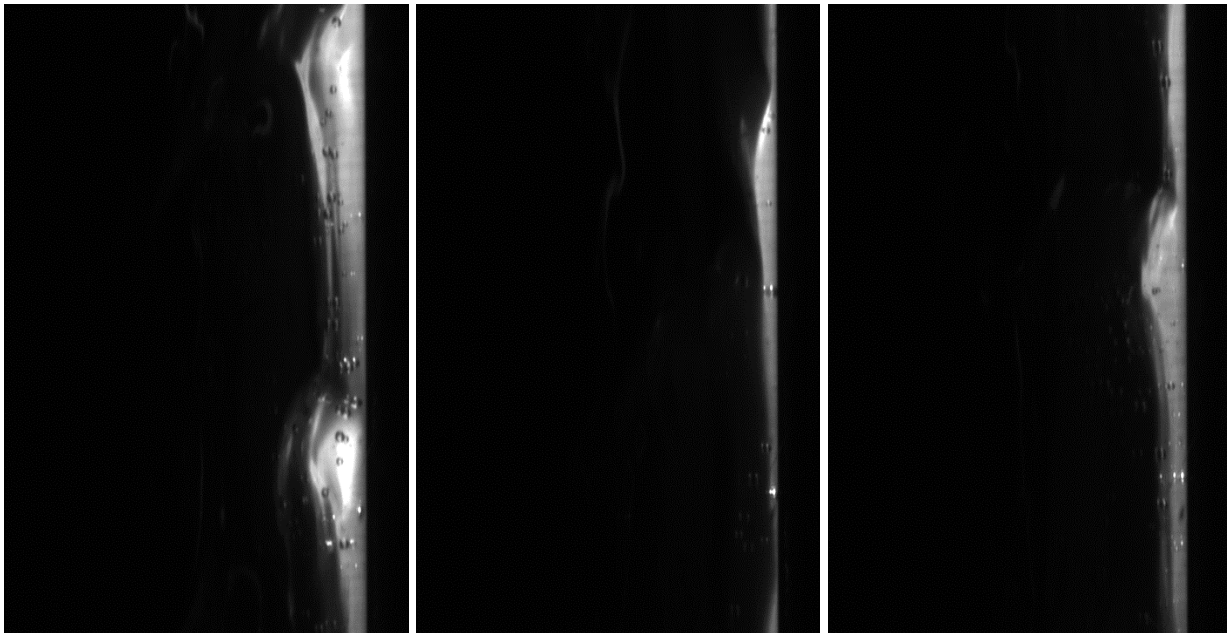


2. Second setup (laser sheet moved away from the center of the pipe closer to the camera):

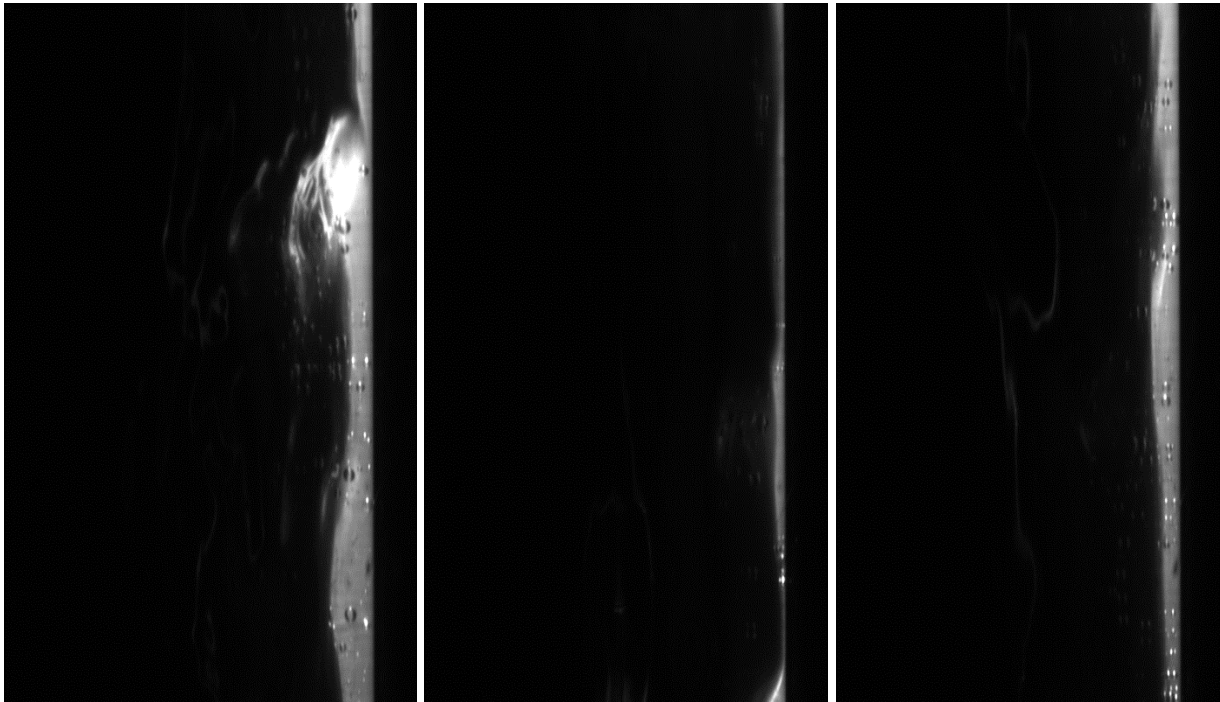
20 LPH (liquid rate) and 1500 SLPM (gas rate) (left to right: maximum, minimum, and average)



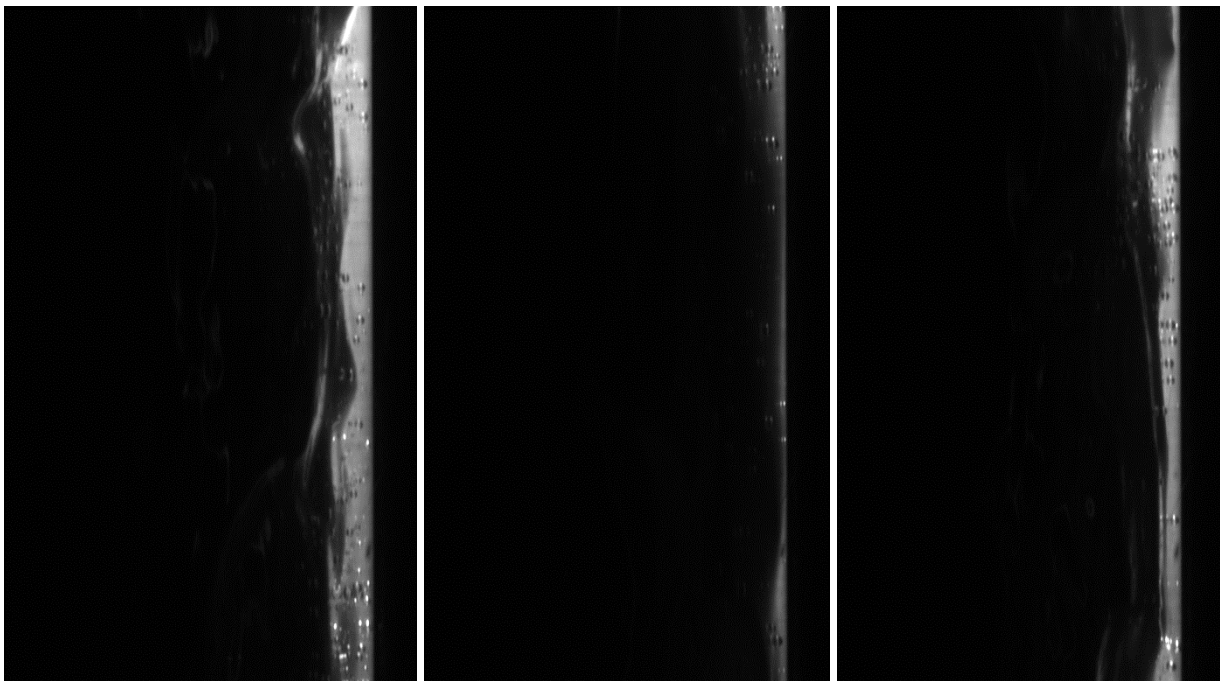
25 LPH (liquid rate) and 1300 SLPM (gas rate) (left to right: maximum, minimum, and average)



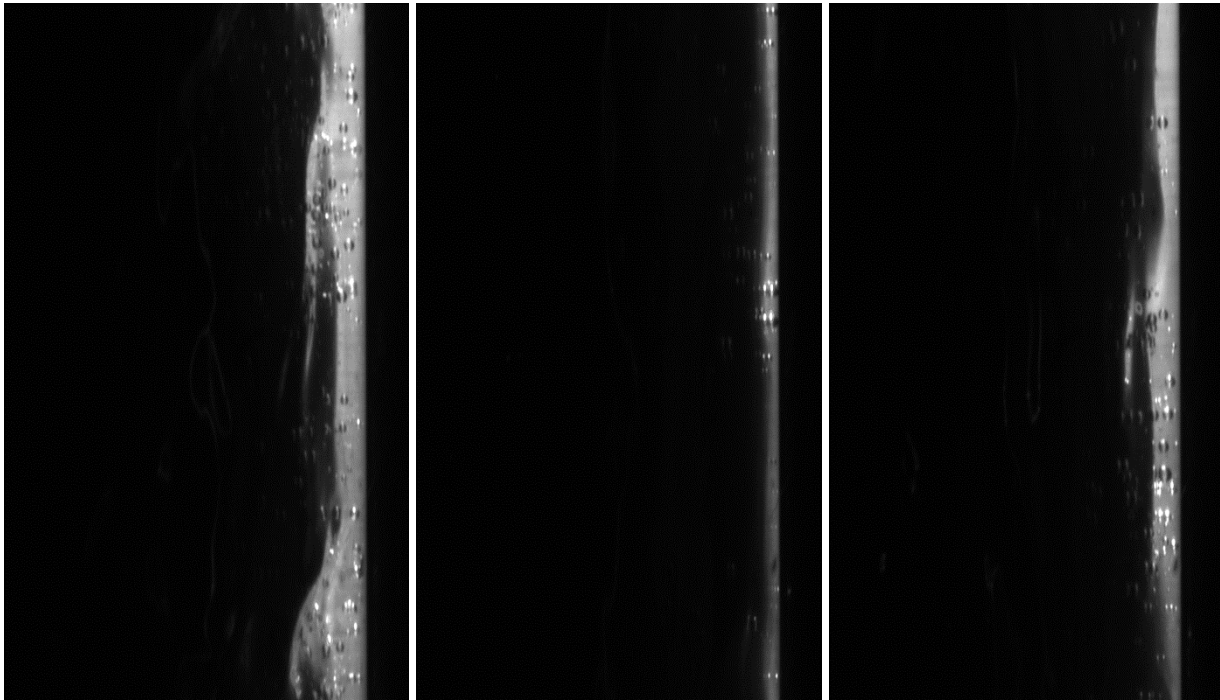
25 LPH (liquid rate) and 1400 SLPM (gas rate) (left to right: maximum, minimum, and average)



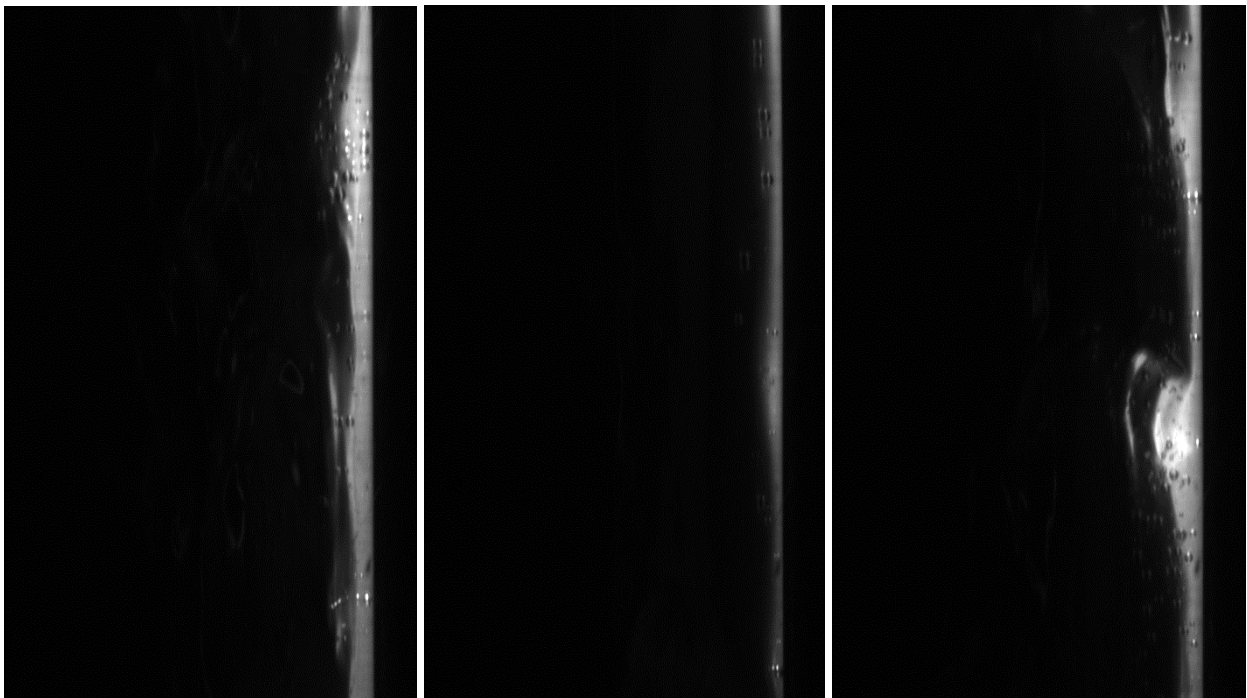
25 LPH (liquid rate) and 1300 SLPM (gas rate) (left to right: maximum, minimum, and average)



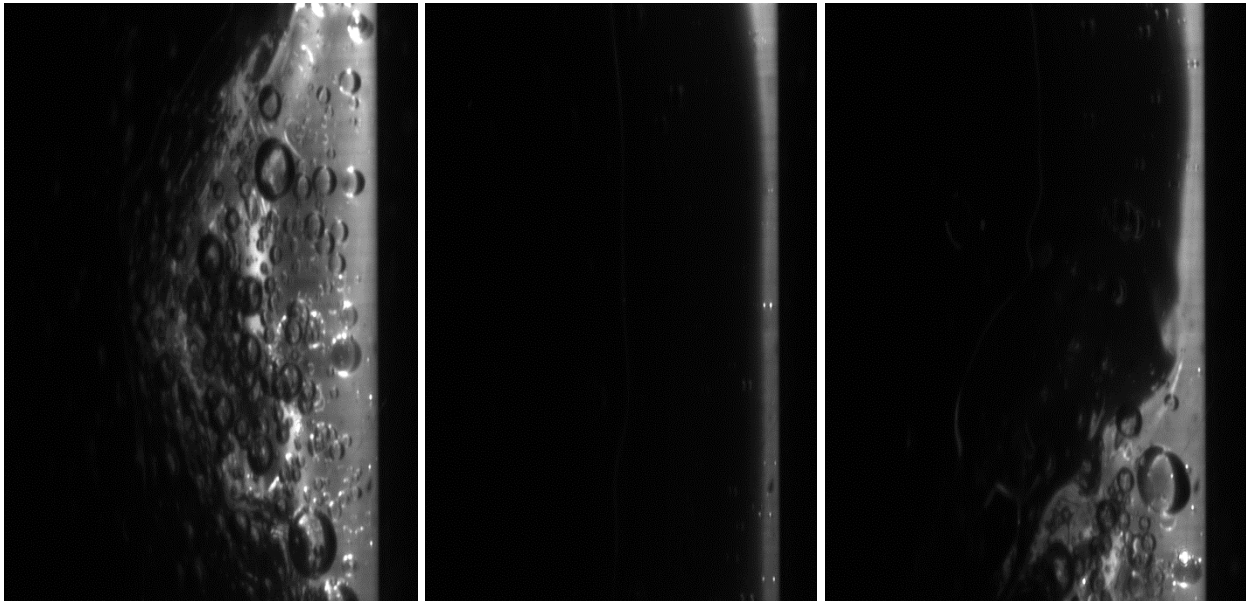
30 LPH (liquid rate) and 1300 SLPM (gas rate) (left to right: maximum, minimum, and average)



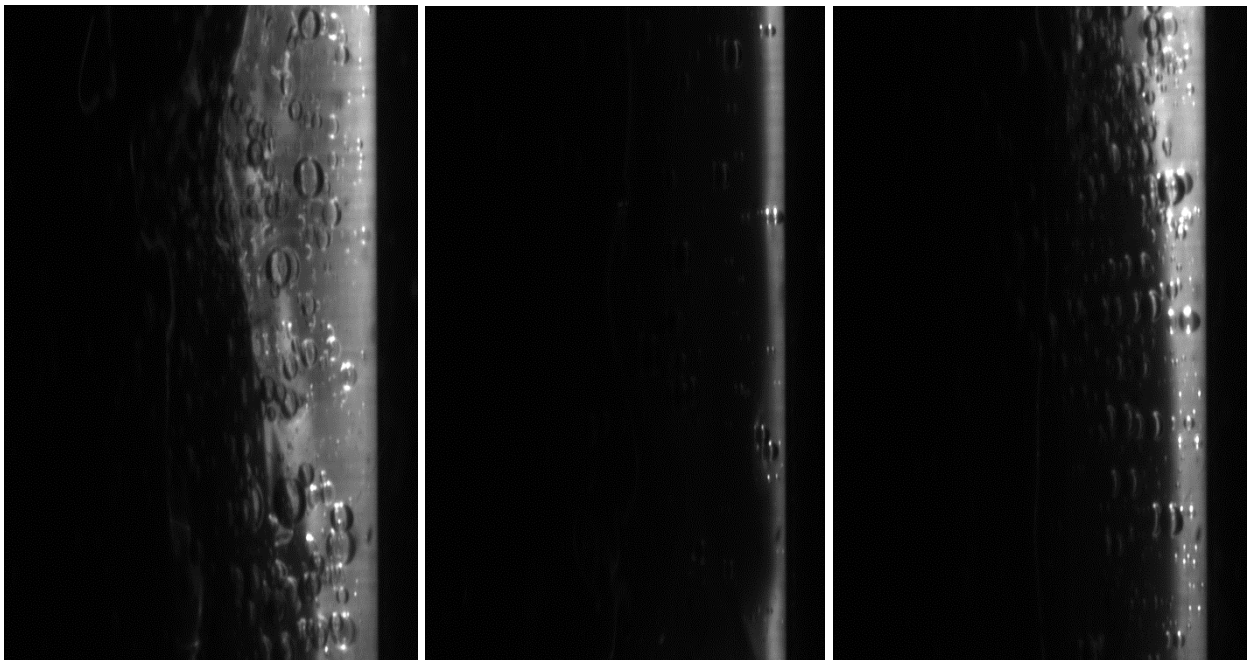
30 LPH (liquid rate) and 1400 SLPM (gas rate) (left to right: maximum, minimum, and average)



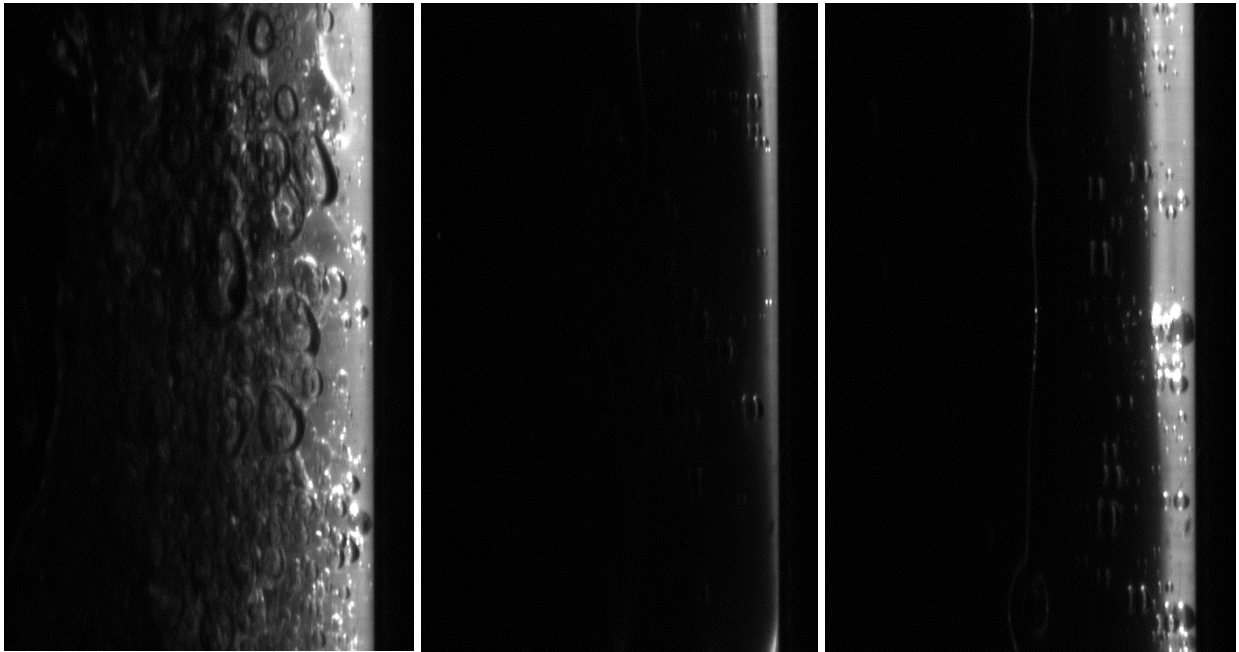
35 LPH (liquid rate) and 500 SLPM (gas rate) (left to right: maximum, minimum, and average)



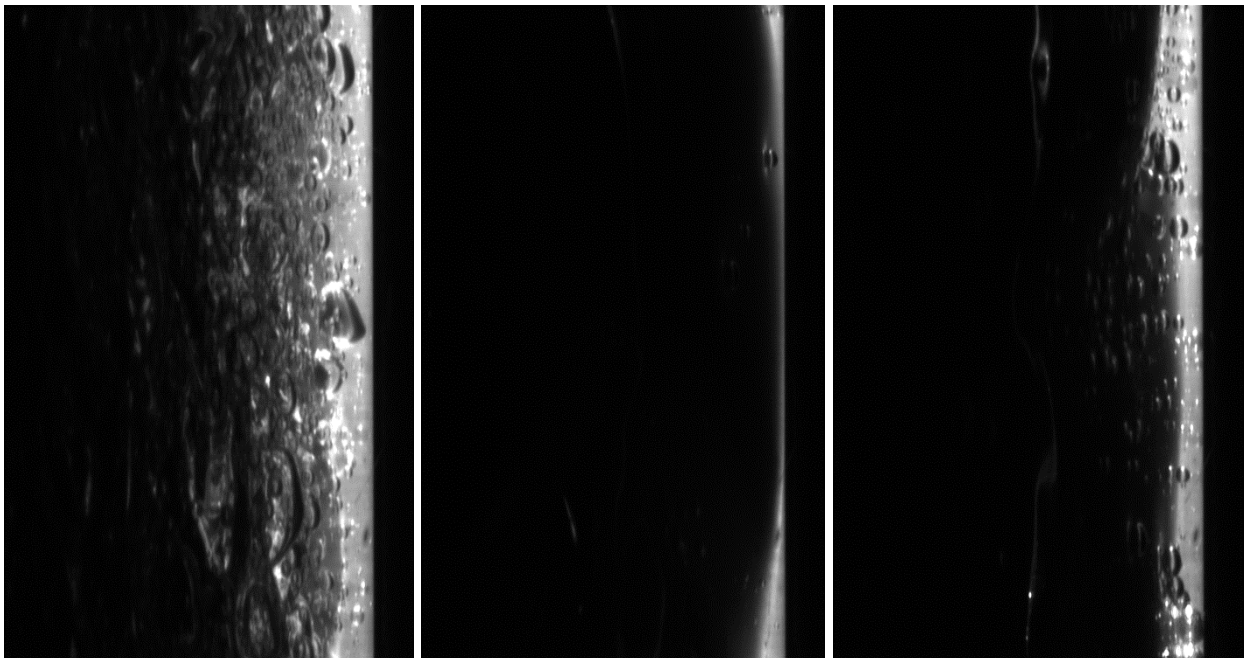
35 LPH (liquid rate) and 600 SLPM (gas rate) (left to right: maximum, minimum, and average)



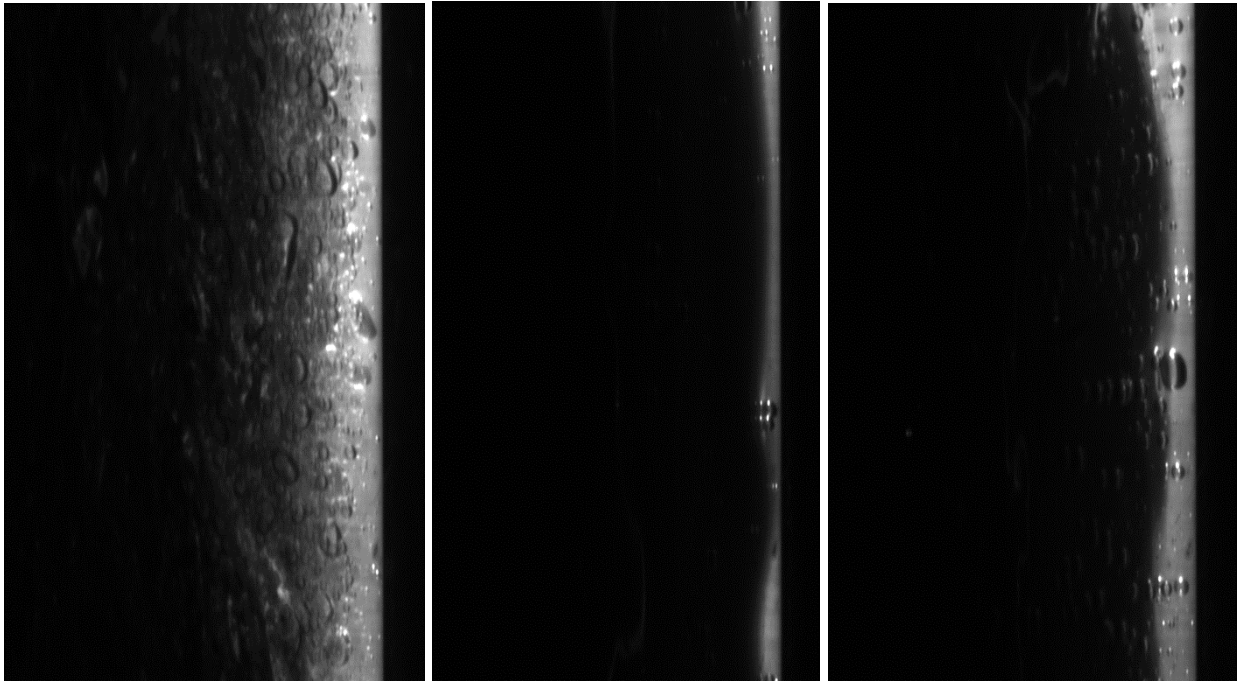
35 LPH (liquid rate) and 700 SLPM (gas rate) (left to right: maximum, minimum, and average)



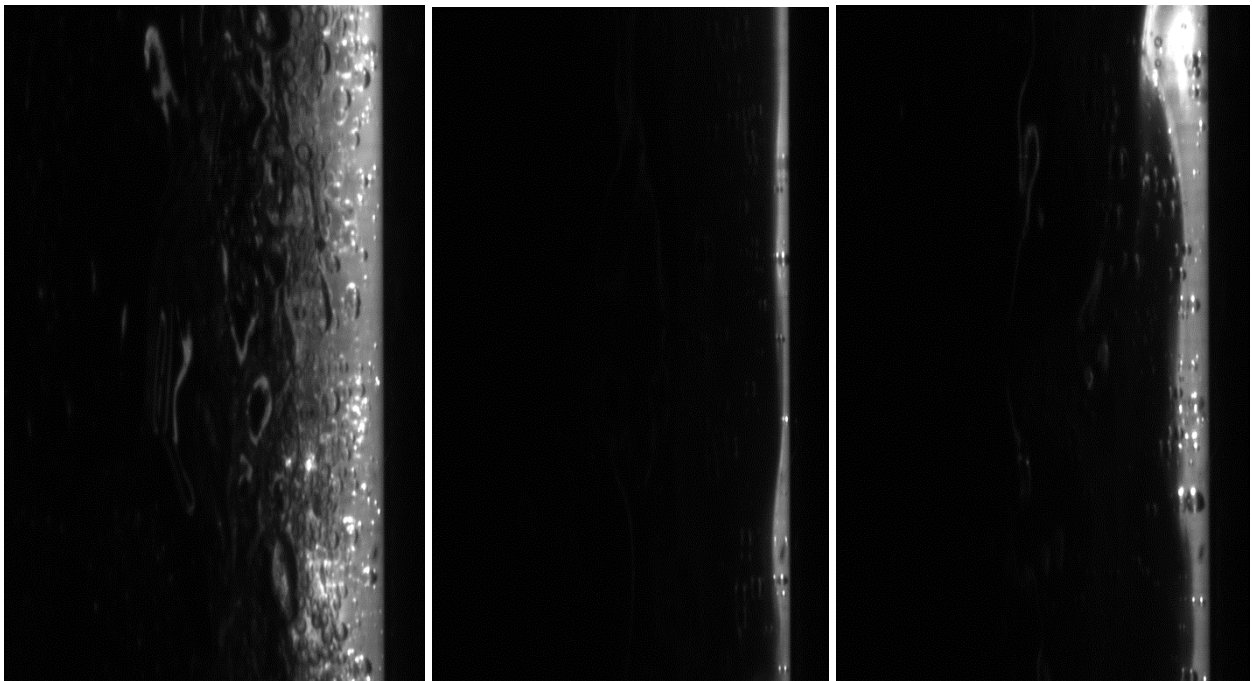
35 LPH (liquid rate) and 800 SLPM (gas rate) (left to right: maximum, minimum, and average)



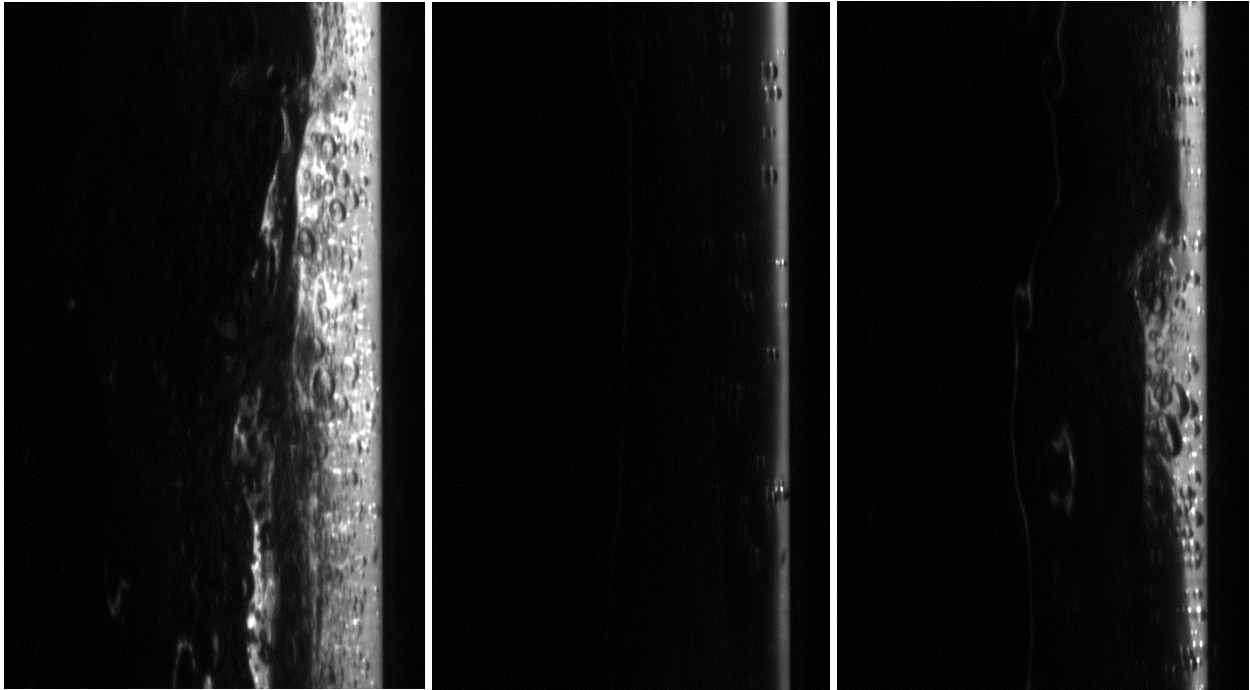
35 LPH (liquid rate) and 900 SLPM (gas rate) (left to right: maximum, minimum, and average)



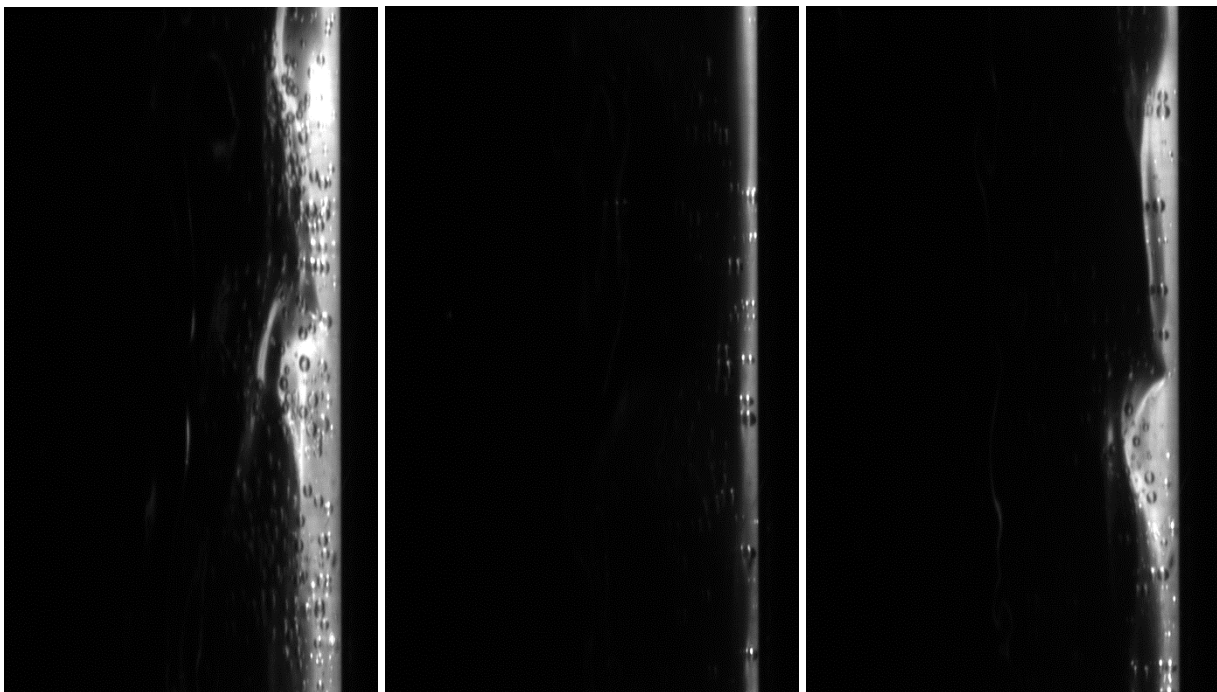
35 LPH (liquid rate) and 1000 SLPM (gas rate) (left to right: maximum, minimum, and average)



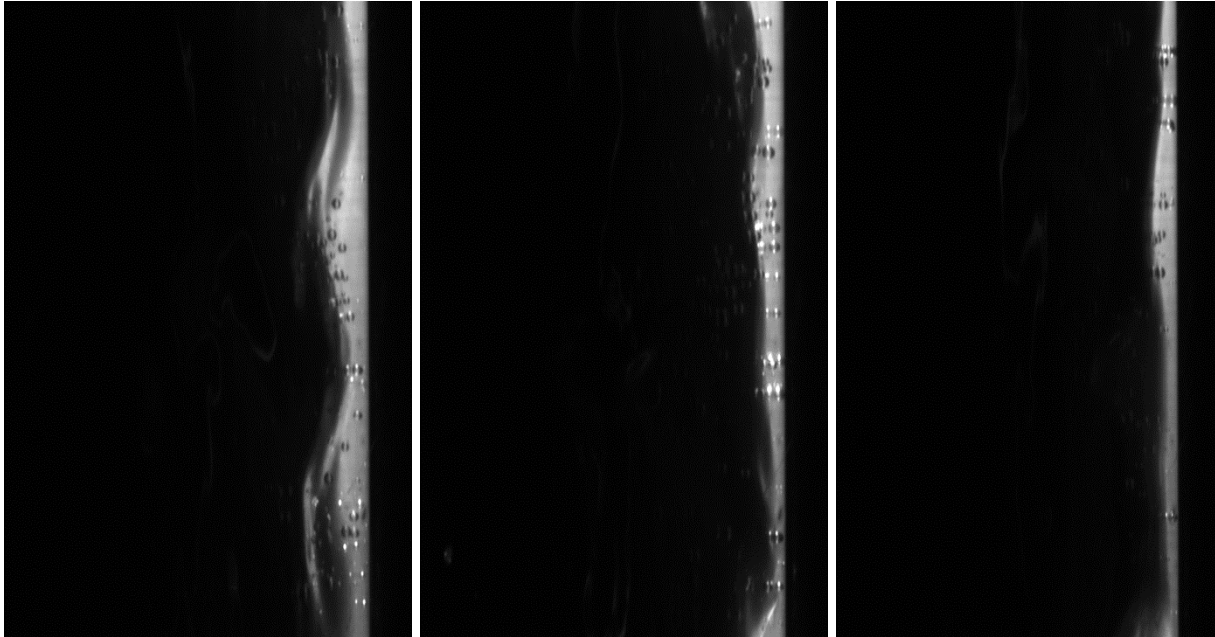
35 LPH (liquid rate) and 1100 SLPM (gas rate) (left to right: maximum, minimum, and average)



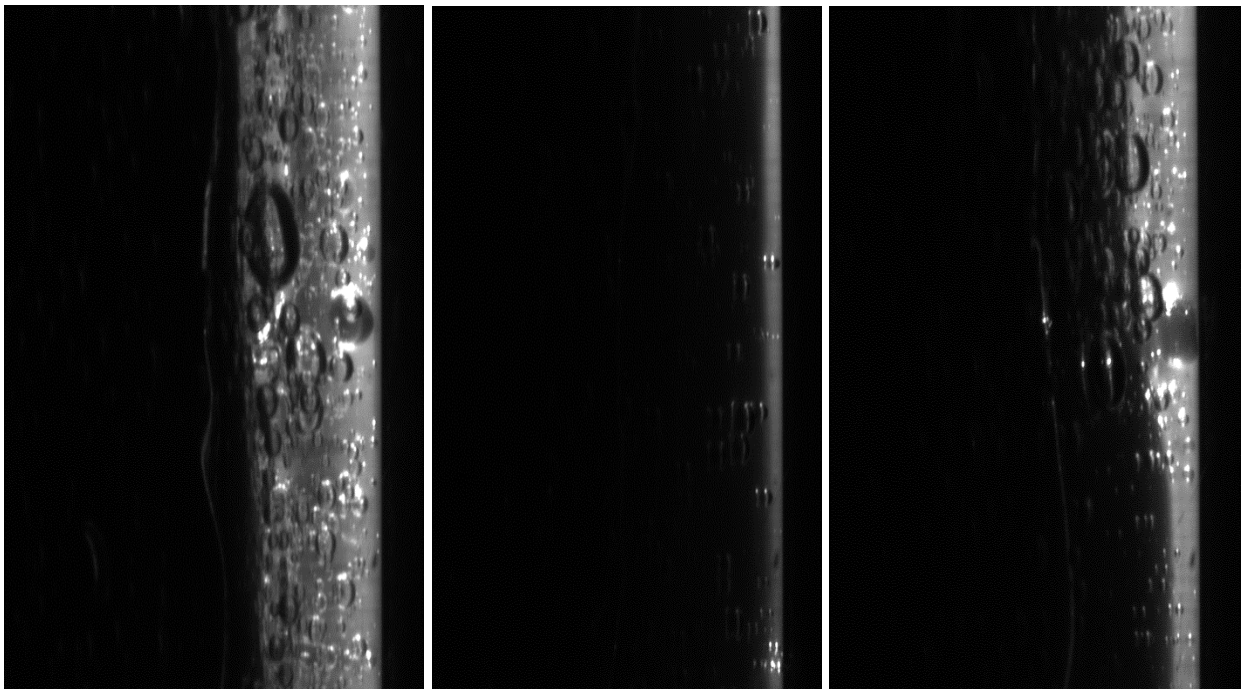
35 LPH (liquid rate) and 1200 SLPM (gas rate) (left to right: maximum, minimum, and average)



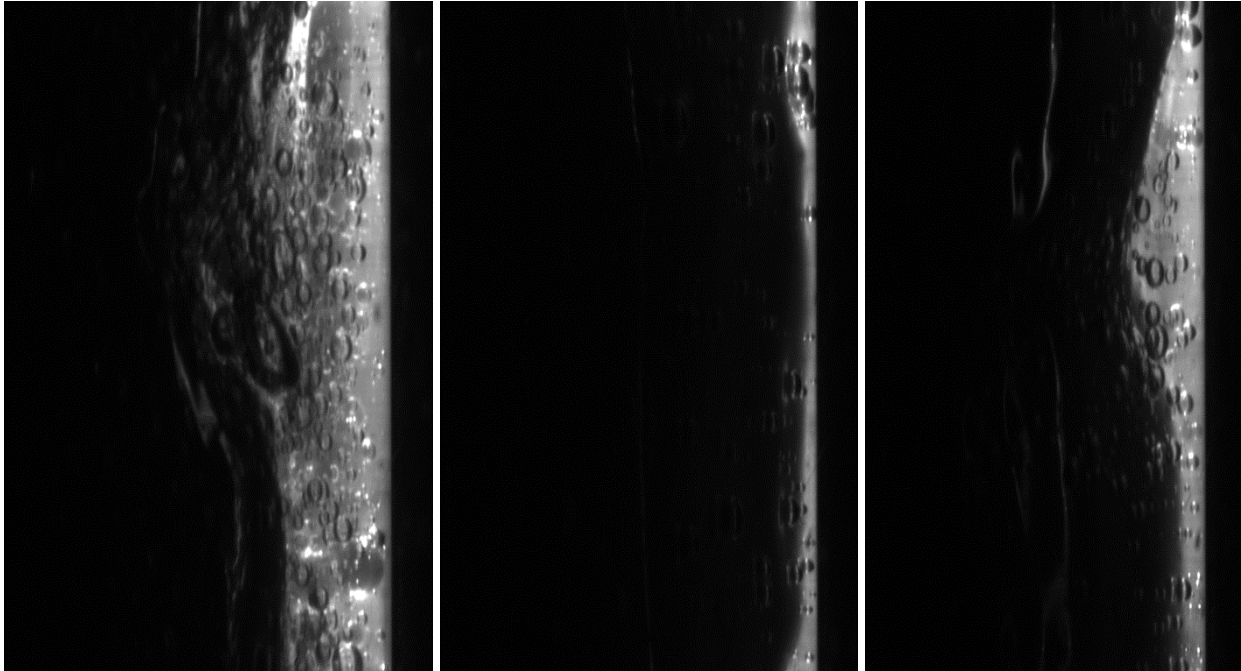
35 LPH (liquid rate) and 1300 SLPM (gas rate) (left to right: maximum, minimum, and average)



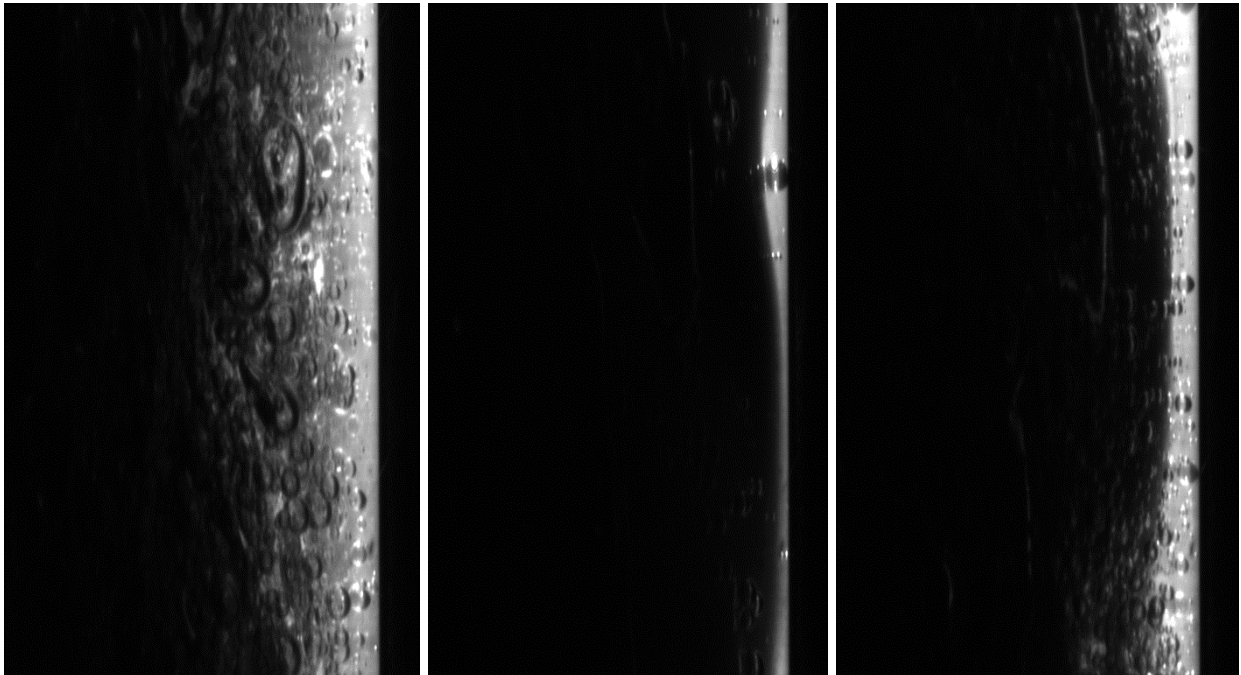
40 LPH (liquid rate) and 500 SLPM (gas rate) (left to right: maximum, minimum, and average)



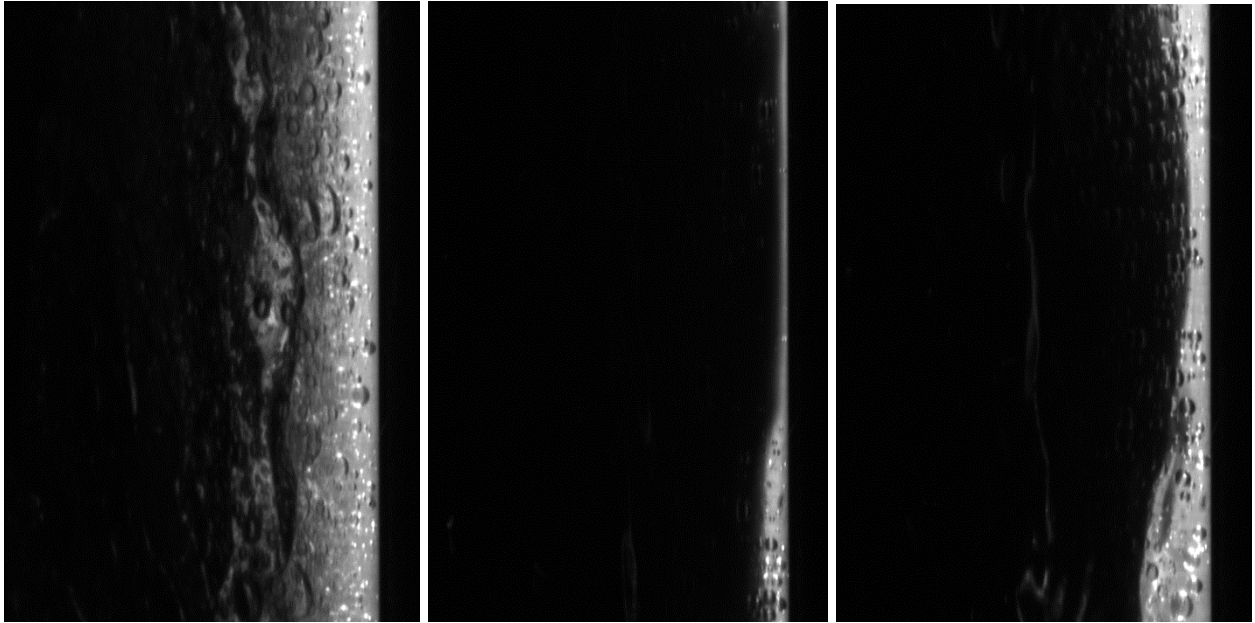
40 LPH (liquid rate) and 600 SLPM (gas rate) (left to right: maximum, minimum, and average)



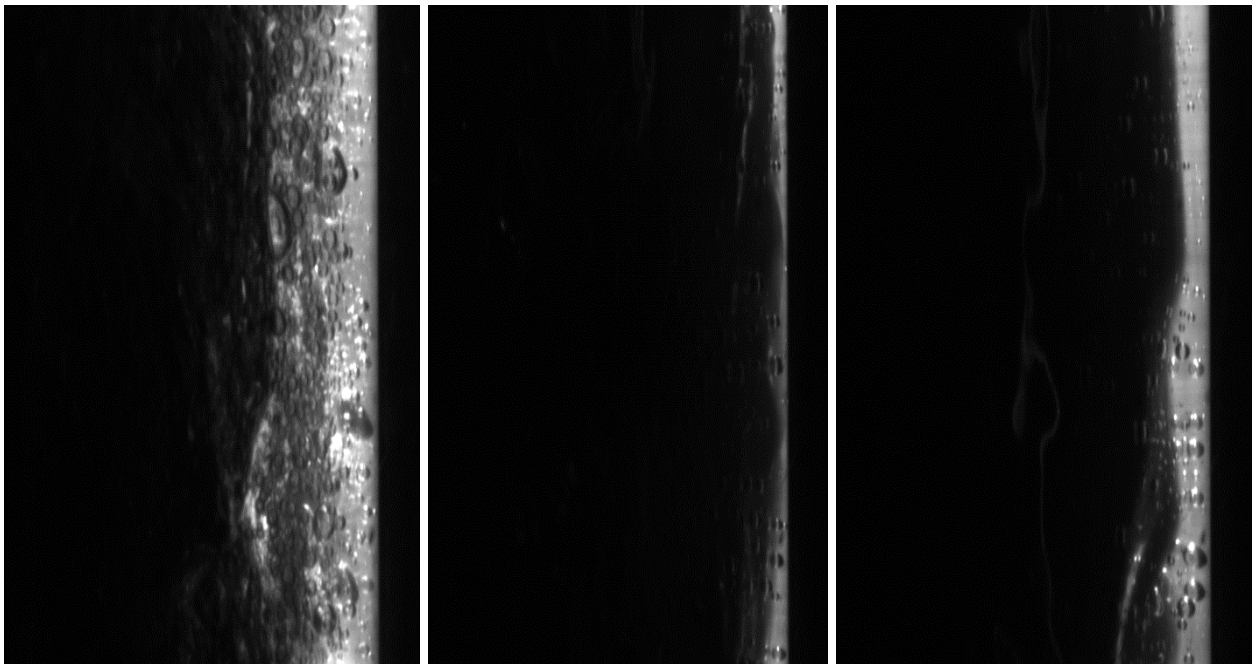
40 LPH (liquid rate) and 700 SLPM (gas rate) (left to right: maximum, minimum, and average)



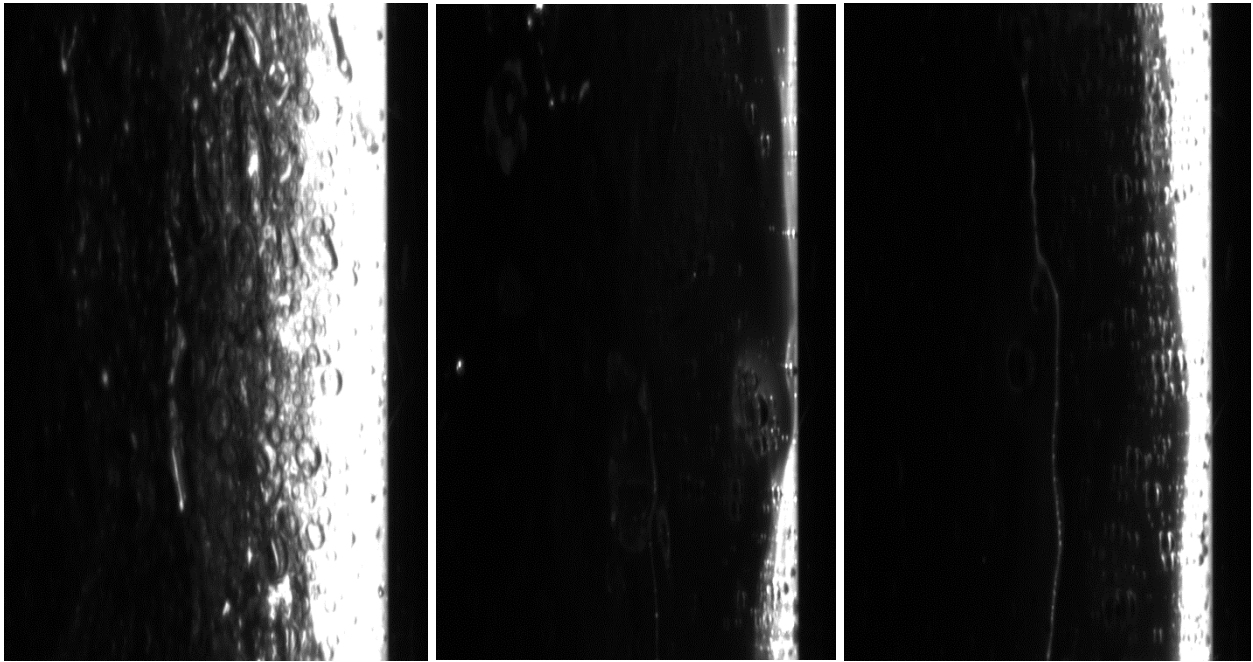
40 LPH (liquid rate) and 800 SLPM (gas rate) (left to right: maximum, minimum, and average)



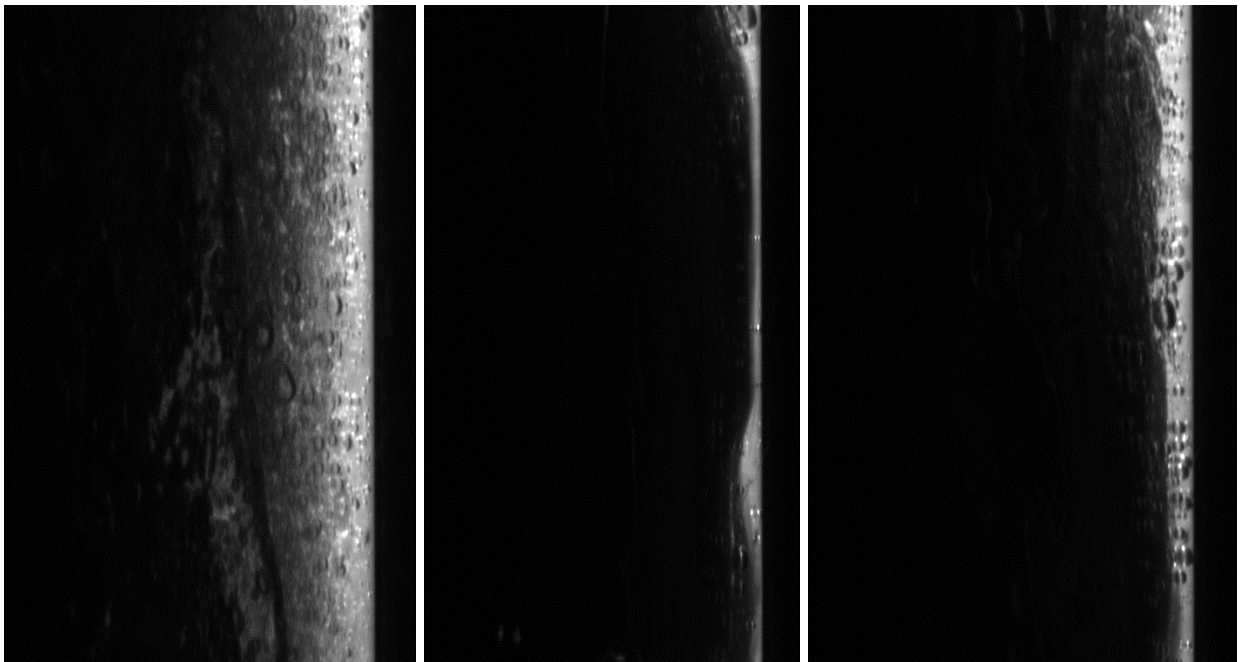
40 LPH (liquid rate) and 900 SLPM (gas rate) (left to right: maximum, minimum, and average)



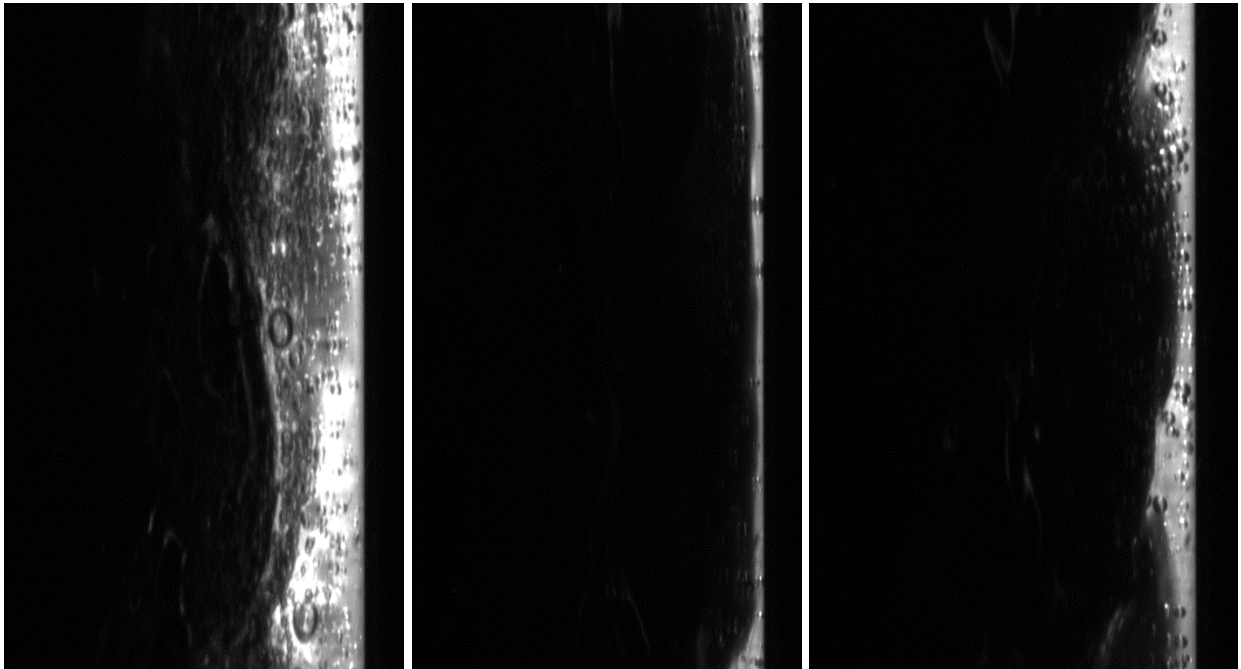
40 LPH (liquid rate) and 1000 SLPM (gas rate) (left to right: maximum, minimum, and average)



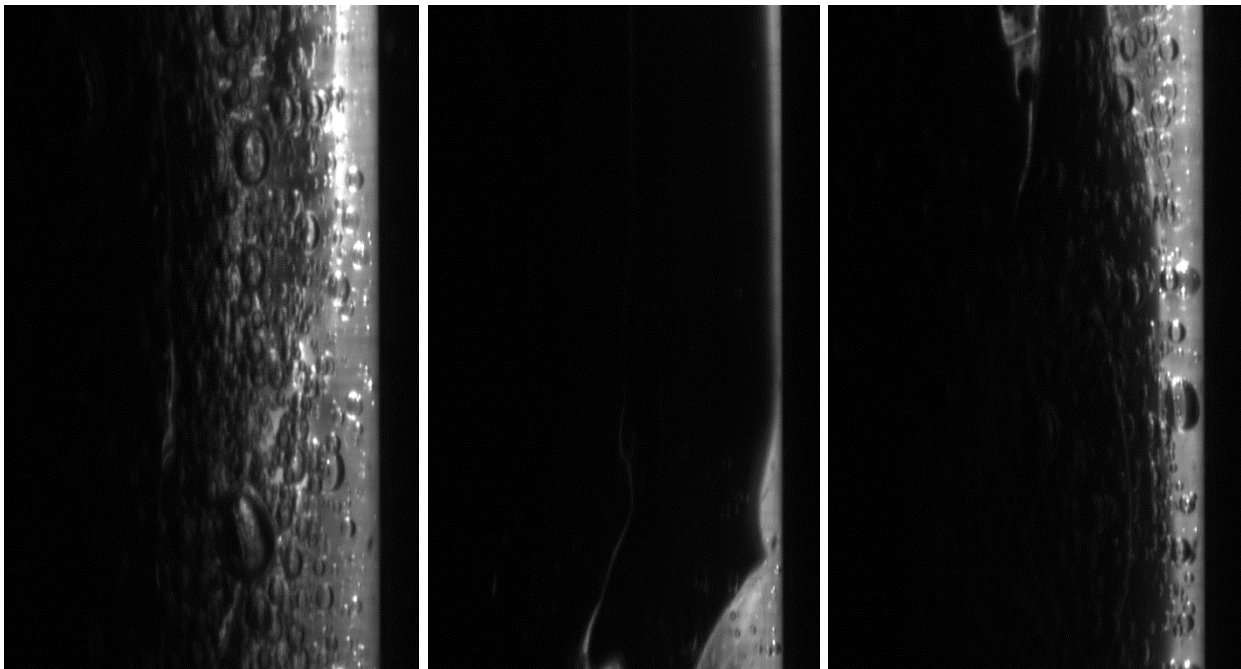
40 LPH (liquid rate) and 1100 SLPM (gas rate) (left to right: maximum, minimum, and average)



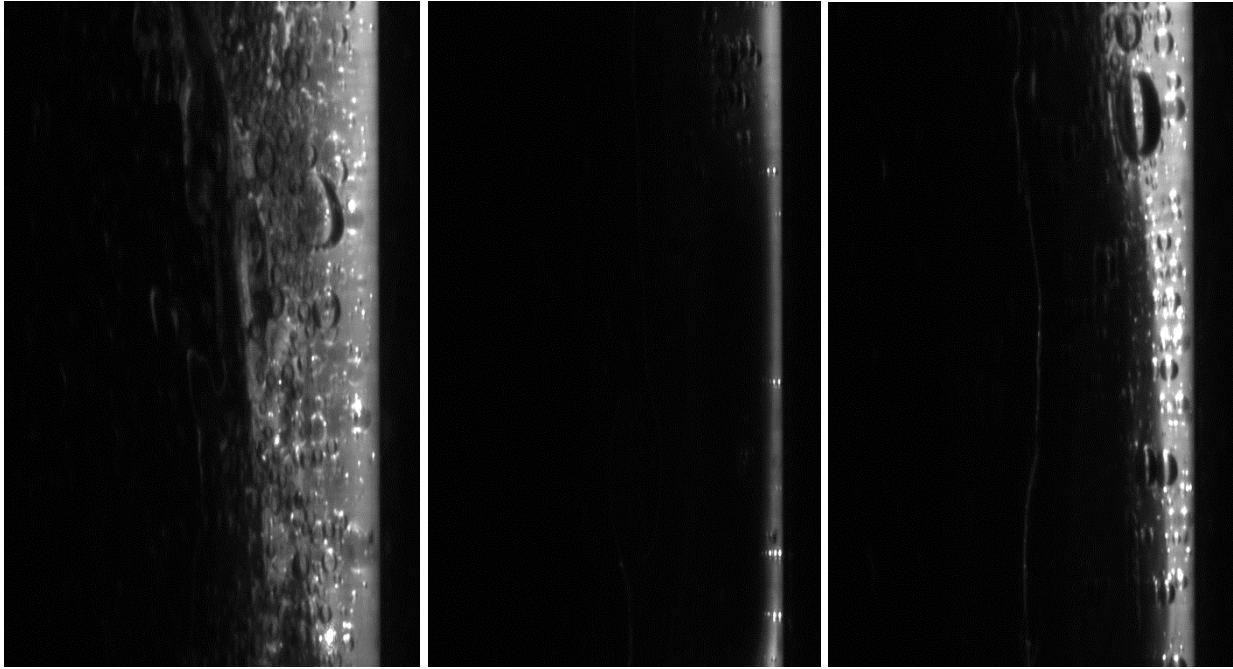
40 LPH (liquid rate) and 1200 SLPM (gas rate) (left to right: maximum, minimum, and average)



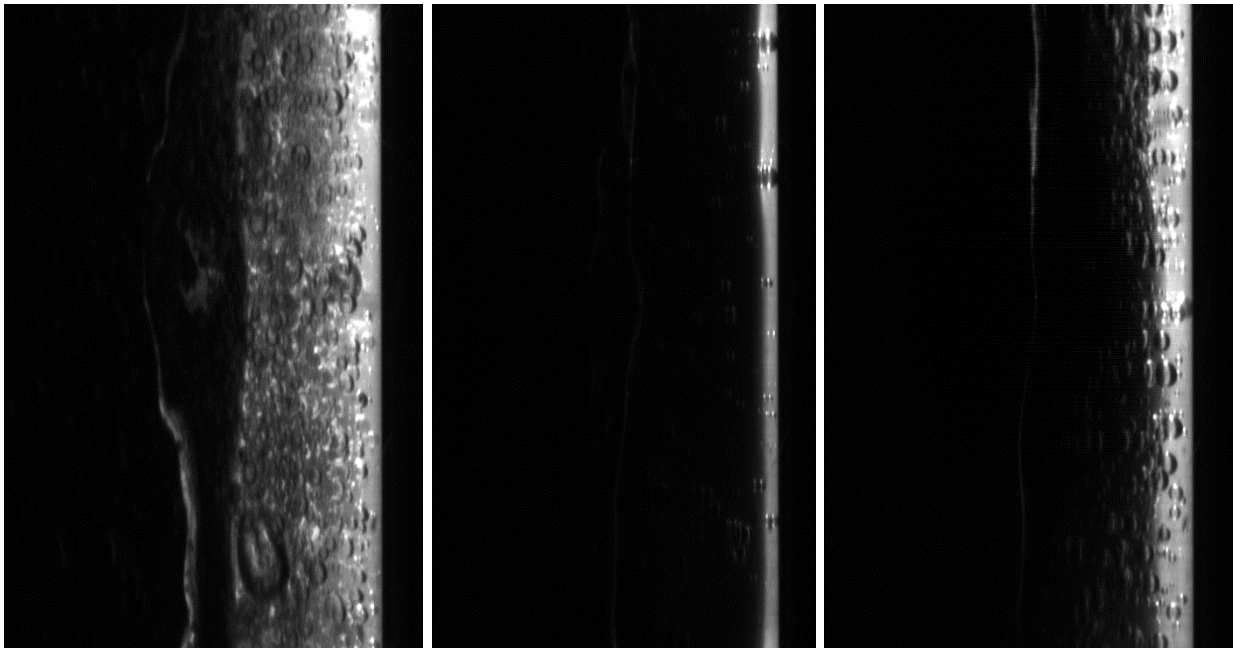
45 LPH (liquid rate) and 500 SLPM (gas rate) (left to right: maximum, minimum, and average)



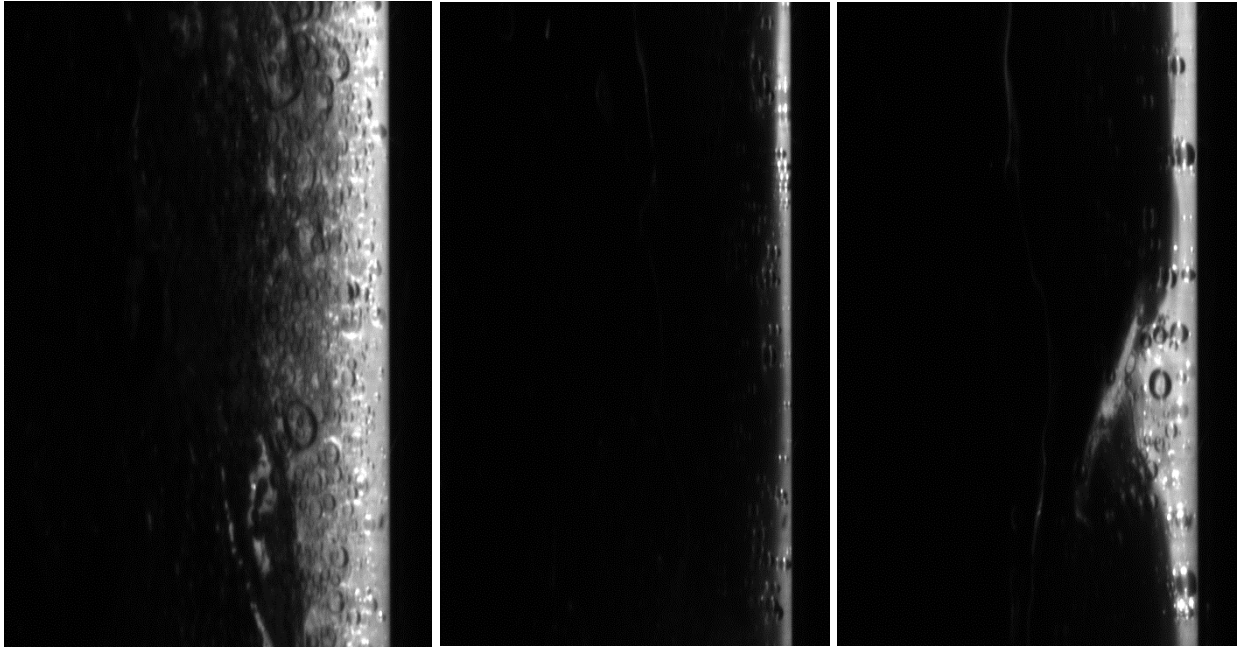
45 LPH (liquid rate) and 600 SLPM (gas rate) (left to right: maximum, minimum, and average)



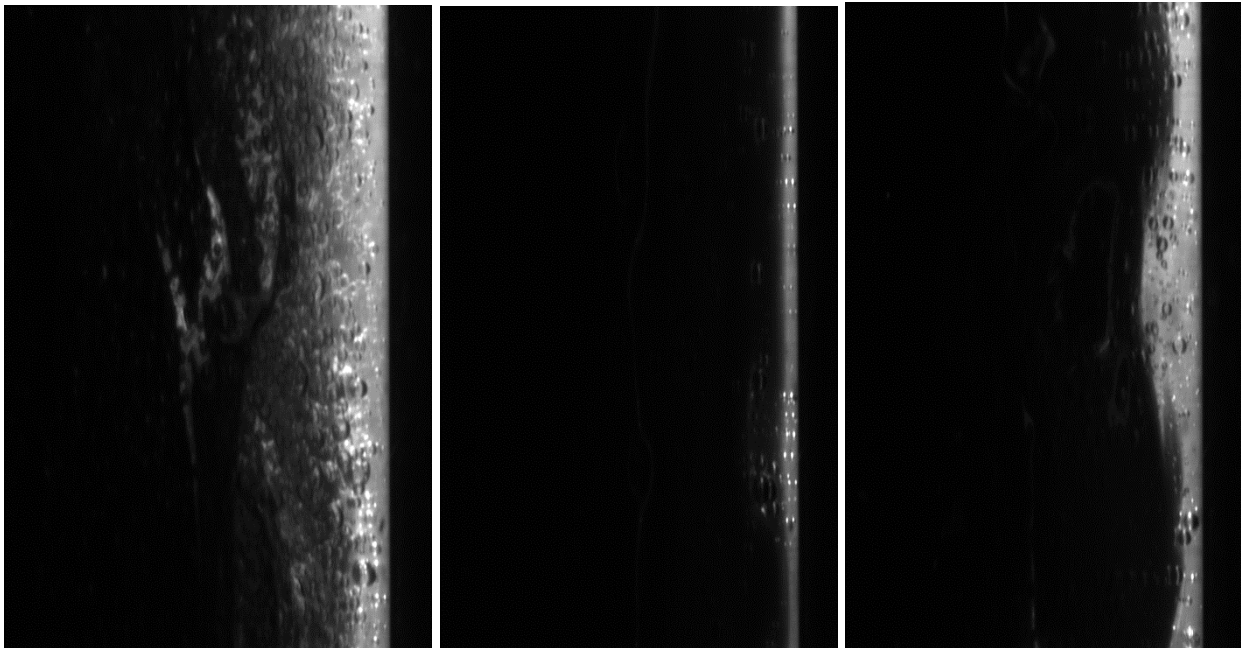
45 LPH (liquid rate) and 700 SLPM (gas rate) (left to right: maximum, minimum, and average)



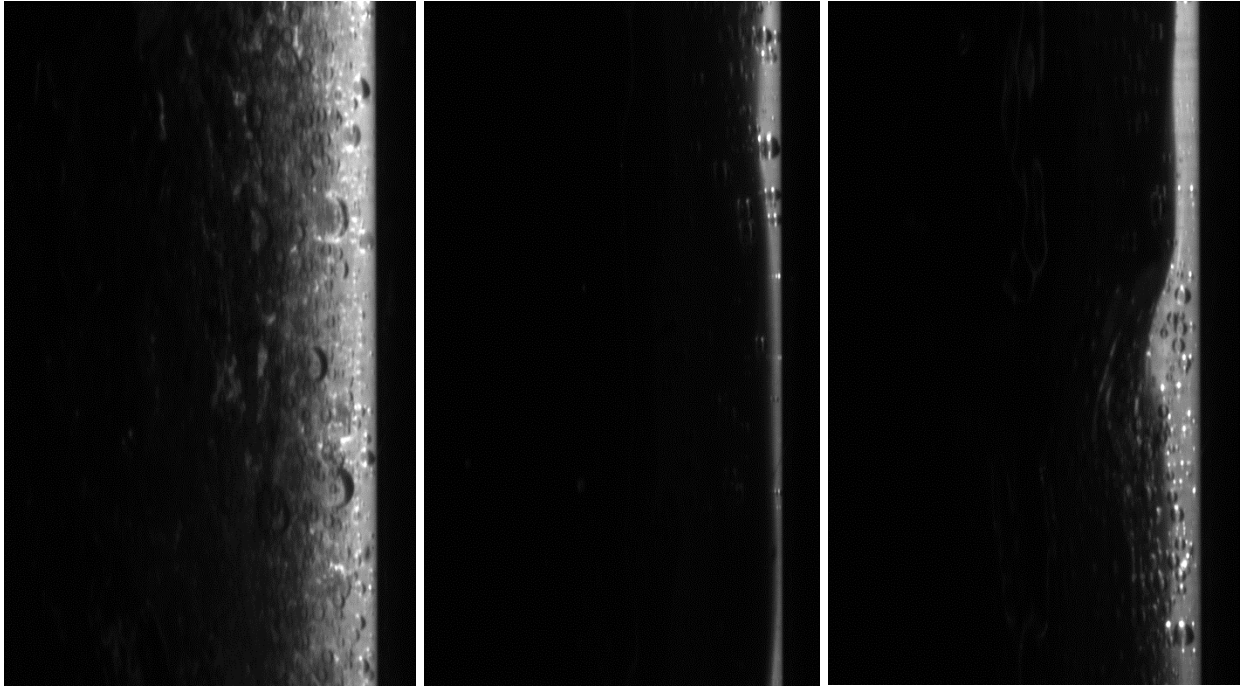
45 LPH (liquid rate) and 800 SLPM (gas rate) (left to right: maximum, minimum, and average)



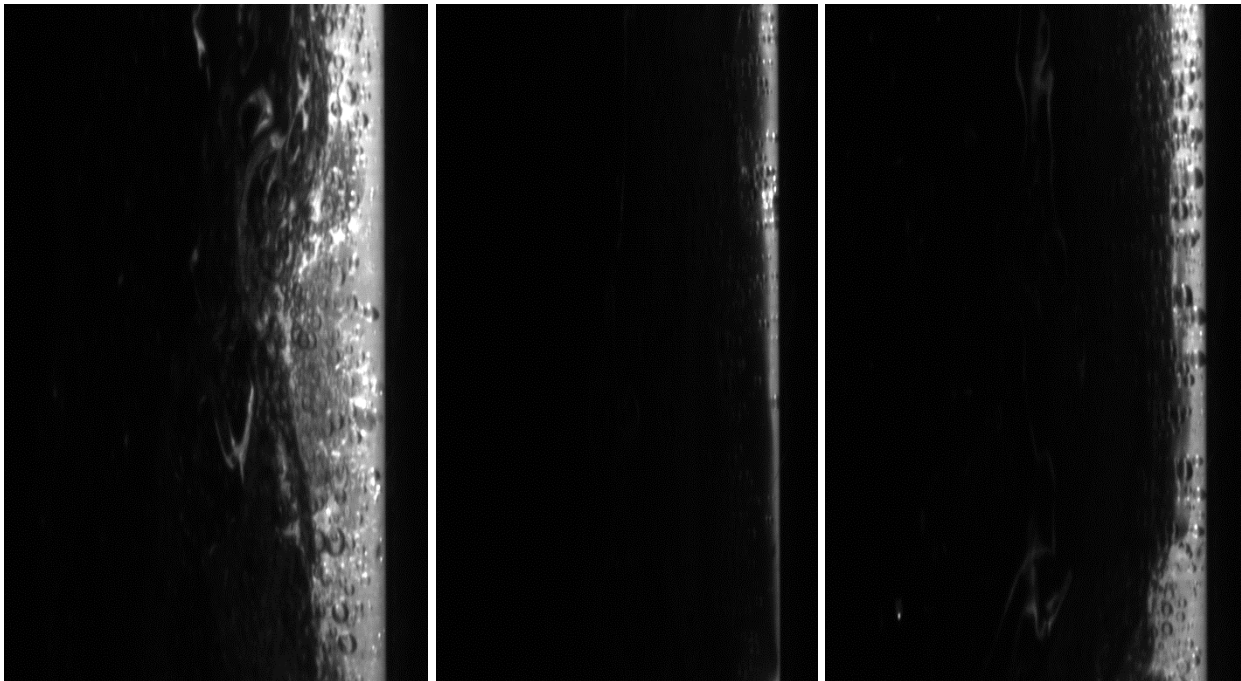
45 LPH (liquid rate) and 900 SLPM (gas rate) (left to right: maximum, minimum, and average)



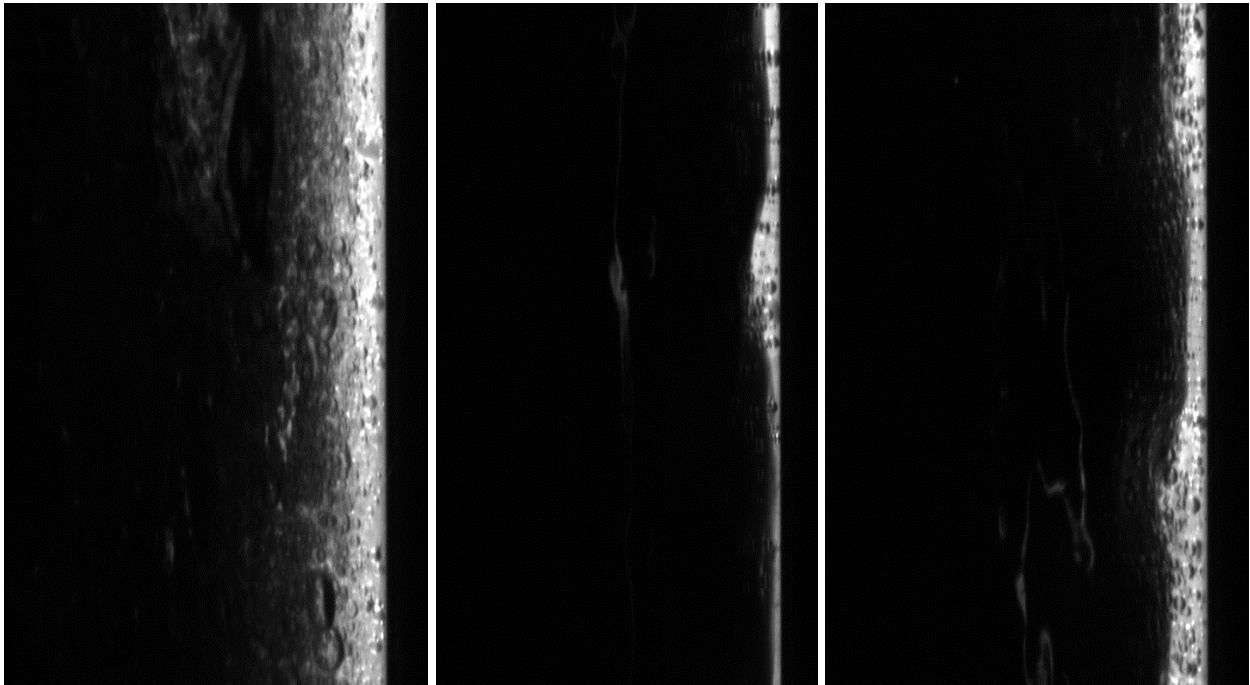
45 LPH (liquid rate) and 1000 SLPM (gas rate) (left to right: maximum, minimum, and average)



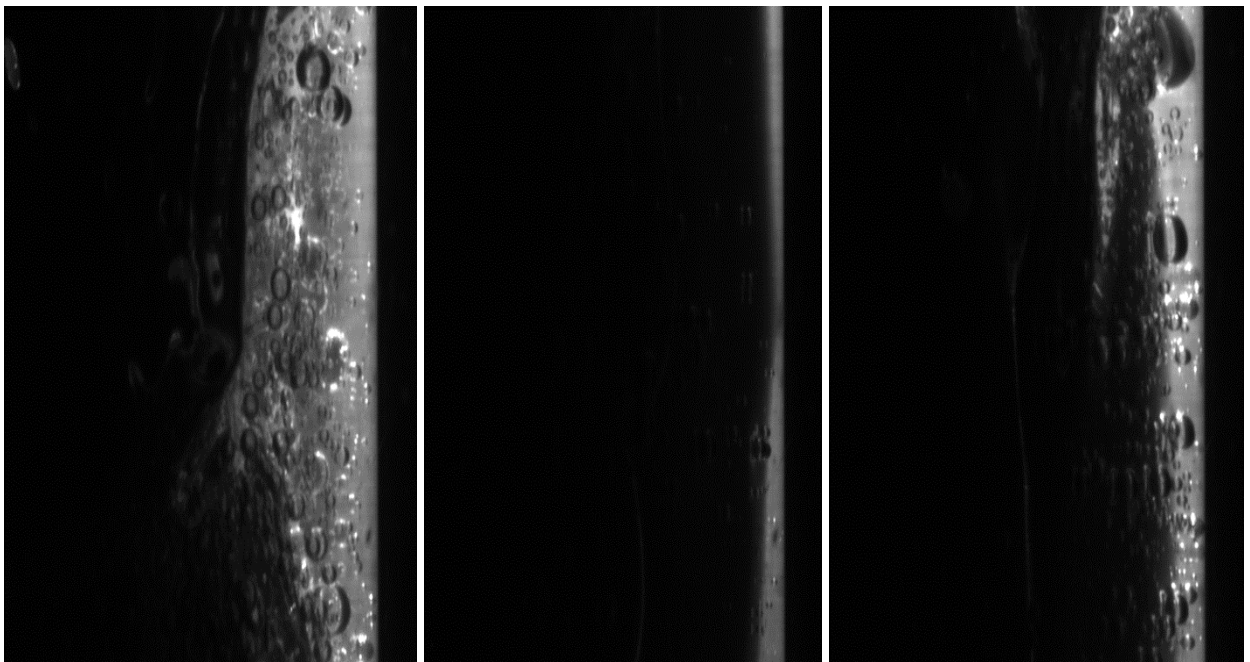
45 LPH (liquid rate) and 1100 SLPM (gas rate) (left to right: maximum, minimum, and average)



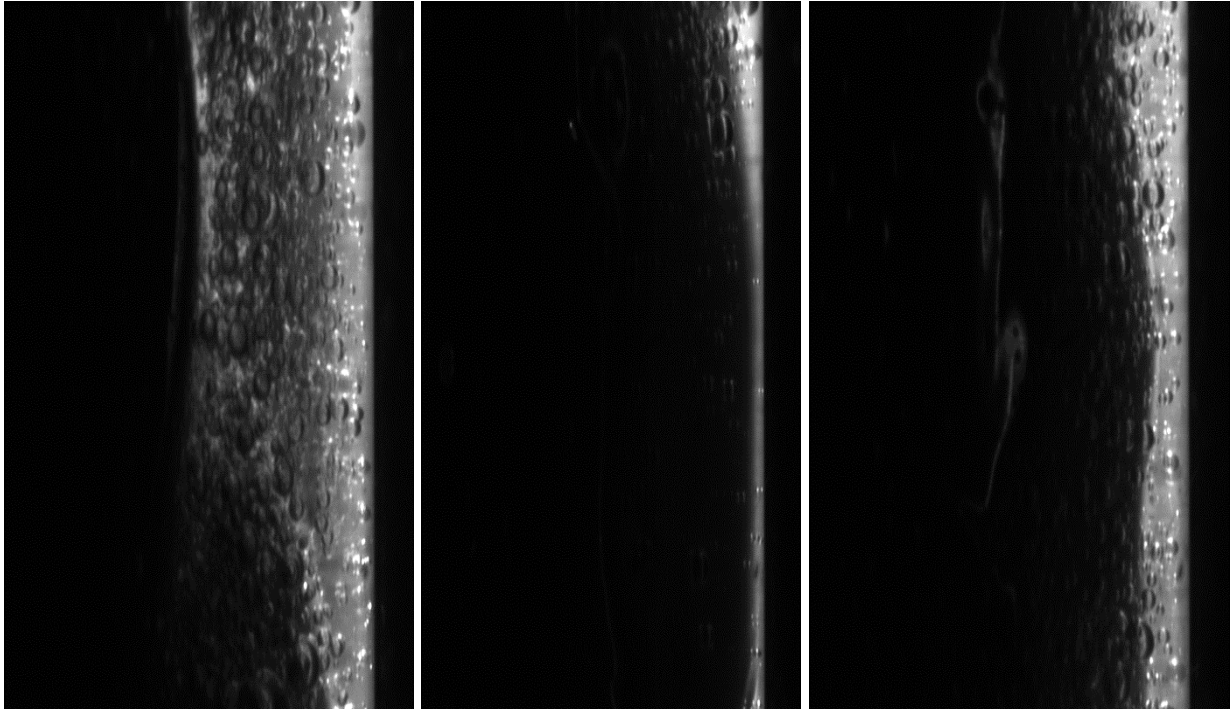
45 LPH (liquid rate) and 1200 SLPM (gas rate) (left to right: maximum, minimum, and average)



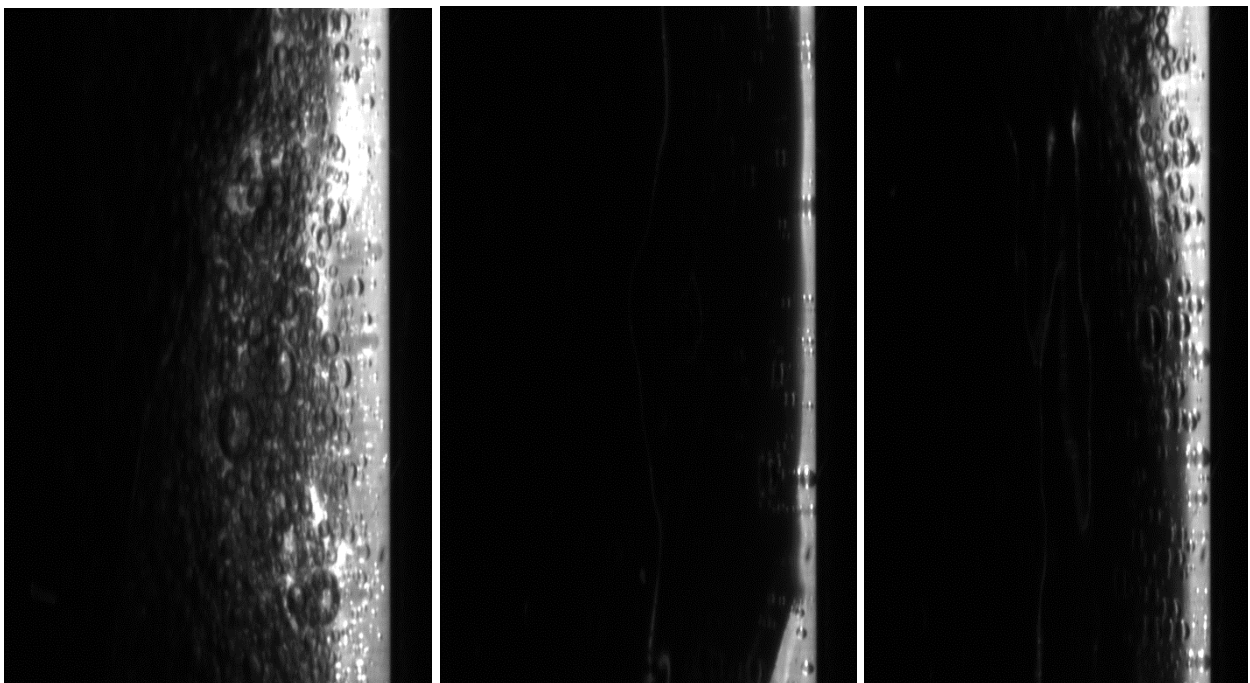
50 LPH (liquid rate) and 500 SLPM (gas rate) (left to right: maximum, minimum, and average)



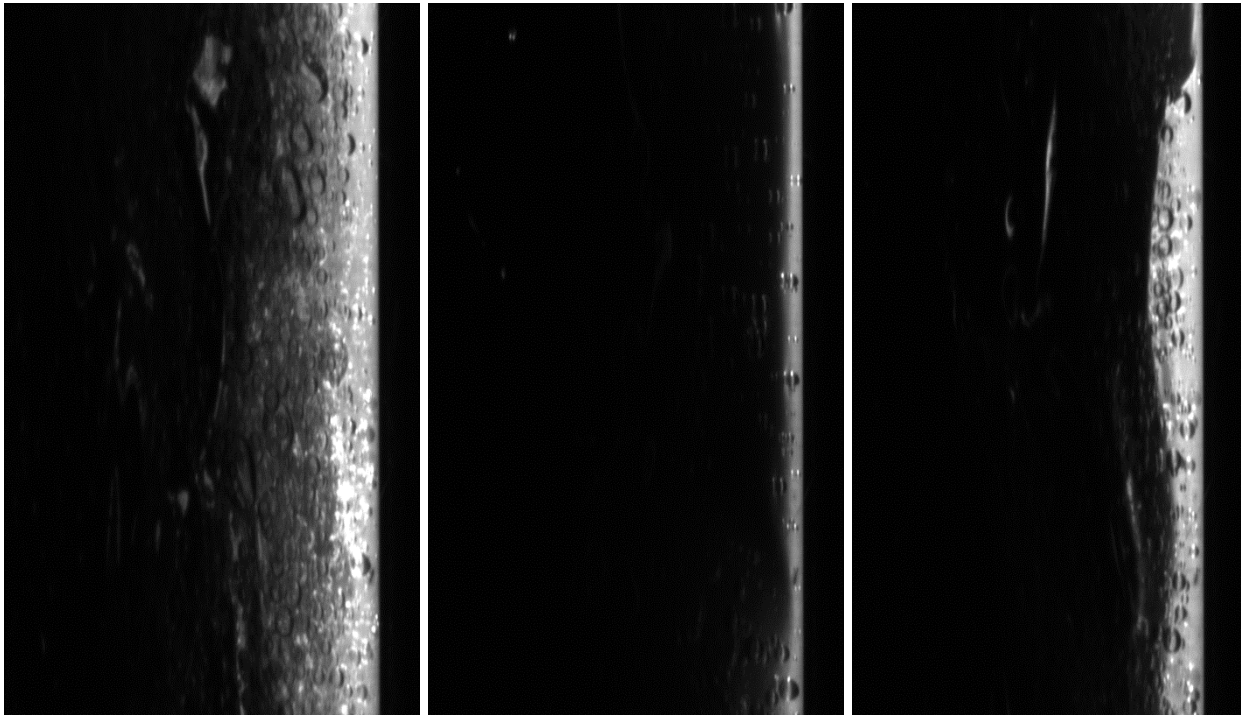
50 LPH (liquid rate) and 600 SLPM (gas rate) (left to right: maximum, minimum, and average)



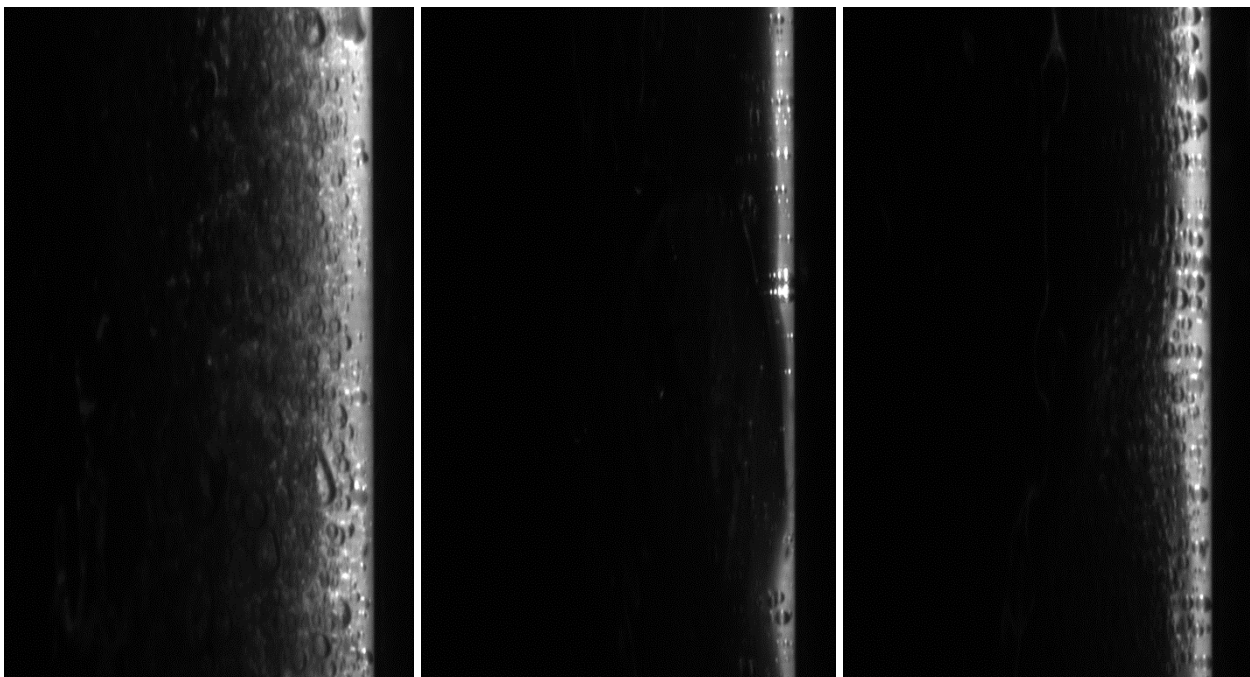
50 LPH (liquid rate) and 700 SLPM (gas rate) (left to right: maximum, minimum, and average)



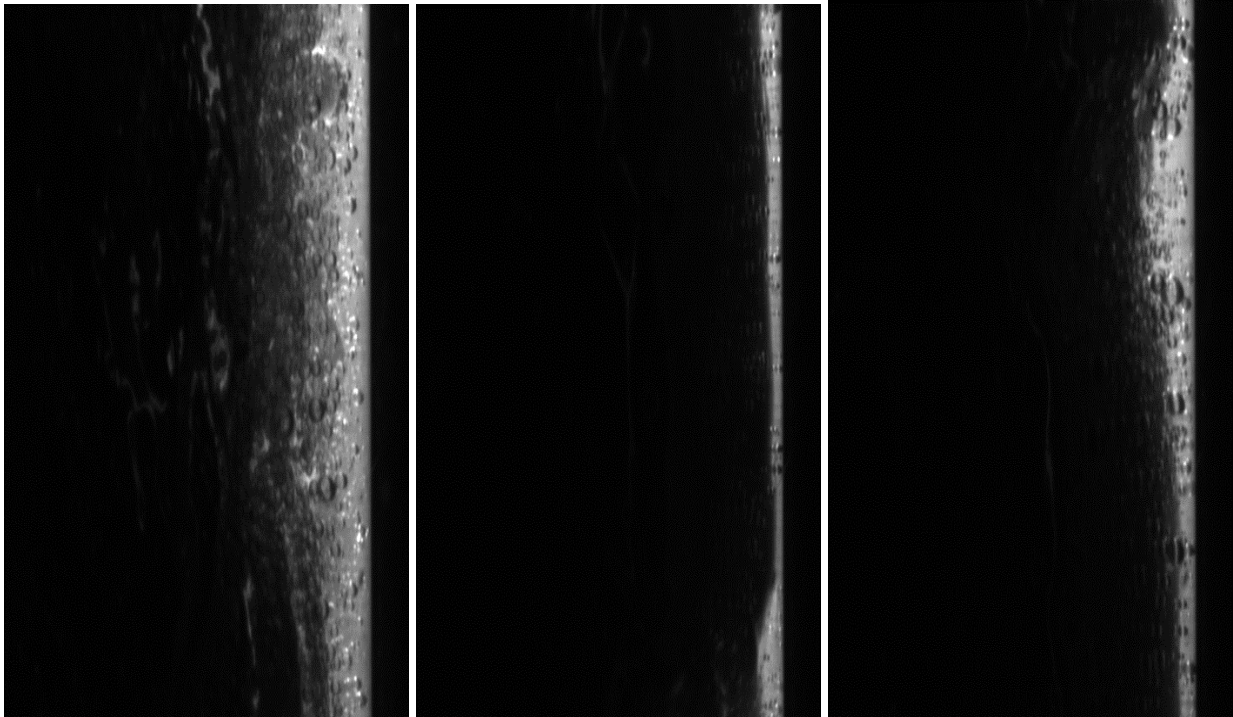
50 LPH (liquid rate) and 800 SLPM (gas rate) (left to right: maximum, minimum, and average)



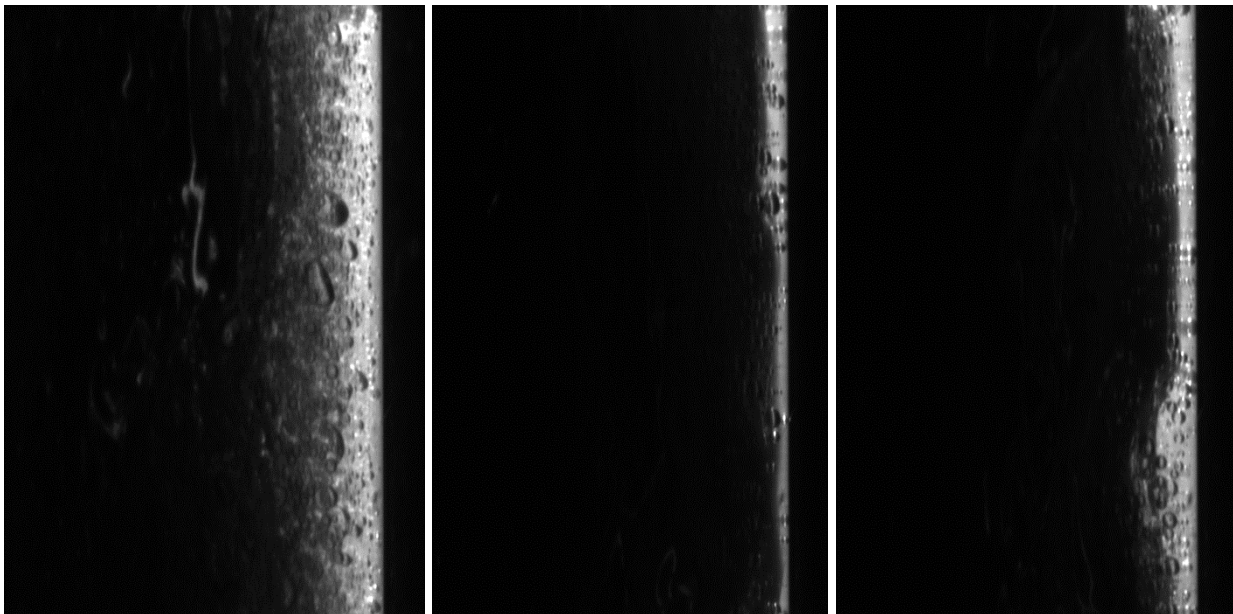
50 LPH (liquid rate) and 900 SLPM (gas rate) (left to right: maximum, minimum, and average)



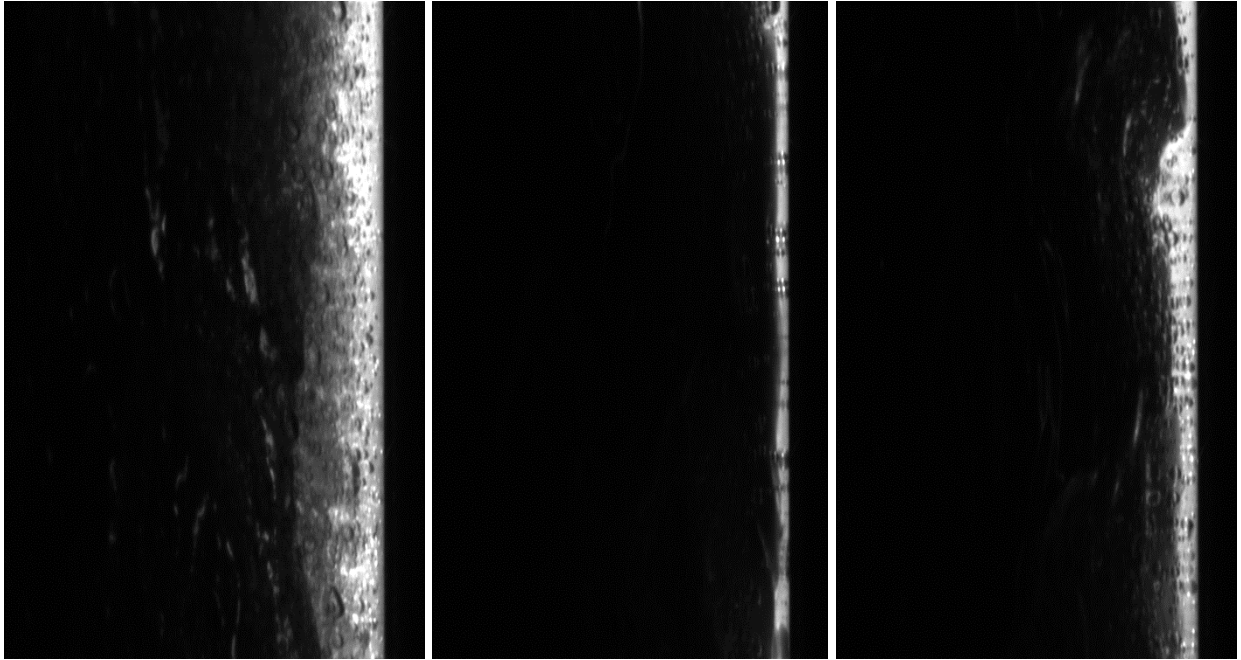
50 LPH (liquid rate) and 1000 SLPM (gas rate) (left to right: maximum, minimum, and average)



50 LPH (liquid rate) and 1100 SLPM (gas rate) (left to right: maximum, minimum, and average)



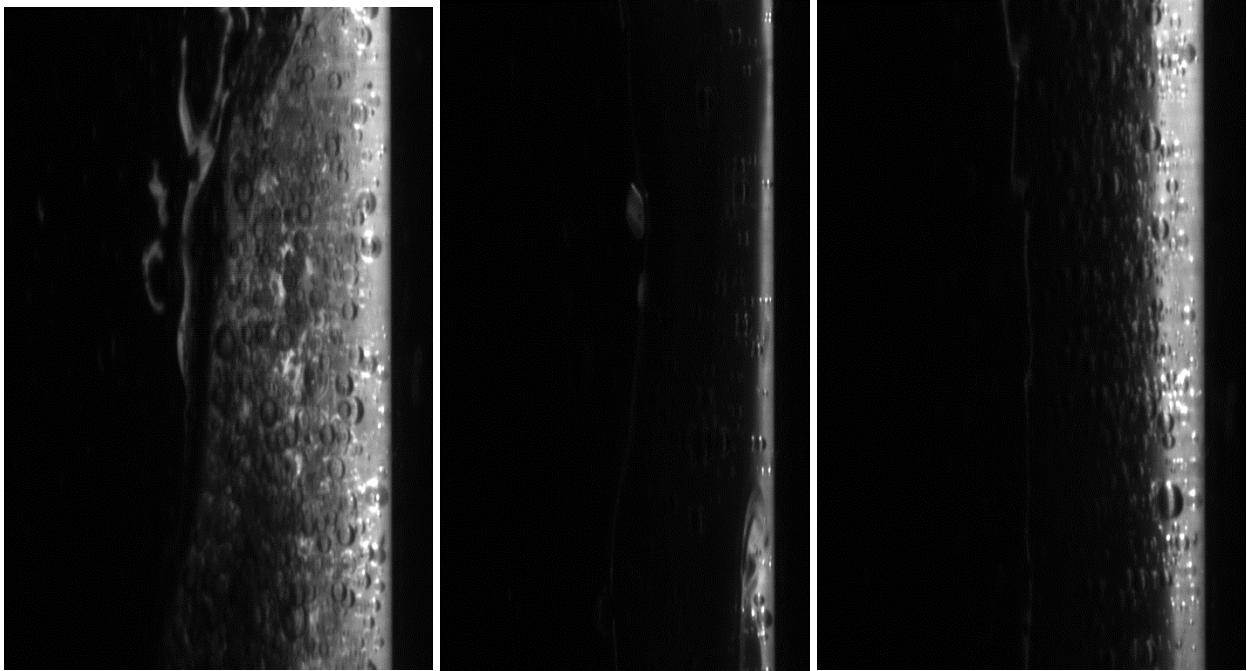
50 LPH (liquid rate) and 1200 SLPM (gas rate) (left to right: maximum, minimum, and average)



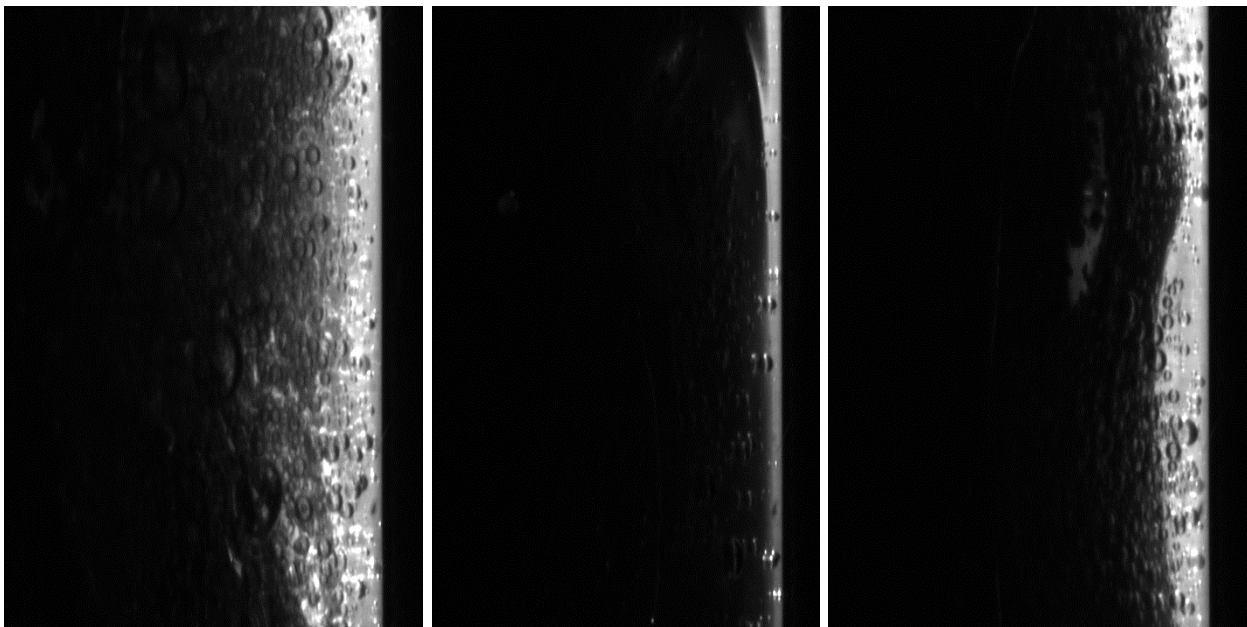
55 LPH (liquid rate) and 500 SLPM (gas rate) (left to right: maximum, minimum, and average)



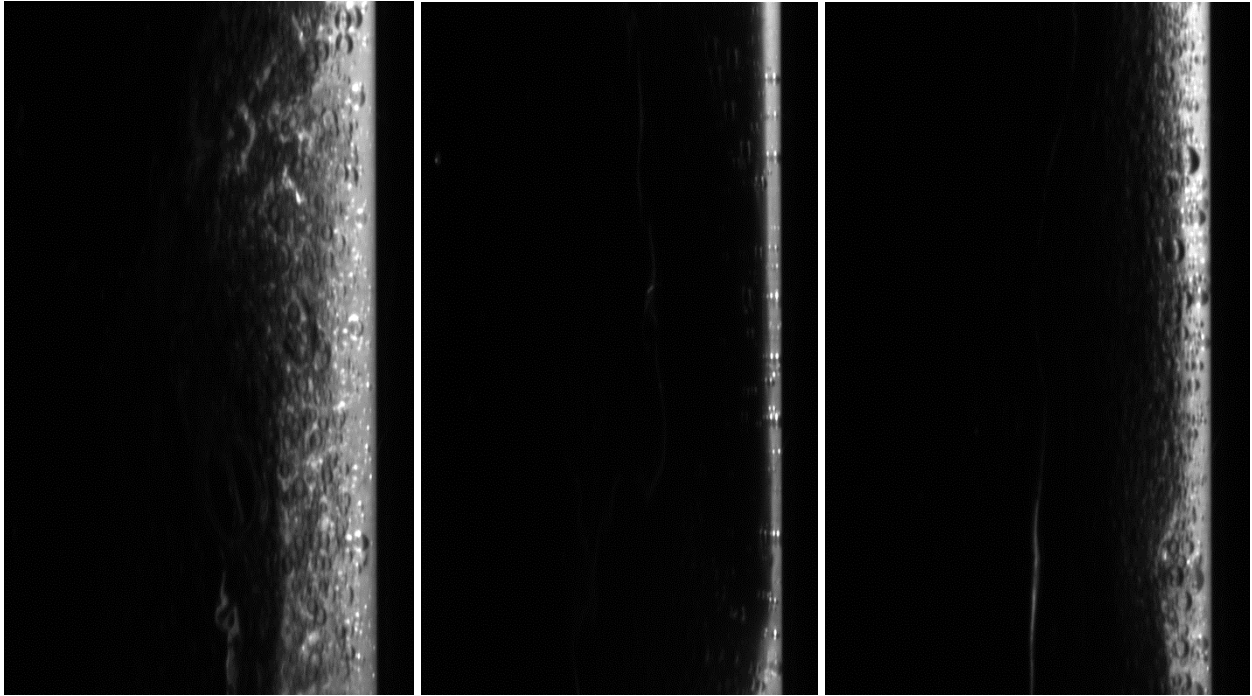
55 LPH (liquid rate) and 600 SLPM (gas rate) (left to right: maximum, minimum, and average)



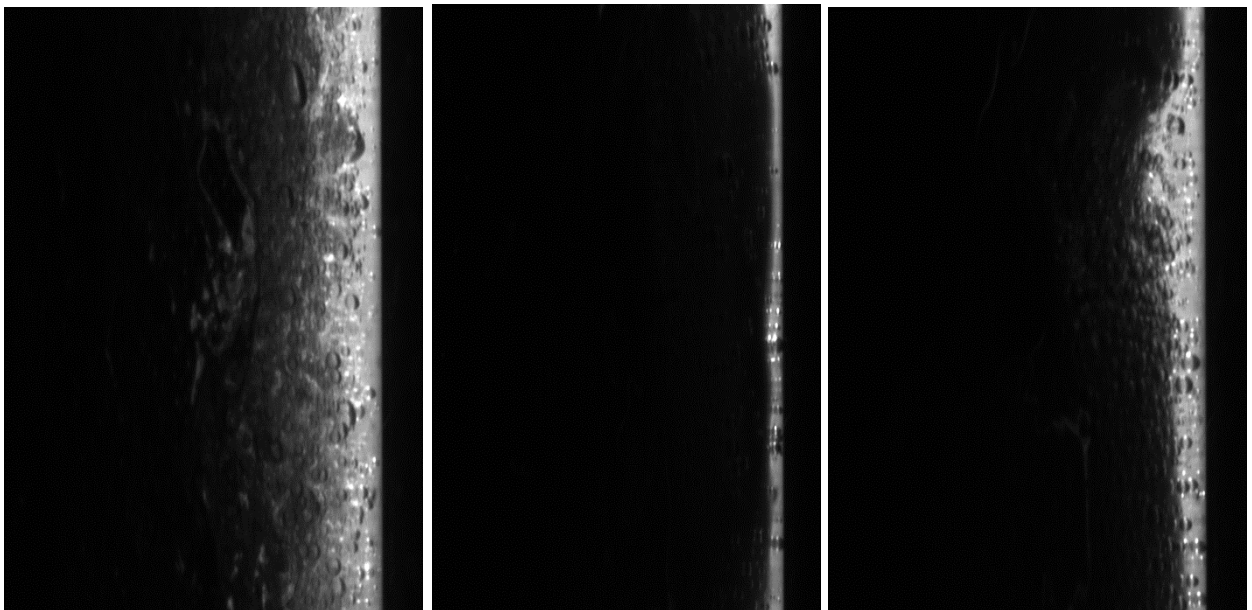
55 LPH (liquid rate) and 700 SLPM (gas rate) (left to right: maximum, minimum, and average)



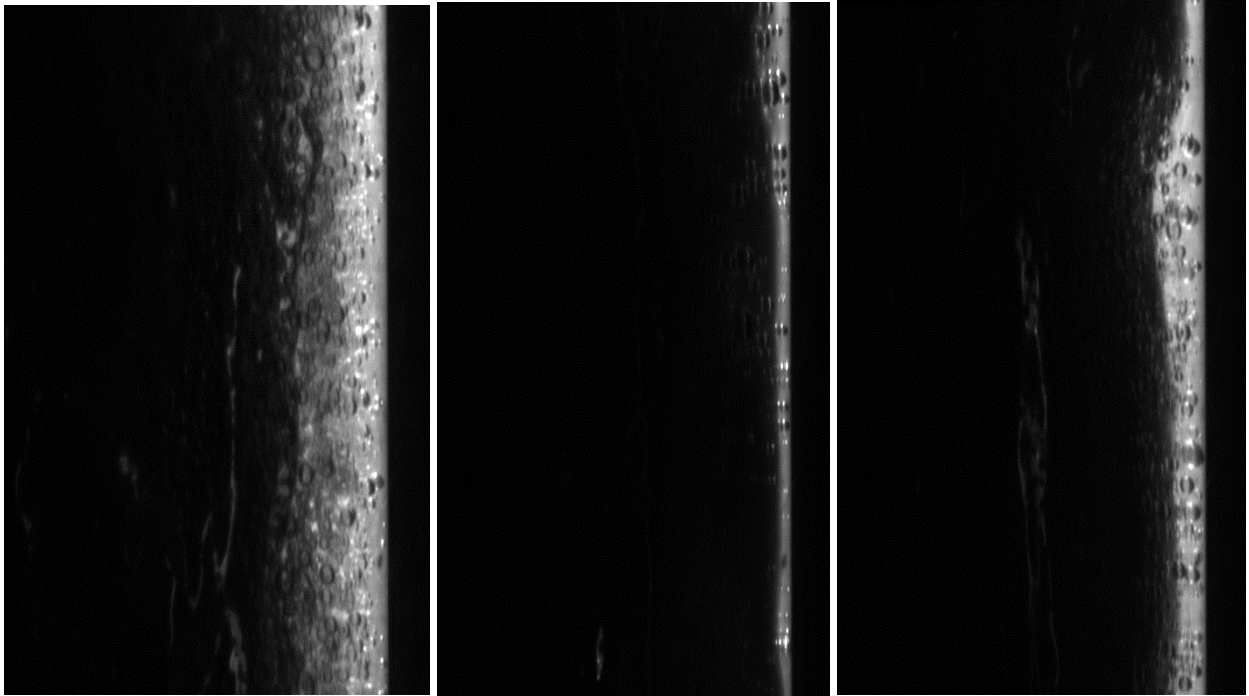
55 LPH (liquid rate) and 800 SLPM (gas rate) (left to right: maximum, minimum, and average)



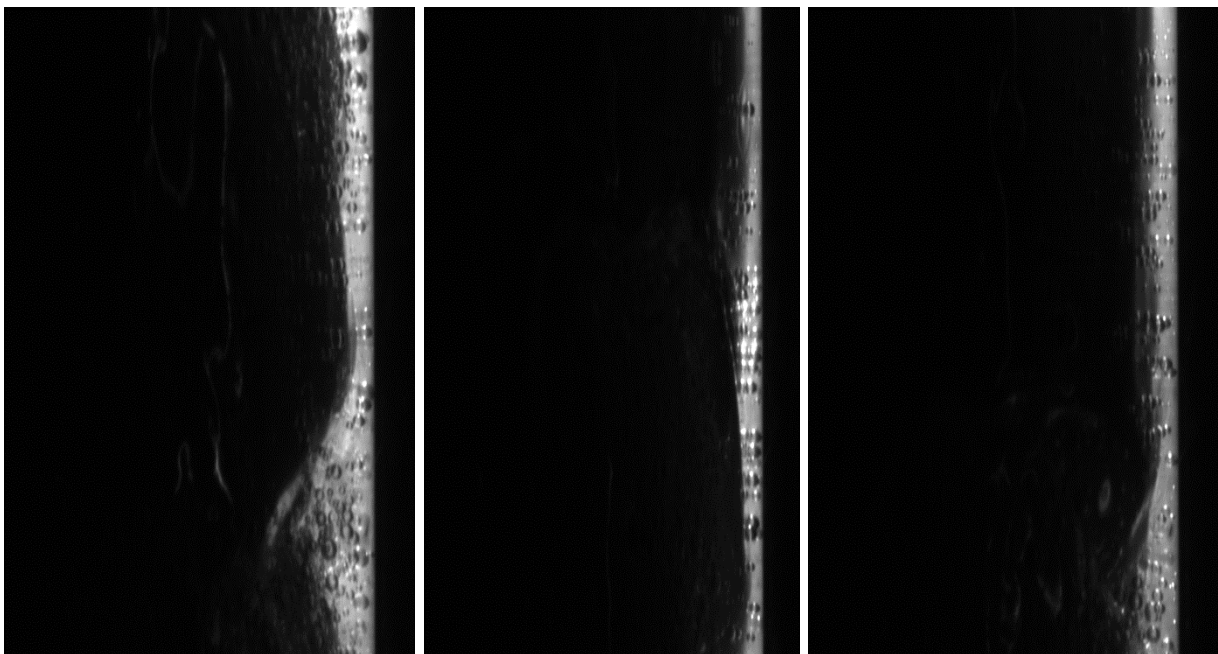
55 LPH (liquid rate) and 900 SLPM (gas rate) (left to right: maximum, minimum, and average)



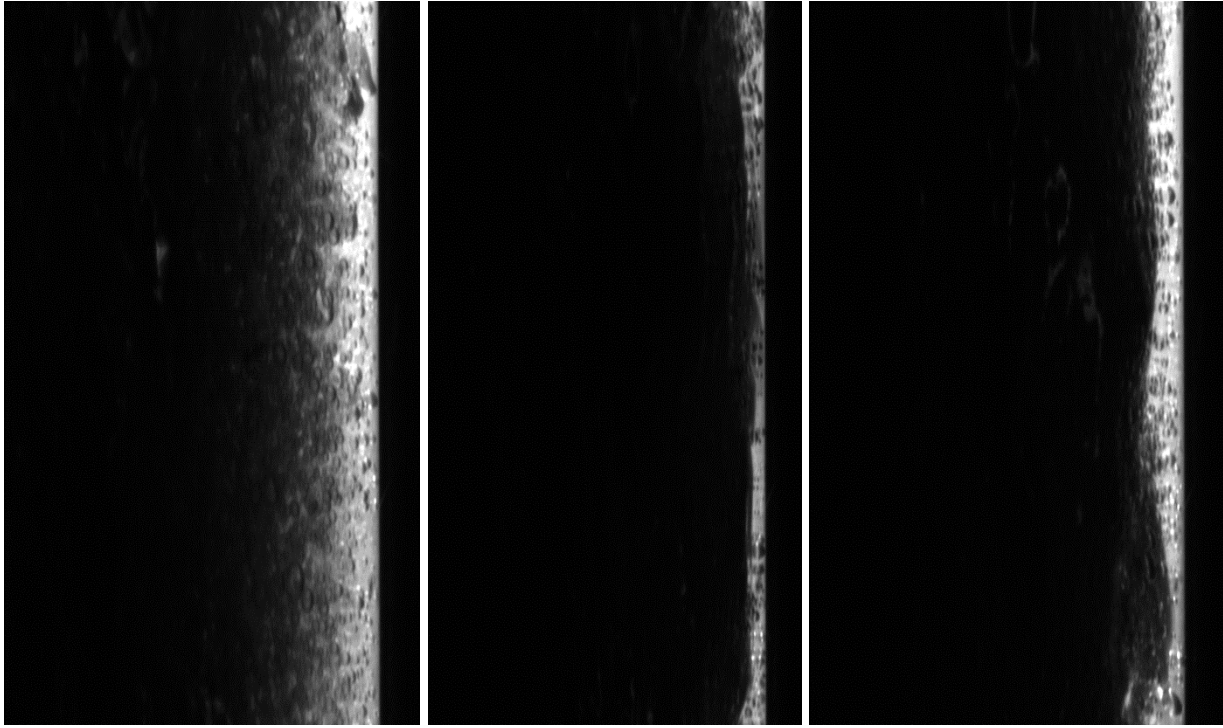
55 LPH (liquid rate) and 1000 SLPM (gas rate) (left to right: maximum, minimum, and average)



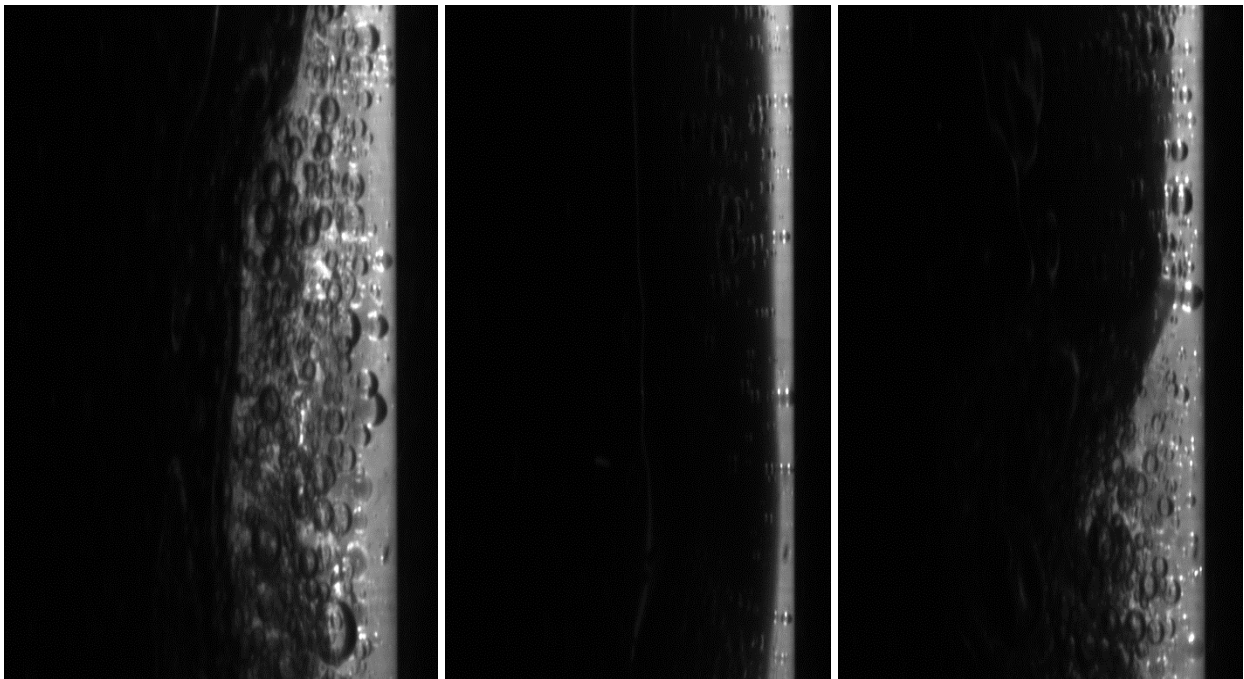
55 LPH (liquid rate) and 1100 SLPM (gas rate) (left to right: maximum, minimum, and average)



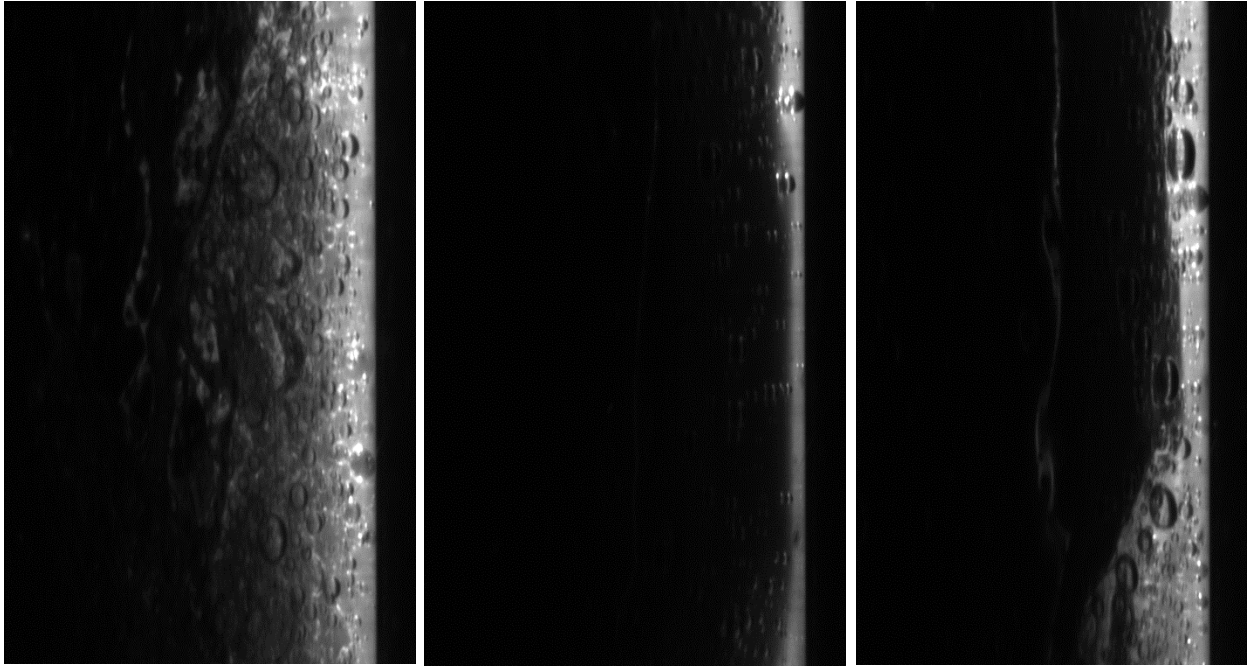
55 LPH (liquid rate) and 1200 SLPM (gas rate) (left to right: maximum, minimum, and average)



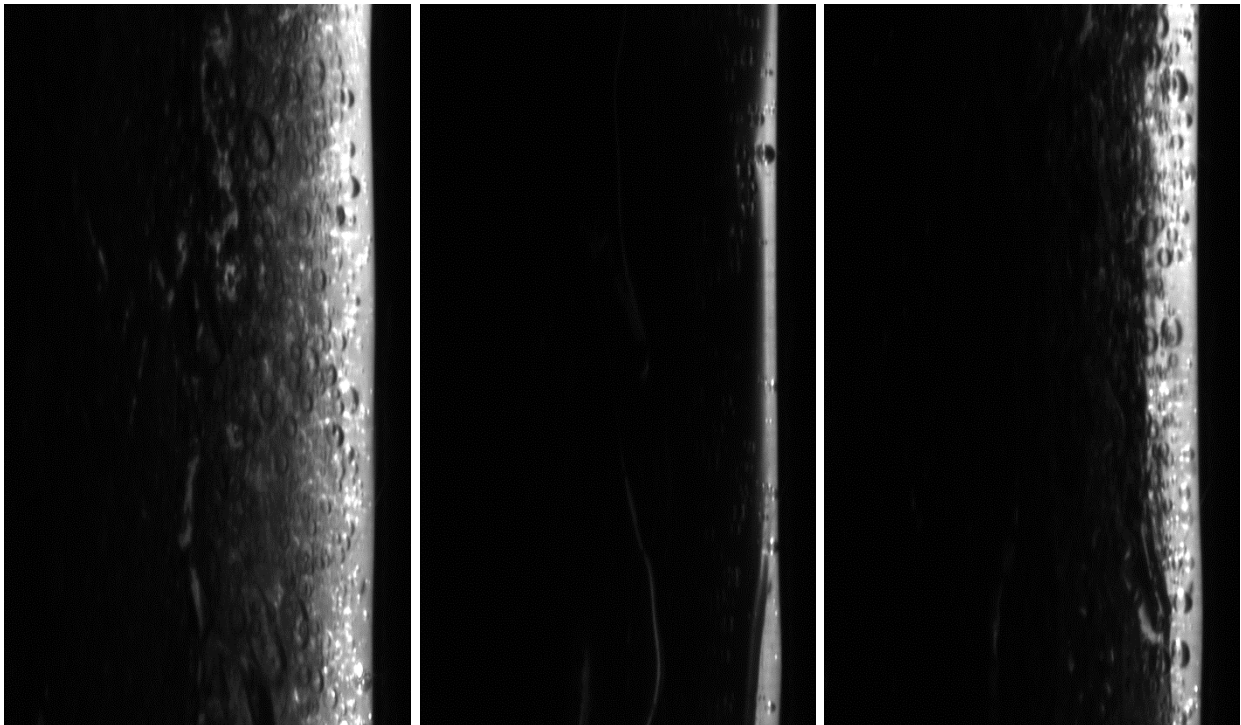
60 LPH (liquid rate) and 500 SLPM (gas rate) (left to right: maximum, minimum, and average)



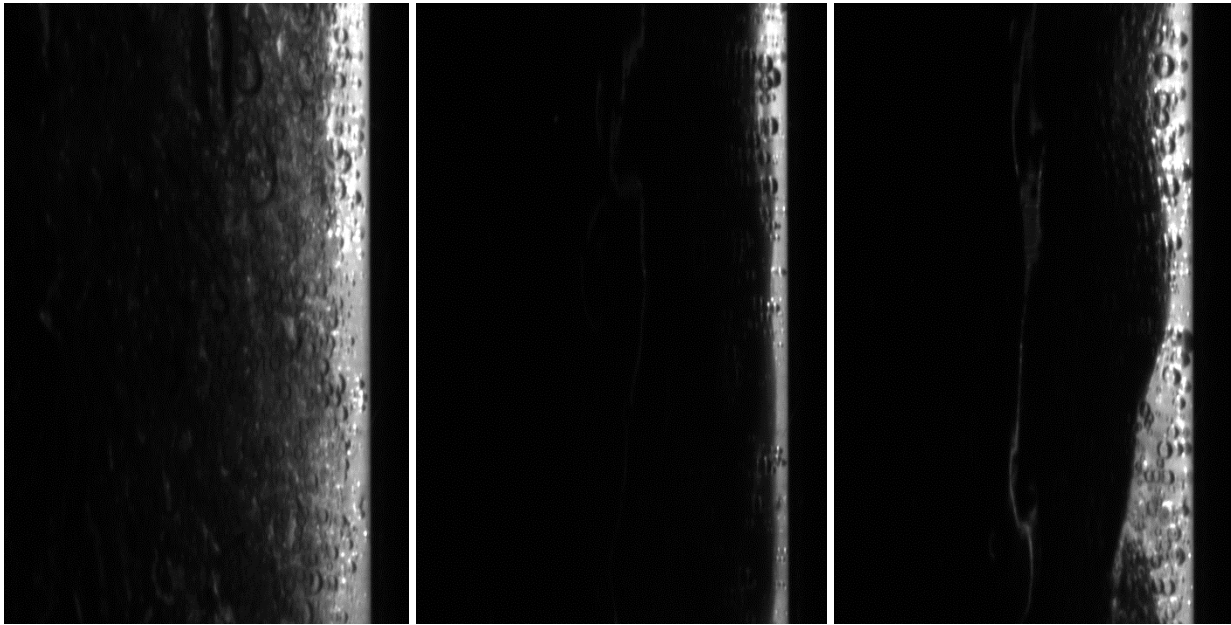
60 LPH (liquid rate) and 600 SLPM (gas rate) (left to right: maximum, minimum, and average)



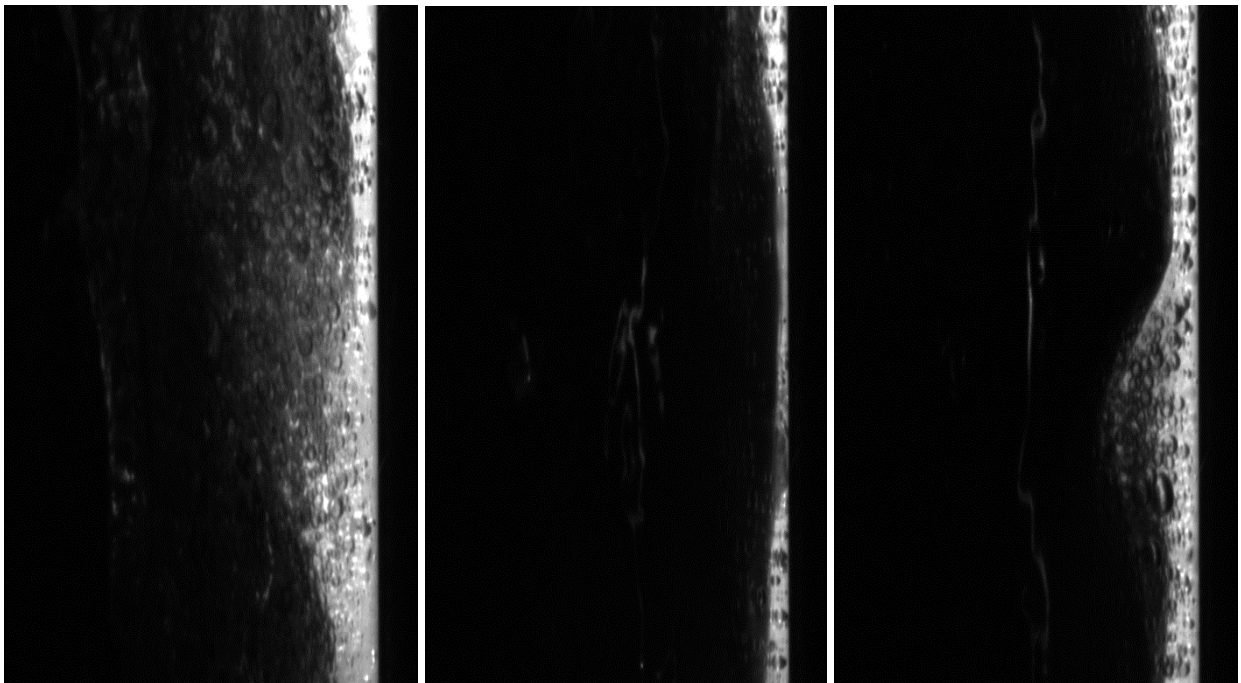
60 LPH (liquid rate) and 700 SLPM (gas rate) (left to right: maximum, minimum, and average)



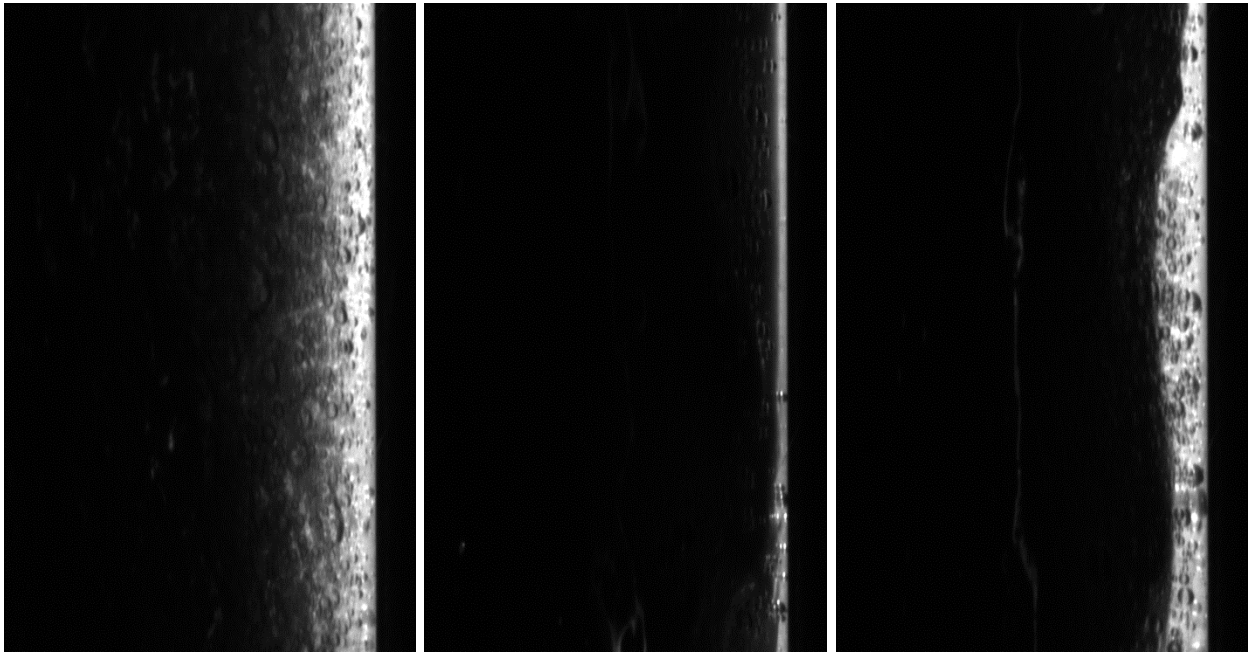
60 LPH (liquid rate) and 800 SLPM (gas rate) (left to right: maximum, minimum, and average)



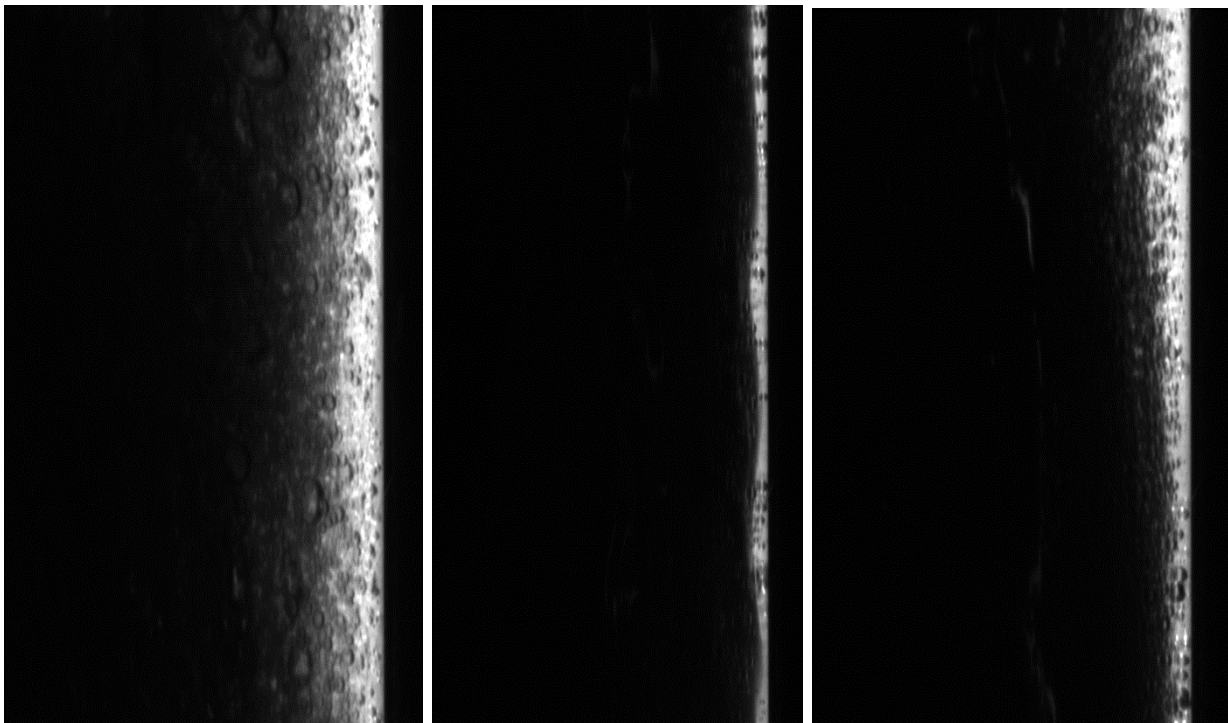
60 LPH (liquid rate) and 900 SLPM (gas rate) (left to right: maximum, minimum, and average)



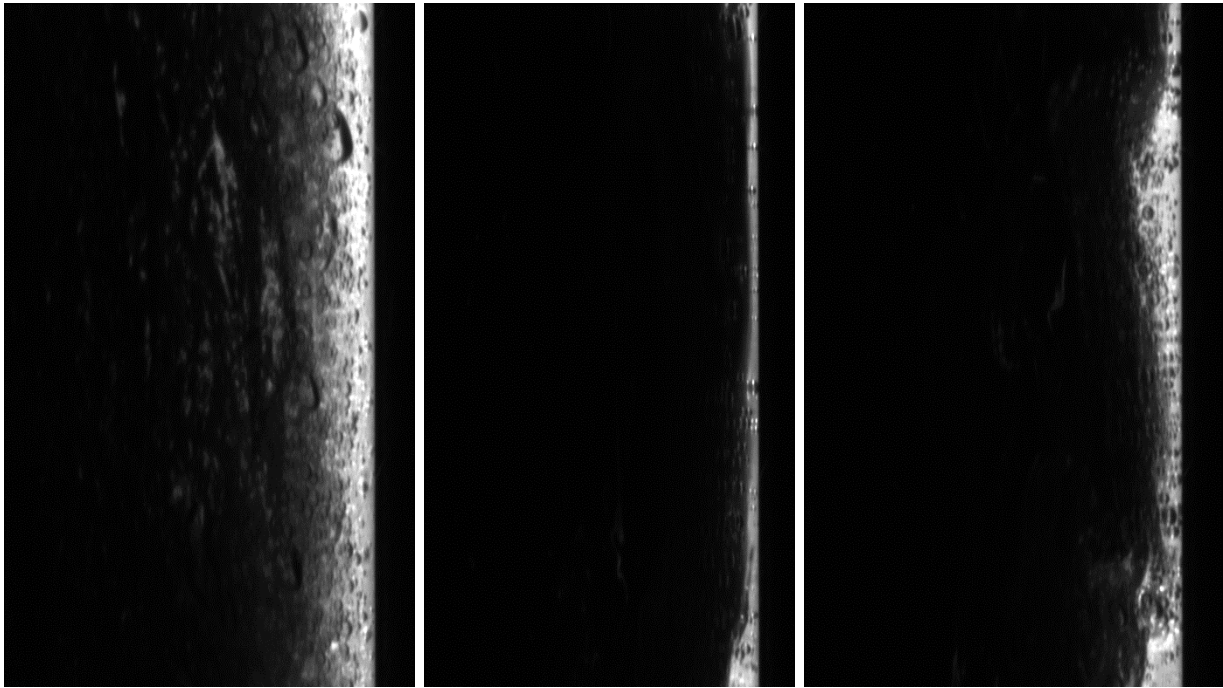
60 LPH (liquid rate) and 1000 SLPM (gas rate) (left to right: maximum, minimum, and average)



60 LPH (liquid rate) and 1100 SLPM (gas rate) (left to right: maximum, minimum, and average)



60 LPH (liquid rate) and 1200 SLPM (gas rate) (left to right: maximum, minimum, and average)



Appendix C

Maximum, minimum and average values of film thickness (laser in the center)

Liquid rate, LPH	20	Film thickness, mm		
		max, mm	min, mm	average, mm
Gas rate, SLPM	500	1.60807	0.00307	0.335
	600	1.1608	0.00536	0.258
	700	0.98013	0.01391	0.212
	800	0.68589	0.01306	0.171
	900	0.65738	0.00478	0.156
	1000	0.42912	0.00961	0.134
	1100	0.43202	1.5E-05	0.11
	1200	0.31825	0.00289	0.088
	1300	0.24315	0.00236	0.072
	1400	0.17658	0.00022	0.064
Liquid rate, LPH	25			
Gas rate, SLPM	500	1.71291	0.02562	0.349
	600	1.24567	0.01894	0.273
	700	1.16679	0.00223	0.231
	800	0.6182	0.00783	0.188
	900	0.55224	0.00021	0.168
	1000	0.00103	0.63014	0.144
	1100	0.37622	0.0008	0.124
	1200	0.36773	0.00388	0.103
Liquid rate, LPH	30			
Gas rate, SLPM	500	1.62864	0.03934	0.365
	600	1.15011	0.02844	0.286
	700	0.83943	0.01138	0.244
	800	1.13245	0.01393	0.213
	900	1.12519	0.00194	0.188
	1000	0.57696	0.00279	0.156
	1100	0.46968	0.0033	0.132
	1200	0.52878	0.00109	0.111

Maximum, minimum and average values of film thickness (laser moved closer to the camera)

		Film thickness, mm		
Liquid rate, LPH	20	max, mm	min, mm	average, mm
Gas rate, SLPM	1500	0.1031	0.02464	0.06256
Liquid rate, LPH	25			
Gas rate, SLPM	1300	0.15188	0.04558	0.09321
	1400	0.12725	0.02525	0.08113
	1500	0.11177	0.02321	0.07095
Liquid rate, LPH	30			
Gas rate, SLPM	1300	0.16702	0.04774	0.10429
	1400	0.14834	0.03487	0.08937
Liquid rate, LPH	35			
Gas rate, SLPM	500	0.79234	0.12822	0.36127
	600	0.6156	0.1471	0.31016
	700	0.61909	0.08041	0.26026
	800	0.56988	0.06799	0.21823
	900	0.44936	0.0757	0.19536
	1000	0.38926	0.063	0.15622
	1100	0.34429	0.06043	0.14487
	1200	0.22518	0.05635	0.12746
	1300	0.28519	0.05199	0.11102
Liquid rate, LPH	40			
Gas rate, SLPM	500	0.75195	0.11214	0.36992
	600	0.67625	0.11639	0.31488
	700	0.61016	0.09889	0.26627
	800	0.53368	0.08247	0.22698
	900	0.5455	0.07921	0.21046
	1000	0.42759	0.05764	0.16743
	1100	0.40297	0.06851	0.15389
	1200	0.37209	0.04911	0.13356
Liquid rate, LPH	45			
Gas rate, SLPM	500	0.78183	0.14499	0.38301
	600	0.71137	0.09764	0.32815
	700	0.70166	0.10911	0.27446
	800	0.51413	0.0874	0.23601
	900	0.47691	0.08858	0.21799

	1000	0.41143	0.07185	0.17191
	1100	0.37762	0.06036	0.16123
	1200	0.30069	0.06713	0.13902
Liquid rate, LPH	50			
Gas rate, SLPM	500	0.77934	0.11226	0.39322
	600	0.71165	0.12946	0.33799
	700	0.68432	0.12283	0.28949
	800	0.52243	0.10609	0.24372
	900	0.44042	0.0968	0.22534
	1000	0.41553	0.08241	0.18208
	1100	0.36839	0.0854	0.16827
	1200	0.31146	0.06498	0.14381
Liquid rate, LPH	55			
Gas rate, SLPM	500	0.79821	0.14736	0.40125
	600	0.74502	0.13213	0.35094
	700	0.60557	0.11972	0.29913
	800	0.52457	0.10484	0.24812
	900	0.47773	0.08342	0.23347
	1000	0.41824	0.08984	0.20098
	1100	0.33751	0.0776	0.17776
	1200	0.52878	0.00109	0.15142
Liquid rate, LPH	60			
Gas rate, SLPM	500	0.71802	0.18678	0.40959
	600	0.65848	0.1417	0.35589
	700	0.62995	0.1231	0.31236
	800	0.52946	0.12551	0.26651
	900	0.51508	0.1081	0.23847
	1000	0.40221	0.08064	0.20566
	1100	0.36436	0.07988	0.17952
	1200	0.33589	0.06712	0.15225